Report No. CG-ONSCEN 03-90

(2)

WESTERN PACIFIC OMEGA VALIDATION ANALYSIS

Verne E. Hildebrand

VISICOM LABORATORIES, INC.
11225 West Bernardo Court
Suite 140
San Diego, California 92127

Final Report, August 1990

Prepared for:

U.S. DEPARTMENT OF TRANSPORTATION
UNITED STATES COAST GUARD
OMEGA Navigation System Center
Alexandria, Virginia 22310-3998

Technical Report Documentation Page

1. Report No.	2. Government Accession No.	3. Recipient's Catalog No.
CG-ONSCEN 03-90		

4. Title and Subtitle	5. Report Date
Western Pacific OMEGA Validation Analysis	August 1990
	6. Performing Organization Code
	8. Performing Organization Report No.
7. Author(s)	
Verne E. Hildebrand	
9. Performing Organization Name and Address	10. Work Unit No (TRAIS)
VISICOM Laboratories, Inc. 11225 West Bernardo Court, Suite 140 San Diego, CA 92127	5462
	11. Contract or Grant No.
	N00123-86-D-0134, D.O. 041
	13. Type of Report and Period Covered
12. Sponsoring Agency Name and Address	Final Report August 1989 to August 1990
U. S. Department of Transportation United States Coast Guard Omega Navigation System Center Alexandria, VA 22310-3998	14. Sponsoring Agency Code

15. Supplementary Notes

Under contract to: Naval Ocean Systems Center
Code 434
271 Catalina Blvd.
San Diego, CA 92152-5000

16. Abstract

This report, the seventh in the Omega Validation series assesses the Omega Very Low Frequency radio navigation system performance in the Western Pacific Ocean area. Our general overview describes (1) a new emphasis for this validations on establishing signal quality through characterizing zones of signal-self-intereference, (2) validation planning, (3) measurements, and (4) analysis undertaken. Regions of self-interference due to equatorial zone propagation are predicted and analyzed for each Omega signal. Zones of poor signal interference caused by propagation the long way around the world (long-path) are predicted and assessed. Navigation accuracy and signal coverage is assessed.

For most of the validation region Omega fully meets navigation expectations. The prediction guidence in the form of Propagation Phase Corrections, zones of poor signal quality (Modal and Long-path), and Station Coverage are largely correct. A relatively small but highly significant zone of predicted inadequate coverage during certain periods of the day was identified and assessed. Navigation support in this zone, which extends approximately between latitude 20°N and 5°S and between longitude 105°E and 120°E, was found to be unreliable at night during periods of strong atmospheric noise.

17. Key Words			18. Distribution Statement
Omega	Correction	Long-path	Document is available to the U.S. Public through the National Technical Information Service, Springfield, Virginia 22161
Navigation	Radio Wave	Phase	
Accuracy	Database	Signal-to-noise	
Propagation	Analysis		
Prediction	Modal		

19. Security Classif. (of this report)	20. Security Classif. (of this page)	21. No. of Pages	22. Price
Unclassified	Unclassified		

Form DOT F 1700.7

NOTICE

This document is disseminated under the sponsorship of the Department of Transportation in the interest of information exchange. The United States Government assumes no liability for the contents or use thereof.

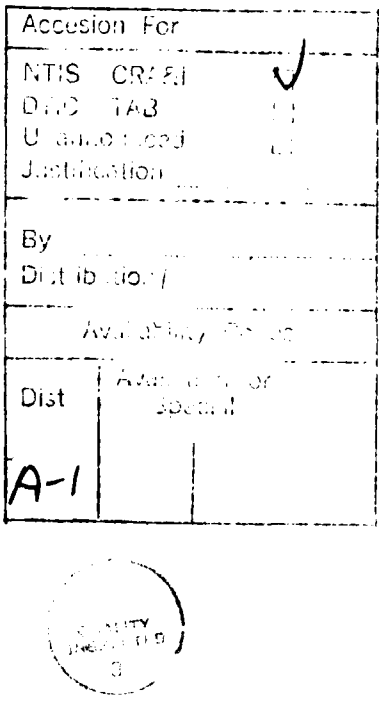

ACKNOWLEDGEMENTS

The author wishes to acknowledge several individuals who have made major contributions to the investigations supporting this Western Pacific Validation Analysis.

Mr. Carl Kugel of the U. S. Naval Ocean Systems Center in San Diego, California, was responsible for the major portion of data processing. His many years of experience were invaluable in ensuring that artifacts of instrumentation were removed prior to our analysis. His guidance was a great aid to understanding the many subtleties and complexities associated with data interpretation.

Mr. Eric Swanson of the U. S. Naval Ocean Systems Center in San Diego, California, provided a wealth of background information, both historical and technical. He contributed to many fruitful discussions regarding coverage assessment and interpretation of theoretical factors.

Mr. Randolph Doubt and Ms. Rebecca Casswell of the U. S. Coast Guard Omega Navigation System Center in Alexandria, Virginia, were instrumental in providing data from the OMEGA MASTERFILE and the shipboard collection program.

Commander R. J. Wenzel, Commanding Officer of the U. S. Coast Guard Omega Navigation System Center and Mr. Randolph Doubt provided extensive valuable guidance in establishing a new emphasis for the remaining Validation Analysis projects.

METRIC CONVERSION FACTORS

Approximate Conversions to Metric Measures

Symbol	When You Know	Multiply By	To Find	Symbol
LENGTH				
in	inches	*2.5	centimeters	cm
ft	feet	30	centimeters	cm
yd	yards	0.9	meters	m
mi	miles	1.6	kilometers	km
AREA				
in^2	square inches	6.5	square centimeters	cm^2
in^2	square feet	0.09	square meters	m^2
yd^2	square yards	0.8	square meters	m^2
mi^2	square miles	2.6	square kilometers	km^2
	acres	0.4	hectares	ha
MASS (weight)				
oz	ounces	28	grams	g
lb	pounds	0.45	kilograms	kg
	short tons (2000 lb)	0.9	tonnes	t
VOLUME				
tsp	teaspoons	5	milliliters	ml
Tbsp	tablespoons	16	milliliters	ml
fl oz	fluid ounces	30	milliliters	ml
c	cups	0.24	liters	l
pt	pints	0.47	liters	l
qt	quarts	0.95	liters	l
gal	gallons	3.8	liters	l
ft_3	cubic feet	0.03	cubic meters	m^3
yd_3	cubic yards	0.76	cubic meters	m^3
TEMPERATURE (exact)				
°F	Fahrenheit temperature	5/9 (after subtracting 32)	Celsius temperature	°c

* 1 in = 2.54 (exactly). For other exact conversions and more detailed tables, see NBS Misc. Publ. 286, Units of Weights and Measures. Catalog No. C13.10:286.

Approximate Conversions from Metric Measures

Symbol	When You Know	Multiply By	To Find	Symbol
LENGTH				
mm	millimeters	0.04	inches	in
cm	centimeters	0.4	inches	in
m	meters	3.3	foot	ft
m	meters	1.1	yards	yd
km	kilometers	0.6	miles	mi
AREA				
cm^2	square centimeters	0.16	square inches	in^2
m^2	square meters	1.2	square yards	yd^2
km^2	square kilometers	0.4	square miles	mi^2
ha	hectares (10,000 m^2)	2.5	acres	
MASS (weight)				
g	grams	0.035	ounces	oz
kg	kilograms	2.2	pounds	lb
t	tonnes (1000kg)	1.1	short tons	
VOLUME				
ml	milliliters	0.03	fluid ounces	fl oz
l	liters	2.1	pints	pt
l	liters	1.06	quarts	qt
l	liters	0.26	gallons	gal
m^3	cubic meters	35	cubic feet	ft^3
m^3	cubic meters	1.3	cubic yards	yd^3
TEMPERATURE (exact)				
°c	Celsius temperature	9/5 (then add 32)	Fahrenheit temperature	°F

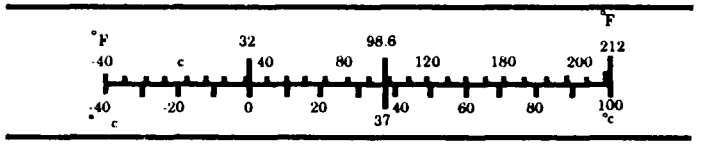

TABLE OF CONTENTS

TABLE OF CONTENTS, Continued

TABLE OF CONTENTS, Continued

TABLE OF CONTENTS, Continued

LIST OF FIGURES

SECTION 3, EXECUTION AND FINDINGS

LIST OF FIGURES, Continued

SECTION 3, EXECUTION AND FINDINGS, Continued

SECTION 4, INTERPRETATION OF VALIDATION ANALYSIS

LIST OF FIGURES, Continued

SECTION 4, INTERPRETATION OF VALIDATION ANALYSIS, Continued

APPENDIX A, GENERATION OF GEOGRAPHIC PLOTS SHOWING MODAL COMPETITION

LIST OF FIGURES, Continued

APPENDIX A, GENERATION OF GEOGRAPHIC PLOTS SHOWING MODAL COMPETITION, Continued

APPENDIX B, MODAL INTERFERENCE DATA ANALYSIS

LIST OF FIGURES, Continued

APPENDIX B, MODAL INTERFERENCE DATA ANALYSIS, Continued

LIST OF FIGURES, Continued

APPENDIX B, MODAL INTERFERENCE DATA ANALYSIS, Continued

APPENDIX C, PRESENTATION OF PREDICTED LONG-PATH INTERFERENCE BOUNDARIES FOR SIGNALS IN THE WESTERN PACIFIC VALIDATION REGION

APPENDIX D, LONG-PATH/SHORT-PATH EFFECTS DATA ANALYSIS

LIST OF FIGURES, Continued

APPENDIX E, NAVIGATION FIX ACCURACY ASSESSMENT

LIST OF TABLES

EXECUTIVE SUMMARY

This executive summary highlights the Western Pacific Omega Navigation Validation. Material presented includes (1) a brief description of Omega, (2) the Omega validation purpose and goals, (3) the objectives and emphasis for this validation, (4) analysis findings, and (5) conclusions.

INTRODUCTION

Omega is a Very Low Frequency (VLF) radio navigation system providing airborne, marine, and terrestrial users with a continuous, worldwide, position-location capability. Omega, which became operational on an interim basis in 1968 and was declared fully operational in 1982, consists of eight transmitters located in Norway, Liberia, Hawaii, North Dakota, La Reunion, Argentina, Australia and Japan. The typical position-fix accuracy achieved with Omega is 2–4 nmi, 2 drms.

The U. S. Coast Guard Omega Navigation System Center (ONSCEN) is assessing the capability of Omega through a validation program consisting of seven regions. Five regions have been validated: the Western Pacific, the North Atlantic, the North Pacific, the South Atlantic, the Indian Ocean and South Pacific (see References). This Western Pacific Validation, revisited, is complete with this report. Analysis of the Mediterranean Sea will consist primarily of data archiving.

The VLF signal properties dictating the quality of Omega operation are received phase and Signal-to-Noise Ratio (SNR). Quality of measured phase is fundamental to position-accuracy. For navigational use or system planning, four types of predictions are used in determining Omega operational characteristics: (1) phase of signals, (2) signal level, (3) atmospheric noise, and (4) signal phase quality. Phase prediction is determined by the Swanson model. SNR is derived from signal level calculations using propagation and noise models. Propagation models are created by the Naval Ocean Systems Center (NOSC) and The Analytical Sciences Corporation (TASC). The noise models use predictions based upon International Radio Consultative Committee (CCIR) measurement data. The most sophisticated model for noise prediction was developed by DECO/ Westinghouse and upgraded by the Naval Research Laboratory (NRL). Signal

phase quality is predicted using a recent set of propagation calculations by TASC as compared with the Overlay and Parametric models of TASC and NOSC, respectively.

Signal phase quality is degraded by self-interference, which results when a signal is dominated by a condition of propagation not intended for Omega use. One type of self-interference occurs, under certain conditions at night, on the direct propagation path when higher-ordered modes are generated and sustained (modal). Another type of self-interference occurs when a signal propagating the long way around the world (long-path), under nighttime propagation, dominates the shorter path (short-path), which is under daytime propagation. The areas where self-interference can occur are called either modal zones or long-path zones. Validations assess conformity of predictions to the received signals.

WESTERN PACIFIC VALIDATION

The Western Pacific validation consists of three parts: (1) planning, (2) measurement, and (3) analysis and reporting.

Planning included (1) predicting navigation performance in the region, (2) identifying areas of predicted signal quality problems, and (3) designing measurements to test predictions. Navigation performance was assessed using theoretical calculations to predict signal level, signal-to-noise ratio, and phase regularity for all signals. Areas having signal quality problems include zones of signal self-interference and poor SNR. Special measurements included use of aircraft to record modal interference patterns.

Measurement included collection of Omega data on aircraft, at fixed sites, and on the Japanese Maritime Safety Agency research vessel, Tsushima. The primary data for assessing signal quality were collected by a U. S. Coast Guard C-130 aircraft, which involved approximately 120 flight hours over a period of 4 weeks during April and May 1986. The fixed-site data aided the calibration of the flight data and helped determine conditions during the flights. Fixed sites did not have atomic reference oscillators; thus the data lack some important controls. The ship, Tsushima, with combined Omega/Satellite receivers made several transits where Omega and Satellite fix data were recorded.

The analysis includes: (1) assessing data and comparing it with predictions, (2) evaluating measured position-fix accuracy, and (3) interpreting the results. Analysis emphasis is on locating signal self-interference and then on testing for good SNR on the other signals. Navigation assessment compares measured with predicted position, using signals found to have good quality.

ANALYSIS FINDINGS

The short-path and the long-path self-interference assessments are presented separately because the different types of interference occur at different times, and because the required analysis work is quite different. Each of the Omega signals was assessed for self-interference in order to establish zones classified by those phenomena that cause the interference. Our findings are that high-quality navigation is achieved for the largest part of the validation region, as shown in Figures 3-4 and 3-5 on pages 35 and 36, respectively. We confirm that certain predicted navigation problems exist in this region.

Short-path Interference Analysis: The short-path predicted modal zones are found to be mostly correct. The data suggest that the predicted highly-extended near station modal zones for La Reunion and Japan should be shortened. This finding is important in that use of the La Reunion signal is vital in the vicinity of Singapore.

Predictions show phase quality to be a problem at night for a sizable area located between about 0° to 15°N latitude and 95°E to 125°E longitude, as shown in Figure 3-6 on page 37. The area is larger and the situation more critical for 13.6 kHz than for 10.2 kHz. Within this sizable area, regions of two-station (Liberia [B] and La Reunion [E]) and three-station (Norway [A], Liberia [B] and La Reunion [E]) coverage are predicted. SNR also is a problem on Norway and Liberia for locations in part of and adjacent to the three-station area. The bearings to Liberia and La Reunion are not favorable for pair selection, thus the navigation quality of the available combinations is limited. The predicted boundaries to the areas of poor coverage are not well defined because of limited measurements. However, the findings collectively support the Analysis Model well enough to lend credence to its predictions.

We found that the nighttime modal problem, which can be severe on all frequencies simultaneously, is strong on the three closest stations: Hawaii,

Australia and Japan. Thus, the more distant stations with longer paths are important for navigation in this region. Modal effects are somewhat dependent on ionosphere conditions, both meteorological and seasonal. This is evidenced in the data by variability in modal occurrence. This variability strongly suggests that boundaries will move about, thus increasing the difficulty of certifying a model.

Long-path Interference Analysis: The TASC calculations of field strength versus distance were extended beyond the station antipodes, and day/night portions were combined to reflect expected propagation conditions at times of specific interest. This extended model, while not elegant, allowed (1) estimating the maximum excursion of the long-path signal into the short-path region, and (2) estimating the time when the boundary between long-path and short-path crosses a monitoring site. This model provided a coupling between the acquired data and the long-path boundary predictions, particularly those predicted by the Parametric Model.

Three stations are predicted and two observed to exhibit long-path interference effects within the validation region; the predicted being Liberia, North Dakota and Argentina. North Dakota was not observed because the needed measurements were not made. The data show requirements for boundary adjustments in all prediction models, but do not directly support placement of the boundaries. This study augments the accumulating evidence that long-path effects are an important and not yet well established factor in navigation signal selection. While the documentation of long-path needs further refinement, the techniques we use are useful and demonstrate the feasibility for additional analysis.

Signal-to-Noise Analysis: The SNR coverage analysis was limited to checks of coverage at fixed sites to determine if inadequate SNR was measured. We find signal loss a significant problem. Poor SNR is an important contributor to the navigation problem. The Western Pacific is an area of high atmospheric noise with the major contributing regions shifting above and below the equator in concert with local summer. Signal loss due to noise occurs between mid afternoon and early night.

Navigation Accuracy Analysis: Spot checks of the data confirm that navigation accuracy for the majority of fixes is within that expected. The analysis thus

focuses on assessing situations flagged as possible exceptions. Our observations suggest that predictions, which are based on mid-latitude models, are not optimal for low-latitude propagation. Examples are given which suggest possibilities for improving predicted phase correction models during the day/night transition times on propagation paths. When the near stations are modal, primary dependence is on use of the far stations. Systematic biases are noted in predictions for transition intervals. Day/night transition intervals for signals from the more distant stations can be long, occupying sixty to eighty percent of the time. Additional prediction refinement to reduce these biases seems warranted. These cited situations concerning model refinements are not considered critical to navigation.

CONCLUSIONS

This validation provides significantly improved perspectives on navigation reliability in the Western Pacific. For most of the validation region, Omega fully meets navigation expectations. Also, the prediction guidance is correct over most areas. The confirmation of a signal coverage problem area is not a new discovery; rather it is a refinement of a well defined problem. The role of a validation is to report findings, and in this case, the findings heavily depend upon predications for extrapolation to locations of boundaries. We recommend that adjustments be made to prediction boundaries and that these findings, after proper review, be included as part of navigation guidance.

In summary, the analysis found that Omega works very well over the vast majority of the Western Pacific validation region. In a significantly large area, up to six of the eight Omega signals can simultaneously incur modal effects during nighttime in the Western Pacific. During daytime adequate navigation is available throughout the region. However, in the vicinity of Cubi Point to Japan, as few as three stations may have adequate SNR. The predicted modal interference and values of inadequate SNR are largely confirmed. An exception is the predicted large northeast-ward extent of the near-zone modal interference predicted for La Reunion and Japan. Long-path self-interference also occurs on three of the eight Omega signals at certain times. These long-path effects add further complexity to the navigation solution. From our analysis, we recommend caution for full reliance on the Omega system in certain locations and under some noise conditions.

THIS PAGE INTENTIONALLY LEFT BLANK

1.0 INTRODUCTION

This section lays the foundation material to support this validation analysis and gives a synopsis of the material presented in the following sections. The background material includes a brief description of Omega, Very Low Frequency Radio Waves, the Omega Validation Program, and the objectives of this validation.

1.1 BACKGROUND

1.1.1 OMEGA NAVIGATION SYSTEM

Omega is a Very Low Frequency (VLF) radio navigation system providing airborne, marine, and terrestrial users with a continuous, worldwide, position-fixing capability (see SWANSON 1983, Ref. 1, for an excellent review). The system, which became operational on an interim basis in 1968 and was declared fully operational in 1982, consists of eight transmitters located in Norway, Liberia, Hawaii, North Dakota, La Reunion, Argentina, Australia, and Japan. These transmitters are given corresponding letter designations [A] through [H]. Omega uses the internationally allocated navigation band between 10 and 14 kHz. The typical position fix achieved with Omega is within 2 to 4 nmi, 2 drms. Omega is operated through international cooperation. The U. S. Coast Guard Omega Navigation System Center (ONSCEN) has management and coordination responsibility for the United States. System synchronization is the responsibility of the Japanese Maritime Safety Agency. Transmitters not on U. S. soil are operated and maintained by host nation agencies. Navigation receivers are produced by manufacturers in several countries.

1.1.2 VLF AND OMEGA

The fundamental measurement in Omega is the phase of the received VLF signal. Omega operates under the predication that measured phase can be related to location on the earth. For navigation, the phase of several received signals (two or three depending upon navigation mode) must be both measurable and of good quality. It is the role of the validations to assess the availability of measurable good quality signals. The received Signal-to-Noise Ratio (SNR) must be sufficiently high to permit accurate and timely phase measurement. Poor SNR on a

received signal can be detected by the receiver, and the signal can be "de-selected" so that this signal is not used for the navigation fix. For reliable navigation, received phase must closely match phase prediction for the receiver location. Unpredictable phase deviations from predictions can occur in certain instances due to signal self-interference. Self-interference results when a signal is dominated by a mode of propagation not intended for Omega use. Undesired modes occur at night on the direct propagation path because higher-ordered modes may, under certain conditions, be easily generated and sustained. Undesired modes also occur when a signal propagating the long way around the world (long-path) under nighttime propagation dominates the shorter path (short-path) under daytime propagation. These phase disruptions caused by signal self-interference are insidious, because they cannot be reliably detected by Omega receivers, and they may exist even on the strongest signals in the area.

VLF signals propagate in a waveguide formed by the earth's surface and the lower boundary of the ionosphere. Both surface conductivity and ionosphere parameters affect the signal attenuation and phase velocity of propagation. Surface conductivity effects are static; they depend on the terrain traversed. Ionosphere parameters are dynamic and are due to variations in the solar illumination (resulting from the earth's rotation and seasons), solar disturbances, and ionospheric wind and electric current systems. Thus, VLF signals incur both (1) variations in phase and amplitude due to navigation receiver location changes (resulting in different static conditions), and (2) time variations due to a dynamic ionosphere. These variations, which must be accounted for in establishing position, are incorporated into navigation phase predictions.

Omega navigation uses four types of predictions versus location: (1) phase of signals, (2) signal level, (3) atmospheric noise, and (4) signal phase quality. Phase prediction is based on the Swanson model. SNR is derived from signal level calculations using propagation models developed by the Naval Ocean Systems Center (NOSC) and The Analytical Sciences Corporation (TASC). The noise models use predictions based upon International Radio Consultative Committee (CCIR) measurement data. The most sophisticated model for noise prediction was developed by DECO/Westinghouse and upgraded by the Naval Research Laboratory (NRL). Signal phase quality is predicted using the Overlay and Parametric models of TASC and NOSC. Each of these prediction models are described in the pres-

entation of the analysis findings. Validations assess conformity of predictions to the received signals.

1.1.3 OMEGA VALIDATION PROGRAM

The U. S. Coast Guard Omega Navigation System Center (ONSCEN) has a program for assessing the overall worldwide capability of the Omega Navigation System. This responsibility is being addressed by a formalized regional validation program described by Scull (SCULL 1978, Ref. 2) and Doubt (DOUBT 1984, Ref. 3). This program, composed of seven validation regions, is presently well along. Six regions have been validated and reported. This Western Pacific Validation augments the first Western Pacific Validation with updated data covering the Australia Omega transmitter and giving emphasis to signal self-interference. The Australia transmitter was not operational at the time of the previous Western Pacific Validation. Previously reported validations include the Western Pacific in the fall of 1977 (KARKALIK 1978, Ref. 4; KARKALIK et al 1978, Ref. 5), the North Atlantic in the summer of 1978 (CAMPBELL et al 1980, Ref. 6; CAMPBELL 1980, Ref. 7), the North Pacific in the summer and fall of 1979 (LEVINE 1980, Ref. 8; LEVINE & WOODS 1981, Ref. 9), the South Atlantic in the spring of 1980 (WATT et al 1983, Ref. 10; WATT 1983, Ref. 11), the Indian Ocean in the fall of 1983 (KUGEL 1984, Ref. 12; SWANSON et al 1985, Ref. 13; KUGEL et al 1986, Ref. 14) and the South Pacific in the fall of 1989 (HILDEBRAND 1989, Ref. 15).

As described in Section 2.3 DATA MEASUREMENT, there are three major data collection categories: airborne, shipboard, and fixed-site measurements. The fixed sites are usually installed before the flights and remain installed to obtain long-term measurement of temporal variation. Shipboard data are obtained when arrangements can be made with ships transiting the regions. Thus, the data collection effort for a given validation may extend up to the time of data analysis and report preparation.

Traditionally, however, the data collection period is more closely associated with the aircraft flights. The flights for the Western Pacific analysis were completed in the spring of 1986.

1.1.4 VALIDATION OBJECTIVE

The major objective for the validation program has always been to report the observed reliability of predictions and the accuracy obtained using the Omega Navigation System. Another objective has been to build up a database to support refinement of phase and signal-to-noise ratio predictions. The perspectives for achieving the primary objective, however, have evolved with time. This evolution is partly due to the "learning curve" associated with Omega utilization and to better insights regarding propagation. We are now greatly benefitting from (1) the lessons learned in the previous validations; (2) the significant refinement of propagation prediction models; and (3) propagation measurements collected over many years. This subsection describes some of the changes in perspectives and the resulting new emphasis placed on the validation process. Most of these new perspectives were incorporated into the previous validation for the South Pacific.

The initial validation emphasis was on signal coverage as defined by Signal-to-Noise Ratio (SNR) and on measuring obtainable navigation accuracy. The previous validations have amply demonstrated that, as predicted by computer models, there is high redundancy of signal coverage in most parts of the world. It has also been more widely appreciated that signal strength does not necessarily lead to accurate navigation. Phase perturbations, caused when a navigation signal interferes with itself, can create complications under certain conditions. These perturbations, collectively called self-interference, are sometimes prevalent in the strongest signals available for navigation. When self-interference can exist, navigation quality can no longer be guaranteed. It is now perceived that a key element in Omega validation must be to assess how well signal self-interference is predicted.

The objectives of this validation are (1) to compare coverage predictions with measurements, with emphasis on signal self-interference; (2) to report on measured navigation accuracy; and (3) to describe observations which differ from predictions.

1.2 VALIDATION SCOPE

The results of this validation are reported in two forms: (1) this validation report for the Western Pacific region; and (2) archive material containing the processed

data and analysis notes generated in the validation. This validation report is prepared as ONSCEN's report to the community describing the validation findings. The archive material is less formal and is intended as a repository for the supporting documentation to the validation results. The archive material is highly technical and data intensive, and of interest primarily to experts who want to check certain aspects of the validation or use the data for other investigations.

The primary focus for this analysis is the use of signals in navigation. The analysis identifies and selects areas and/or boundaries of special interest or concern first in terms of coverage from a single station and second in terms of coverage from all stations. An assessment is then made of the total signal resources available for navigation in the area or across the boundary of concern.

We note that the focus on navigation has served well in establishing analysis guidance and in organizing the presentation material. However, in order to determine signal quality for use in navigation, it has also been necessary to build a case for selecting good signals. Starting with theory, we build a model for guidance. We then use the model to identify signals of good/poor quality. We have maintained an orientation that emphasizes location. In addition, when appropriate, we have addressed the total Omega signal assets available for navigation in an integrated manner.

General: The steps in this validation consist of (1) planning, (2) acquiring data, (3) selecting and reviewing models for analysis guidance, (4) interpreting data based upon derived guidance, and (5) communicating the findings through comparison of results with previously published predictions.

Three major topics are addressed: (1) occurrence of good/poor phase quality, (2) occurrence of adequate/inadequate signals (SNR), and (3) expected/observed navigation accuracy. The phase quality factors addressed are problems of signal self-interference (modal interference, higher-ordered mode dominance, and long-path interference).

Phase Quality: This validation places maximum emphasis on locating signal self-interference regions and only a minimum on assessment of SNR coverage. It is increasingly clear that self-interference can be an important factor in achieving navigation reliability. The geographic extent of self-interference is much

greater than was realized at the time Omega was developed. Each of the Omega signals is assessed for zones of self-interference occurrence and classified by causing phenomena. The short-path (modal effects) and long-path self-interference assessment is presented separately because of occurrence at different times and because the required analysis is quite different. In addition, the theoretical support available to us for modal analysis is much stronger than for long-path. We were unable to evaluate the long-path effects in nearly as much detail as the modal effects.

The signal self-interference analysis has four major parts: (1) a description of the guidance derived for assessing modal interference and higher-ordered mode dominance; (2) a presentation and interpretation of the data with respect to modal effects; (3) a description of the guidance used to assess long-path effects on navigation; and (4) a presentation and interpretation of the data with respect to long-path interference. The guidance for parts one and three is derived from (1) the results of signal prediction calculations; (2) coverage diagrams; (3) previous experience; and (4) a preliminary overview of the data.

Signal-to-Noise Quality: What is important in the SNR analysis is to determine from the collection of signals with predicted "good" phase that a sufficient number have adequate SNR. A minimal effort was expended in investigating the signal-to-noise aspect of signal coverage. The focus is on determining whether at least three usable signals, having reliable phase and adequate signal, are available at all times (including accounting for station down times) over the Western Pacific region. Since poor phase quality and poor SNR do not necessarily coincide in time, the time factor is important. As noted previously, experience has shown that signal coverage predictions of SNR are generally adequate for station selection. Furthermore, much evidence exists that atmospheric noise variability is so high that the uncertainty of validating SNR from limited measurements argues against adjustment of contours based on the limited data of validations. As emphasized by Swanson in the Indian Ocean Validation report (SWANSON 1985, Ref. 13), inadequate SNR can be sensed and compensated for in data processing by the navigation equipment. We note that SNR is predicted to be a problem in the Western Pacific during some seasons and time intervals. As an example, the overlay predictions show 3 signals with adequate SNR in the vicinity of Darwin at 0600 GMT in February. The three signals are La Reunion, Australia and

Japan. The time of this prediction is at the beginning of the thunderstorm build-up period. Thunderstorm activity dies down after 1100 GMT, about three hours after sunset on the Japan propagation path. To emphasize the time factor, we note that the Japan signal incurs some modal interference after sunset. The high noise plus nighttime modal effects could result in only two station providing reliable phase.

Navigation Accuracy: Assessment of navigation accuracy is only meaningful when good quality signals are used. Thus, the process for assessing navigation accuracy is (1) to determine, for those locations where measurement data are available, what signals are predicted to be good and when, and (2) using good signals to measure the statistical accuracy of position fixes for representative propagation conditions. Good signals are determined by the phase and signal quality analysis described above. Representative propagation conditions include times of various path conditions, all daylight, all night, or in transition.

Data were selected from both fixed sites and ship transits for assessing navigation accuracy.

In addition to the above presented background material, the following subsection gives an encapsulated description of the material presented in this report.

1.3 REPORT OVERVIEW

Before proceeding with the main body of the report, we consider it helpful to give the reader an overview of the flow of information, along with some important findings. First, to set the stage, it must be appreciated that Omega validation is an immense undertaking, only slightly eased by dividing the world into seven regions. The Western Pacific is a relatively small region that has unusually difficult navigation problems. Omega signal propagation is very complex, involving many propagation factors and variables. To cover this region, the ideal assessment would involve a sampling strategy, both spatial, and temporal, that far exceeds any realistic budget. As a consequence of these considerations, the validation is conducted with extremely sparse data. Accordingly, heavy use is made of theoretical predictions.

Section 2.0, Methodology, provides a foundation for the analysis presented in Section 3 EXECUTION AND FINDINGS. A reader not well versed in Omega, VLF propagation theory, and past validations may find this material particularly helpful. It is important to recognize that the validation program started over 14 years ago and that each validation experience, as well as much other research, has contributed to the knowledge base. The philosophy for conducting the validation analysis has changed over time. Thus detail is provided to cover aspects that may be new to the reader.

Material reviewed includes (1) an examination of those guiding principles that are particularly germane to a validation analysis, (2) a description of how these principles are used to guide the preparation of a validation and analysis plan, (3) the preparation of a plan, and (4) the implementation of the plan for data collection and interpretive analysis. Emphasis is given to a description of those factors contributing to reduced navigation accuracy.

Section 3.0, Execution and Findings, provides a summary of the measurement operations, data assessment, selection of analysis guidance models, and the data analysis and interpretation effort. This section sets the stage for the evaluation and comparison of Omega coverage prediction presented in Section 4 INTERPRETATION OF VALIDATION ANALYSIS. The sequence of presentation follows the previously described philosophy that (1) navigation accuracy assessment should be conducted on good quality signals, and (2) to select good quality signals, a determination must first be made on signal quality. Thus, much of the report addresses the determination of when and where signal quality is reduced due to signal self-interference, i.e. modal and long-path effects. An analysis overview is presented in this section, which contains sufficient detail to provide a flavor for the overall activities. More details on analytical guidance are presented in Appendices A (for modal effects) and C (for long-path effects). Amplifying details on data analysis and interpretation are presented in Appendices B (for modal effects) and D (for long-path effects).

Since the analysis must depend heavily upon models for interpretation of the data and for extending results from measurements to regions where no data were obtained, these appendices contain a large amount of material. We used three sources of guidance: two coverage models, the Overlay and

Parametric model, and a recent set of Omega signal propagation calculations. Each source differed somewhat in placing important boundaries. We believe that the most recent propagation calculations provided important contributions to our findings. Unfortunately the calculations required extensive conversion (shown in Appendices A and C) to allow direct comparison with the other models and to be useful for geographic predictions. Our interpretation is heavily based upon the insights gained from this conversion process. Furthermore we feel that the insights have important consequences for predictions. Also, as will be noted in the presentation, we have to derive assessments that require a great deal of inference. We felt that in order to provide adequate support for the assessments, a large number of somewhat weak cases needs to be presented.

Our findings show that for the vast majority of the validation region, (shown in Figures 3-4 and 3-5 on respectively pages 35 and 36), high-quality navigation is achieved. Predictions show phase quality to be a problem at night for a sizable area centered about 10°N, 110°E as shown in Figure 3-6, page 37. The areas for 10.2 kHz and 13.6 kHz are similar in location, although the severity of modal competition is less for 10.2 kHz. Poor SNR is a problem for adequate station selection in the same area that has modal problems. This finding is consistent with predictions for this area.

Section 4.0, Interpretation of Validation Analysis, places the validation findings in perspective with expectations and the three coverage predictions (the material of Appendices A and C, the Overlay model and the Parametric model). We found that all models were largely in good agreement. Yet we find small but important differences. The differences are important for both refining coverage prediction and for establishing the credence of predictions for use in areas where confirming measurements have not been made. Adjustments to predictions of signal self-interference are recommended. Such adjustments provide better guidance for determining where and when certain signals should not be used for navigation. The predicted area for only two-station coverage at night, centered about 10°N, 110°E and at 13.6 kHz, would not occur if the La Reunion predicted modal interference does not extend as far as predicted. We believe the reliability of the Norway signal is questionable in this same area due to

SNR for some receivers. These factors make the navigation problem very real. Furthermore, the system has lost robustness in this area because there is no backup for station down-time.

The comparison of multiple models is particularly important in that the system user, or at least the manufacturer of user equipment, needs a source of system coverage information. Overlay and Parametric models have been available for some time. While the model outlined in this report is at present an engineering analysis tool, it is the most current, most detailed and easiest to use for purposes of validation. The community will benefit from each model and from knowing the similarities and differences between them.

Section 5.0, Summary and Conclusions, shows that over most of the Western Pacific validation region, Omega fully meets navigation expectations and that prediction guidance is correct. The identification of an area of inadequate signal coverage is not so much a new discovery as it is a confirmation and refinement of previous predictions. The role of a validation is to report findings. It is noted however that the findings have made extensive use of predictions to extend interpretations from locations of actual measurement to locations of expected boundaries.

2.0 METHODOLOGY

This section describes the principles and processes used in this validation. This material is intended to provide an amplifying foundation for the analysis presented in Section 3 EXECUTION AND FINDINGS. A reader well versed in Omega, VLF propagation theory, and past validations may choose to skim this material. Since the methodology for conducting the validation analysis has changed significantly over time, and since the self-interference effects may be new material for some readers, we provide more detail to cover these aspects.

2.1 VALIDATION GOALS

This subsection documents the planning processes, from evaluating the validation needs to defining specific analysis tasks. The analysis criteria and the processes used for the validation are established here. The focus is on the navigation product. Thus, the order of presentation for deriving validation guidance builds from providing a navigation service (the bottom line) through the chain up to the basic knowledge making such a service feasible.

2.1.1 GUIDING PRINCIPLES

Omega was conceived and implemented to provide worldwide, low cost, moderately accurate navigation services using VLF radiowave signals. Omega's intended use is primarily for in-transit navigation with other means used for transit end points. Although the system accuracy design goal was 2 to 4 nautical miles (2 drms), accuracy of 1 to 2 nautical miles was visualized and on average is realized where the signals have good phase quality.

Uncertainties in propagation prediction and geophysical variabilities lead to less accuracy at certain times and locations. Part of the validation challenge is to determine (1) when and where navigation accuracy is less than optimal, and (2) what accuracy can be achieved with the available signals of good quality.

Assessing position-fixing accuracy and its variability is greatly facilitated by understanding how relevant geophysics governs position fixing and how its dynamics contribute to position uncertainties. The following discussion builds a chain from the navigation product to each of the contributing physical elements. The chain is then examined for guidance in achieving the validation objectives.

How Omega uses VLF for position fixing. The fundamental measurement used in Omega is the phase of the VLF signal. The navigation service provides both stable signals for phase measurements and predictions of the expected phase at any position and time. The prediction part of this service is being validated. Accurate phase prediction is dependent on establishing reliable values for signal propagation parameters that vary in a complex manner with position and time.

The most basic method for obtaining a position fix (using hyperbolic phase difference curves) requires that phase be measured on a combination of three signals at one frequency to provide two Lines-of-Position (LOPs). The signals must be chosen so that the derived LOPs have sufficient angular separation to allow accurate location of their intersection. Four common frequencies are transmitted from each station. When mode 1 propagation is dominant, these frequencies have a well-defined phase relationship at the receiver. Phase is measured as a part of a cycle. Since the same phase value recurs at regular distance intervals separated by a cycle of propagation distance, a phase measurement can represent many positions. The distance interval covering a full cycle of measured phase is called a lane. Each frequency produces a different phase repetition pattern; thus different lane widths. Phase measurements are compared on up to four frequencies to establish a position for that frequency combination. This position is unique over a larger distance interval than a position determined from any single frequency. Defining position within the range of this interval is required of the user and is not a consideration of the validation. Optimal navigation is obtained from strong signals having good geometries and predictable phases. The ideal navigation process selects the best combinations of signals for position fixing. Accuracy of a position fix generally can be improved by using additional frequencies and stations. The challenge is to correctly weight signals in a position-averaging process. Geometric relationships can be calculated in a receiver from rough position fixes and SNR can be measured; both can be applied as weighting factors. Phase quality presently cannot be determined within the navigation receiver, nor can it always be reliably predicted due to uncertain propagation factors. Thus, the best approach is to deselect signals whose phase quality may be in question.

The validation assessment determines the accuracy of phase prediction at selected representative times, locations and Omega frequencies. Since phase pre-

dictions are made for expected conditions, validations assess deviations from predicted phase, and if possible, determine the cause. Phase prediction amounts to propagation prediction, which in turn amounts to prediction of the parameters that govern propagation. Such parameters may be empirical.

Phase deviations that create complications are integral to the navigation signals. They result from higher-ordered mode dominance and/or signal self-interference. Higher-ordered mode dominance can occur at nighttime along certain radials from the transmitter. Signal self-interference has two dominant mechanisms: (1) round-the-world, long-path propagation interfering with the short-path, and (2) modal interference created when the different modes of propagation within the bounded earth-ionosphere waveguide are of comparable amplitude.

The long-path/short-path self-interference results from the fact that the Omega signals propagate long distances with relatively low attenuation and that the propagation conditions on the two paths may be different.
These propagation differences include the following:

(1) Propagation attenuation is significantly less for eastward propagation relative to westward propagation;
(2) Signal attenuation is significantly different for day versus night propagation; and
(3) Signal attenuation varies with the conductivity of the earth's surface.

The modal interference occurs as a result of two conditions. The first, near modal, occurs close to the transmitter, where the received signal is composed of many propagated modes, each having a different phase velocity and attenuation. The higher-ordered modes generally dampen rather rapidly but have sufficient strength close to the transmitter to produce an interference pattern. However, when the transmitter is at a low latitude or low mid-latitude, the interference pattern may extend to large distances under nighttime propagation. The second condition, mode conversion, occurs at nighttime for propagation across or near the geomagnetic equator (over approximately ±20 degrees magnetic latitude) and possibly for propagation across very low-conductivity terrain such as the Greenland icecap. Energy is imparted to the higher-ordered modes which then can achieve amplitudes comparable to the dominant first mode. For both conditions, one of the higher-ordered modes may become the dominant mode. Each mode (several may be of comparable amplitude) propagates at a different

velocity. Thus, the phase may vary in a complex manner with distance. The interference causes the measurement of phase to deviate (lead and lag) from what is expected if propagation is only via mode 1. On occasion, the deviations are large enough to cause a cycle jump. A cycle jump implies a switch in dominant modes. This switch may occur at a fixed measurement site without a cycle jump. In this case the switch is evidenced when a large phase change occurs that differs from the expected mode 1 diurnal pattern. Once a higher-ordered mode becomes dominant, it may stay dominant over a large distance interval. When mode conversion takes place, energy is removed from and added to the first-ordered mode in unpredictable amounts. Consequently, the phase of the signal during and following mode conversion is no longer reliably predictable. Since phase fluctuations, mode switching, or higher-ordered mode dominance are not a part of the Omega navigation model, their occurrence results in position errors. Accurate predictions of regions where phase deviations can occur are needed to guide station deselection. Such predictions are particularly important, because no other means presently exists for mitigating conversion effects.

Use of Prediction Models. Four types of predictions for Omega have been used in past validations. These are predictions of navigation phase, signal coverage (i.e., boundaries within which phase is considered reliable and within which SNR is predicted adequate), best selection of station pair combinations, and regions of signal self-interference. The primary prediction is average incident phase from all stations for any receiver location, time-of-day, and season. Phase predictions assume that the first-order mode is sufficiently dominant that received phase will increase regularly with distance from a transmitter. Propagation parameters used in the average phase predictions are "fine tuned" using the OMEGA MASTERFILE of phase data, gathered through a network of monitoring sites. The OMEGA MASTERFILE is a database maintained by ONSCEN that contains hourly phase and phase-difference data from the worldwide network of OMEGA monitor sites. Because the OMEGA MASTERFILE database is quite large and includes measurements from widely dispersed locations around the world, average predictions should be quite accurate where the phase varies systematically with distance. It is the role of a validation to assess, within a region, the accuracy of position fixes to the greatest extent practical.

Coverage predictions are generated using full wave calculations of signal propagation, integrated with an atmospheric noise prediction model. Predictions are

average signal quality, SNR, and phase "purity." Two types of displays are produced: *Overlays* showing contours of SNR and phase quality threshold boundaries, and *Parametric Displays* showing signal navigation quality using symbology as the indicator. Both of these types of displays are presented and used in Section 4.1.2 COMPARISON OF ANALYSIS WITH COVERAGE PREDICTIONS to assess the analysis findings. Composite signal coverage predictions are extensions of basic coverage prediction that show coverage of all stations versus location on a single diagram.

Modal interference, mode switching, and higher-ordered mode dominance predictions are made using full-wave calculations. Achieving accurate position fixing requires knowing how the phase behaves with time and position. The presence of higher-ordered modal effects on a signal must be ruled out. If phase always changed regularly with distance (this was the basis for Omega design), prediction would be less complex. Unfortunately under nighttime propagation, important cases occur when received phase varies in a much more complex manner.

Validation requires determination of the actual existence of a predicted condition or quality. Ideally, sufficient analysis would be conducted to assess both time and position variability of the predictions. Unfortunately, the ideal case does not exist; much ingenuity is required to test the predictions from the few measuring sites, most of which cannot be optimally located for achieving these objectives. Some tests would have to be made to determine how far and how well extrapolations can be made from the specific measurement locations. A less desirable but more practical alternative is to simply report agreement or disagreement between predictions and measurements.

The quality of average phase predictions is best validated from well-surveyed fixed-site measurements of received phase with a high-quality reference oscillator. Phase-difference measurements, which are obtained by comparing phases between two received signals, are used when a highly stable local reference oscillator is not available. While complicating the interpretation, phase-difference data are a satisfactory substitute. To test phase prediction, care must be taken to ensure that the measured signal is not contaminated with unwanted components such as signal self-interference or local interference.

In the next subsection we discuss the plan for deriving the validation products.

2.2 VALIDATION PLAN

This subsection describes conversion of goals to planned practical accomplishment at an overview level, discusses what can be done and what is practical, describes use of theoretical guidance and predicted performance, describes types of measurements, reasons for use, their historic value and interrelationships, and describes problems of implementation, site selection and operational factors.

The Western Pacific validation technical activity was divided into three phases: (1) planning; (2) measurement; and (3) analysis and reporting.

2.2.1 PLANNING SUMMARY

The planning phase entailed the following activities:

- Use of models to predict navigation performance in the region.
- Identification of areas where signal self-interference is predicted to be a problem and explore boundaries in the region where SNR = –20 dB and –30 dB.
- Design of measurements to test for predicted signal self-interference and SNR boundaries.

For both planning and analysis, propagation and phase prediction models are relied upon to indicate the likely occurrence of inadequate signal quality. Naval Ocean Systems Center (NOSC) personnel made assessments of Omega navigation performance in the validation region using theoretical calculations of Omega signal propagation. Predictions of signal level, signal-to-noise ratio, and phase regularity were made for all Omega signals available in the Western Pacific region. Tools used were the NOSC state-of-the-art propagation models (FERGUSON 1970, Ref. 16; BICKEL et al 1970, Ref. 17; PAPPERT et al 1972, Ref. 18; SNYDER 1981, Ref. 19) and The Analytical Science Corporation (TASC) amplitude prediction model (GUPTA et al 1979, Ref. 20). These tools provided the best means for assessing the modal structure dependence upon distance, magnetic azimuth, magnetic dip angle, and ionospheric profile parameters.

Next, boundaries in the region were identified beyond which $\Delta\emptyset > 20$ CEC and SNR < -20 dB and < -30 dB. The waveguide-mode prediction model showed the regions where potential navigation accuracy problems exist. The calculations indicated where observations of Omega signals should be made. These regions

were determined as functions of geophysical conditions (i.e., solar illumination and season). The planning phase is described in detail in Subsections 2.3 DATA MEASUREMENT and 2.4 A PLAN FOR VALIDATION ANALYSIS. The planning phase has been documented by the Naval Ocean Systems Center in an informal unpublished repcrt entitled "Western Pacific Omega Validation Test Plan" by C. P. Kugel (KUGEL, private communication).

2.2.2 MEASUREMENT SUMMARY

The measurement phase entailed the following activities:

- Collection of Omega data to test the predictions with monitors at fixed sites, on aircraft, and on ships.
- Obtain navigation fixes both with Omega and with satellite navigation for reference.

The objective of the measurement phase was to provide data for assessing position fix accuracy of both fixed and mobile recording sites and for verifying the predicted location, extent, and time evolution of both modal zones and SNR boundaries. Seventeen aircraft flights were conducted, six fixed sites were located within the validation region, and two major ship transit segments conducted by the Japanese Maritime Safety Agency recorded data. The data collection locations/transits and the data gathered are described in Subsection 3.2 DATA ASSESSMENT.

2.2.3 ANALYSIS SUMMARY

The analysis phase consisted of the following activities:

- Refine predictions of signal self-interference zones and format for suitable comparison with data
- Assess modal effects in validation region and compare with predictions
- Evaluate signal/noise measurements and compare with predictions
- For signals of good phase quality and adequate SNR, assess position fix accuracy
- Interpret results

The models and techniques used and the detailed results are described or referenced in the subsections entitled 3.3 SIGNAL SELF-INTERFERENCE ANALYSIS, 3.4

LONG-PATH INTERFERENCE ASSESSMENT, 3.5 SIGNAL-TO-NOISE RATIO ASSESSMENT and 3.6 NAVIGATION ACCURACY ASSESSMENT.

2.3 DATA MEASUREMENT

The major measurement activities included the following:

- In-flight measurements on dedicated flights;
- Long-term measurement of temporal variation at fixed sites;
- Shipboard phase and position measurement from ship measurements made by the Japanese Maritime Safety Agency.

The selected boundaries for magnitude of phase fluctuation and SNR were used as one basis for selecting fixed monitor sites, aircraft flight paths, and ship transits. Availability of installation sites was another basis.

2.3.1 SITE SELECTION

The selection of sites and stations to be monitored at each site required tradeoffs between the kinds of data needed and the practical aspects of obtaining the data. Placement of monitors was made largely for practical support reasons. A requirement was that the selected sites provided good data for checking predictions and provided calibration points for the aircraft instrumentation.

To obtain the optimum set of data within the bounds of the available resources, a combination of data collection efforts were undertaken:

(1) Long-term fixed-site recording, primarily utilizing those sites that were set up for obtaining data for the OMEGA MASTERFILE;
(2) Short-term fixed-site recording, using much higher time resolution and calibrated (at the time of the site visit) for measurement of signal-to-noise ratio and to calibrate the aircraft collected data;
(3) A series of aircraft flights that transited the area; and
(4) Placement of navigation receivers upon a ship transiting this region.

2.3.2 MEASUREMENT OPERATIONS

The measurement activities were conducted in three separate operations: fixed-site monitoring, measurements aboard an aircraft, and independent shipboard operations conducted by the Japanese Maritime Safety Agency. Each of these measurement operations will be described in this subsection.

2.3.3 FIXED SITES

ONSCEN has established a global network of monitoring sites as part of the continuing evaluation of Omega signal behavior throughout the world. Normal monitoring operations were conducted by on-site personnel and collected data forwarded to ONSCEN. For selected sites, NOSC personnel conducted calibration measurements that allowed obtaining "absolute" signal field strength data. The procedure was to use special equipment to calibrate the amplitude measurements made with the fixed-site MX-1104 Omega Monitor Receivers, and then to use data from these receivers to calibrate the aircraft data during flyovers. Equipment at the fixed sites compares received phase with either an internal oscillator or precision external standard and records the data on magnetic tape. Depending upon the quality of the reference frequency, the data are processed by ONSCEN as measured phase or Line-of-Position (LOP) phase differences and included in the OMEGA MASTERFILE data bank. OMEGA MASTERFILE data were excerpted for selected sites.

The calibrated signal amplitude and phase monitoring equipment installed at the ONSCEN sites is basically the Magnavox MX-1104 receiver with a variable attenuator in the calibration line. Data from all sites consisted of SNR and phase relative to the local oscillator for seven stations and the calibration channel at the three frequencies of 10.2, 11.3 and 13.6 kHz. The selected sites for amplitude calibration had attenuated calibration signals injected at the receive antenna. (The interested reader is referred to reference 14, Indian Ocean Validation, Section 3, for more information on equipment characteristics and calibration methods.) The calibration signal was adjusted to be comparable in amplitude with the received noise, thereby calibrating the observed noise variations. SNR of the signal measurement channels was then converted to signal amplitude by removing the calibrated noise effects.

2.3.4 MOBILE RECORDING

Mobile data collection activities included ship transits and aircraft flights.

U. S. Coast Guard C-130 Aircraft Flights. Technical staff from NOSC and ONSCEN flew special monitoring equipment on a series of flight radials across the validation region. Most of the flights were nearly along a radial from one of the Omega transmitters. Monitoring equipment was installed aboard a C-130 cargo

aircraft operated by the U.S. Coast Guard (USCG). The aircraft flights encompassed approximately 120 flight hours and a total mission duration of 4 weeks during April and May 1986. The aircraft was equipped with two Litton LTN-211 Omega Navigation System (ONS) receivers and the Hewlett-Packard 3581 Wave Analyzer/Selective Level Meter for data measurement.

Shipboard Data. The Japanese ship Tsushima with Magnavox MX-1157 Omega receivers installed on board made several transits in the validation area between July 1986 and March 1987. Ship personnel collected frequent navigation-fix data with the MX-1157 receivers. The data were recorded and forwarded to ONSCEN. Data supplied consisted of taped readings of fix quality and fix error recorded at five or six minute intervals covering times of satellite passes.

The Magnavox MX-1105 Omega/Satellite receiver equipment configuration for shipboard installations is similar to that for the ONSCEN ground monitors, in that the basic components are the receiver and MFE-5000 cassette recorder. The MX-1105 is similar to the MX-1104 but also incorporates a receiver for TRANSIT navigation satellite fixes and uses speed log and gyrocompass information to enhance position determination.

2.4 A PLAN FOR VALIDATION ANALYSIS

This subsection describes the analytical plan prepared for the validation analysis. The spirit of a plan is indicated by using the future tense. We believe the future tense helps to communicate the perspective of a planning viewpoint, that is, expectations prior to undertaking the actual analysis. The analysis experience, described later, identifies how the analysis had to deviate from the plan. This plan is intended to be both a living document, to be modified by experience, and a guide for the remaining validations. As noted previously, the validation effort concentrates on analysis of modal interference effects, and therefore this discussion centers on these procedures.

A plan for data analysis and interpretation: The first priority will be to determine, by site location, what propagation characteristics are predicted to exercise a dominant influence on the signals. Primarily, this determination process identifies useful signals and segregates regions where higher-ordered modes, long-path interference and poor SNR have a major effect.

Analysis of flight signal level data will be conducted first to identify possible regions of multimode occurrence. Calculations of field strength versus distance made by TASC (GUPTA 1980(a), Ref. 21) and supplied by ONSCEN also will be reviewed and compared with flight data. The South Pacific analysis showed that the flight data did not always evidence modal effects that were either predicted or observed at fixed sites. The reasons for not showing modal effects are attributable to (1) either the time of the flight; (2) variation in the occurrence of modal effects; or (3) sufficient higher mode dominance so as to mask an interference effect. Thus, it is now known that the flight signal level data are not as reliable an indicator of modal effects as originally expected.

Fixed-site data analysis will be grouped into two categories based upon data analysis: data affected and data not affected by multimode. Data affected and not affected by multimode will be used to check the predicted boundaries of multimode effects. The fixed sites generally are not well placed to test predicted modal zone boundaries, so care will have to be taken in interpretation of the observations. Data not affected by multimode will be reviewed for consistency with Propagation Phase Corrections (PPCs) recorded in the OMEGA MASTERFILE. Noted gross inconsistencies of measured LOPs with PPCs will be flagged (ideally, the measured station pair phase difference plus the PPC equals the LOP).

For this validation, none of the fixed sites used atomic frequency references. Thus, special processing of the received phase will have to be made to remove as much of the reference frequency drift as practical. The corrected phase of individual transmissions will be scanned to detect significant deviations from the expected diurnal pattern. Deviations will be flagged and correlated between frequencies as a test for multimode. Occurrence of multimode will be noted.

Minimal assessment of measured SNR will be made to test for adequacy of signal coverage when the number of good stations is in question, primarily due to modal zone problems. SNR predictions will be tested at fixed sites for those stations predicted to have low SNR and primarily for those times when and locations where adequate signal coverage could be a problem. It is known that many of the fixed sites had, at times, severe interference problems. Thus care will have to be taken in noise level interpretation.

Shipboard data will be used to augment fixed-site data, primarily to test for modal interference. Ship transits were made at places providing a much better test of

modal zone boundaries than available from fixed sites. Therefore, an investigation will be made to determine if modal effects can be determined from the shipboard data.

A navigation accuracy assessment will be conducted as the final phase of the validation analysis. The assessment will consist of two parts: examination of data from fixed sites, and from shipboard measurements. The analysis process will depend on the type of data available. First, all data sets known to contain signal self-interference and inadequate SNR will be removed from the analysis files. Since no sites used an atomic frequency reference, phase-difference data will be compared with predicted phase difference for selected station-pair combinations.

Planning Comments: A more detailed description of the analysis processes used is presented in Section 3.3 SIGNAL SELF-INTERFERENCE ANALYSIS and Section 3.5 SIGNAL-TO-NOISE RATIO ASSESSMENT. We note that this planned process was modified significantly, especially with respect to using aircraft data as the focus for identifying modal conditions. From the analysis of prediction calculations and from the early stages of data analysis, it became evident that much of the modal competition was not easily recognized in the flight data. Consequently much more dependence was placed upon fixed-site data.

3.0 EXECUTION AND FINDINGS

This section provides the details of the validation effort, in this sequence: Measurement Summary, Data Assessment, Signal Self-Interference Analysis, Long-path Interference Assessment, Signal-to-Noise Ratio Assessment, and Navigation Accuracy Assessment.

3.1 MEASUREMENT SUMMARY

This subsection summarizes the measurement part of the validation: what flights were conducted and when, what fixed sites were operated and what transpired, and what ship transits were made and data collected. Measurement activities are compared to the plan and expectations.

The validation regions are basically centered on large ocean areas; consequently data collection is often challenging. In the Western Pacific, possible monitor site locations are along (1) the northern coast line of Australia, (2) the islands strewn across the region, and (3) the Japanese islands.

Within the Western Pacific, a major concern is that modal interference will occur on many Omega signals; namely Hawaii (Station C), North Dakota (Station D), La Reunion (Station E), Argentina (Station F), Australia (Station G), and Japan (Station H). For these transmissions, modal effects are expected to be most severe in the western portion of the validation region (largely from the Philippines westward). The aircraft flights are oriented so as to obtain optimum information on the transmitters near the validation region. Fixed sites were either a part of the long-term monitoring program or were chosen to aid calibration of the aircraft flight data and to assist in determining if the conditions measured during overflight are typical.

To review, combinations of data collection efforts are undertaken which consisted of (1) long-term fixed-site recording, primarily utilizing sites set up for obtaining data for the Omega navigation OMEGA MASTERFILE, (2) short-term fixed-site recording, usually with much higher time resolution and calibrated measurements of Signal-to-Noise Ratio (SNR), (3) a series of aircraft flights which transited the area, and (4) data collected from navigation receivers aboard the Aids to Navigation Research Vessel, Tsushima, operated by the Japanese Maritime Safety Agency while operating in this region.

The fixed-site recording stations for the Western Pacific, designated by circled dots, are presented in Figure 3-1. The primary sites are within the hatched area indicating the validation region. Fixed sites for the Western Pacific are Japan, Yap, Cubi Point, Brisbane, Darwin, and Singapore. Secondary sites lying outside this validation region are also used to measure signals traversing the region. The data collected at the fixed sites were obtained with MX-1104 receivers.

The flight data for assessing modal structure were collected by a U. S. Coast Guard C-130 aircraft. The flight paths for the Western Pacific region are shown in Figure 3-2. The flights are generally flown at night when the most serious modal effects are expected to occur. As noted, obtaining all-night propagation paths for widely dispersed transmitters is not possible. Thus many of the signals are recorded with the day/night terminator crossing the propagation path during at least part of the flight. A listing of flight schedules is shown in Table 3-1.

Omega, Transit satellite, and Global Position System (GPS) satellite fixes were made and compared for data collected on the ship, Tsushima, operated by the Japanese Maritime Safety Agency. The ship tracks for which data are analyzed are shown in Figure 3-3. The ship transits provide additional spatial information through much of the validation area.

3.2 DATA ASSESSMENT

This subsection describes the database acquired, assesses its quality, cites archival repository for data, provides examples to illustrate type and quality, and emphasizes aircraft data and modal effects.

Three types of measurements can be made from the received signals when calibrated: (1) signal levels, (2) signal-to-noise ratio, and (3) phase. Different measurements are analyzed for each recording configuration, aircraft, fixed site and ship.

Measurements of signal level versus distance from flights are used to test for evidence of modal interference. It was expected at the time of data collection that the aircraft data would provide the primary determination of modal interference caused by trans-equatorial propagation. The criterion used for identifying severe modal interference in the data is that the signal level variation between

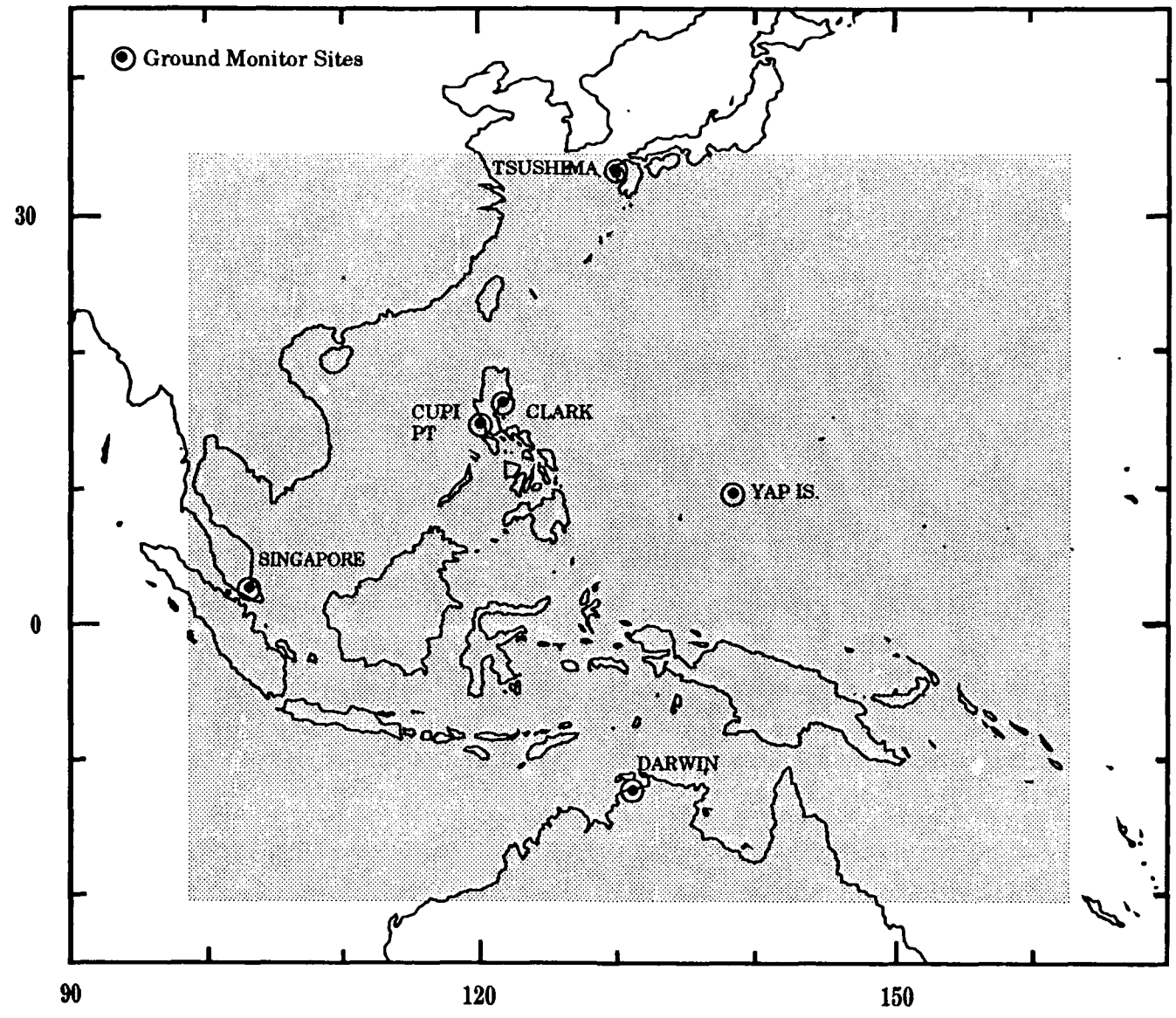

Figure 3-1. Western Pacific Omega Ground Monitor Sites

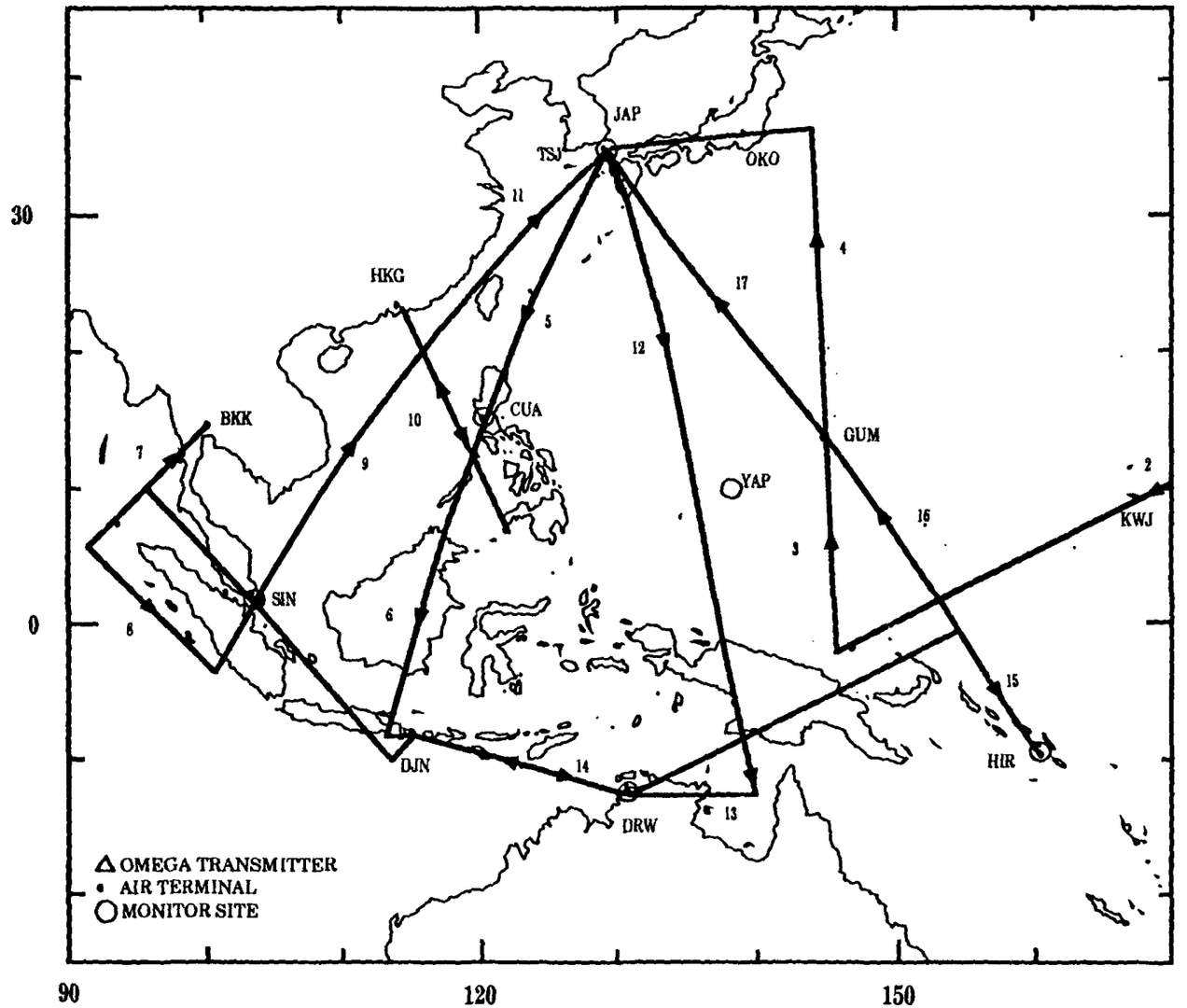

Figure 3-2. Flight Itinerary for USCG C-130 Aircraft

A/C FLT. NO	DEPARTURE					ARRIVAL					GND RON HRS
	ID	LOCAL Date	LOCAL Time	ZULU Adj.	ZULU Time	ID	LOCAL Date	LOCAL Time	ZULU Adj.	ZULU Time	
01	SAN	04/11/86	1040	+7	1740	HNL	04/12/86	1533	–14	0133	7.9
02	HNL	04/13/86	2003	–14	0603	KWA	04/13/86	0215	–12	1415	8.2
03	KWA	04/14/86	1945	–12	0745	UAM	04/14/86	0210	–14	1610	8.4
04	UAM	04/16/86	1937	–10	0937	OKO	04/16/86	0015	–15	1515	5.6
05	OKO	04/17/86	2200	–9	1300	CUA	04/17/86	0427	–16	2027	7.4
06	CUA	04/19/86	1927	–8	1127	DJK	04/19/86	0012	–17	1712	5.8
07	DJK	04/20/86	1846	–7	1146	BKK	04/20/86	0014	–18	1814	6.5
08	BKK	04/22/86	1928	–7	1228	PYL	04/22/86	0225	–16	1825	6.0
09	PYL	04/25/86	2158	–8	1358	HKG	04/25/86	0635	–16	2235	8.6
10	HKG	04/26/86	2308	–8	1508	HKG	04/26/86	0643	–16	2243	7.6
11	HKG	04/28/86	1946	–8	1146	TSJ	04/28/86	0130	–15	1630	4.7
12*	TSJ	05/01/86	2014	–9	1114	YAP	05/01/86	0410	–14	1810	6.9
13*	YAP	05/03/86	2039	–10	1039	DRW	05/03/86	0311	–15	1811	7.5
14	DRW	05/04/86	2054	–9	1124	DRW	05/04/86	0331	–15	1801	6.6
15	DRW	05/06/86	2034	–9	1104	HIR	05/06/86	0607	–13	1907	8.1
16*	HIR	05/09/86	2223	–11	1123	UAM	05/09/86	0321	–14	1721	6.0
17	UAM	05/10/86	2117	–10	1117	OKO	05/10/86	0313	–15	1813	6.9

* Sunrise or Sunset Transition During Flight

Table 3-1. Flight Schedule for Western Pacific Omega Validation

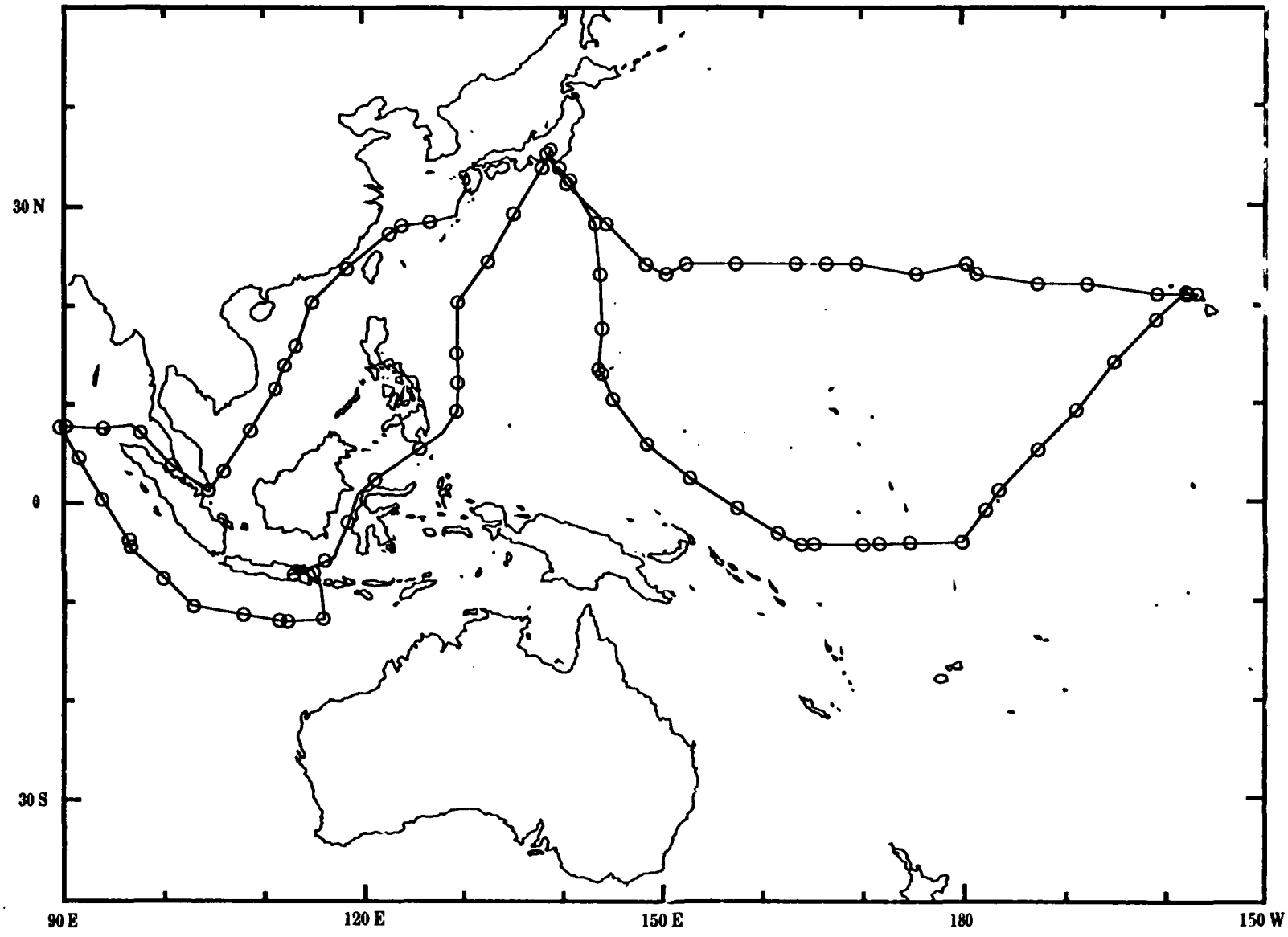

Figure 3-3. Locations for Omega Shipboard Measurements, Navigation Research Vessel TSUSHIMA

successive relative maxima and minima exceeds 20 dB. It is found that modal competition from traversing equatorial modal conversion zones does not always produce fade patterns easily identifiable in flight data. Aircraft data are plotted as field strength in microvolts/meter versus distance in megameters. Local interference and static noise is a significant problem as much of the variation indicating modal competition is masked by this noise.

Analysis of phase data from flights is not practical. Reference oscillator phase offsets were sufficiently large that insufficient data points were available between cycles of drift to determine corrections.

The fixed-site phase data are selected as the primary source for determining modal effects. The original plan was for this data to augment aircraft data in order to confirm observations and determine temporal variation. As was learned in the South Pacific validation, the aircraft amplitude data alone do not provide a clear indication of modal effects. Using fixed-site data works well, although many local interference problems exist and frequent data gaps occur. Because of reference oscillator drift, strong local interference and many other reasons, extensive processing generally is required to obtain the needed information.

Fixed-site amplitude data are used to determine SNR. Most of these data are archived for future reference.

Shipboard data obtained on the Tsushima are used to the extent possible to confirm the existence of modal interference in the ocean areas where fixed-site data are not available. These data are generally of good quality. The data provided to us consist of daily segments coinciding with satellite fixes. These generally occur during daylight and early evening hours at the ship. Thus we have almost no data for full nighttime periods on propagation paths.

As we show next, the experience gained in the South Pacific validation makes it possible for us to extract much more information from all types of data.

3.3 SIGNAL SELF-INTERFERENCE ANALYSIS

This subsection describes the analysis conducted to assess the occurrence of self-interference on the navigation signals. The overview presents a rationale for our order of presentation. This is followed by a general description of the analysis models developed to guide analysis. A detailed description of the model development is contained in Appendices A and C. The analysis is then summarized, again with amplifying details provided in Appendices B and D. This subsection sets the stage for evaluation and comparison of Omega coverage prediction presented in Section 4 INTERPRETATION OF VALIDATION ANALYSIS.

3.3.1 VALIDATION ANALYSIS OVERVIEW

The presentation is given as follows: (1) a discussion of the analysis guidance derived from results of signal prediction calculations, coverage diagrams, previous experience and a preliminary overview of the data, and (2) presentation and interpretation of the data sequentially by location. The primary interest is navigation, which depends upon signal availability, obtainable phase accuracy, and established confidence in predictions. Navigation is position oriented; thus we have chosen to focus on position and position accuracy as the analysis key. Our analysis presentation identifies and selects subregions and/or boundaries of special interest or concern, and then assesses the total signal resources available for navigation as related to the subregions and boundaries. The analysis is most effective when the data from all frequencies are compared for evidence of self-interference. Likewise, we feel that the total information content in the Omega navigation signals requires emphasis as a resource for navigation; thus the analysis of all frequencies is integrated.

A factor in conducting this and other validations is that resource constraints, time, data, and cost all impose important limitations on establishing definitive conclusions. As described below, a less than ideal match often existed between the predictions of important regions and boundaries and the available data for assessment.

3.3.2 ANALYTICAL GUIDANCE

Several investigations have been made of Omega Signal Coverage that include consideration of signal self-interference (GUPTA 1980(a), Ref. 21; SWANSON 1983,

Ref. 1; NALBANDIAN 1986, Ref. 22; GUPTA 1988, Ref. 23; and HILDEBRAND 1989 Ref. 15). Each of these investigations offered significant insights for our analysis. Predictions made by Gupta and Swanson are compared with results of this analysis in Section 4 INTERPRETATION OF VALIDATION ANALYSIS. Nalbandian and Tench produced a PC computer-based software program that displays signal coverage, the day/night terminator, and great circle propagation paths on maps. This software helped gain insight into the various geophysical factors contributing to predicted and observed signal reception. NOSC provided mode-sum calculations for selected station propagation radials that correspond with selected flight paths. These calculations provide the most detailed samples of mode structure versus distance. The continuing work of TASC in support of ONSCEN has produced the most useful overall information. Their series of calculations is particularly useful because the strength of each contributing mode is plotted along with the mode sum. Our work in the South Pacific validation establishes the validity and value of this analysis process and provides an important learning phase. This learning phase is ongoing as new insights are continually being derived.

No attempt was made to evaluate the merits of the various prediction models. Actually we have found all the models used to be beneficial. Please note that all of these models are theoretical and thus cannot be expected to predict in detail the observed real world. Nevertheless, the models can provide a great deal of insight regarding what can be expected and how to interpret what is observed. Our primary goal in using predictions/calculations is to obtain guidance for the analysis interpretation. Following the analysis presentation, a comparison is made of our analysis products and various predictions.

Phase deviation is defined as any condition where the navigation signal is not dominated by the mode for which the system was designed, i.e., mode 1 and short-path propagation (see Section 2.1.1 GUIDING PRINCIPLES for discussions on propagation theory and self-interference/modal factors).

Phase deviation effects are placed into five categories for this analysis:

> **Near Modal**: Mode competition originating close to a transmitter when higher-ordered modes are strongly excited; this can extend to large distances when the attenuation rates of competing modes are only slightly

different. At nighttime, higher-ordered modes are often initially stronger than the first-ordered mode.

Mode Conversion: Mode competition resulting from propagation factors other than near modal, usually as a result of mode conversion occurring in propagation within the equatorial zone or across very low conductivity terrain.

Shadow Zone: Applied to the zone of uncertain phase quality following propagation through a mode conversion zone.

Mode Switching: A higher-ordered mode achieving dominance at some distance from a transmitter; this results when an initially weaker higher-ordered mode has a lower attenuation rate than the first mode.

Long-path: Phase unpredictability caused by the long-path signal's domination or interference with the short-path signal.

The phase deviation analysis consists of preparing charts of zones for each station where signal quality is suspect due to various modal conditions cited above. The charts and analysis guidelines were then compared with the data collected on aircraft flights, at fixed sites and on the Japanese research ship Tsushima. The long-path interference assessment was done separately, because this effect predominates when the short-path is in daylight. The other effects occur when the short-path is mostly in darkness. Analysis guidelines rather than formalized charts were prepared.

Our most detailed guidance for determining the possibility of one of these phase deviation conditions is derived from a series of calculations for Omega signal field strength versus distance for 10.2 and 13.6 kHz, produced by TASC for ONSCEN (GUPTA 1988, Ref. 23). A sample of a calculation is shown in Appendix A, Figure A-1. This series of calculations is the most complete set available. These calculations are for static conditions in time, either all day or all night on the propagation path. The modal effects occur only at night. No predictions are made when daylight exists on part of the path. When we compare these plots with previous calculations, significant differences are found. As with the South Pacific validation, rather than use existing geographic displays, we consider it prudent to convert the information in this series from radials to geographic plots

showing zones where phase deviation can occur for each station. The creation of the geographic plots is described in Appendix A GENERATION OF GEOGRAPHIC PLOTS SHOWING MODAL COMPETITION.

The first task is to examine the sets of calculations for each station in order to identify the possibility of one or more of the three modal conditions above. The three most important model features useful for analysis guidance are (1) the structure (signal fluctuation with distance) in the mode sum, (2) what modes contribute to the mode sum, and (3) what mode is dominant in the validation region. This information is derived and compared for the two frequencies, 10.2 and 13.6 kHz, for which calculations are available. One important additional consideration is to assess how the propagation might differ for seasons other than the April-May time frame when the principal data were acquired. This assessment is based largely on intuition and determination of differences in solar illumination patterns.

The results of the geographic plot preparation are described for each of the stations in the following subsections.

3.3.3 DISCUSSION OF ANALYTICAL GUIDANCE

We must emphasize that this material is prepared for analysis guidance. The material is intended to serve as a benchmark to assist in interpreting the data. The charts we devised are not intended, at this stage, for navigation guidance.

The Omega navigation system is designed with redundant signal coverage. Conservatism suggests a policy of station deselection if the phase quality is in question. Thus, our analytical approach is first to determine, by geographic areas, which signals are candidates for deselection at some time during the diurnal day because of predicted unusable phase. Then, using available "good" phase signals, we determine the expected navigation capability by taking into account SNR and geometry factors. We emphasize those subregions where the largest number of signals are flagged for possible unusable phase. At this stage we make no allowance for possible time differences in deselection times. If many signals are in question, it is much more important to determine the correctness of the prediction. On the other hand, if good signal redundancy exists, deselecting a signal is of little consequence.

Composite charts showing zones where modal effects occur for 10.2 and 13.6 kHz are made from the charts for each station which are described in Appendix A. These composite charts are shown in Figures 3-4 and 3-5 for 10.2 and 13.6 kHz respectively. These composite charts show the locations of possible unusable phase that may occur at some time during the diurnal day. The shading of the zones of different coverage shows the number of station signals that are in question. The shaded legend shown to the right of Figures 3-4 and 3-5 covers five levels. The predicted always good signals are called out in each zone. For 10.2 kHz (Figure 3-4), a small zone centered near 10°N, 110°E has five signals of possible unusable phase. The always good phase signals are Norway, Liberia and La Reunion. As will be noted later, the Norway signal may have inadequate SNR at critical times. Adjacent to this zone are four zones showing four rejects and four good stations. The area within the boundary surrounding these five zones is of the greatest interest. Where modal effects occur, the time sequence of occurrence will be somewhat different for each station. Considerations of differences in occurrence time are deferred until later as these calculations provide no guidance on this matter.

For 13.6 kHz (Figure 3-5), a smaller zone of six questionable signals is predicted, centered near 10°N, 105°E. The good signals are Norway and Liberia. There are four adjacent zones containing five questionable signals. As shown in Figure 3-5, the 13.6 kHz signal also has two additional zones where only three signals are predicted to provide good coverage. These zones are all covered by four or more signals at 10.2 kHz. Assuming that these zone locations are valid, the concern would be during times of good station shutdown and then primarily for lane resolution. Again we note that inadequate SNR, considered later, may reduce the number of useful stations.

A composite chart, shown in Figure 3-6, combines the zones containing four or more signals of possible unusable phase for 10.2 and 13.6 kHz. This figure is presented to flag these areas that need particular attention in the analysis. Unfortunately, the zones of most concern lie primarily within segments not well covered by aircraft or fixed-site validation measurements. Some shipboard data were collected on one transit through this area. The lack of data for the areas shown in Figure 3-6 contributes significantly to the uncertainty of analysis interpretation.

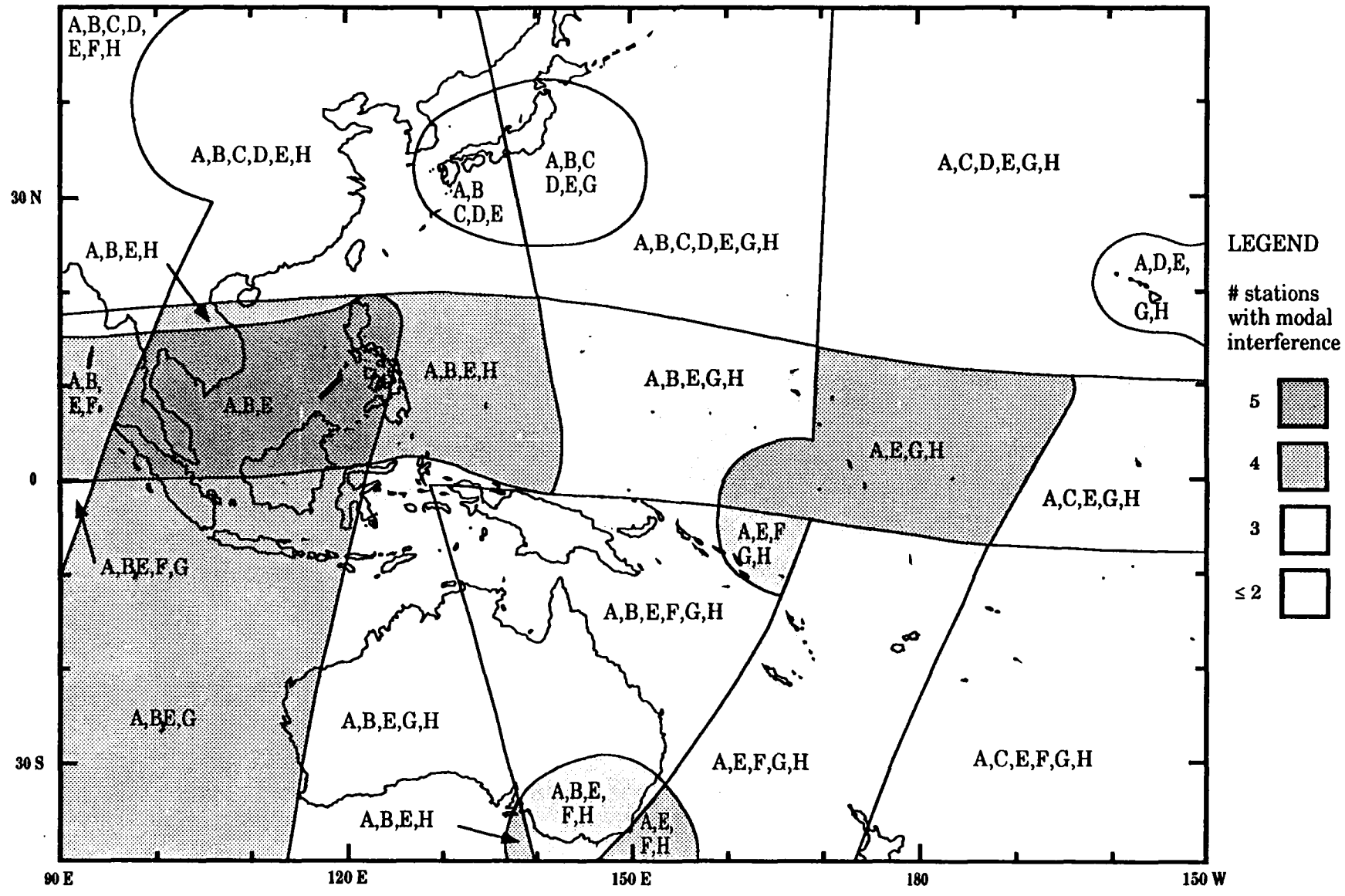

Figure 3-4. Composite Map of Modal Zones at 10.2 kHz

LEGEND NOTE: If a region is marked "A,E,G,H" it means the predictions are that stations A, E, G, and H NEVER have modal interference in that region. The other stations MAY have modal interference - but not necessarily at concurrent times.

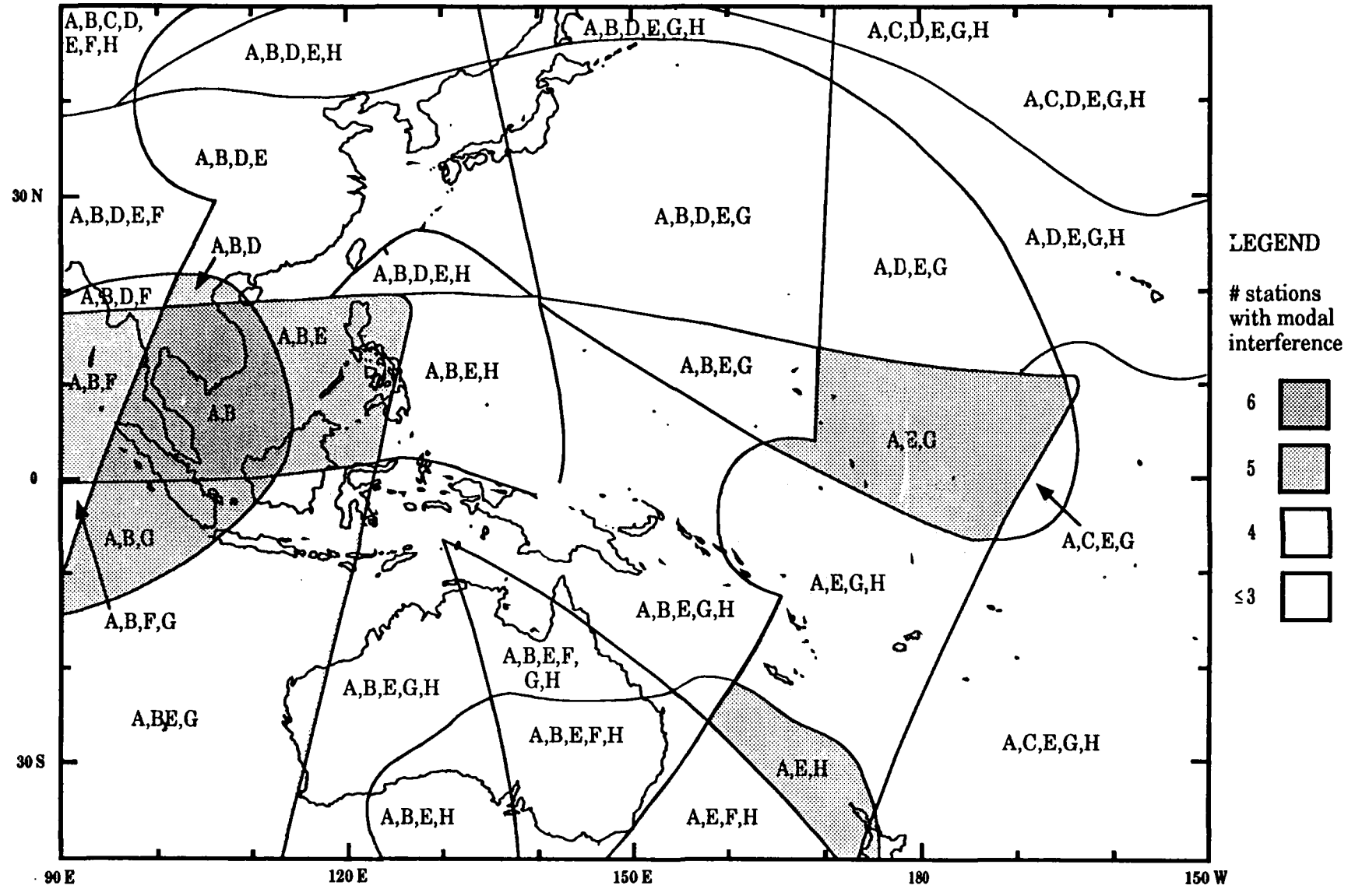

Figure 3-5. Composite Map of Modal Zones at 13.6 kHz

LEGEND NOTE: If a region is marked "A,E,G,H" it means the predictions are that stations A, E, G, and H NEVER have modal interference in that region. The other stations MAY have modal interference - but not necessarily at concurrent times.

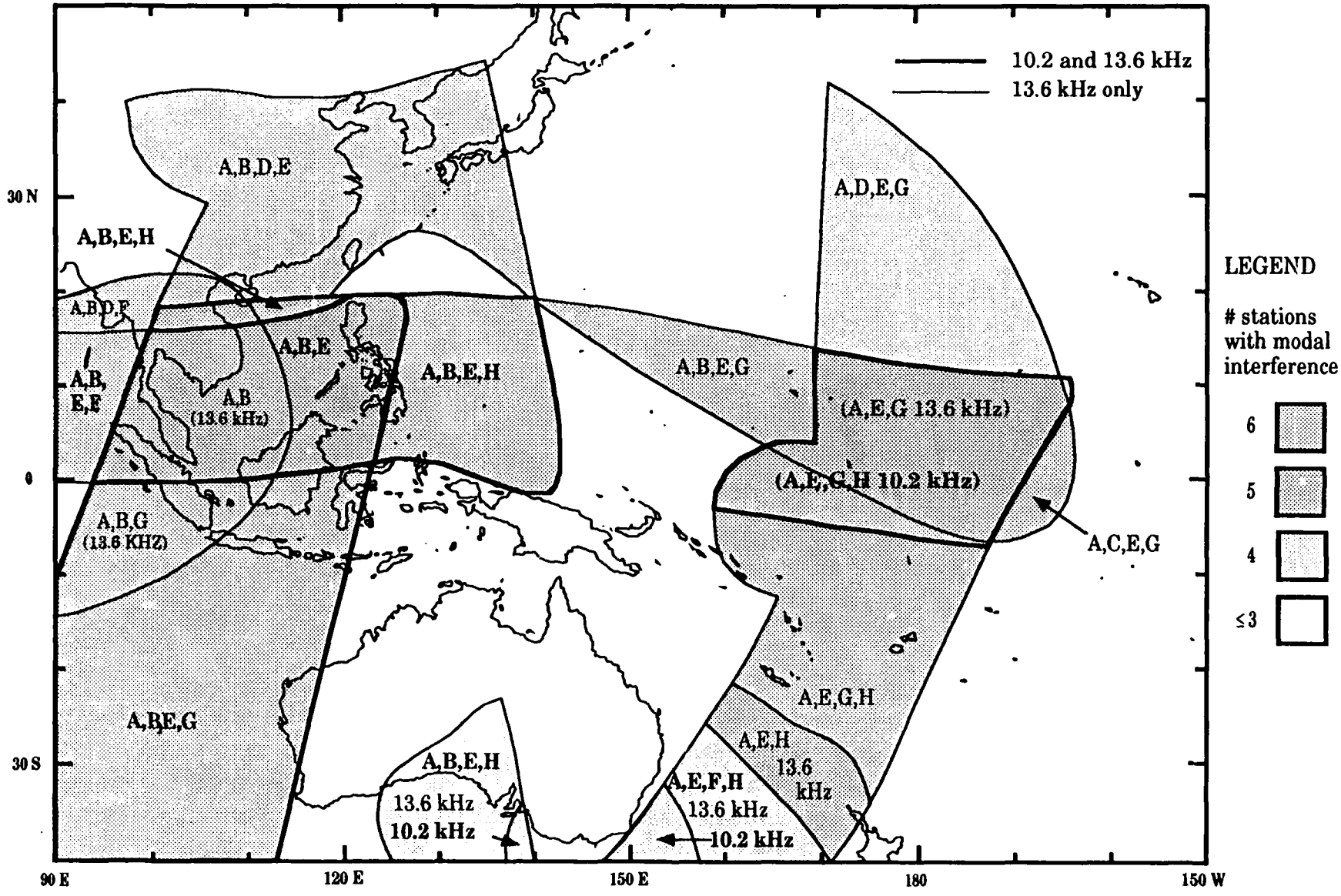

Figure 3-6. Composite Map of Modal Zones at 10.2 and 13.6 kHz

LEGEND NOTE: If a region is marked "A,E,G,H" it means the predictions are that stations A, E, G, and H NEVER have modal interference in that region. The other stations MAY have modal interference - but not necessarily at concurrent times.

The propagation prediction calculations prepared in this manner are used as guidance for data analysis assessment and as a model for extending measurements to the total Western Pacific validation region. We reemphasize that these charts are for nighttime propagation on each signal path and thus are time static; they do not take into account the diurnal variability of the zones of unusable phase. They are also seasonally static; variations in solar illumination at the poles are not integrated into the analysis. While these charts are considered a good model for validation data assessment, further interpretation is needed to derive navigation guidance. Navigation interpretation is considered later in the analysis.

3.3.4 DATA INTERPRETATION

DATA INTERPRETATION OVERVIEW. The data interpretation is a complex process involving extensive preparation of the data and the comparison of many different data segments to achieve the interpretation presented here. The results of this interpretation are summarized in this subsection. A more detailed description of the interpretation process and findings is presented in Appendix B.

The procedure we use in Appendix B for data interpretation is to work across the validation region from east to west. We break up the region into areas largely based on natural boundaries defined by signal conditions. The process used for each area is (1) to determine for each station the dominant mode and signal amplitude structure along flight paths, ship tracks and fixed sites predicted by the calculations, (2) to compare flight amplitude data with calculations, and (3) where available, to examine fixed-site or ship phase data for possible modal effects.

The fixed-site phase data are used for two purposes. First, a check is made to determine, as much as possible, the propagation conditions at the time of flights. Second, a check is made to determine how the data at flight time are related to the total data set available at that site.

The fixed-site data are processed in several different ways depending upon the stability of the frequency reference at the measurement site. None of the stations had atomic frequency references. At sites where the reference frequency was stable, the cumulative phase difference is measured between successive midpath

noon times on the best quality signal. This phase difference is then incrementally subtracted from all measurements. The ideal result has a nearly stable diurnal phase curve for each measured signal. In most cases, the reference oscillator frequency offset is sufficiently constant over a 24-hour period so that the corrected phase plots can easily be evaluated for signal self-interference. When the reference oscillator is not sufficiently stable, phase-difference data between two received stations are examined. In using phase-difference data, an attempt is made to use a strong signal containing only a first mode as a reference for evaluating those signals suspected of having modal interference. We use Japan if it is not modal; otherwise we use the La Reunion signal.

We note that it is easier to recognize the existence of modal competition in the presence of normal propagation variability by comparing the diurnal-phase data between multiple frequencies.

MODAL COMPETITION DATA ANALYSIS SUMMARY. As noted in the overview for this subsection (Subsection 3.3.1 VALIDATION ANALYSIS OVERVIEW), the primary focus for analysis is based on position. Position is what the navigator is interested in. The positions of recorded data are along aircraft flights, along ship transits, and at fixed recording sights. We find that the analysis is more definitive when it is possible to examine an area within the region that has a natural focus. An example of such a focus is the geographic area for predicted onset of equatorial modal effects for specific stations. We examine such a selected area through the integration of as many data resources as practical. For instance, west of Hawaii we use the combined data from aircraft flights, ship transits and the Hawaii fixed site to assess the equatorial modal boundaries of Hawaii, North Dakota and Argentina. The assessment of each station contributes to the interpretation of propagation for other stations. In this manner, the analysis taken collectively produces a more coherent picture.

The ship data are more representative of fixed sites (little position change with time) and tend to be more isolated from the other measurement places. The shipboard data are useful for assessing modal effects as well as for conducting a qualitative check on position-fixing accuracy.

We group the analysis into four geographic areas: (1) Hawaii to Guam, (2) Guam to, but not including, Cubi Point in the Philippines, (3) Japan vicinity, and (4)

west of Cubi Point to Singapore. These areas form natural divisions because of predicted phenomena and available data. The first area, west of Hawaii, includes the onset of equatorial zone mode conversion for the Hawaii signals and the predicted long extent of the 13.6 kHz near modal zone for the Japan signal. Equatorial mode conversion zones for North Dakota and Argentina, which start east of Hawaii, also extend clear across this area as well as most of the validation region. The second area, Guam to the Philippines, includes the predicted eastern edge of the Australia equatorial mode conversion zone. It also includes the conversion zones from the first area. The third area, in the vicinity of Japan, is selected because of the special interest in checking the Japan transmitter and because of the concentration of traffic around Japan. The fourth area, the Philippines to the western edge of the region, includes the eastern edge of the Japan signal equatorial mode conversion zone as well as the continuation of conversion zones for Hawaii, North Dakota, Argentina, and Australia. This area is predicted to be very difficult for navigation because of modal effects and high atmospheric noise levels.

Generally we identify each of the four areas with an easily recognized landmark. However, we make the bounds for any given area vague. The reader is referred to Appendix A for maps showing predictions of phase quality for each of the signals. Each summary of our analysis findings is grouped into two parts; the first highlighting the predicted important characteristics and the second citing the conclusions of the analysis. The following discussion describes the four areas.

West of Hawaii to Guam (Hawaii, Flights 1 and 2, and Southeast Ship Transits): This area is characterized by having three stations predicted always good (Norway, La Reunion and Australia) and five stations predicted to have nighttime modal problems at some locations within the area. Most modal problems occur because of equatorial zone mode conversion. Specific predicted phase problems are noted in the following commentary for each station. The data consists of measurements on (1) Oahu Hawaii, (2) flights from Hawaii to Kwajelein and from Kwajelein to Guam, and (3) the Tsushima ship transit from Japan to Hawaii and then a loop south to the equator and back to Japan. The data for the flight from Hawaii to Guam were from along the extended 254° radial of Hawaii through Kwajelein (see Figure 3-2) and then a dogleg to Guam.

The data confirm the existence and approximate boundaries of the predicted nighttime equatorial modal conversion zones for Hawaii, North Dakota and

Argentina. The Liberia signal east of Kwajelein is long-path most of the time. The La Reunion and Australia signals are good at all times. Norway has good phase but was not be received at all times in Hawaii. The ship reception of Norway was evidently good, this being in mostly daytime when noise is highest. The Japan 10.2 kHz signal is predicted good at all times, while the 13.6 kHz phase quality may be questionable between Japan and Kwajelein.

The data suggest that the equatorial modal zone boundaries may fluctuate several degrees latitude with variations in propagation conditions. However, the data set is too small to provide more than a suggestion.

South Central Area, Guam to 130° East Longitude (Flights [3 & 4], 12, 13, [15, 16 & 17], Yap, and Darwin; excluding the vicinity of Japan): This area is characterized by having four stations predicted always good (Norway, Liberia, La Reunion and Japan), and four stations predicted to have nighttime modal problems at some locations within the area. Modal problems occur because of equatorial zone mode conversion. The eastern edge of the predicted equatorial mode conversion zone for Australia signals is within this area (see Appendix A, Figure A-18). The data consist of measurements on Yap, flights on two radials from Australia (Flights [3 & 4] and [12 & 13]) and on two radials from Japan (Flights [15, 16 & 17] and [12 & 13]).

The equatorial modal effects noted to the east for the Hawaii, North Dakota, and Argentina signals were predicted and observed for this area. Our prediction is for the equatorial mode conversion zone for the Australia signals to begin west of Guam and extend westward to the edge of the validation region. Modal effects are detected on flight data for locations north of Yap. Modal effects are only weakly evident at Yap. Thus the data only partially support the Australia modal prediction. The Norway signal, while weak, has good phase quality. Japan signals are good at all times and locations. The aircraft data only weakly support placement of modal boundaries.

We conclude that Norway, Liberia, La Reunion and Japan provide good signals throughout the area. We note that the Japan signal radial to Darwin probably delineates the eastern edge of its equatorial mode conversion zone. The Australia signals are good below their mode conversion zone. The North Dakota signals are good above their mode conversion zone.

North Central Area; Japan and Vicinity Flights (Overflight radials of Japan transmitter and Japan fixed site): This area is selected to give focus to the documentation of the near modal zone of the Japan Omega station and to assess navigation capability in the high traffic area of Japan. Because the Japan signal has no diurnal phase change, the reference oscillator drift can be very accurately measured and removed from all other station records.

The combined flight and monitor site data generally support the predictions for modal effects. Good signals in the vicinity of Japan are Norway, Liberia, North Dakota and La Reunion. We note that Norway SNR can be marginal when thunderstorm activity is high in a broad area around Japan. The North Dakota signal is weak. Thus, closer to noise sources, such as at Taiwan and Hong Kong, this signal may not be trackable. The Hawaii signal has good phase quality at Japan most of the time, but we detected significant modal effects on about ten percent of the days. We have no data on the Argentina signal that are predicted unusable in this area. The Australia signal shows strong evidence of being in the shadow zone of the equatorial zone mode conversion. Modal interference is strong at night on 10.2 kHz and 11.3 kHz. The 13.6 kHz signal produced a characteristic mode 1 diurnal phase curve on almost all days.

We conclude that in this area navigation is adequate but not particularly redundant.

Western Area; Philippines to the Western Regional Boundary (Flights 6, 7, 8, 9, 10, and 14; the fixed sites, Cubi Point and Singapore; and the Tsushima SW transit): This area is predicted to be the most difficult for navigation in the Western Pacific validation region. Here the Japan equatorial mode conversion zone is added to the other zones. As noted in Figure 3-4 the nighttime good signals at 10.2 kHz are limited to Norway, Liberia and La Reunion for most of the area. For 13.6 kHz (Figure 3-5), La Reunion may be modal over part of the area, leaving Norway and Liberia the only signals always good at night. We note later in SNR analysis that Norway coverage can be unreliable at both 10.2 kHz and 13.6 kHz, at least in the eastern part of this area.

With respect to the database and its quality, the sample size west of Cubi is very sparse. The Cubi data, while requiring an extensive amount of processing work, generally provided good results. For Singapore, the only other fixed site in this

area, data interruptions occurred essentially daily. In most cases, we cannot remove reference oscillator drift effects. For the aircraft data, noise problems are more severe. We believe the aircraft noise problems are due to both generally higher atmospheric noise, and in several cases, weaker signals. For the Tsushima ship, the phase records are highly inconsistent . In most cases, we are unable to establish systematic reference oscillator drift trends and thus are not able to decipher data of individual station phase. For the ship data, we resort to interpretation of SNR and phase-difference data. In this section we show some ship SNR data to illustrate findings. However, the findings for each case are based upon assessment of all available data.

The combined flight, monitor site, and shipboard data generally support the predictions for modal effects. Good signals in this area are Liberia and La Reunion. We note that Norway SNR can be insufficient when thunderstorm activity is high within this area. The North Dakota signal is very weak and modal. At times this signal may not be trackable. The Hawaii signal has bad phase quality at night all of the time below 20°N latitude. The Argentina signal is weak and shows some modal effects where measured in this area. The Australia signal shows strong modal effects above the equator. The Japan signal shows strong modal effects below about 20°N latitude. The data show that signal coverage (addressed in Subsection 3.5.5 COMPARISON OF PREDICTIONS WITH FINDINGS), may be inadequate on many stations during nighttime propagation conditions.

3.3.5 SUMMARY OF SIGNAL SELF-INTERFERENCE ANALYSIS

The signal self-interference analysis consist of preparing charts of zones where signal quality is suspect due to various types of modal self-interference. The interference conditions considered are (1) near-zone modal, (2) mode conversion zones, trans-equatorial or trans-polar, and (3) zones of higher-ordered mode dominance following mode conversion, i.e. the shadow zone. These charts are then compared with measurements from aircraft flights, fixed sites and ship transits. The zones predicted modal shown in the figures of Appendix A and the composite charts of modal zones (Figures 3-4 and 3-5) are found to be largely correct. Please note that these composite charts do not include time intervals for the conditions cited.

It is worth restating that the modal problem is largely a nighttime propagation phenomenon. When a path is in daylight, these modal problems go away.

However, these problems may exist for each station for a large part of the day/night transition times on the propagation path.

Several adjustments to the predictions of modal problem areas are suggested by the data, primarily that the eastern boundary locations of the equatorial mode conversion zones are all further east than our model predicts. We note that some calculations provided by NOSC personnel show evidence of mode structure to the east of our predicted boundaries. We do not have enough NOSC calculations to assess the boundary placement. For the boundaries nearest the transmitters we observe considerable variability between measurements. Again we have insufficient data to determine the statistics of this variability or the envelopes that fully contain the boundaries. We conclude that in order to be conservative, the modal zone boundaries should be located at least 3° in geographic latitude further from the center than our prediction. We believe that placing the boundary along a constant magnetic latitude is logical.

We continue to be frustrated in our assessment of the predicted large extent of the 13.6 kHz near zone to the southeast for midlatitude stations located north of the equator and northeast for stations located south of the equator. We were unable to test the predictions for Hawaii and Japan in the South Pacific validation. In this validation we are also frustrated in our attempts to assess the Japan and La Reunion predictions. The sparse clues we are able to glean suggest that these lobes can be reduced somewhat from the predicted. Again, data are insufficient to reliably determine what adjustments can be safely made.

Clearly use of signal deselection is important to achieving navigation quality over much of the Western Pacific region. At most locations sufficient signal redundancy exists such that conservatism in signal selection is good practice. For an approximately trapezoidal zone from (15°N, 125°E) to (0°N, 94°E), caution is needed for signal deselection because of the number of stations incurring modal effects. A key factor to is knowing when specific signals are reliable. We will consider the time spans of reliable signal coverage for the total set of eight signals in Subsection 3.6 SIGNAL TIME AVAILABILITY.

3.4 LONG-PATH INTERFERENCE ASSESSMENT

3.4.1 OVERVIEW

The objective in assessing long-path interference effects is to determine, within the validation region, whether the coverage predictions adequately determine when and where stations need to be deselected. The determination needed is the placement of the boundary for the long-path zone. This boundary shows the long-path's maximum extent into the short-path region.

The occurrence of long-path signal interference has a quite different pattern in terms of location and time than the above-described short-path signal self-interference. Long-path interference can extend in either direction from the signal antipode, depending upon which propagation direction along the great circle paths has the lowest signal loss. Typically the long path/short-path boundary will move along each great circle path in a daily cycle from an initial location to its maximum extent on one side of the antipode, back through the antipode to the its maximum extent on the other side of the antipode, and then return to its initial location. The maximum extent along any given radial of the long-path signal into the short-path side occurs when any nighttime propagation conditions are completely on the long-path. The most extensive long-path interference is almost always to the east of the antipode of each station. However, terrain conductivity and solar illumination conditions have a strong influence on the location of the long-path/short-path boundary.

The assessment of long-path effects is challenging because identification of the effects must be inferred from the measurement data that are (1) a composite of many possible phenomena, (2) seldom acquired at optimum locations, and (3) from a few locations that are widely separated. For these reasons interpretation of the data depends heavily upon using a model to guide the interpretation. In this analysis we use only data from fixed sites to test for long-path effects.

3.4.2 ANALYTICAL GUIDANCE

Our assessment of long-path effects for the South Pacific validation required development of a guidance model. We were not able to acquire a model for predicting long-path effects that we considered adequate to provide the needed

guidance. Yet we found the data almost impossible to interpret without some guidance as to what to expect. Our requirement was and is to assess the prediction of boundaries that are far from the locations where data is available. We concluded that the most useful parameter is the time dynamics of boundary movement. The parametric model that provides the best description of long-path effects does not provide the needed time and spacial detail. Consequently, for the South Pacific validation we prepared a simple model by extending TASC Omega propagation calculations as described in Appendix C. This model is used in this analysis.

The technique (described more fully in Appendix C) consisted of a simple drafting procedure to extend the field strength predictions beyond the 19 Mm distance provided by TASC. The major challenge is to account for the fact that the long-path prediction has to include a mix of day and night propagation. We expect that modeling propagation across a terminator cannot be well represented without using full-wave computational techniques. Thus our method is at best a first order approximation consisting of connecting the appropriate extended segments of TASC's day and night propagation calculations. Nevertheless the resulting predictions proved useful in guiding our data interpretation.

Since the long-path (which has most of the night path) always includes at least as much daylight propagation as the extension beyond the antipode, the method for connecting the day and night portions must be carefully considered. When day is on the first part of the path, the higher-ordered modes are highly attenuated before the night portion begins. Thus, except for mode conversion (as occurs in the equatorial conversion zone), the nighttime fields are expected to have mostly mode 1 content. When night is on the first part of the path, the higher-ordered modes are highly attenuated after the day portion begins. Thus the daytime fields, extending into the long-path region, would be expected to have mostly mode 1 content. Based upon this reasoning we used only the mode 1 component of the TASC predicted signals to construct the boundary of long-path dominance. The method used is illustrated in Appendix C.

The data collection locations were seldom at the long-path boundary's maximum extent. We need to devise a means of estimating this maximum extent relative to the measurement locations. For sites within the long-path region part of the time, prediction of the time of boundary crossings provides a test of the model.

Two crossings occur each day, one as the boundary moves outward from the antipode and one as it moves towards the antipode. The prediction of these crossings requires estimating how the boundary moves in relation to the terminator. This movement is related to the maximum extent of the boundary, to the relative attenuation rates of each path, and to the rate of movement of the terminator along the path. For this analysis we simply used calculations of the day/night terminator positions on the earth's surface to estimate where to switch from day-to-night propagation, or vice versa. More refinements to this model are easy to devise and should be added for future analysis.

Comparison of measured crossing times relative to predicted ones provides guidance for adjusting the predictions. The adjusted predictions are then used to determine the maximum extent boundary of long-path effects. The findings of this comparison analysis is described in the next subsection.

3.4.3 DATA INTERPRETATION

A summary of findings regarding long-path effects is presented here; a more detailed description is in Appendix D. The model predicts that three of the eight Omega stations have long-path effects within the Western Pacific validation region. These stations are Liberia, North Dakota, and Argentina. For these stations long-path effects were confirmed on at least Liberia and Argentina. The phase records of both of these stations exhibited long-path effects at Brisbane. For Liberia, the boundary of primary interest for this analysis is to the west of the antipode. We conclude that the long-path zone boundary lies slightly inside our prediction. We estimate from the data analyzed that the boundary should be placed near or west of 140°E longitude at 30°S latitude. Data from sites placed at other locations in Australia should be examined to properly locate the Liberia long-path zone boundary.

For the North Dakota signals, we are not able to assess the long-path boundary. The reason is that either this channel was used for calibration or the signals were highly contaminated with equatorial zone modal effects.

For the Argentina signals, we detect long-path signals at Brisbane for about two months of the year, centered around early July. Argentina signals were not recorded at the sites closer to the antipode, so we do not know what the boundary

dynamics might be. We estimate that the Argentina long-path boundary does not extend much south of Brisbane.

As noted in Appendix D, we are not able to conduct a complete assessment of long-path boundaries. Yet the findings make a small contribution to our knowledge of long-path characteristics.

3.4.4 DISCUSSION OF LONG-PATH EFFECTS FINDINGS

The investigation of long-path effects was cursory. Thus we hesitate to make definitive claims. The dearth of data is a severe hindrance to establishing definitive conclusions. Our simple model predicts that long-path effects cover large areas and for long time intervals. While our analysis does not provide a good test, we are confident that the predictions give a realistic indication of the long-path problem and thus of the importance of validating locations of long-path zone boundaries. Again, since signal deselection is the likely method for mitigating long-path conditions, the placement of boundaries can easily be made larger than needed except where there is a shortage of reliable signals.

In conclusion we feel that this described analysis technique provides a good start for assessing/validating long-path effects. The guidance obtained allowed us to make some estimates of long-path zone boundaries; the data show that adjustments are needed for the Liberia and Argentina long-path boundaries. The model can easily be used and further calibrated with additional measurements. The evidence clearly shows that long-path effects are an important part of coverage prediction. We consider the data obtainable from any single validation region to be insufficient because of measurement site locations relative to zone boundaries and because of the wide separation between sites. However, it is expected that if an analysis includes many regions and the data are used to validate and refine a model, high confidence can be achieved in using a model to place long-path zone boundaries.

We know of no thorough analysis of long-path boundary dynamics. Since long-path is an important contributor to invalidating signals propagating to the west and since these signals are often in short supply, we recommend a detailed investigation of long-path boundary behavior.

3.5 SIGNAL-TO-NOISE RATIO ASSESSMENT

This subsection describes the signal-to-noise ratio analysis and presents the findings on how well the measurements support the predictions. SNR topics presented are SNR Data, Observed SNR Performance, SNR Predictions, Comparison, and Summary.

3.5.1 SNR DATA

The SNR data measured for the validation were received on Magnavox MX-1104 receivers at the fixed sites. Signal injection calibration techniques developed by NOSC were used to determine signal levels and noise. Received SNR from the Omega stations are assessed at five Western Pacific monitor sites: Japan, Cubi Point, Yap, Darwin, and Singapore. The data are provided in the form of computer-generated plots for two-week periods of the average and standard deviation of SNR for three frequencies: 13.6, 11.33, and 10.2 kHz. Figure 3-7 is an example of the SNR versus time curves. The data of this figure show constantly high values of SNR. The solid line depicts the average value of SNR for each time of measurement. The dotted lines show the spread about the average encompassed by one standard deviation of SNR. The data were collected between the months of January and August 1986. The data from different sites cover different time spans.

3.5.2 OBSERVED SNR PERFORMANCE

The SNR versus time curves were examined to identify the occasions when the SNR fell below two thresholds, –20 dB and –30 dB. When either the average SNR or the upper or lower standard deviation fell below the threshold, the time was recorded. Rather than mask the data with statistics, we choose to describe general trends and to cite worst case examples of SNR for stations where problems exist at a particular cite. The following paragraphs discuss the SNR results by monitor site.

Japan Site: We reported from data collected in the February/March time period for the South Pacific validation analysis, that all the SNR observations from five Omega transmitters (Hawaii, North Dakota, Argentina, Australia, and Japan) were greater than –20 dB at all three frequencies for all hours of the day. Also, for the La Reunion station, the lower standard deviation curve for the 10.2

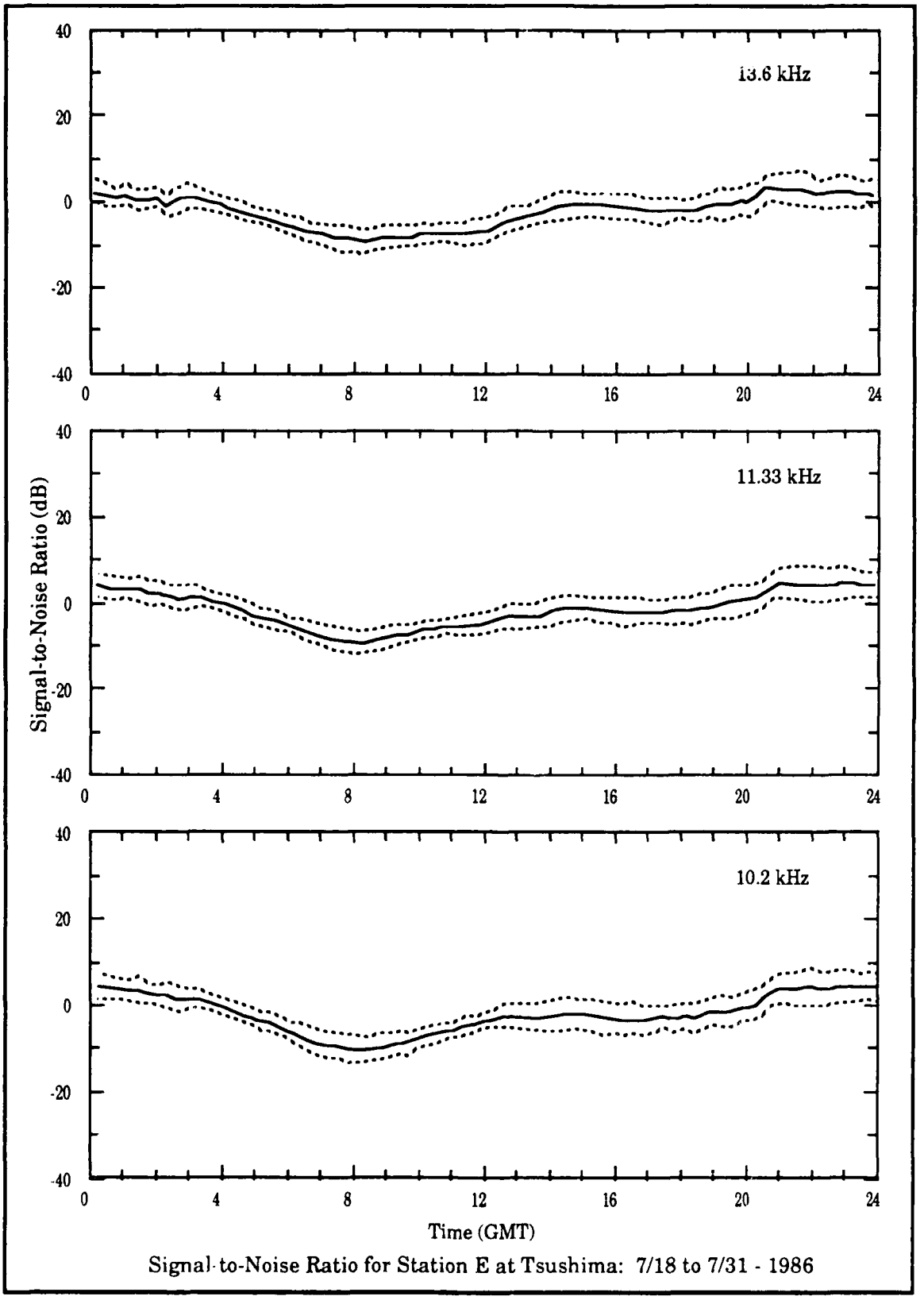

Figure 3-7. Example Showing SNR for La Reunion at Japan

kHz signal fell below the threshold for periods of two hours, between 0200 and 0400 GMT during January and between 1230 and 1430 GMT during April.

In this analysis, which covers the local summer months, we get different results. Here only the La Reunion and Japan station signals remain above the –20 dB threshold at all times. No measurements are available for Argentina. In Figures 3-8 through 3-12, we show the worst case conditions for each station where the lower standard deviation reaches less than –20 dB SNR. We note that all cases are for the last half of July and that the worst time typically is in the 0600–0800 GMT time span. The conditions we illustrate are generally less severe in other periods. Since in this season the predominant noise results from thunderstorms in the broad area around Japan and the time span is midafternoon, we expect the poor SNR to be highly correlated between the different station signals. As will be shown in the next subsection (Subsection 3.5.3 SNR PREDICTIONS), these finding are in good qualitative agreement with noise predictions. Clearly, on some days a low sensitivity navigation system would have only the Japan and La Reunion signals available.

Cubi Point Site: During the analysis period, the SNR observations are greater than –20 dB at all three frequencies on the La Reunion and Japan signals. Data are not provided for July. The Liberia signals are above the –20 dB threshold at all times, except for the later half of April when the 10.2 kHz frequency average level just touches the threshold at 0900 GMT. The lower standard deviation curve at 10.2 kHz is below this threshold from 0700 to 1100 GMT. The lower standard deviation curve at 10.2 kHz is also below this threshold for a similar time period during August.

The Australia signals are above this threshold, except for periods in April and August when the average and lower standard deviation curves dip below this threshold at certain times. We show these conditions in Figure 3-13. We note that the SNR minima are at sunset/sunrise times or during the night on the propagation path.

For Norway signals, the lowest SNR generally occurs between 0700 and 1300 GMT. As shown later, this time interval is the period of highest predicted noise. No July data are available. The seasonally worst periods are late April and early August. This implies that July would also be included in the worst periods. At

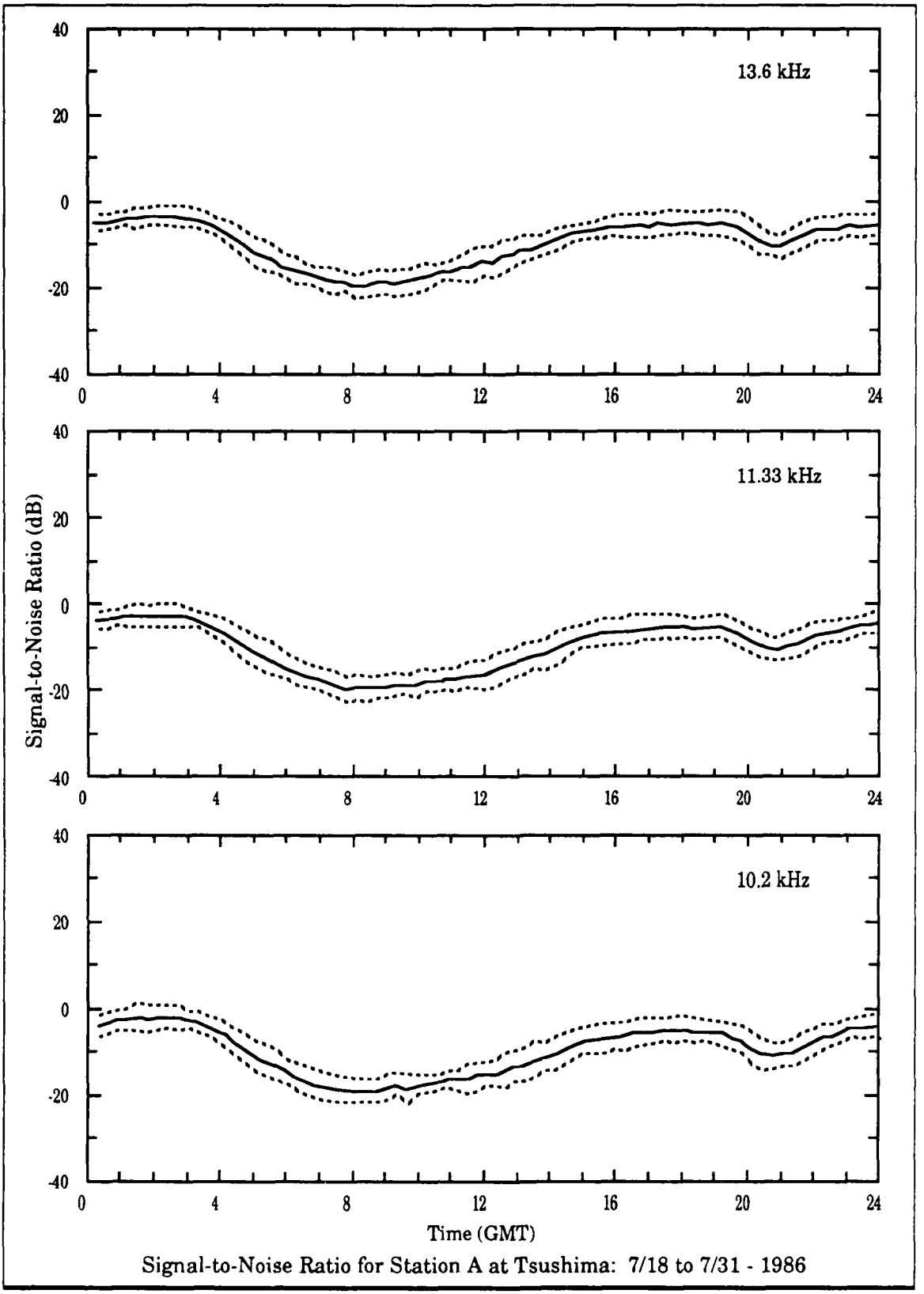

Figure 3-8. Worst Case SNR for Norway at Japan

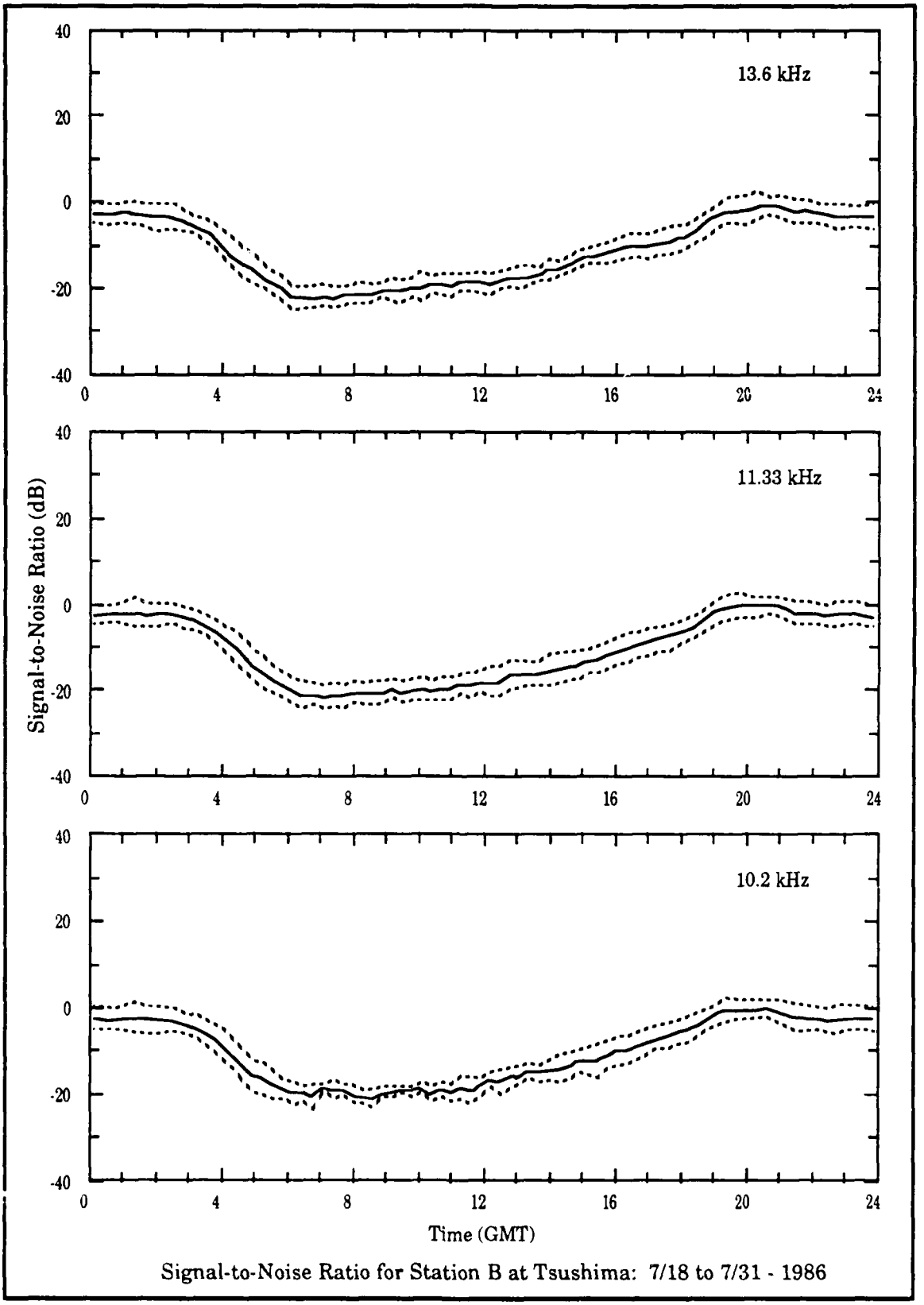

Figure 3-9. Worst Case SNR for Liberia at Japan

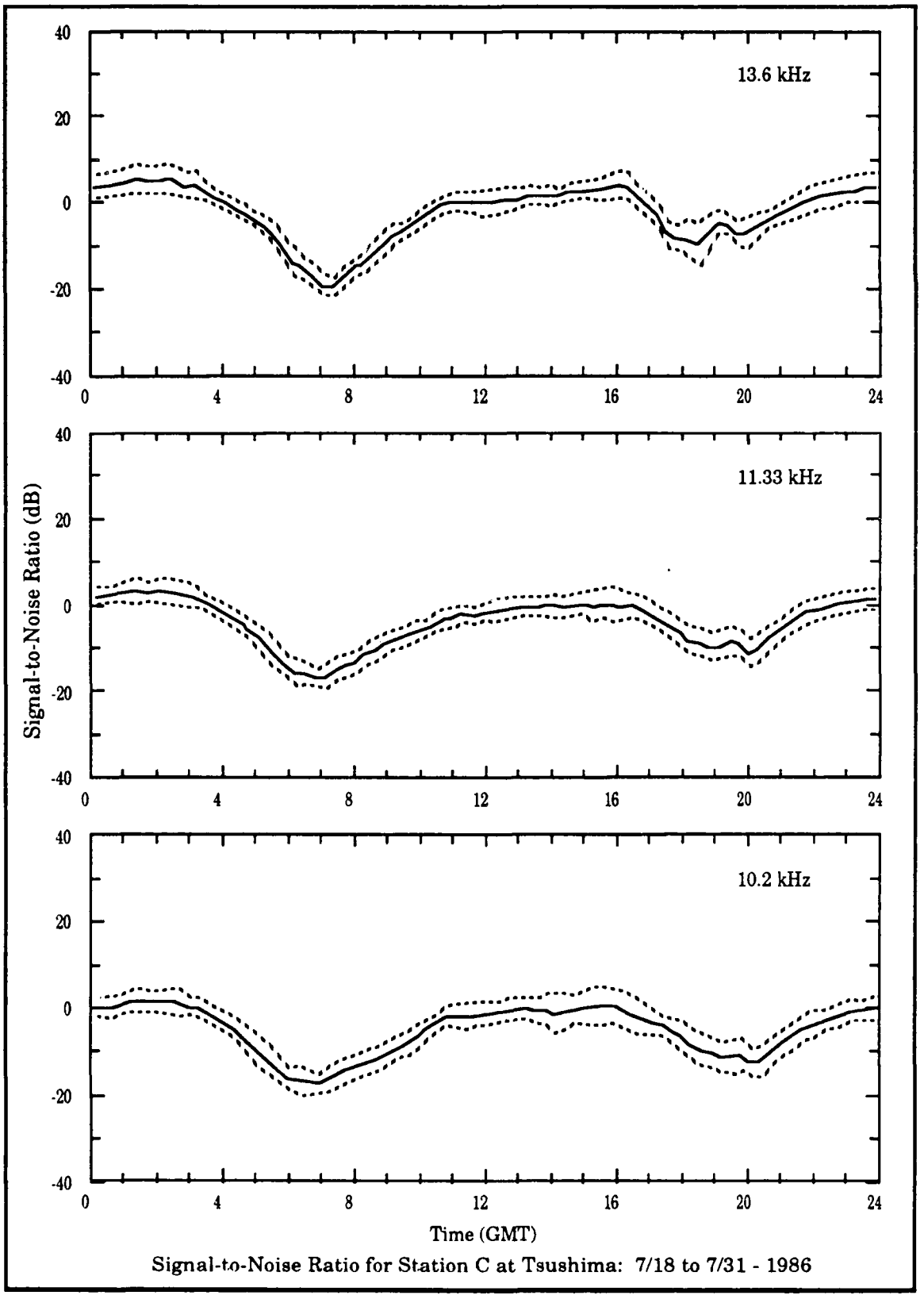

Figure 3-10. Worst Case SNR for Hawaii at Japan

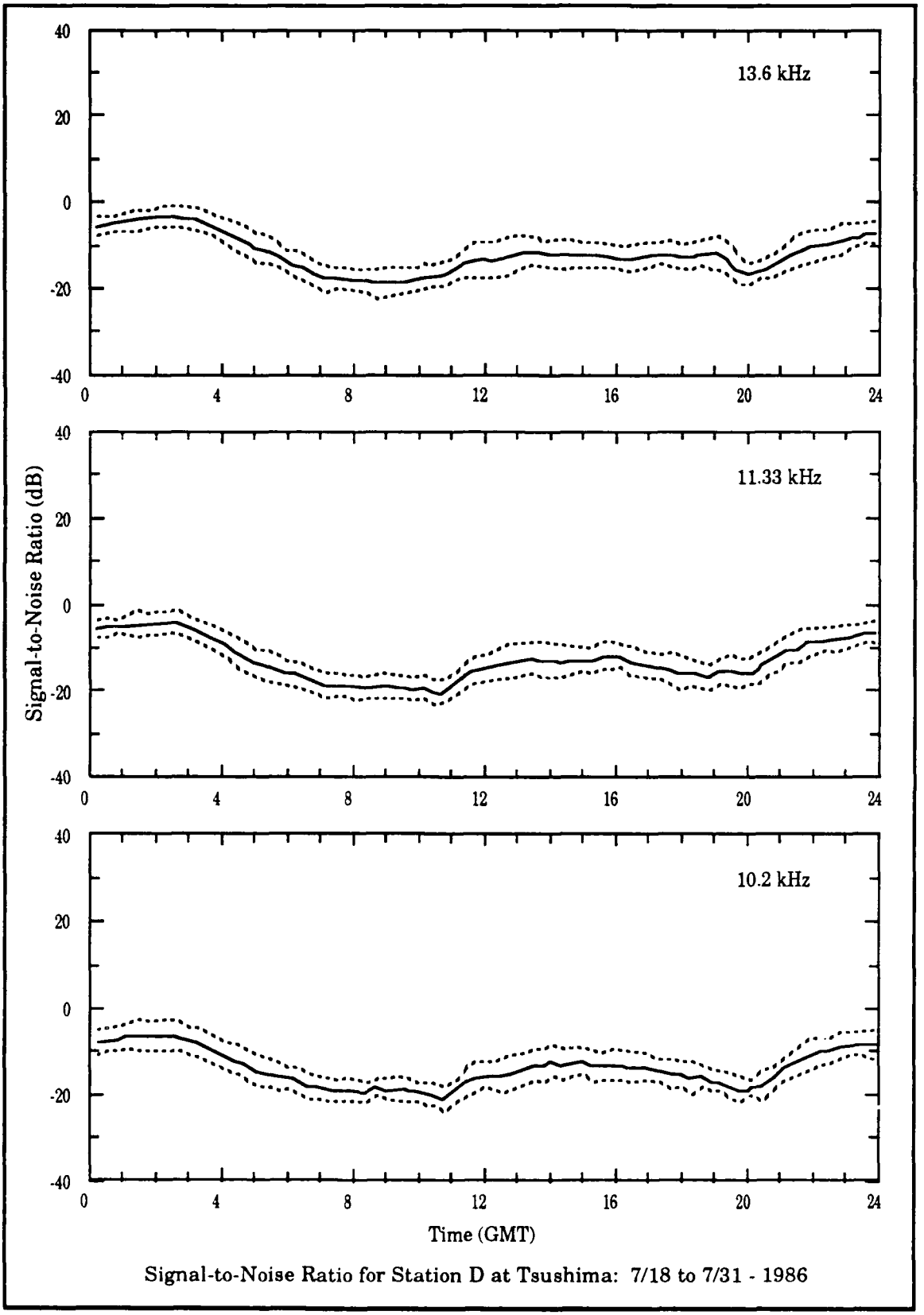

Figure 3-11. Worst Case SNR for North Dakota at Japan

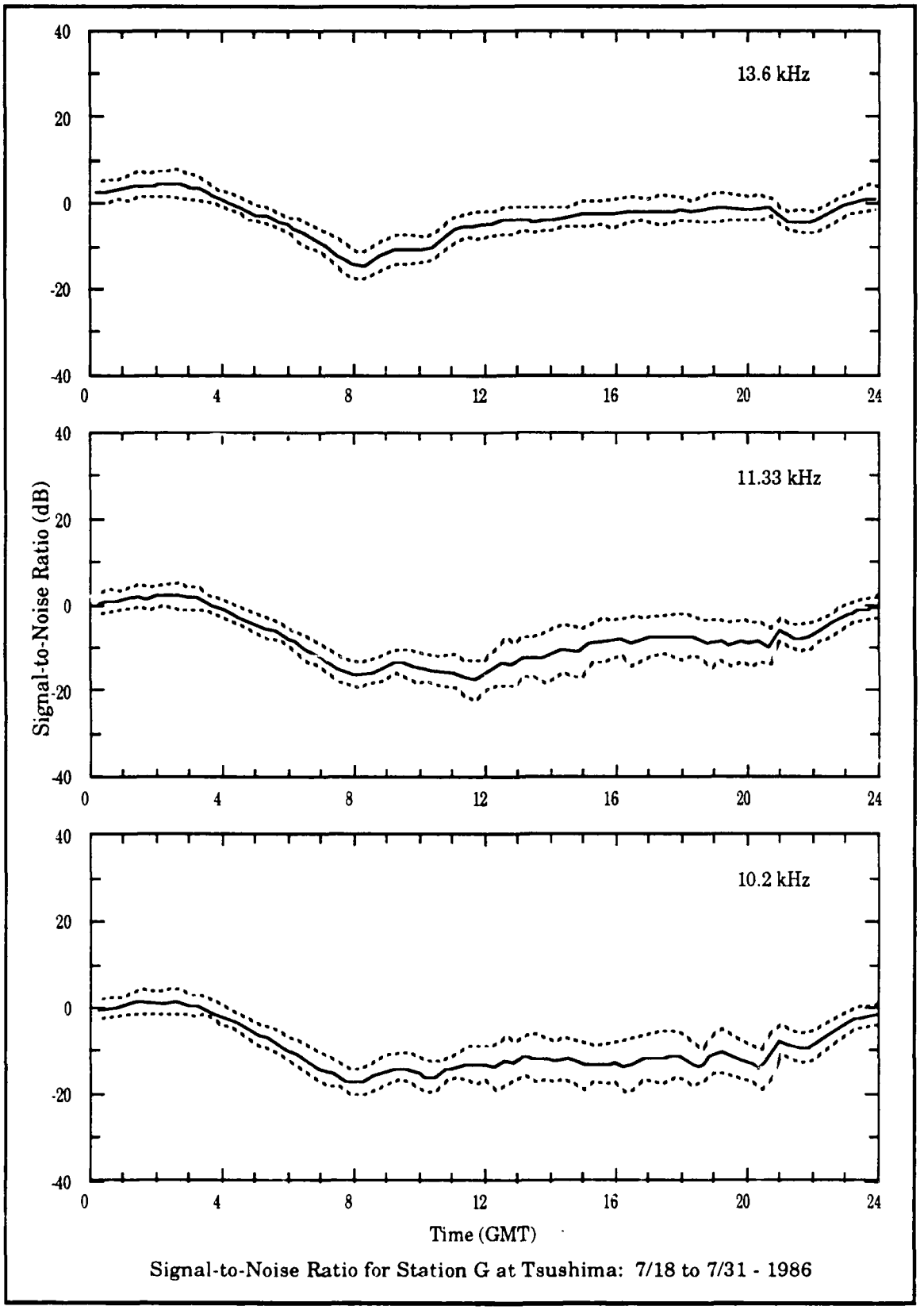

Figure 3-12. Worst Case SNR for Australia at Japan

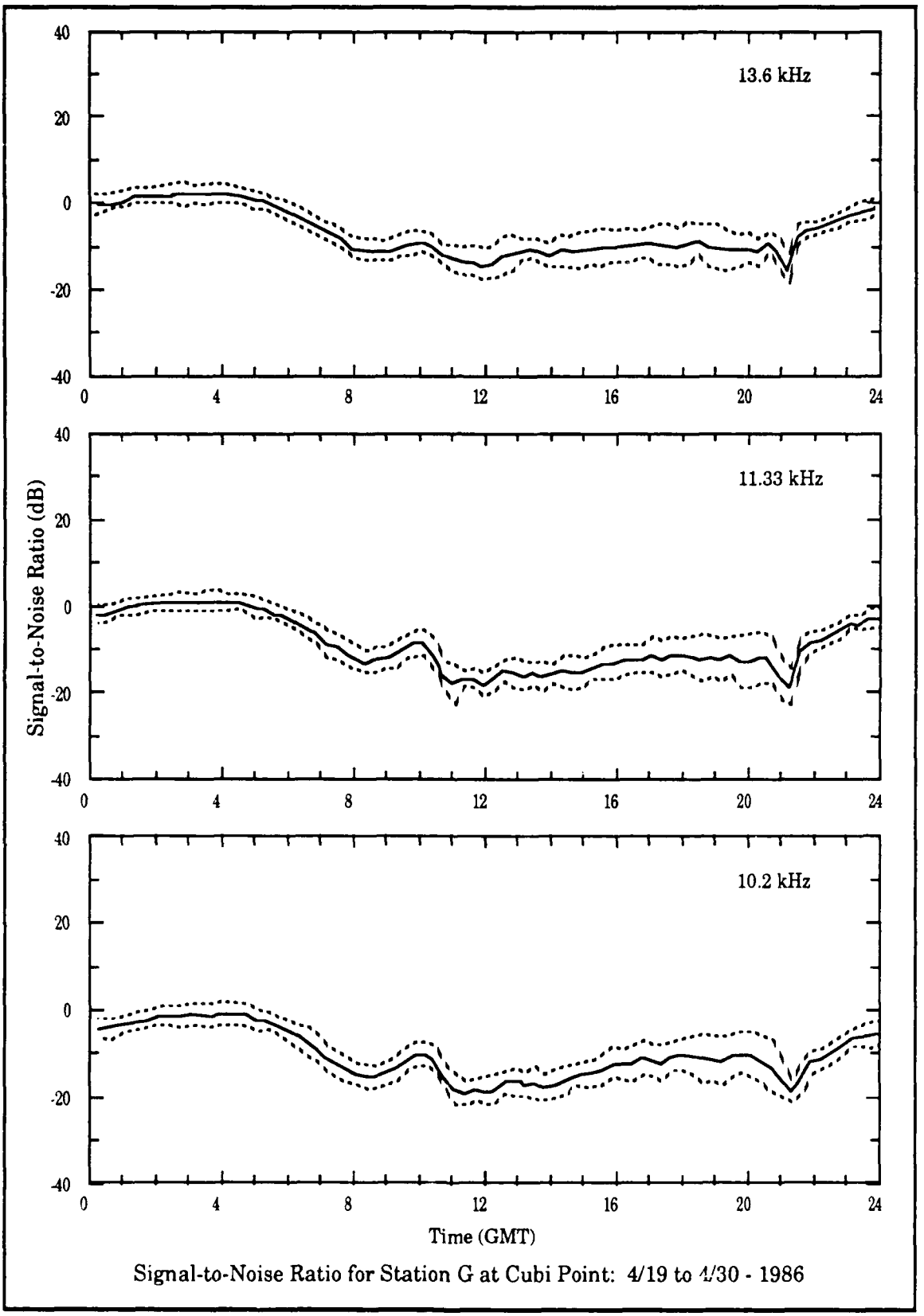

Figure 3-13a. Worst Case SNR for Australia at Cubi Point 4/19 to 4/30 - 1986

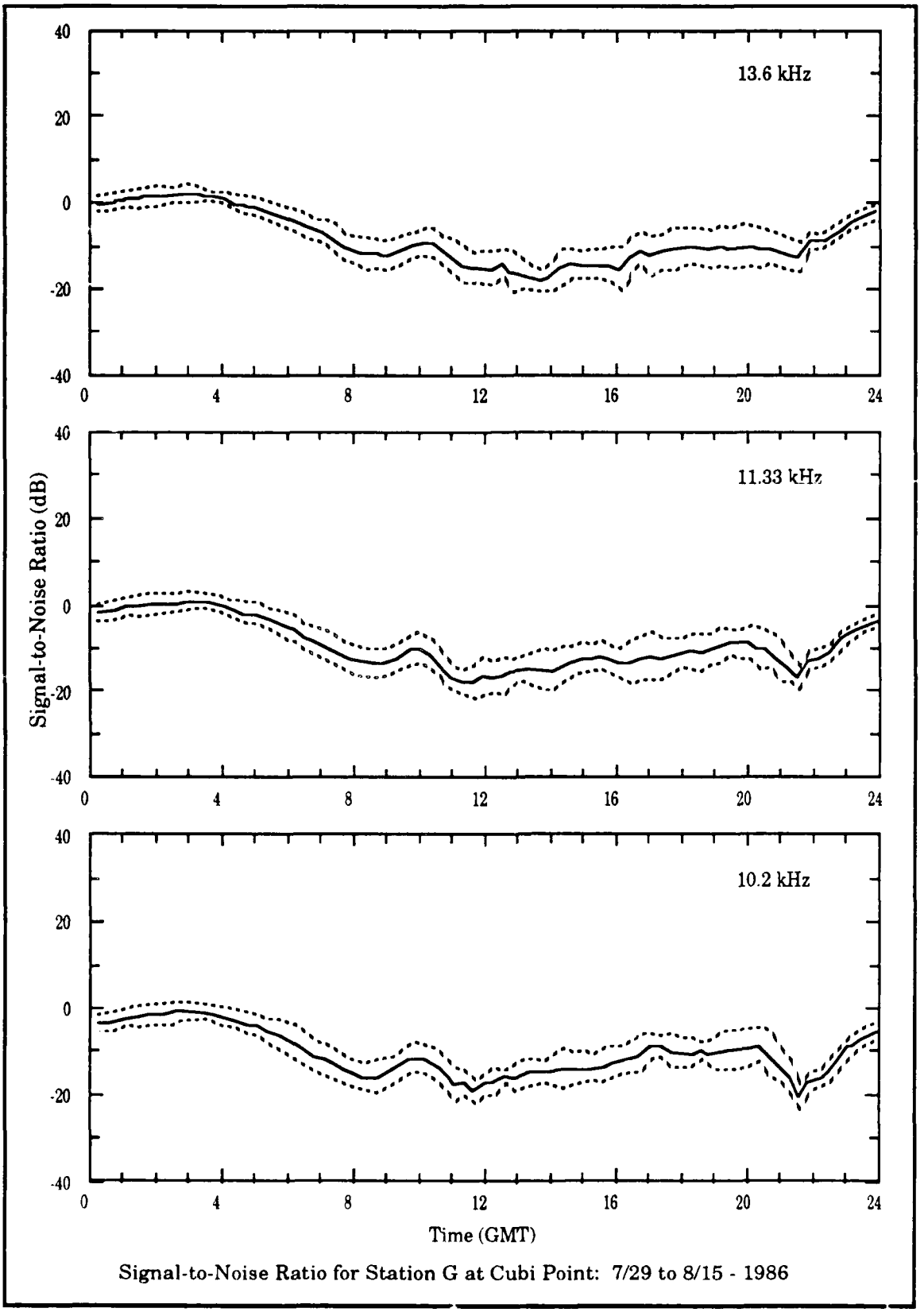

Figure 3-13b. Worst Case SNR for Australia at Cubi Point 7/29 to 8/15 - 1986

these date and time intervals, the average SNR drops below –20 dB on all frequencies. At 10.2 kHz we suspect signal loss occurs on some days, as the standard deviation becomes very small. A small standard deviation under conditions of poor SNR is attributable to small sample size. We note that part of this time interval covers early night at Cubi Point, a time when some other signals are modal.

For Hawaii signals, during July/August between 2300 and 0600 GMT, the daytime 10.2 kHz signal is close to the –20 dB threshold. Also, as shown in Figure 3-14, signal fades occur during transition times where tracking is regularly lost. On radials beyond Cubi Point and at times of high thunderstorm activity, we expect the Hawaii signal to be below the –20 dB threshold much of the day.

The North Dakota signals are generally weak at Cubi Point. On high noise days, both the 10.2 kHz and 11.3 kHz signals are typically not received for 4 to 6 hours at each of the transition times. During local daytime and high noise, the 10.2 kHz signal is below the –20 dB threshold most of the time.

Yap Site: Interpretation of SNR at Yap is complicated by the high local noise created by the local Loran-C facility. We have not attempted to determine how the local noise degrades signal coverage. The SNR observations are greater than –20 dB on the La Reunion, Australia and Japan signals at all three frequencies during this analysis period. The data cover May and June. The observed high noise months of April and August at Cubi Point are also expected to be high noise periods at Yap. We find the SNR for all stations to be quite variable between two-week intervals. This variability is not consistent with daily or seasonal trends in thunderstorm activity. As we show in the next section, we conclude that the local noise dominates the measurements. The following comments should be taken only as observations.

The Norway signals, as shown in the example of Figure 3-15, are particularly weak in late May and early June. We note that at 10.2 kHz the upper standard deviation curve is below the –20 dB threshold most of the time. At 13.6 kHz, the average signal level reaches about –28 dB between 0400 and 0800 GMT. This signal is not received on some days during this period.

The Liberia signals are generally below the –20 dB threshold between 0400 and 1500 GMT. All three signals go through a broad SNR minimum during this time

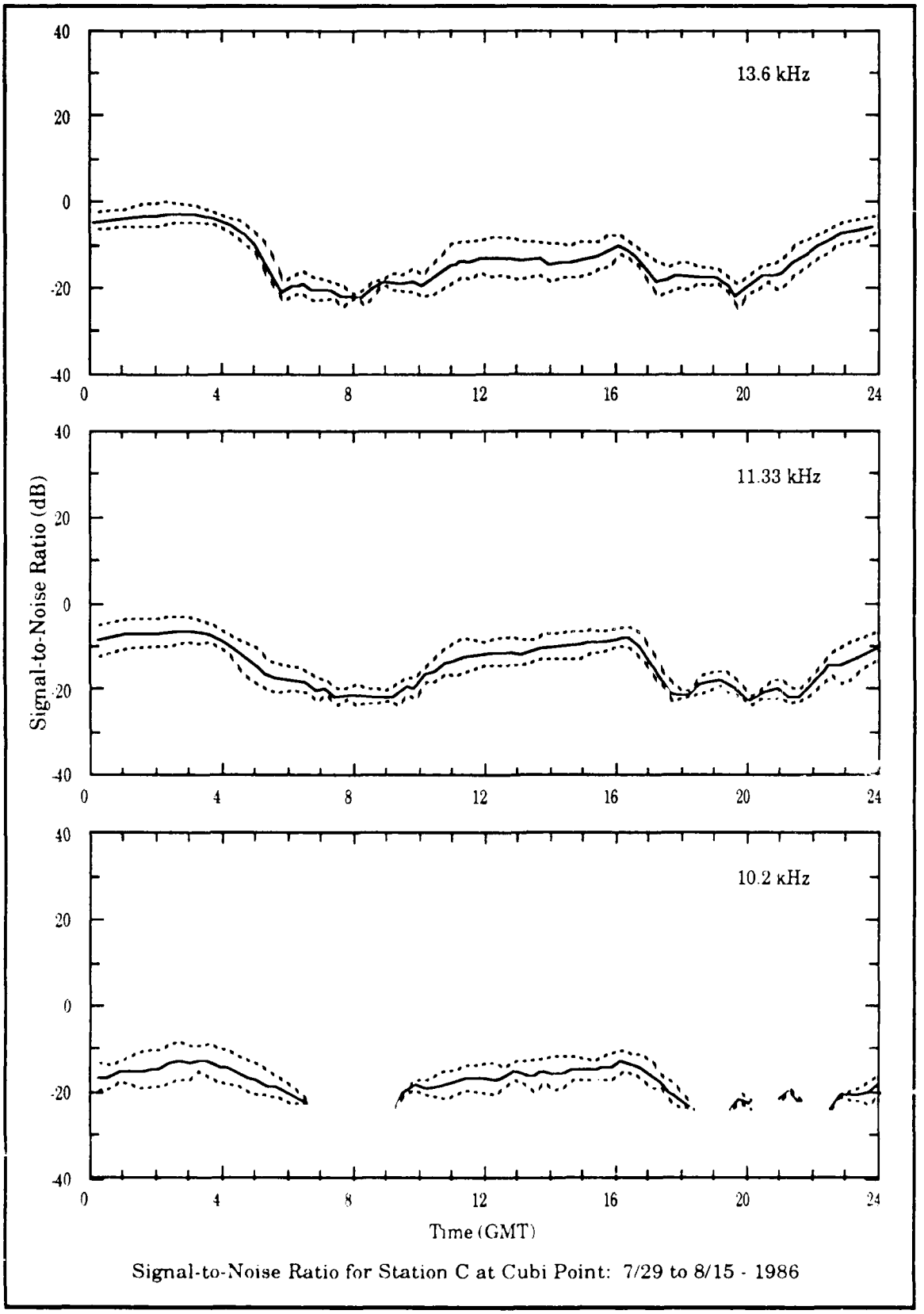

Signal-to-Noise Ratio for Station C at Cubi Point: 7/29 to 8/15 - 1986

Figure 3-14. Hawaii SNR Recorded at Cubi Point

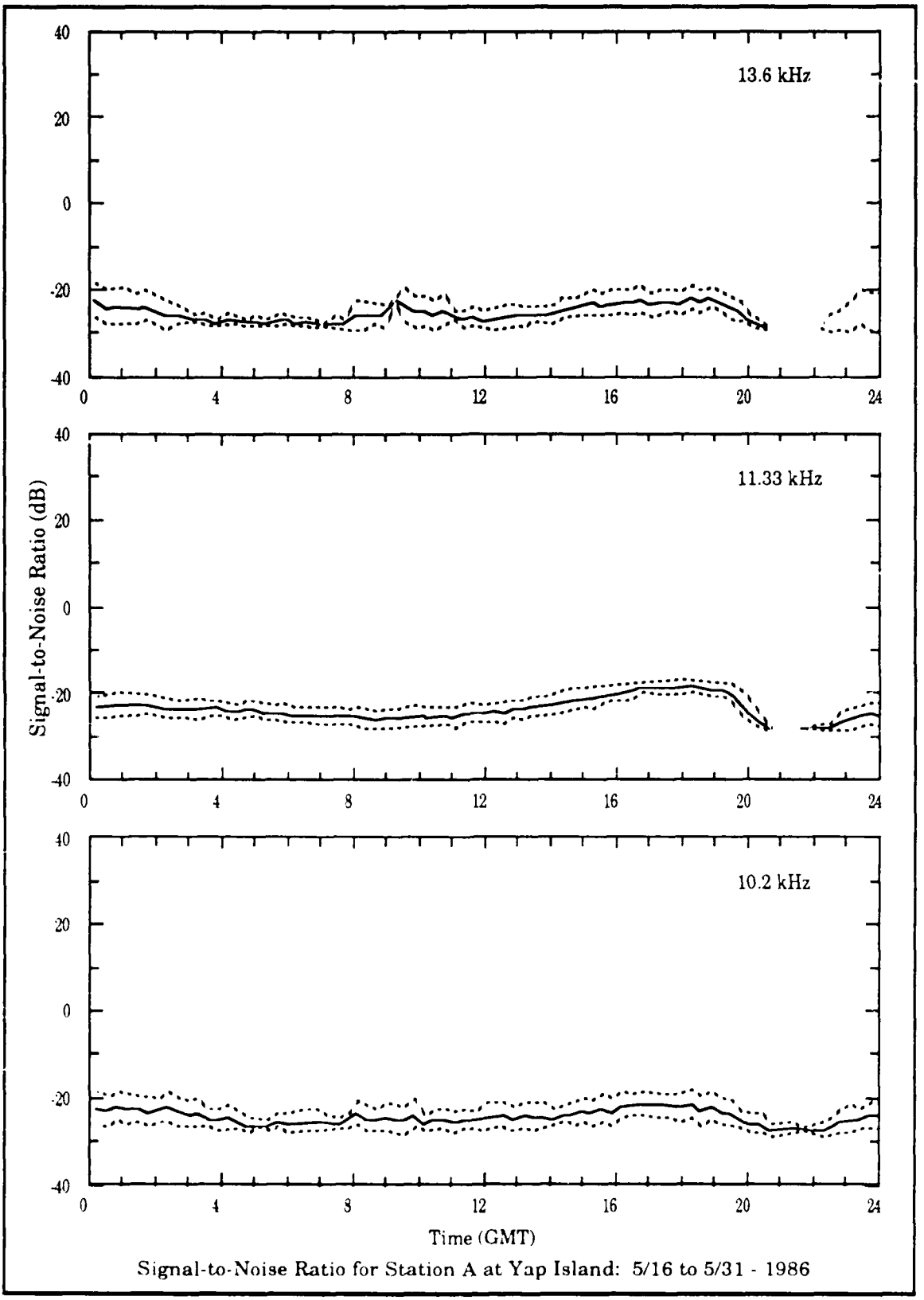

Figure 3-15. Norway SNR Recorded at Yap

interval. The 10.2 kHz signal may be below reception threshold on some days between 0700 and 1000 GMT.

The Hawaii signals are very weak during the sunset/sunrise transition intervals. Each of these intervals lasts about four hours. For the 10.2 kHz signal during daytime, the standard deviation lower curve is at or near the –20 dB threshold during most of the sample periods.

The North Dakota signals are below the –20 dB threshold most of the time. Reception is frequently lost for periods of several hours on all frequencies.

Darwin Site: The stations with good SNR at all times and frequencies are Liberia, La Reunion, Australia, and Japan. The data cover the months of May through July. We note that this measurement interval corresponds to a relatively low predicted noise period for Darwin.

The SNR of the Norway signals varies somewhat between the two-week intervals of averaged data. The signals have highest SNR near 0300 and 2000 GMT and lowest SNR near 1000 GMT. Reception is frequently lost for several hours at a time between 0800 and 1600 GMT. The highest SNR achieved is typically about –15 dB. For January noise, the highest SNR based upon the predicted increase in noise would be –21 dB.

The average SNR of the Hawaii signals is generally above the –20 dB threshold during times of all daylight on the propagation path. The lower curve of one standard deviation is below this threshold about 30 percent of the time.

The average SNR of the North Dakota signals is generally near the –20 dB threshold between 2000 and 0400 GMT. Most of the time the lower curve marking one standard deviation is below this threshold. Many periods of signal loss are evident during the hours between 0400 and 2000 GMT.

The average SNR of the Argentina signals is generally near the –20 dB threshold, except for signal fades that occur between 2100 and 2330 GMT. Between 0000 and 0800 GMT, when the signal SNRs are usually the lowest, the average SNR may occasionally drop below the –20 dB threshold.

Singapore Site: The stations with good SNR at all times and frequencies are Norway, Liberia, La Reunion, Australia and Japan. The data cover the months of May, August, September, November and December.

The average SNR of the Hawaii signals is generally above the –20 dB threshold during times of all daylight on the propagation path. The lower curve of one standard deviation is below this threshold about 40 percent of the time.

We question the validity of the North Dakota data because the relative SNR values and time patterns do not appear appropriate.

The average SNR of the Argentina signals generally vary around the –20 dB threshold between 1600 and 0400 GMT. Between 0400 and 1600 GMT the signals are not recorded a high percentage of the time.

3.5.3 SNR PREDICTIONS

In this part of the analysis, we use two sets of predictions. First we examine noise predictions from CCIR data for each measurement site (ZACHARISEN and JONES 1970, Ref. 24). These predictions consist of hourly values for each month of the year. Since signal level predictions for a selected hour are the same for each month, the predicted SNR is directly related to the relative predicted noise. Second, we examine SNR coverage contours produced by TASC (GUPTA et al 1980 (b), Ref. 25) to estimate how geographical coverage relates to the measurement sites.

NOISE PREDICTIONS. For this analysis, we use 10.2 kHz predictions of noise for a 100 Hz receiver bandwidth. (Receiver performance is typically defined in signal sensitivity relative to 100 Hz bandwidth atmospheric noise.) In Figure 3-16 through 3-20, we show the highest and lowest predicted noise during the year for each hour. If the highest or lowest values all occur within a month, the month is indicated next to its corresponding curve. If the values are from different months, the month, by number, is marked across the plot.

Japan: For the Japan site, the data for July represent the worst case SNR. As noted, the period of highest local summer noise extends between 0500 and 1600 GMT. Sunset occurs at about 1000 GMT in July and August so the strong noise lasts 6 hours after local sunset.

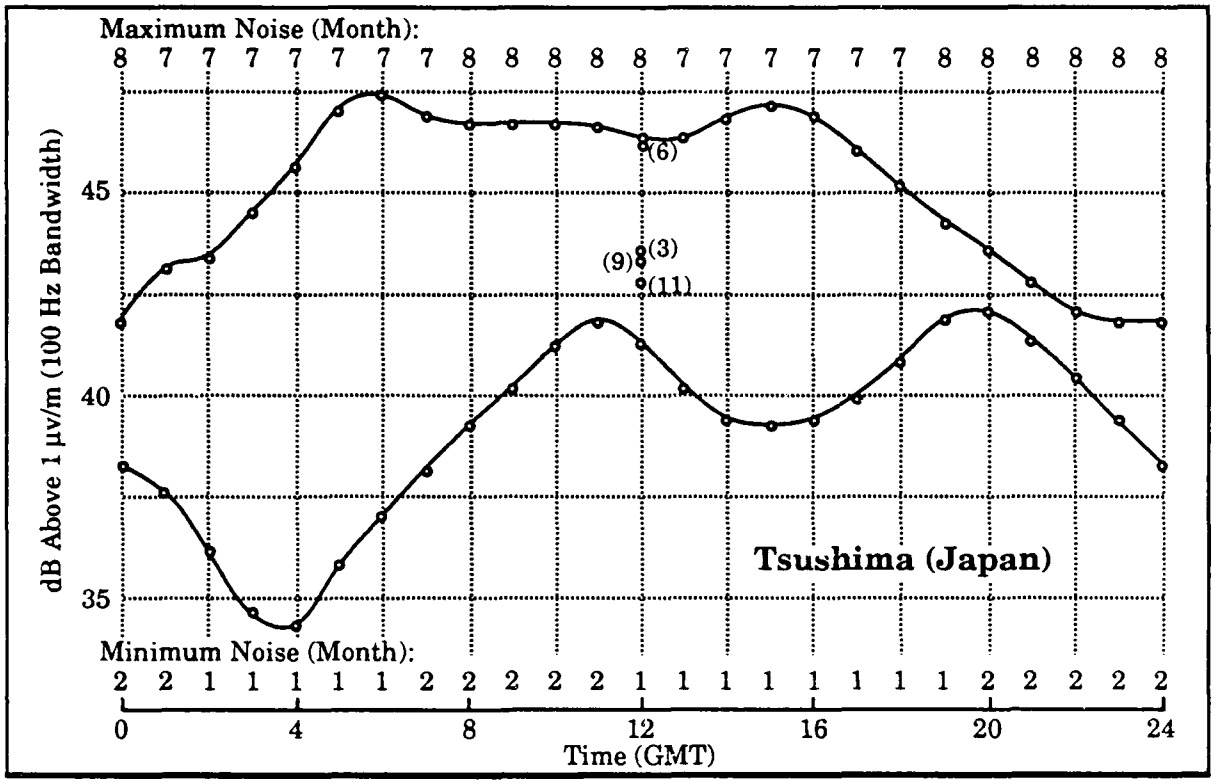

Figure 3-16. Predicted Noise Range at Japan

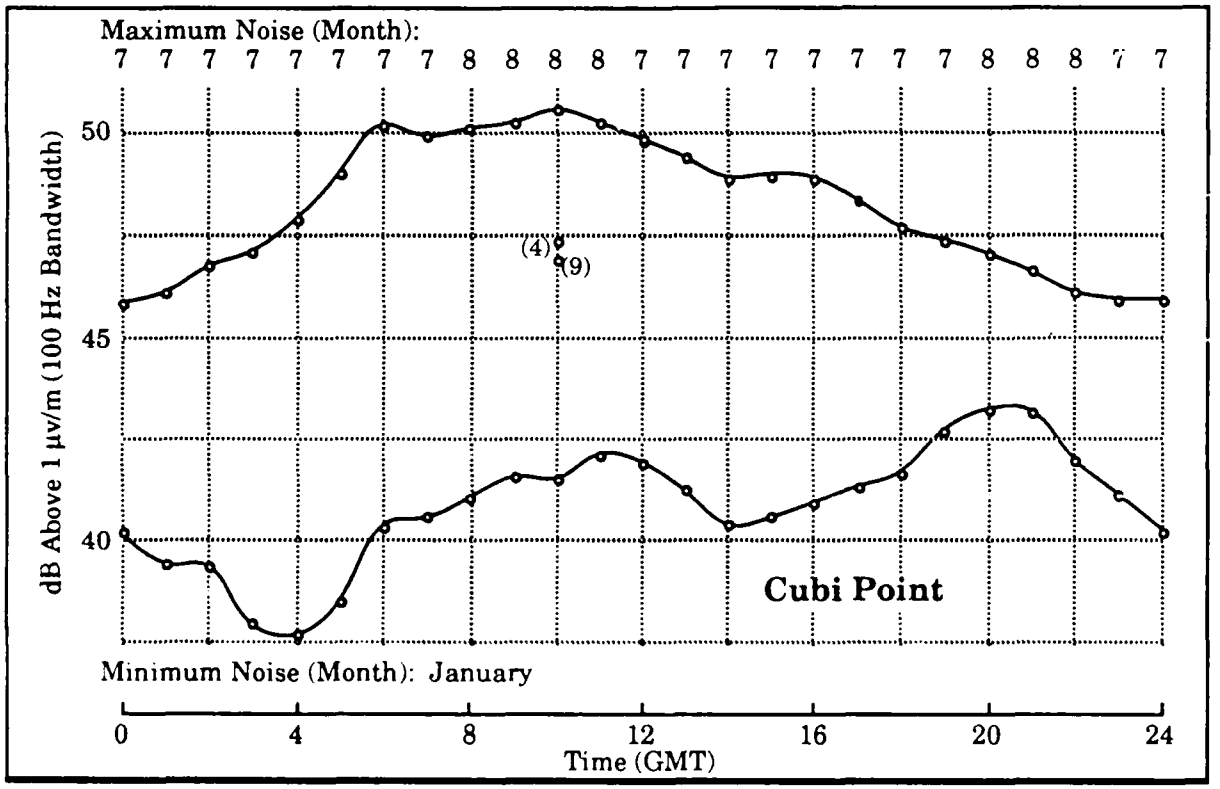

Figure 3-17. Predicted Noise Range at Cubi Point

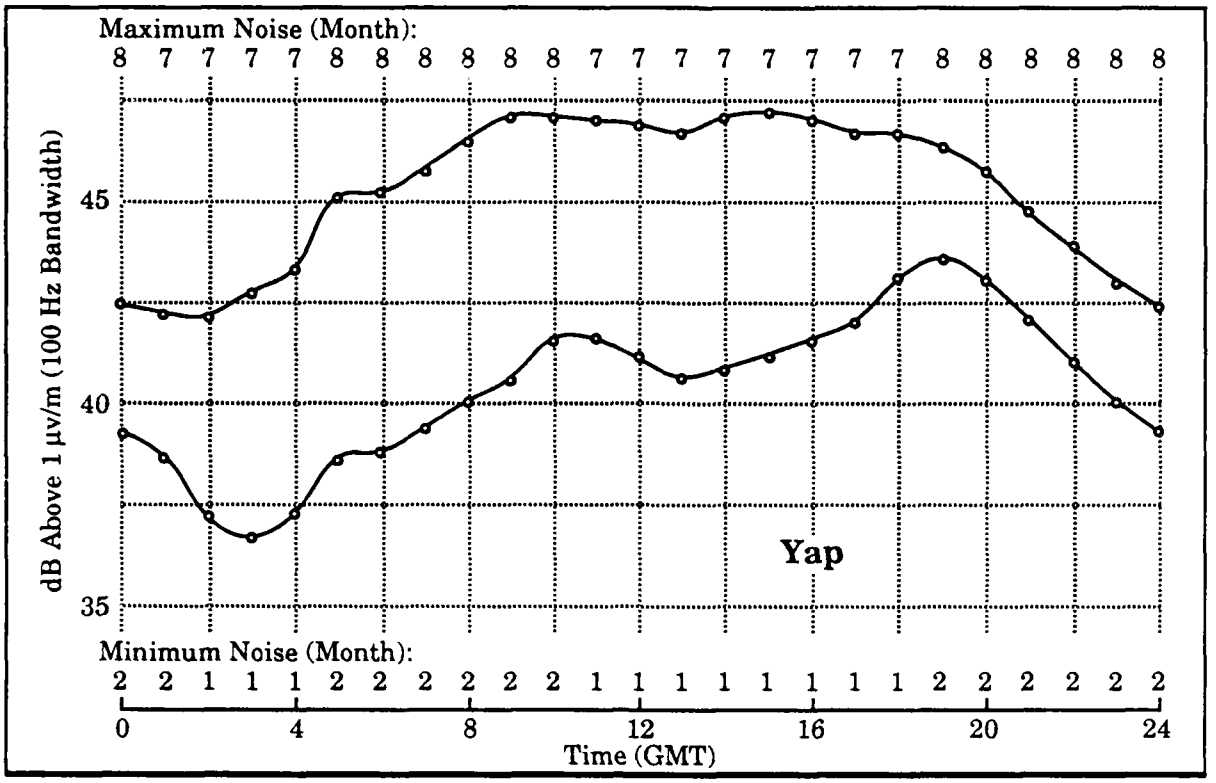

Figure 3-18. Predicted Noise Range at Yap

In Figure 3-16, we also show noise values at 1200 GMT for several other months (indicated by numbers in parentheses), to illustrate how noise varies with season. At Japan the noise is near its peak value for June, July and August.

Cubi Point: For the Cubi Point site, the highest noise levels shown in Figure 3-17, occur during July or August, but noise is also strong in June. The time interval of peak noise is from 0600 to 1200 GMT. Local sunset occurs near 1000 GMT during July/August. Thus the noise is strongest when the sunset amplitude fade occurs on many of the signals. The peak noise is predicted stronger at Cubi Point than at Japan by about 3 dB. This prediction is consistent with the observed occasional loss of the Norway signal at Cubi Point but not at Japan.

Yap: For the Yap site (Figure 3-18), the noise also peaks in July or August. The noise is near peak values for a long time interval, from 0800 to 1900 GMT. Local sunset occurs near 0830 GMT during July/August. Thus the period of peak noise is mostly at night. The three strongest stations, La Reunion, Japan and Australia, are all free of modal problems in this vicinity. During off times for one of these three stations and at peak noise times, selection of an additional station could be a problem.

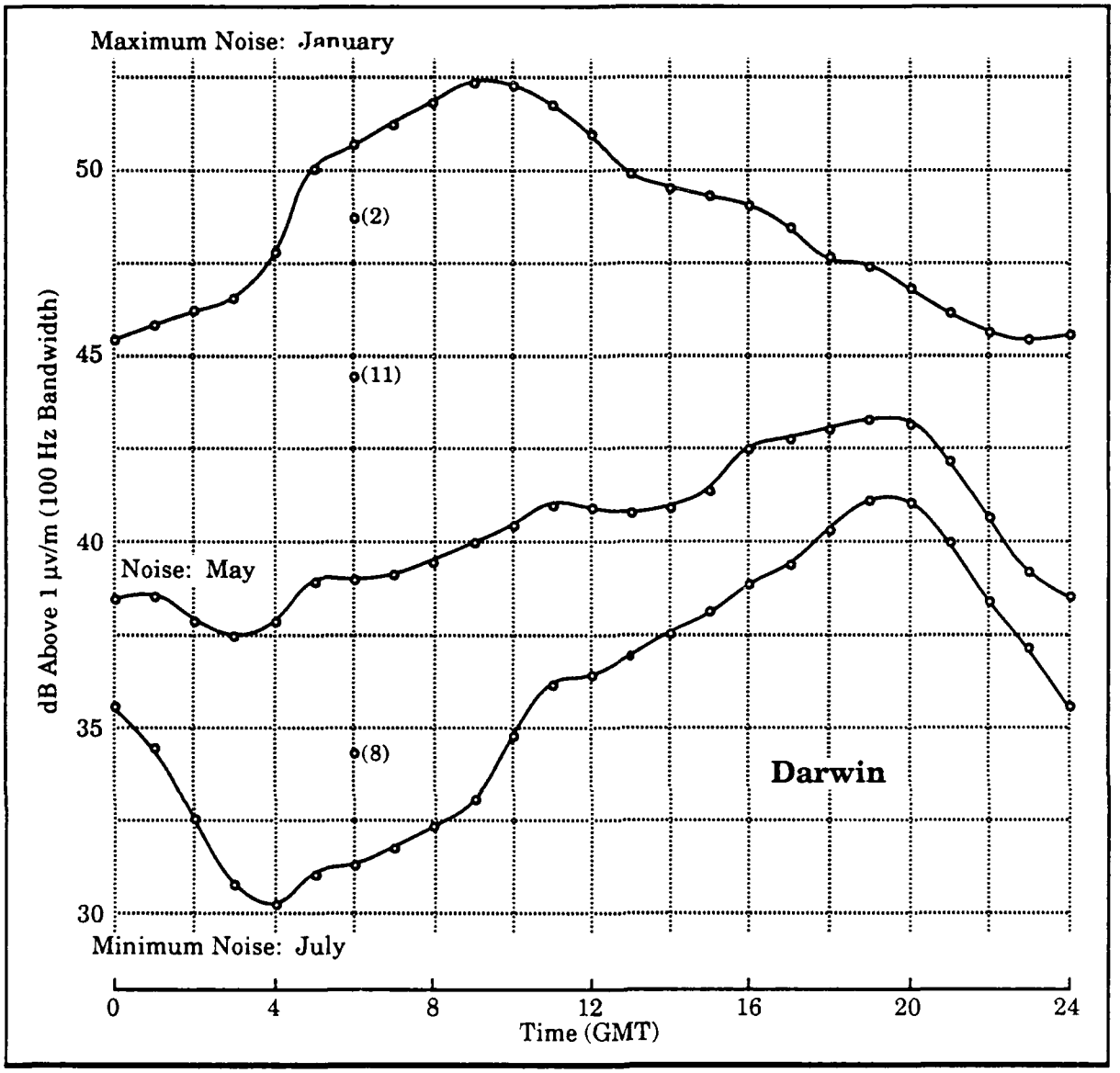

Figure 3-19. Predicted Noise Range at Darwin

Darwin: For the Darwin site, the seasons are reversed relative to the other sites, thus the highest predicted noise levels occur during January. Figure 3-19 shows the predicted highest noise level in January and the predicted lowest noise level in July. Also shown is the predicted noise level for May, the highest noise period for which data are analyzed. We note that at 1000 GMT the predicted May noise level is 12 dB below the predicted peak. If this 12 dB difference is added to the May SNR measurements, the Liberia signal would have a –28 dB SNR between 0800 and 1200 GMT in January. The La Reunion SNR would be –15 dB. The Norway, Hawaii, North Dakota, and Argentina signals likely would not be usable because of the poor SNR noted in the previous section. Local sunset

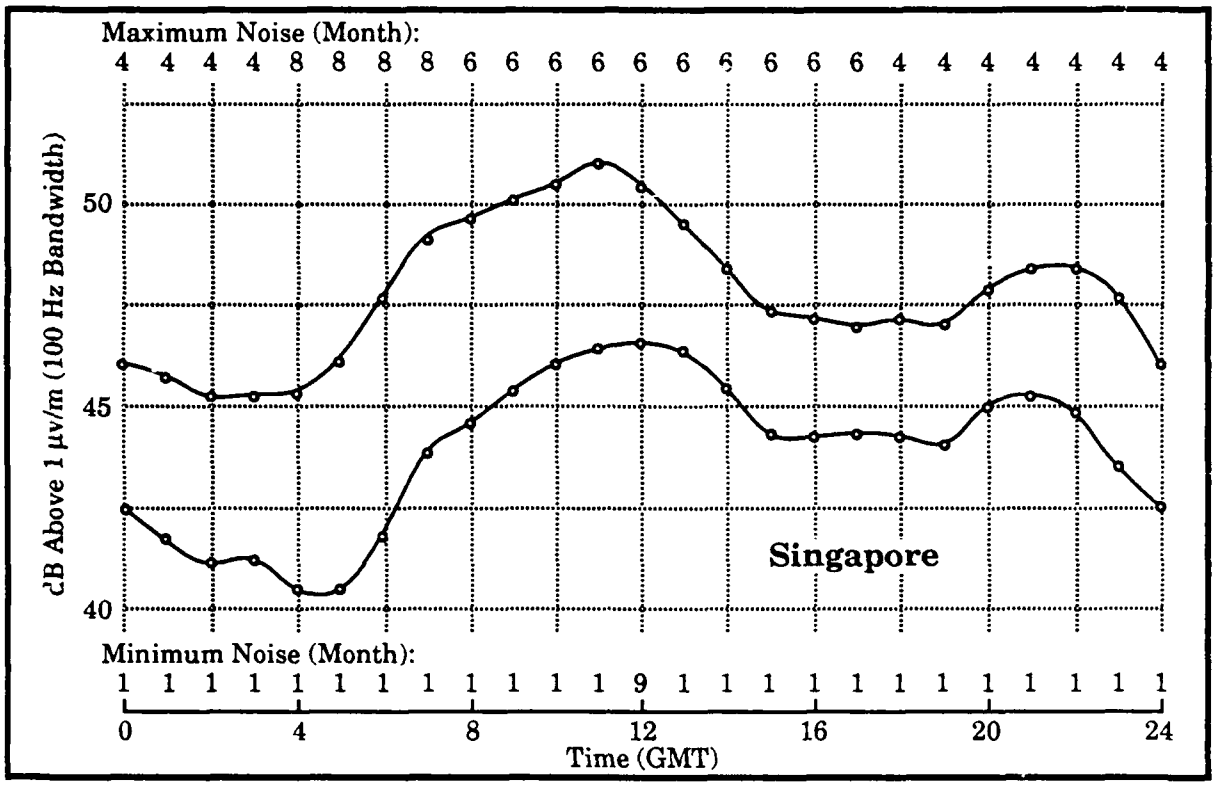

Figure 3-20. Predicted Noise Range at Singapore

occurs in January near 0900 GMT, after which the entire propagation path from Japan is dark. Slightly to the west of Darwin where the Japan signal is definitely modal at night, it is possible that only the Australia and La Reunion signals are of good navigation quality for a few hours after sunset.

Singapore: For the Singapore site (Figure 3-20), the peak noise occurring in June at 1100 GMT, is typical of the other sites. Local sunset occurs near 1030 GMT for July/August. Of the always good SNR stations (Norway, Liberia, La Reunion, Australia and Japan), Japan and Australia definitely become modal after 1030 GMT. None of the marginal SNR stations have good quality phase after this time so the decrease in noise after 1000 GMT doesn't help.

COMPARISON OF NOISE PREDICTIONS WITH DATA. Some data for each of the monitoring sites were analyzed by Carl Kugel of NOSC to extract levels of noise. The amount of data that could be analyzed were determined by the degree of local man-made noise interference, the quality of calibration, the frequency drift of the receivers and available manpower. Here we compare the noise level data with the CCIR/ITS noise predictions.

Japan Noise: Shown in Figure 3-21 are predicted and measured noise values for several intervals from mid April through June. Our observations are: (1) that measured peak noise for each interval is less than predicted, ranging from 2 dB in April to 4 dB in June, (2) the time of measured minimum noise is later by about 3 hours than predicted and the minimums are lower, by as much as 8 dB, and (3) for May and June the noise remains high throughout the night. We note on these and the following figures, the 0600 and 1800 GMT times correspond to the coverage predictions to be subsequently described. Also, local sunset and sunrise is marked to show how the noise patterns relate to these times.

Cubi Point: The predicted and measured noise is shown in Figure 3-22. Key comparisons are: (1) the predicted peak noise for each interval is higher than

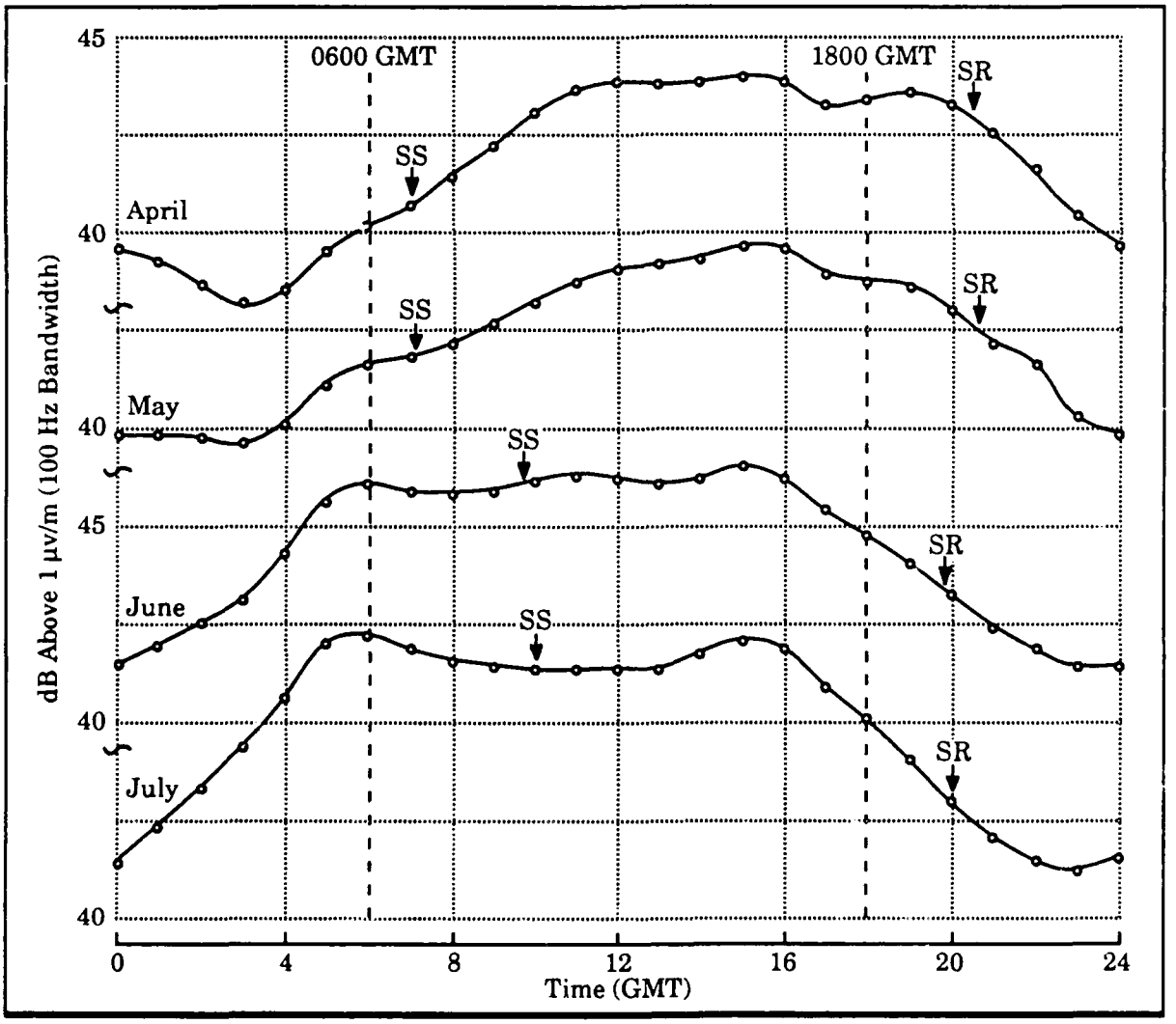

Figure 3-21a. Predicted (ITS/CCIR) Noise at Japan; 10.2 kHz

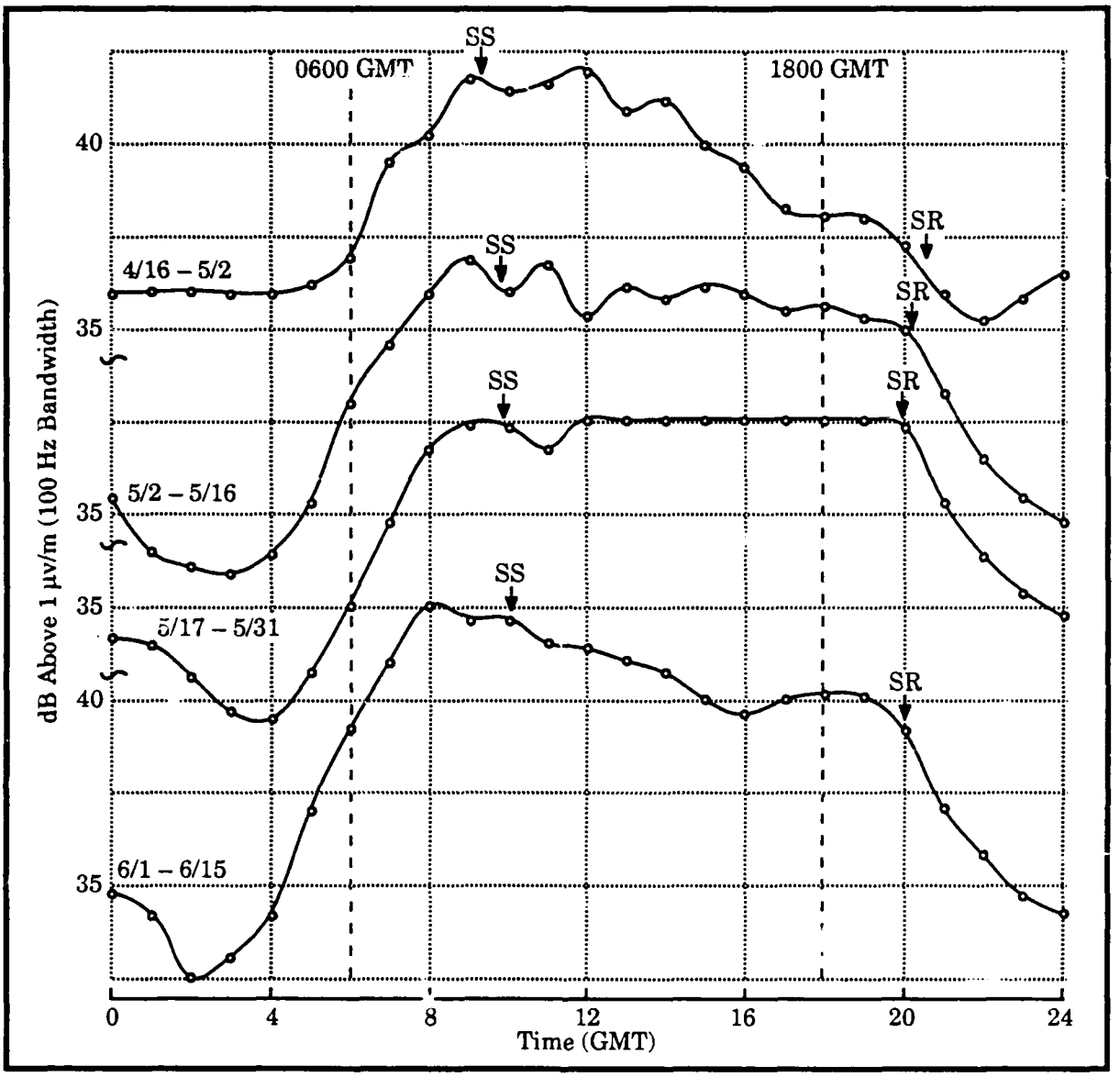

Figure 3-21b. Measured Noise at Japan; 10.2 kHz

measured, ranging from 3 to 10 dB, (2) the time of minimum noise occurs about 3 hours later than predicted and the minimum is 6 to 14 dB lower than predicted, and (3) in local summer, the noise peaks before sunset and subsequently decreases throughout the night. The 0400 GMT, which approximately marks the beginning of noise buildup in summer at all the sites, is also noon at Cubi Point. This finding supports the expectation that most of the noise is from afternoon storm buildup in and west of the Philippines.

Yap: A comparison of noise levels and diurnal patterns between predicted and measured noise (Figure 3-23), clearly demonstrates that local interference is

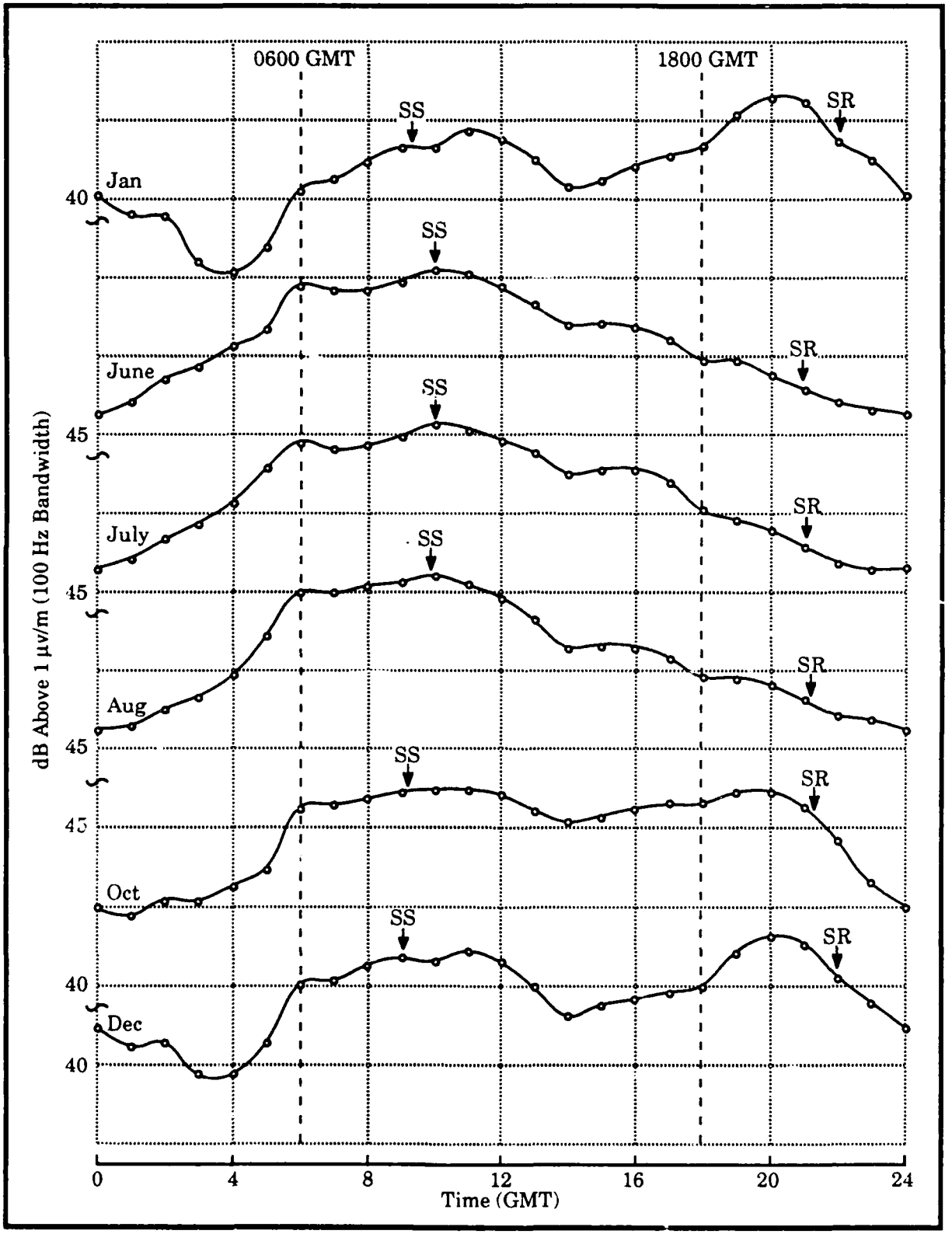

Figure 3-22a. Predicted (ITS/CCIR) Noise at Cubi Point; 10.2 kHz

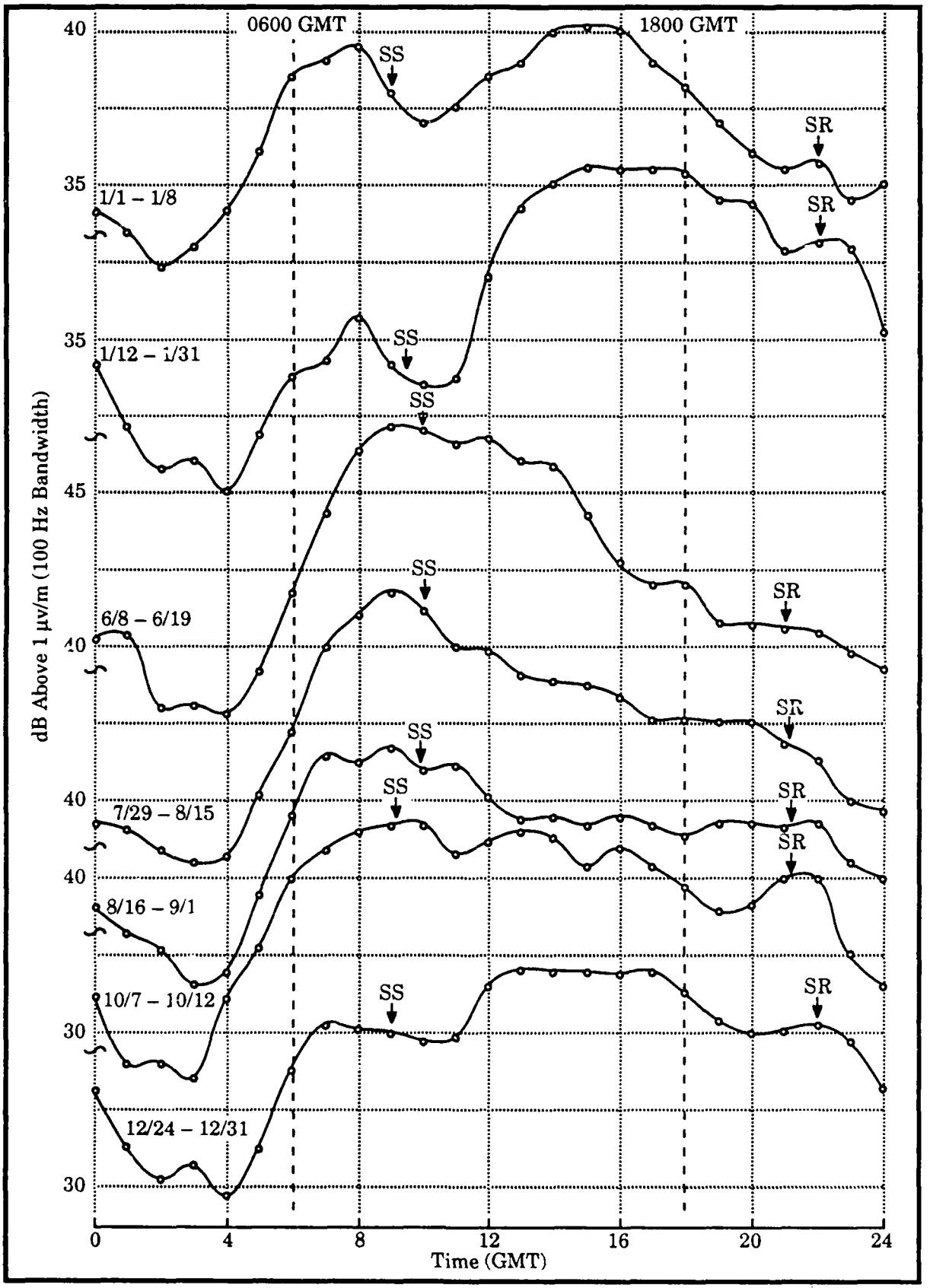

Figure 3-22b. Measured Noise at Cubi Point; 10.2 kHz

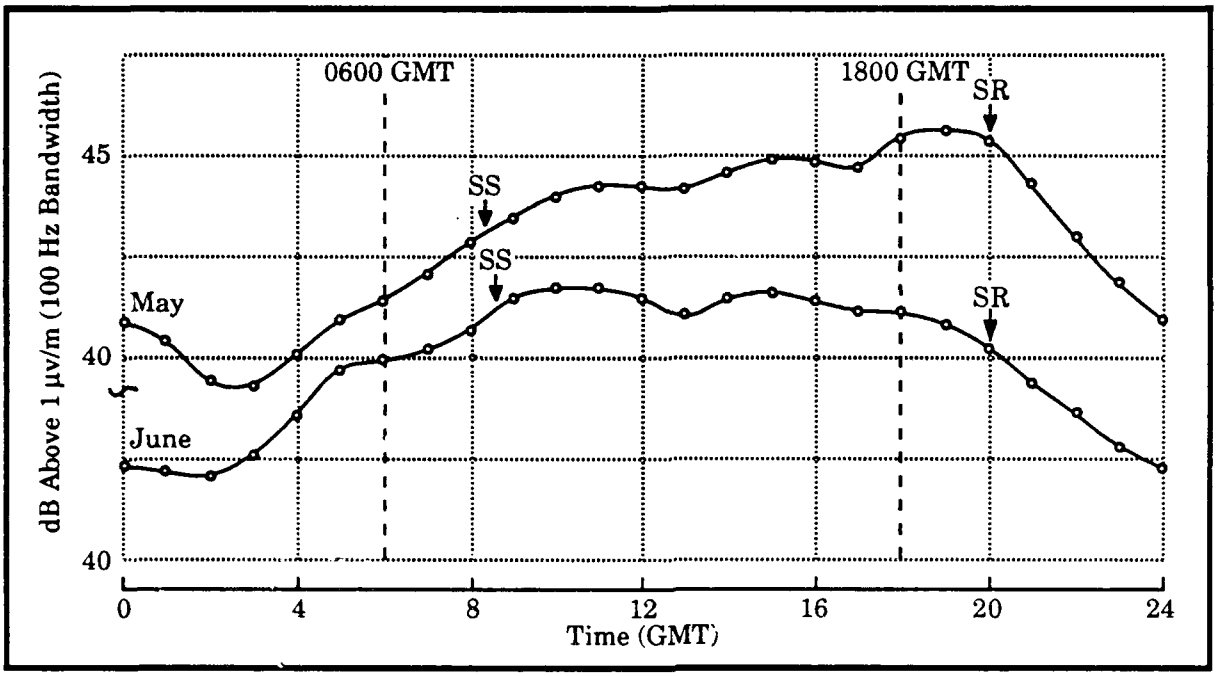

Figure 3-23a. Predicted (ITS/CCIR) Noise at Yap; 10.2 kHz

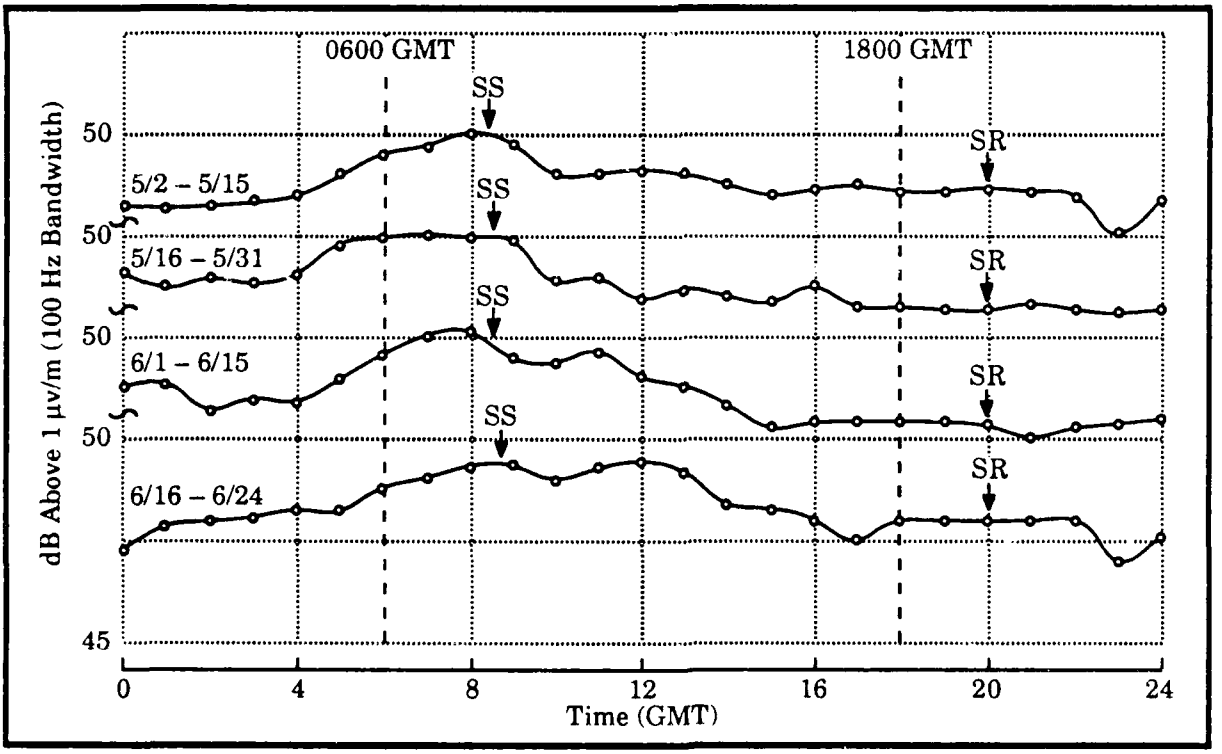

Figure 3-23b. Measured Noise at Yap; 10.2 kHz

dominant. Thus, the Yap data provide minimal information on atmospheric noise conditions and signal coverage boundaries. However, we include both the Yap noise data and the earlier presented measured SNR, as we believe useful information can be extracted. If inferences are made from measurements at other sites and about the noise predictions, estimates of coverage at Yap can be derived.

Darwin: The short sample of measured noise is compared with predicted in Figure 3-24. Since Darwin is 13° south of the equator, the local noise is expected to follow a seasonal pattern that is out of phase from the above sites. Yet the time pattern of the measured sample for May is more similar to the June data at Cubi Point than to the May predicted values. Intuitively, we are much more comfortable with the measured shape than the predicted shape. (This is because the thunderstorm regions that would be primary contributors around 0900 GMT are much closer to the receiver than thunderstorms which are expected to be active around 1900 GMT.) Darwin is about as far south as Cubi Point is north of the equator. Yet the May (fall) measured Darwin noise at 0900 GMT is 42 dB while at Cubi Point, the October (fall) noise is about 37 dB. We caution that the 3 day period of measurements is far too short to draw conclusions on averages and trends.

Singapore: The limited measured noise data are compared with predictions in Figure 3-25. We note that the measured noise buildup pattern is similar to the other sites and that the post-sunset decrease is less that at the other sites. We interpret the continuation of noise over a longer period to result from the proximity of thunderstorm centers to the east and west of Singapore extending for a longer distance and thus more difference in time history. We note that the August 0900 GMT noise is within –2 dB of that measured at Cubi Point. The 2000 GMT noise is 1 dB below the Cubi Point noise. The predicted noise peak at 1100 GMT for August is 9.5 dB above that measured. The predicted and measured noise range is very similar if all values are offset about 6 dB.

In summary, we find that the measured noise is consistently lower than predicted at all sites. This finding should be checked against other analysis to determine if the measurements are representative. We also find consistent differences in measured versus predicted diurnal pattern of the noise. Here we

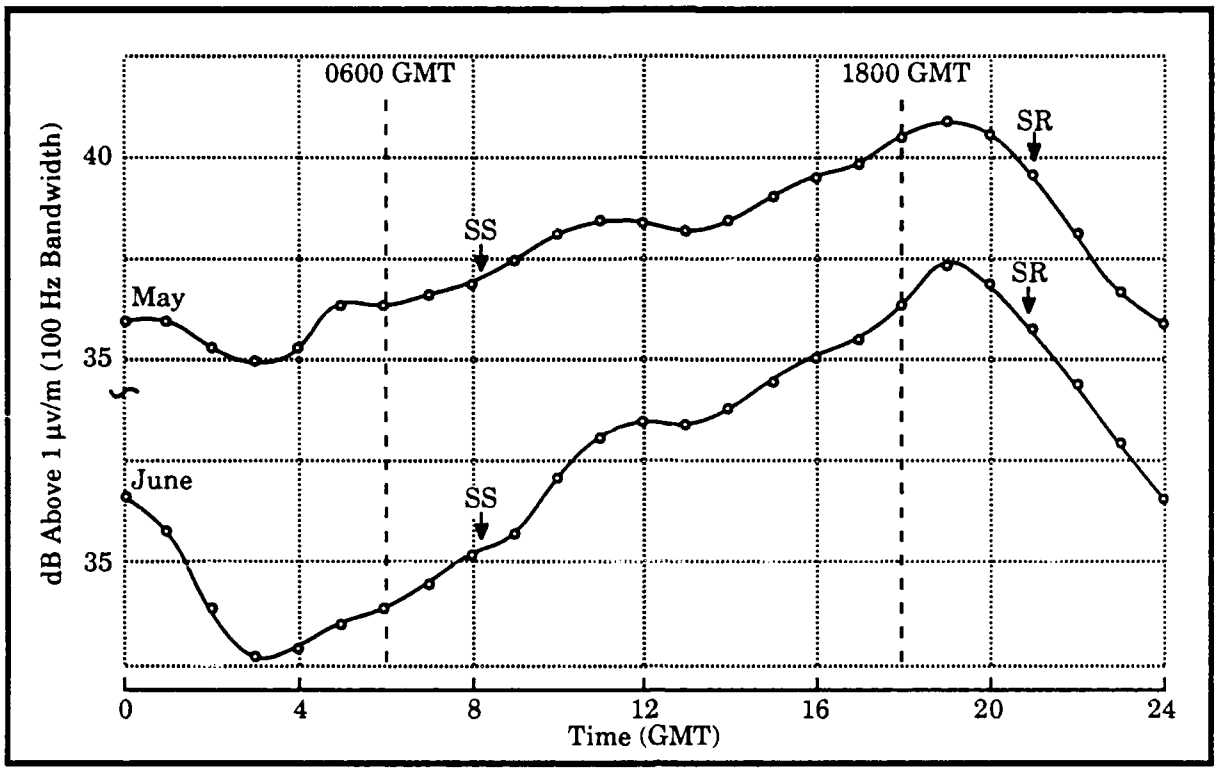

Figure 3-24a. Predicted (ITS/CCIR) Noise at Darwin; 10.2 kHz

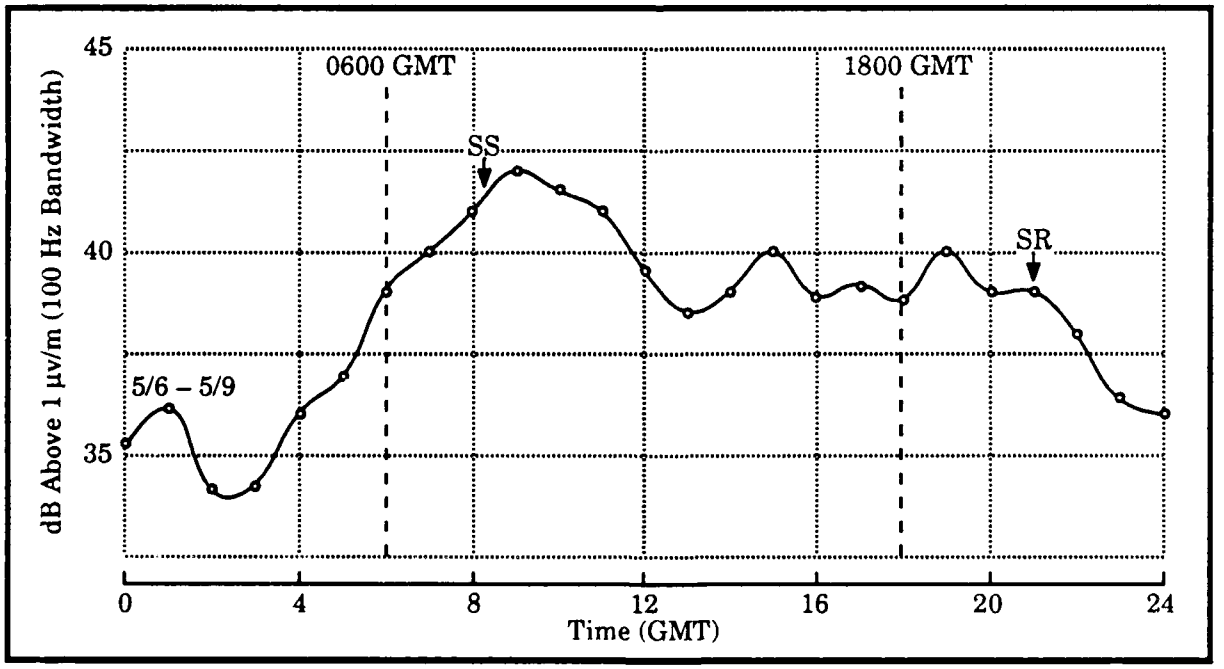

Figure 3-24b. Measured Noise at Darwin; 10.2 kHz

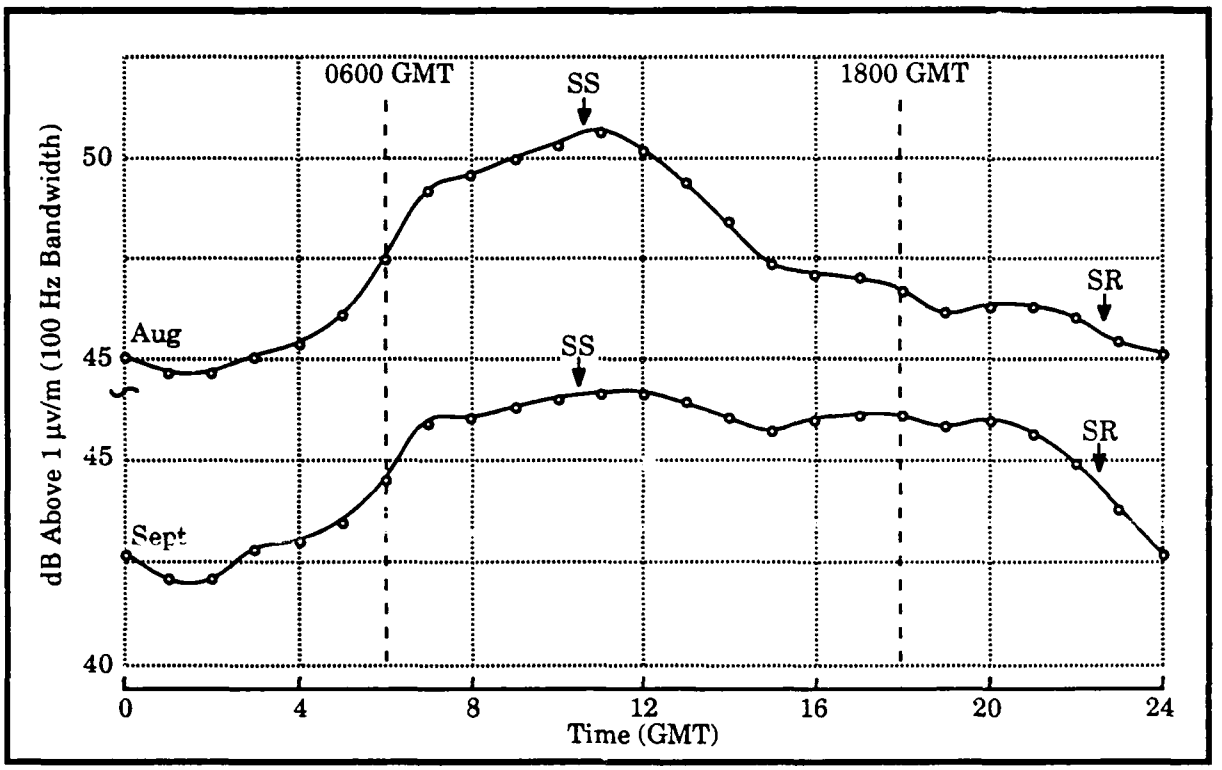

Figure 3-25a. Predicted (ITS/CCIR) Noise at Singapore; 10.2 kHz

are confident, because of our intuition about thunderstorm activity, that the measured patterns are more representative than the predictions.

3.5.4 EXAMINATION OF SNR PREDICTIONS

Prediction of Omega signal coverage is based upon plots of signal contours prepared by TASC for ONSCEN (GUPTA et al 1979, Ref. 20; and GUPTA 1980(b), Ref. 25). Signal contour diagrams for –20 and –30 dB SNR for each of the stations are compared with the measured SNR at each of the monitor sites. Reference 25 contains 64 figures showing coverage contours for individual stations for two times (0600 and 1800 GMT) on four months (February, May, August and November). Because it is not practical to discuss all of these predictions in detail, we will concentrate on the greatest coverage concerns and highlight important findings.

3.5.5 COMPARISON OF PREDICTIONS WITH FINDINGS

In this section, we select the Norway signal as a focus to describe our analysis and to illustrate certain key features of both the coverage model and measurement findings. We choose Norway and focus on the area between Cubi Point and

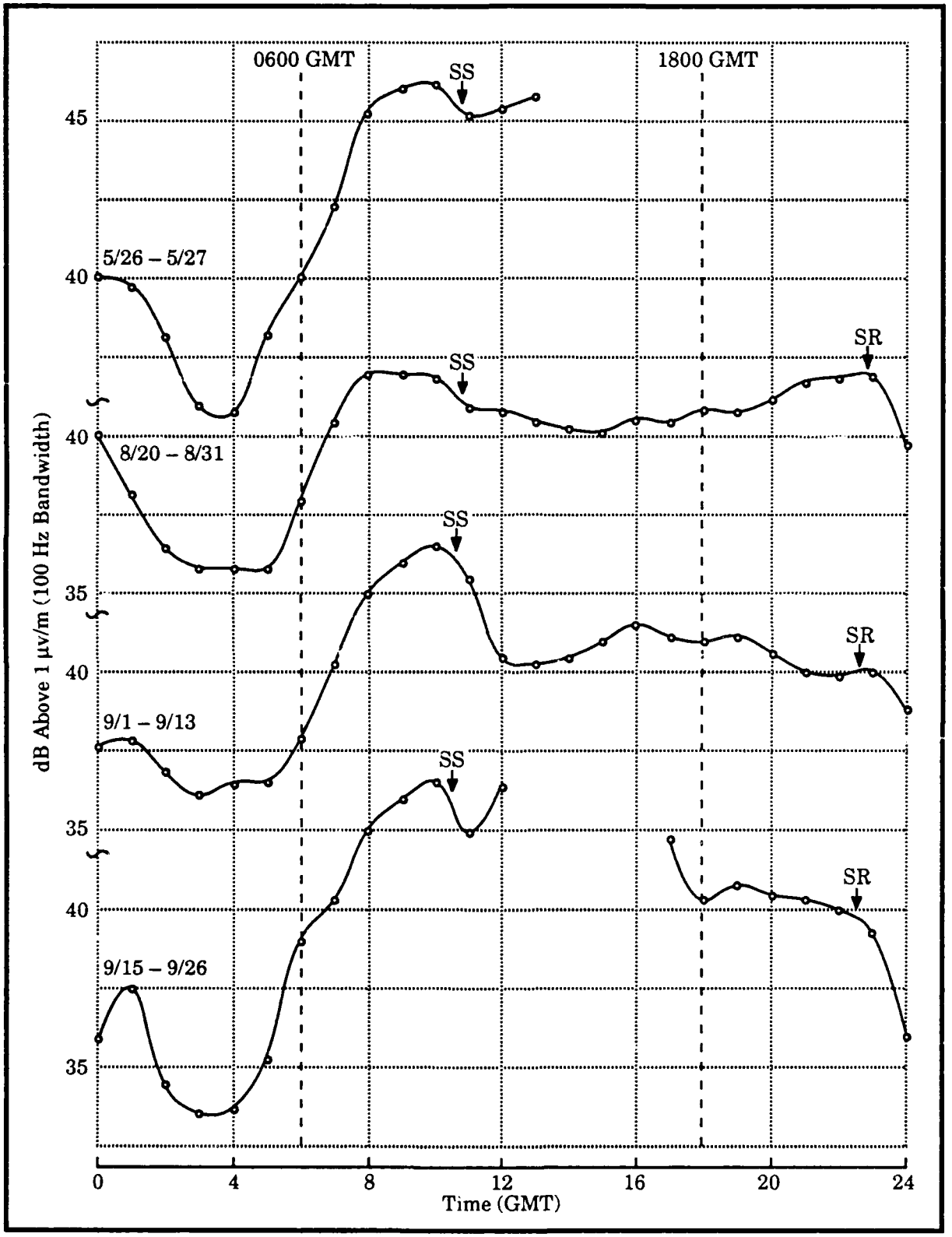

Figure 3-25b. Measured Noise at Singapore; 10.2 kHz

Singapore because of the predicted importance of the Norway signal to reliable navigation. Coverage for Norway at 0600 GMT for the predicted months is shown in Figures 3-26 through 3-29. At the other prediction time, 1800 GMT, full coverage is predicted for Norway throughout the validation region. Noon at the center of our focus area (about 10°N, 110°E) is about 0330 GMT. At 0600 GMT, the propagation path is all daylight except for February and November when the sunrise terminator is just east of Norway. These predictions show that for the –20 dB SNR coverage: (1) no coverage exists at this time during February and May, (2) coverage is limited to the northern end in November, and (3) near full coverage of the region is predicted for August. For the –30 dB SNR coverage prediction: (1) the least coverage in this region occurs in February, (2) most of Australia is not covered in May and November, and (3) full coverage occurs in August.

For all stations SNR is predicted lower at 0600 than 1800 GMT. For Liberia, at 0600 GMT in February, the –20 dB contour extends from the northern tip of the Philippines in a broad arc to the western edge of Borneo down to just west of Australia. In May and August, this contour is to the west of most of our focus area. In November the contour is almost vertical just west of the Philippines and at the equator, arcs east to near Darwin.

For Hawaii, the signal is shown below –20 dB SNR to the west and the south of the Philippines for most of the predictions, at both 0600 and 1800 GMT. In May and August for 0600 GMT, the predictions for this focus area are SNR < –30 dB.

For North Dakota, west and south of the Philippines, the SNR is predicted below –20 dB at all times and below –30 dB in May and August.

For La Reunion the SNR is predicted above –20 dB at all locations, dates and times.

For Argentina the SNR is predicted below –30 dB at almost all locations, dates and times.

For Australia in May, the –20 dB contour extends from just south of Cubi Point to south of Singapore for both 0600 and 1800 GMT. In February and August the upper half of our focus area is predicted below –20 dB SNR.

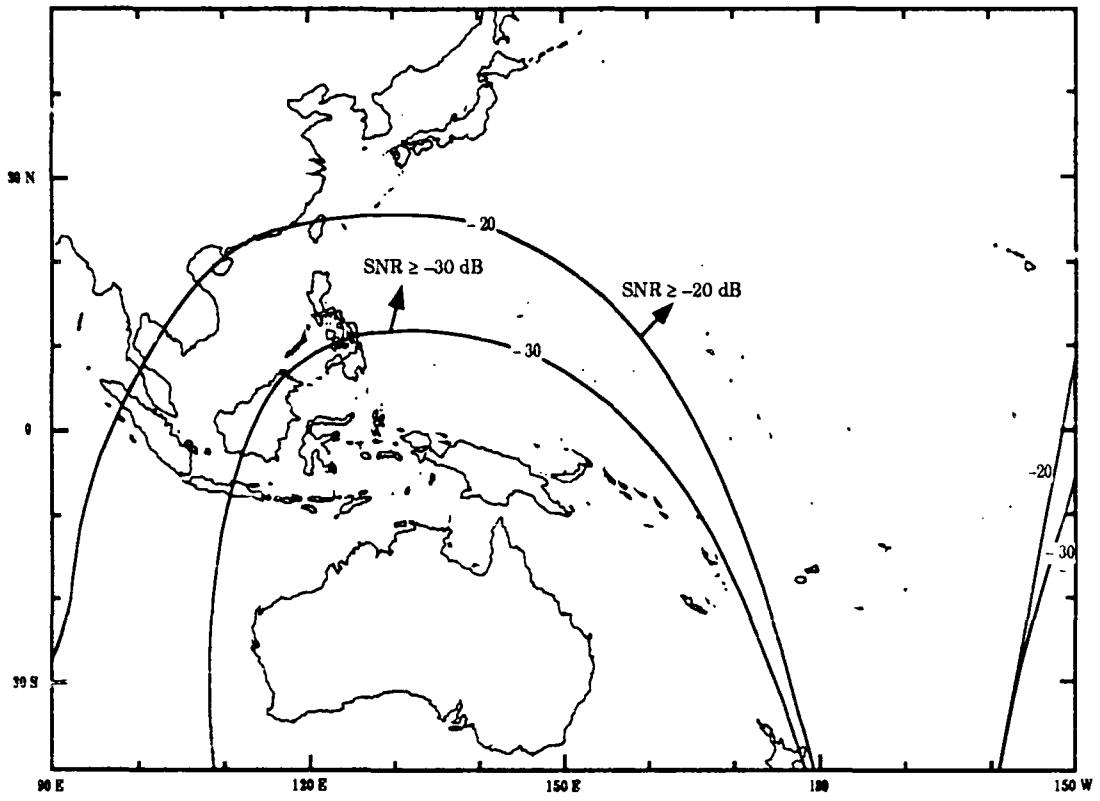

Figure 3-26. Norway SNR Coverage in February at 0600 GMT

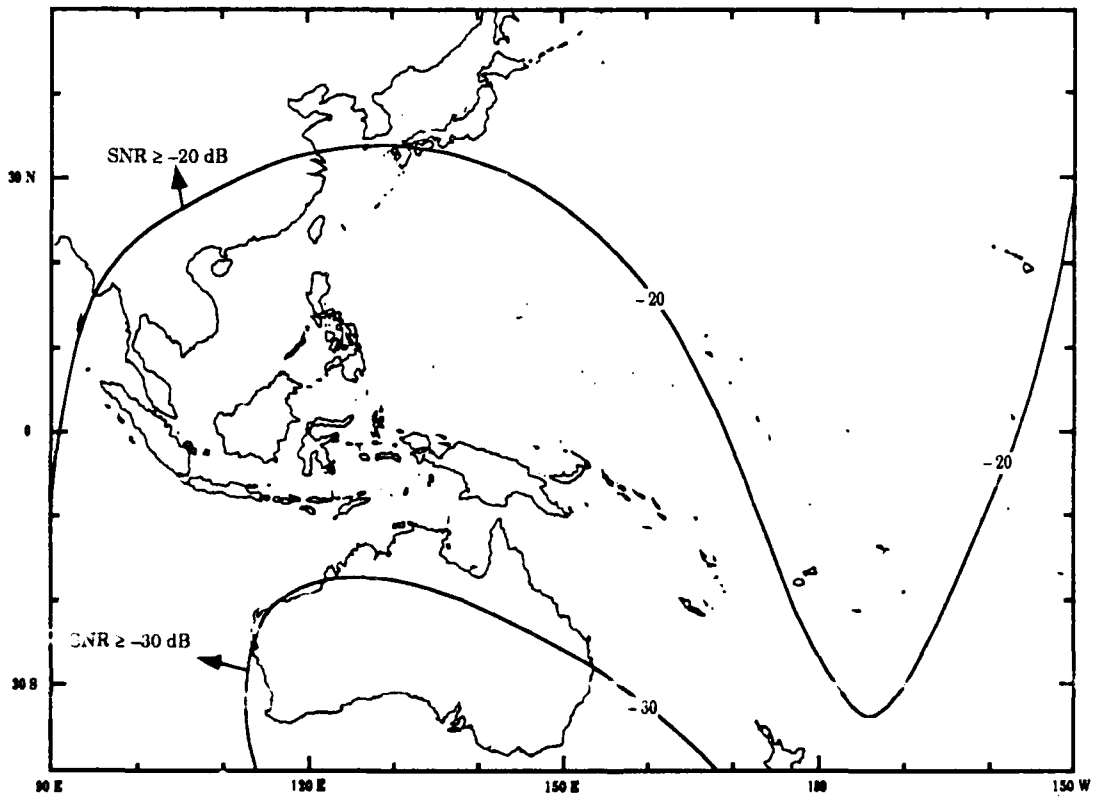

Figure 3-27. Norway SNR Coverage in May at 0600 GMT

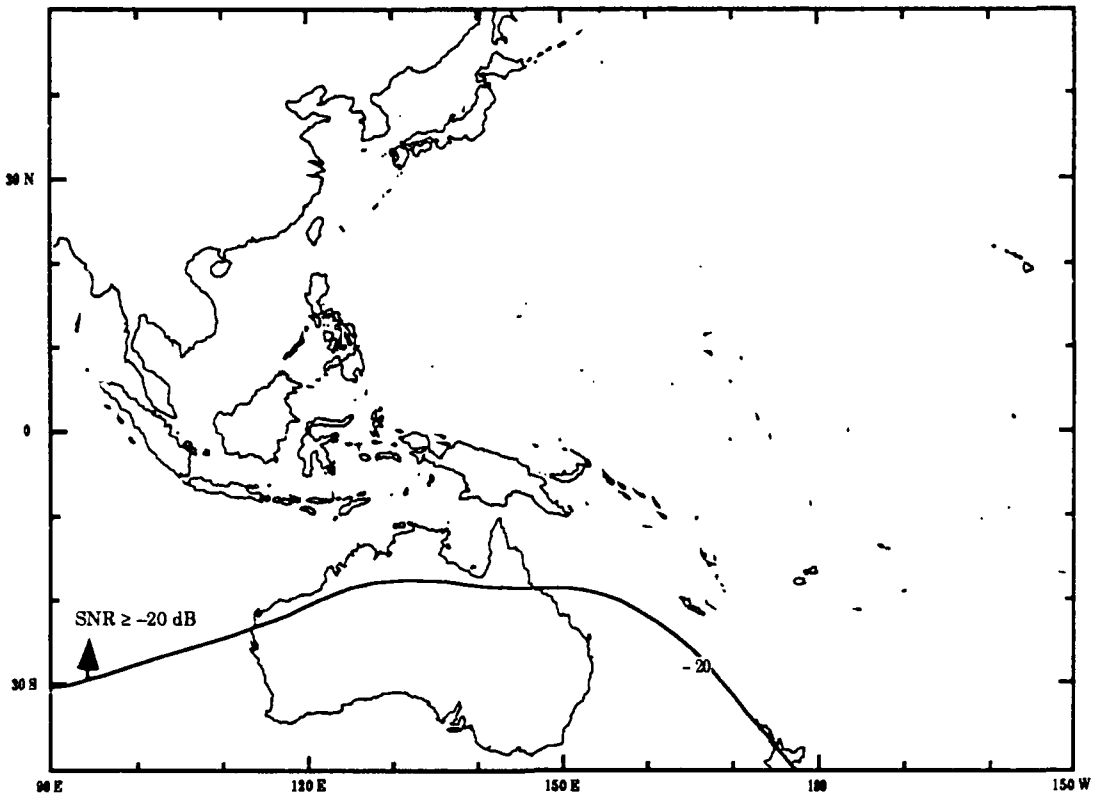

Figure 3-28. Norway SNR Coverage in August at 0600 GMT

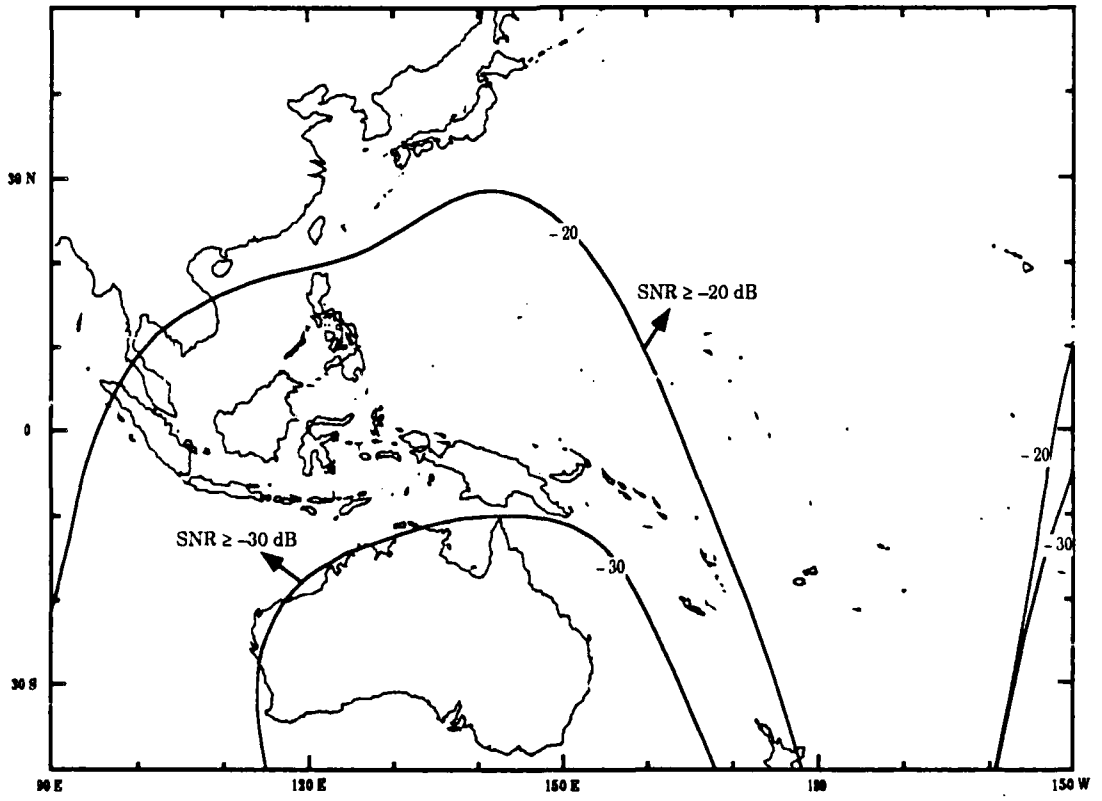

Figure 3-29. Norway SNR Coverage in November at 0600 GMT

For Japan, the –20 dB SNR contour extends in February at 1800 GMT from just south of Jakarta to the east and then curves south just east of 120°E longitude. Otherwise good coverage is maintained.

In summary, the La Reunion, Australia and Japan signals generally provide good predicted SNR coverage, with the Australia signal possibly slightly below –20 dB SNR during May and August north of an arc from Singapore to Tsushima, Japan. The North Dakota and Argentina signals are predicted marginal or not usable. Hawaii is predicted below –30 dB SNR in our focus area in the local afternoon and early evening during May through August. The area of marginal SNR for Liberia is mostly to the east of the modal zones for Australia and Japan. The Norway coverage remains the major concern because of needed coverage when Hawaii, Australia and Japan are modal.

While focusing much of our analysis on Norway signal coverage, we emphasize that all predictions have much in common. They all use the same noise model, thus the noise over the area is the same for any given date and time. The propagation model is the same, thus any observations of signal strength relative to predictions would be applicable to calculations for other stations and paths.

In reviewing the Norway coverage contours shown in Figures 3-26 through 3-29, we are surprised that the best coverage occurs in August and the poorest in February. While we have no details, we expect the signal strength calculations vs. location to be the same for each of these months; i.e., that of a daylight path. Thus any variations must be due to noise.

The Cubi Point measurements and noise predictions provide a good test. The Darwin and Singapore measurements, while not as complete, help to provide confirmation. First we examine measurements of signal level as shown in Figures 3-30 and 3-31 for Cubi Point and Singapore, respectively.

Shown in the top graph of these figures is the average received signal level versus time for the data intervals indicated. A second data interval is presented in the bottom graph for Singapore. Also marked are sunrise and sunset times for the path end points and the times for TASC SNR contour predictions. We note that the measured signal level varies through the 24-hour period, gradually decreasing after sunrise at Norway and reaching a minimum a few hours after sunset at the receiving site. During sunrise and sunset transitions times the

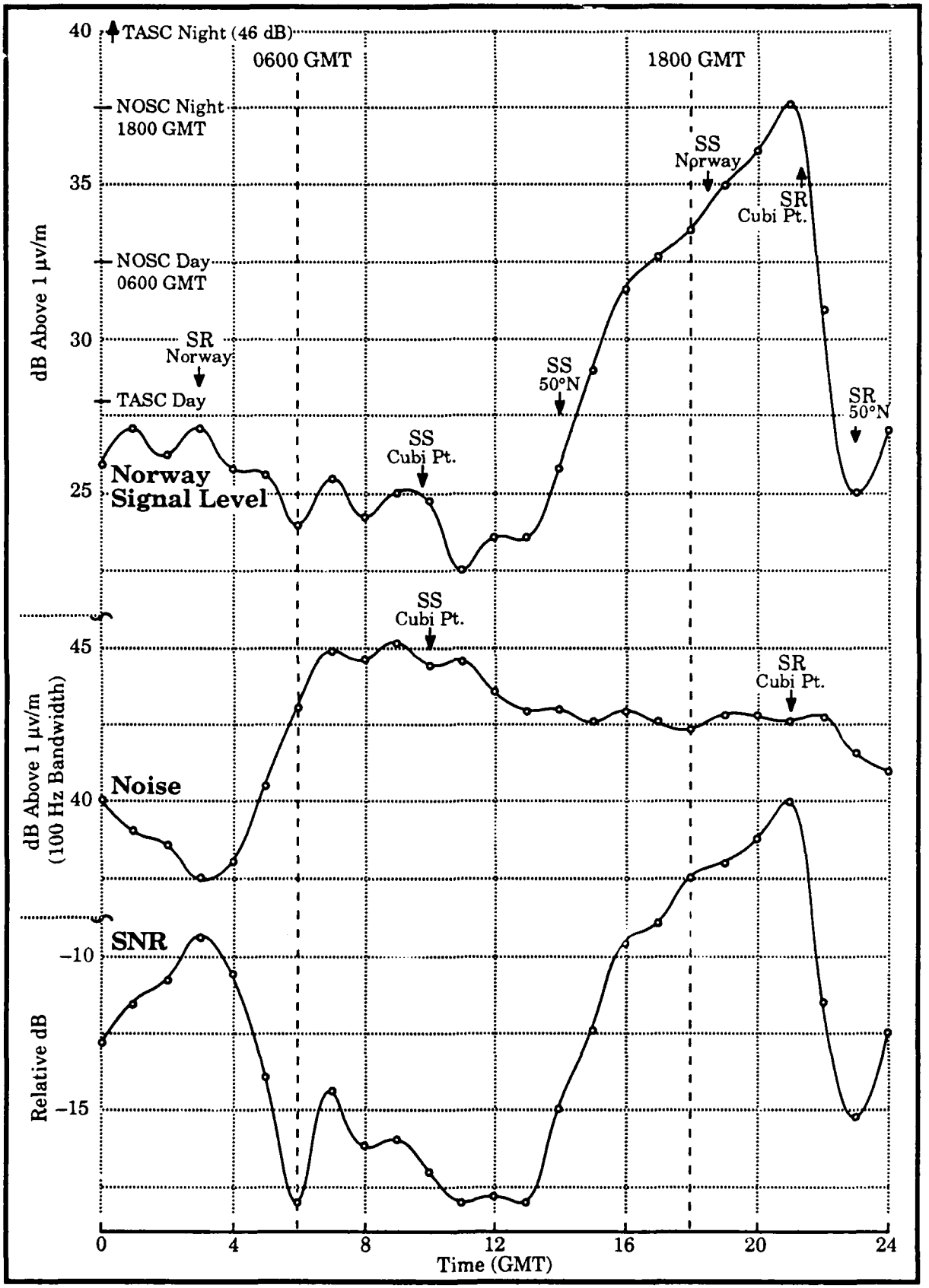

Figure 3-30. Cubi Point Measurements at 10.2 kHz, 8/16 – 9/1; 69° Radial, 7.52 Mm Path Length

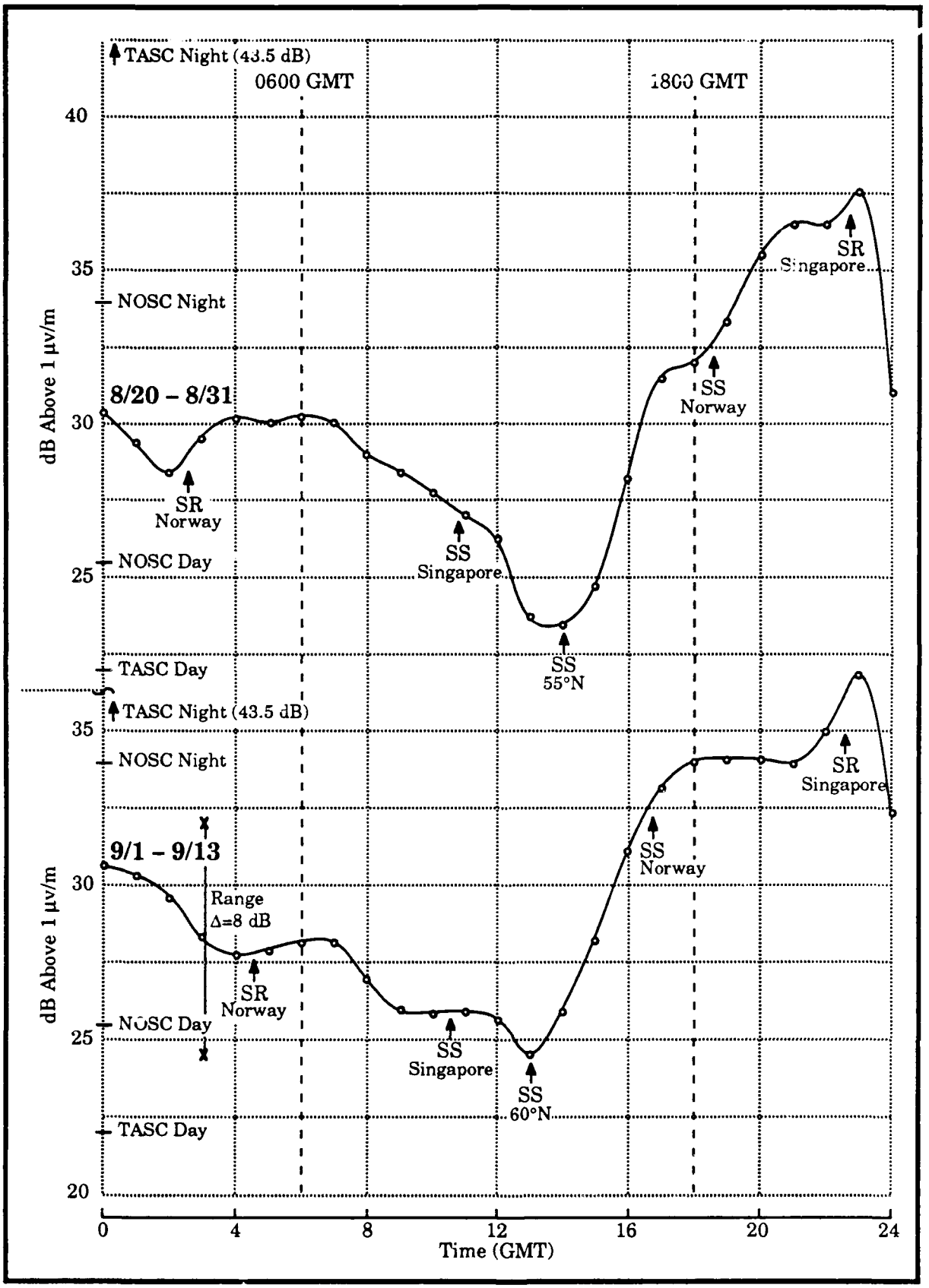

Figure 3-31. Signal Level, Norway at Singapore; 10.2 kHz

amplitude change is relatively rapid, accounting for most of the diurnal change (10 to 12 dB), during the time period where the terminator intersects the path below 60°N latitude. However during daylight, the amplitude continues to decrease; a larger decrease is noted at Singapore. On the vertical scale we note signal levels computed by NOSC (J. Bickel, private communication) and TASC (GUPTA 1988, Ref. 23). The TASC calculations are those used by us for our modal analysis and probably were not used for the SNR coverage diagrams. We note that at Cubi Point, both calculations are high for the 0600 GMT (daytime) prediction while at Singapore, the NOSC calculation value is close to the minimum signal observed (1400 GMT) and the TASC value is a few dB below. This example of a comparison of calculated signal levels with measured is typical for this analysis. Differences of 4 to 5 dB are frequently observed, thus we would conclude some refinement is desired for reliable signal level prediction.

The 1800 GMT prediction is more typical of night propagation, although it is noted from both figures that not much stable night occurs on these paths at these times. The NOSC calculations for night are within the measured range of values while the TASC predictions are 8 to 10 dB too high. For prediction purposes we note that in late August and early September, the Norway signal levels are weakest during the periods of strongest noise.

In Figure 3-30 we show the measured noise and SNR for the last two weeks of August. This noise is also shown in comparison with noise for other months in Figure 3-22b. Here we note that the SNR pattern between 0000 and 1300 GMT largely reflects the noise pattern. Between 1300 and 2400 GMT the pattern more closely follows the signal level pattern. We note that the SNR reaches –18 dB at its lowest. From all of the measurements we conclude that the noise at 0900–1000 GMT is representative of worst case noise for all months.

Next we examine signal levels and SNR at Cubi Point for the 0600 and 0900 GMT times for various months where data are available. As shown in Figure 3-32, the signal levels are reasonably constant throughout the year at both times. The January and February levels are about 3 dB higher; we believe due to night or near night conditions at Norway. The SNR is highest in late January at both times being –6 and –8 dB for respectively 0600 and 0900 GMT. The February values are –8.5 and –14 dB for the same respective times. In June, July and August, typical values of SNR for 0600 GMT are –20 dB. The values at 0900 GMT

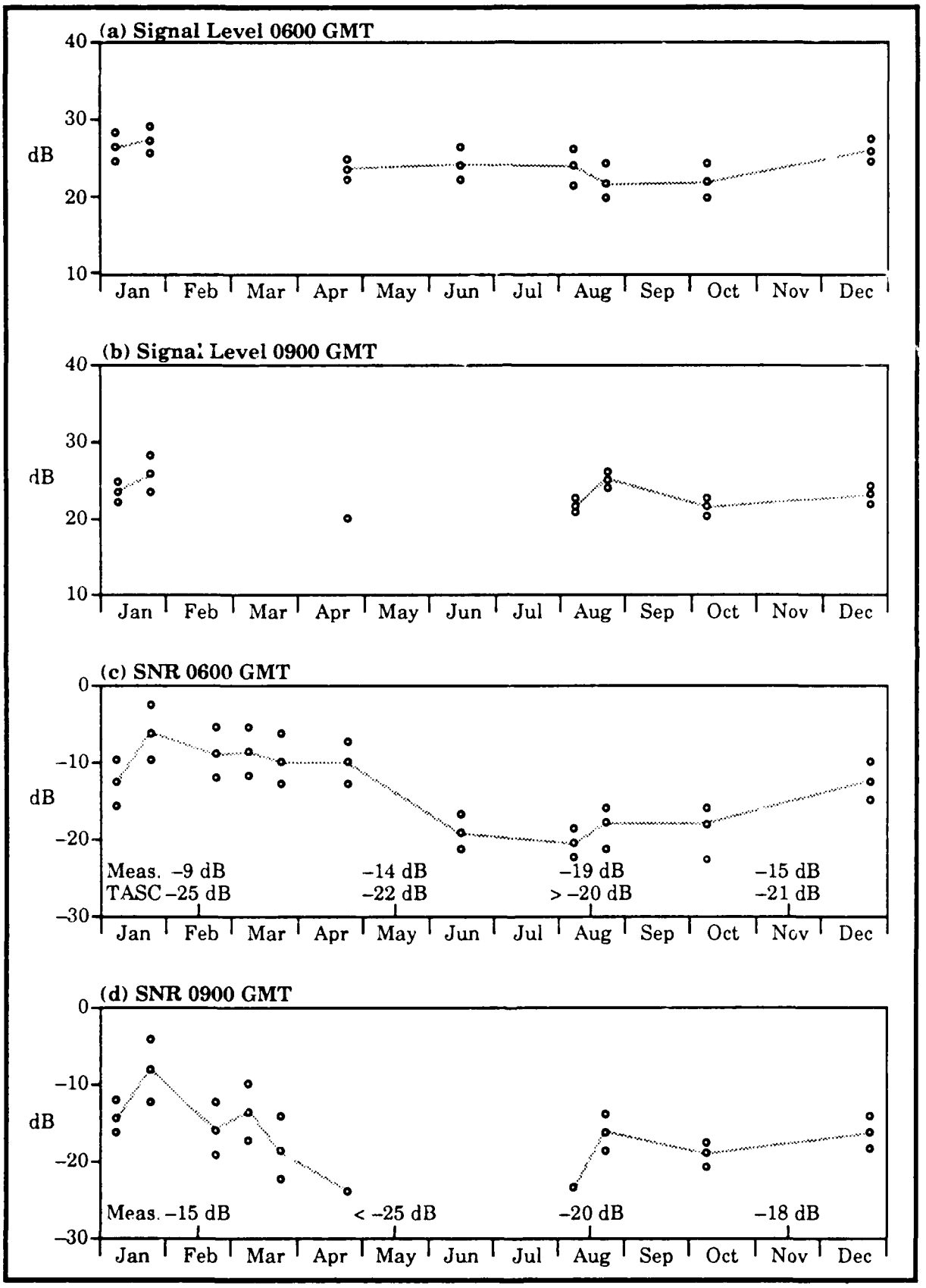

Figure 3-32. Norway Measured Signal at Cubi Point, 10.2 kHz

are below measurement threshold (about –25 dB) except for the last part of August where –16 dB is recorded. We note that the SNR level reached –18 dB at 1100, 1200 and 1300 GMT for this two week interval.

From this example and other analysis, we conclude that the seasonal trends shown by the predictions for 0600 GMT are not correct. Assuming that the measured SNR is representative of long term averages, the –20 dB contour should be placed north of Cubi Point at 0600 GMT from mid May to mid August. The –30 dB contour probably is near Cubi Point between 0900 and 1300 GMT during June and July. By 1300 GMT the Australia and Japan signals have been in total night for three hours. We would expect these conditions to be representative across the South China Sea at 15°N latitude.

We do not have good data over a sufficient season span at either Darwin or Singapore to conduct a detailed analysis. Darwin data show that SNR can drop below tracking threshold in May, June and July. We have no December, January or February measurements, but our examination of literature showing occurrence of thunderstorms strongly indicates that most of the noise incident at Darwin is generated north of Australia for all months.

For these reasons, we would expect the –20 and –30 dB SNR contours for Norway to lie north of Australia during the Austral summer, but well south of our area of special interest.

In summary, the evidence shows that the SNR coverage predictions for the Western Pacific should be used with much caution. Coverage is only a problem when the Australia and Japan paths are modal, i.e. at night on these paths. During months of high noise (June, July and August), the data suggest that the Norway signal SNR can be insufficient for at least those hours into the modal periods for Australia and Japan. All noise measured at times of peak amplitude was less than predicted for the respective locations. If the noise per chance, was below average during the validation measurements, the situation could be worse than we surmise.

3.5.6 SUMMARY

The Western Pacific provides the exception to the generalization that redundant SNR coverage exists for Omega signals. Two sites, Japan and Cubi Point, incur

times when the possibility exists that only two station coverage is available. At Yap three station coverage is measured for some time intervals. Such a condition does not allow for any station off-air time. The predictions generally confirm the analysis of SNR data. However, the model differs from observation in several important respects. Also the times selected for prediction do not cover the worst case situations.

3.6 SIGNAL TIME AVAILABILITY

The analysis to this point compares data with models that are basically static in time. Time dynamics is a very important factor that somehow has to be added. We must rely heavily on measurements and extrapolation to locations of interest. The measurements made close to a location of interest can help us estimate when in the diurnal cycle various phenomena are likely to or can occur and how this might relate to a propagation path's orientation with respect to its modal zone boundary. Extrapolation is used because it is the only means we have to geographically translate findings.

Much of the data indicate that modal effects, when present, can occur from near the beginning of sunset on the propagation path to near the end of sunrise on the path. Modal effects are observed to be somewhat ionosphere-dependent, as noted by the percentage of occurrences. These percentages are expected to change as the seasons progress. Some of the boundaries are thus expected to move; the question is how much.

Long-path interference depends upon relative illumination of two paths. The maximum extent of long-path occurs when the short-path has the greatest ratio of daylight.

Our goal here is to simply place our findings in perspective in reference to navigation use. More refinement is needed to provide guidance for actual navigation. Our interpretations are not sufficiently refined to show time variability of signal quality as a function of location. For this reason we only provide one representative location; this is for a receiver a' [illegible]'N, 112°E.

In Figure 3-33, we show time availability of all eight stations for this selected location for two months, August and February. Shaded rectangles indicate times

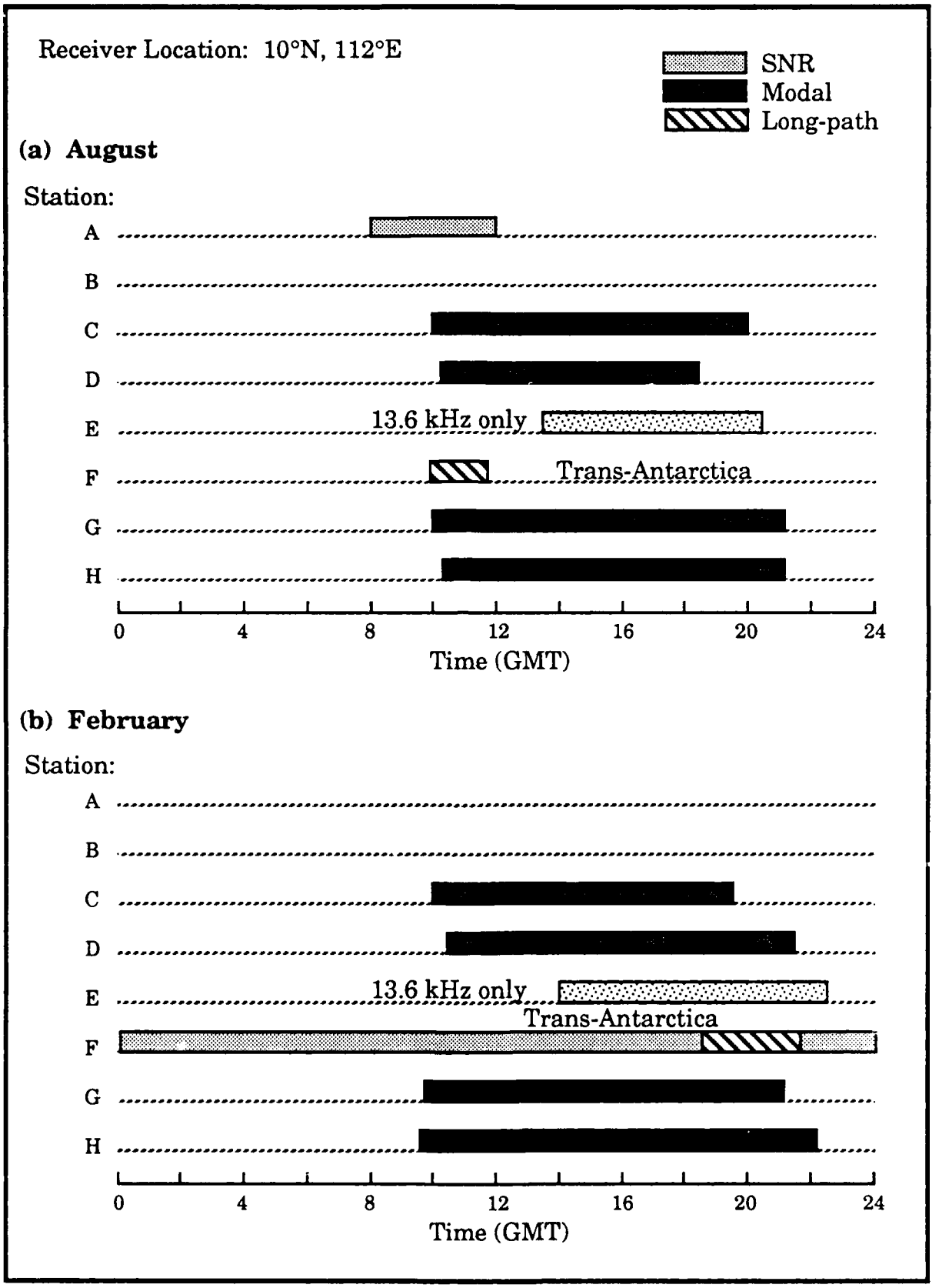

Figure 3-33. Times Requiring Possible Signal Deselection

when we predict degraded signal quality for each signal. The cause of degradation is indicated by the keys. We do not expect the La Reunion signal to be modal at this location but it could be slightly modal further west at 13.6 kHz. If it were modal the times of occurrence are predicted by the shown rectangle. Also note that in February the all-day path across Antarctica for the Argentina signal causes its level to be too low to receive.

This figure clearly shows that the occurrence times of reduced signal quality have considerable overlap. It is for the reason we claim that the western one-third of this validation region is a real problem area for nighttime Omega navigation. We point out that if a deselection model is based upon 4-hour time blocks (a common choice for predictions), deselection would be required for 4 of the 6 blocks.

3.7 NAVIGATION ACCURACY ASSESSMENT

3.7.1 OVERVIEW

In undertaking the accuracy assessment phase of this validation, our perspective is that the nominal accuracy of OMEGA has been well established in past validations. We expect that the demonstrated accuracy is valid in the Western Pacific validation region. For this reason we have chosen a new emphasis for accuracy assessment. In previous analyses, the available database was essentially processed into statistical compilations of measured LOPs and compared with predictions. In contrast, we have made spot checks using small data samples and representative locations and conditions. Our method, while confirming accuracy, is to primarily identify deviations from predicted accuracy and to focus on factors that can lead to improved utilization of Omega. This section, with the amplifying support of Appendix E, presents highlights of our findings.

3.7.2 DISCUSSION

In order to conserve resources and to focus on the principle objective (that of flagging deviations from predictions), we have been very selective in data processing. First, signals that have been identified as having problems from the other analysis (trans-equatorial modal, long-path interference or trans-polar) were not examined in this phase. Second, spot checks and quick scans were made to confirm close agreement with predictions. When the data did not meet our expectations

a more detailed analysis was undertaken. Generally our expectations were based upon predictions and what we considered reasonable variability due to propagation effects. Where trends are noted, we use illustrative examples to describe the observed effects.

The analysis reported in Appendix E consists of two major parts:

(1) Samples of tabulated two week segments of phase-difference data which are compared with the computed PPCs (Propagation Phase Corrections) to illustrate observed trends, and

(2) Samples of measured LOPs acquired during ship transits showing navigation fix accuracy and illustrating observed trends in signals.

We are unable to examine phase data, thus we make use of phase-difference data. This type of analysis does not allow us to attribute observations of the propagation to a single path. The illustrations provided, both fixed site and the shipboard measurements, are from receiving sites not having an atomic reference oscillator. As a result, the interpretation of deviations from predictions is more complicated than with the South Pacific validation analysis.

3.7.3 SUMMARY OF ACCURACY ANALYSIS

We found that, except for a few significant exceptions to be described, OMEGA phase-difference accuracy is as specified. When signals are good, the median values are close to predicted and the deviation from the median is quite small; well within 15 CECs for the median, 10 CECs deviation from the median during midday on a path, and 25 CECs deviation at night. The observed day/night phase change generally was not as close to the predicted.

One significant exception is observed biases during the day/night transition times. Systematic deviations from predicted phase were observed. As shown in Appendix E with several examples, all diurnal transition periods could benefit from adjustments.

Many of the good signals in the Western Pacific validation region undergo long transition times. For this reason, improving navigation accuracy for these times has added significance. The observed biases, occasionally as much as 30 CECs, appear to be reducible through improved calibration.

For a range of locations, the selection of "good" is highly limited. Several measurements show that both phase disturbances and SNR are a serious problem. The ship transit data confirm the navigation problems evidenced at fixed sites.

Over much of the area, the phase-difference data do not fit predictions as well as expected. We suspect that some modal effects are involved, but in general the equatorial ionosphere may be different. We take this evidence as a flag to more thoroughly check propagation outside the predicted conversion zones. We concentrate so heavily on conversion effects that any other phenomena are not given due attention.

Overall, these findings fit the patterns established in other sections of this report and previous validations. OMEGA generally provides the navigation accuracy expected. Further improvements to propagation predictions can and should be made. Our increasing knowledge of VLF propagation and its attended geophysics, adds to the awareness of complex factors determining the quality of navigation signals and consequently to our ability to refine navigation guidance.

4.0 INTERPRETATION OF VALIDATION ANALYSIS

This section places validation findings in perspective with expectations and other coverage predictions, and states specifically what was found to agree or disagree with those expectations and predictions.

In this section a comparison is made between the analysis findings reported in Section 3 as related to our *analysis model* and the two principal types of coverage prediction models: the *coverage overlay* (GUPTA et al 1980(a), Ref. 21), and the *parametric prediction* (SWANSON 1983, Ref. 1). The later two prediction models have been available for some time and are used in navigation planning and analysis. Charts of each model prediction, showing individual station signal coverage of good quality phase, are presented as part of the comparison (for example, see Subsection 4.2, Figures 4-4, 4-5, and 4-6).

4.1 PREDICTION MODELS

The foundation on which these models are built is highly complex. The reader is referred to the referenced documents for a description of model details. All three predictions are based primarily on theoretical models with feedback derived from measurements. Each theoretical model relies heavily on the fullwave propagation computational techniques developed at NOSC. In addition, in the development of each model, extensive use has been made of calculations prepared by TASC. Different sets of calculations made at various times were used by the different developers. Each model incorporates expert judgment of the developer.

For each model only those features which address signal self-interference are considered. Again we emphasize that modal interference occurs at night on the short propagation path, while long-path interference occurs during the day on the short-path. For the coverage Overlay Model, the display used is the predicted boundary line beyond which phase deviation is predicted greater than 20 centicycles (CEC). For the Parametric Model, symbols are used to geographically present navigation signal quality. Table 4-1 defines the symbols used in the charts. The symbols of particular interest are (N) for Near interference, (M) for Modal, (L) for Long-path, and (–) for Disturbed. We note that the Parametric Model covers only 10.2 kHz predictions.

Character	Limitation/ Meaning	Elaboration
N	Near	Within 1 Mm of the station and potentially subject to skywave-groundwave interference
A	Antipode	Within 2 Mm of the antipode and subject to antipodal interference
#	No Signal	SNR worse than –40 dB in 100 Hz bandwidth
M	Modal	Second mode dominates or is within 1 dB of first mode
L	Long-path	Long-path dominant or equal to short
–	Disturbed	Unwanted self-interference within 10 dB; either long-path or second mode
3	SNR in –30's	$-40 < \text{SNR} \leq -30$ dB in 100 Hz bandwidth; Usable with a well installed good receiver
2	SNR in –20's	$-30 < \text{SNR} \leq -20$ dB in 100 Hz bandwidth
1	SNR in –10's	$-20 < \text{SNR} \leq -10$ dB in 100 Hz bandwidth
0	SNR in 0's	$-10 < \text{SNR} \leq 0$ dB in 100 Hz bandwidth
Blank	Loud and Clear	Signal should be well received by a poorly installed mediocre receiver under water

Table 4-1. Parametric Coverage Display Code

4.2 COMPARISON OF THE VALIDATION ANALYSIS WITH COVERAGE PREDICTIONS

The analysis findings are compared with the two published models, addressing in sequence the predictions for each station. For the following discussion, the prediction models described above are called the Analysis Model (developed in Section 3), the Overlay Model (GUPTA 1980(a), Ref. 21), and the Parametric Model (SWANSON 1983, Ref. 1). The process is to compare the predicted coverage for each station by showing a selected figure for each model and by discussing the findings in relation to the models.

(A) NORWAY

For Norway signals, all models (Figures 4-1, 4-2 and 4-3) show that the region is essentially free of modal effects.

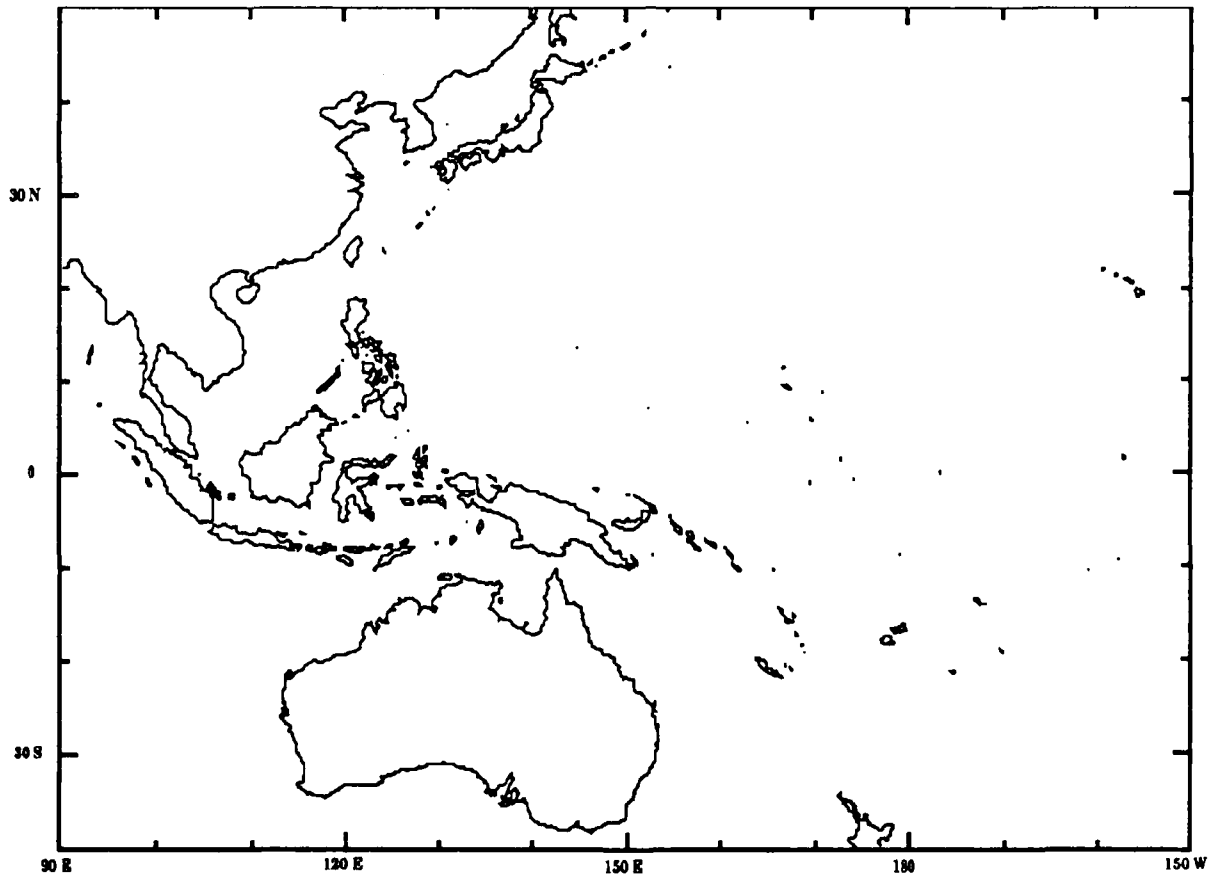

Figure 4-1. Norway Signal Modal Free Area; Analysis Model

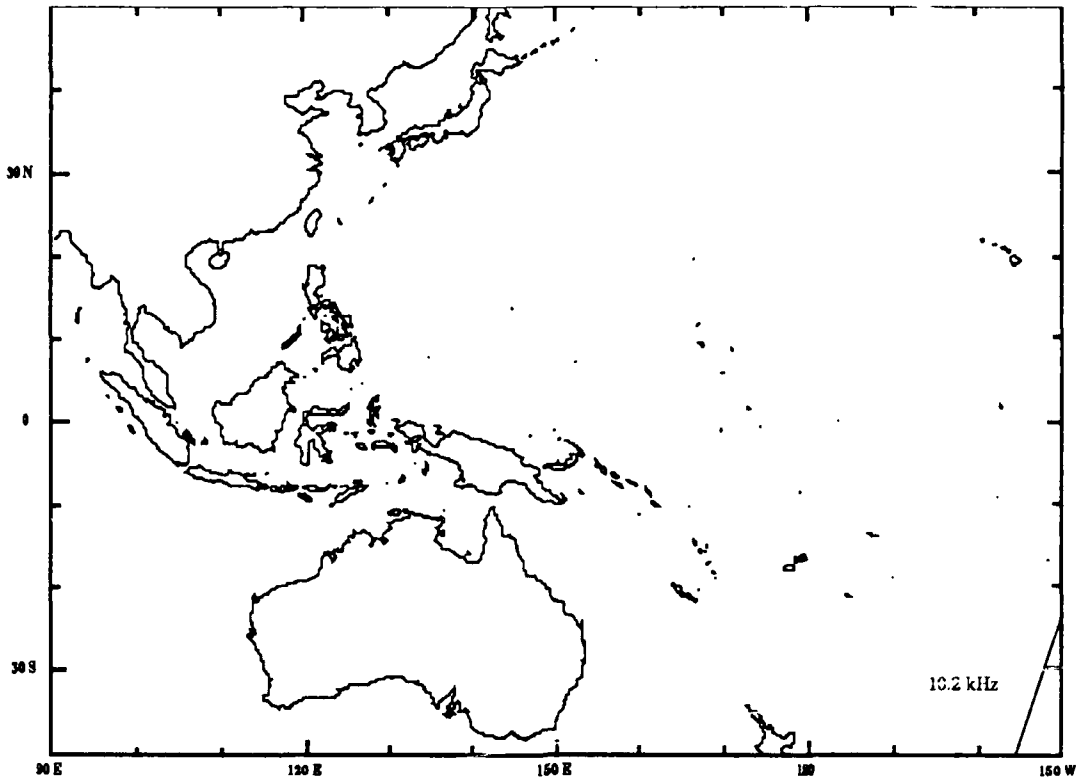

Figure 4-2. Norway Signal Modal Zone; Overlay Model

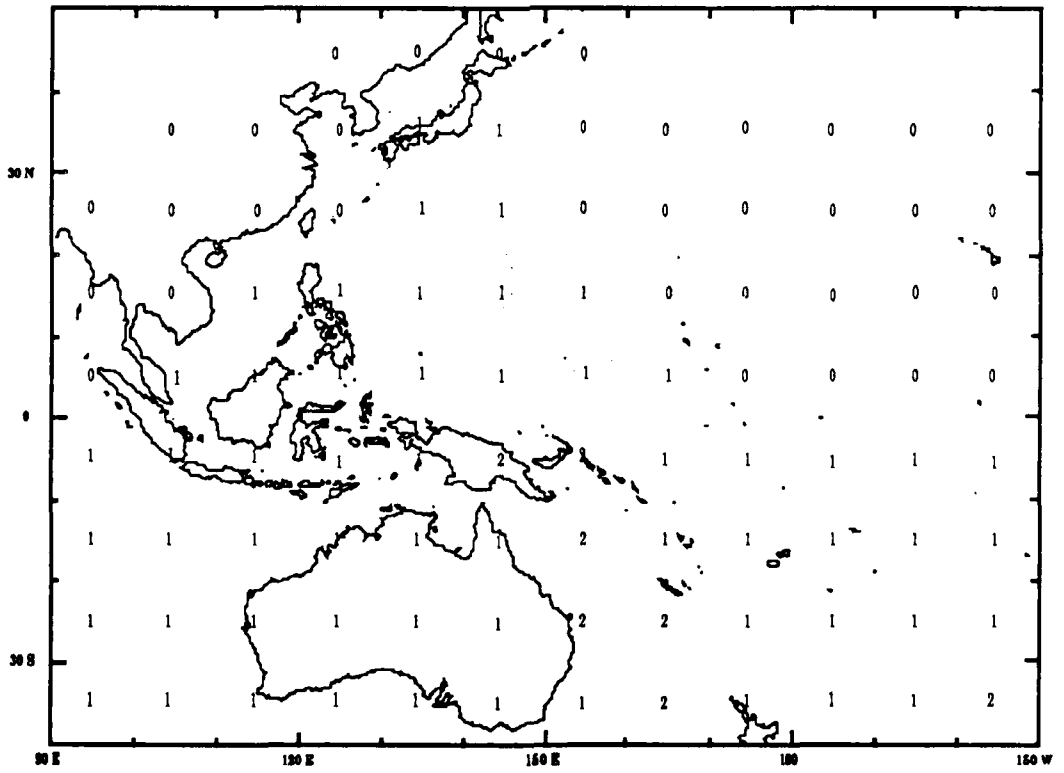

Figure 4-3. Norway Signal Quality; Parametric Model

(B) LIBERIA

The Analysis Model (Figure 4-4) places the modal effects for both 10.2 and 13.6 kHz on the same boundaries. The Overlay Model (Figure 4-5) shows the 10.2 kHz signal to extend further west than the 13.6 kHz signal. The difference in boundary placement is within the area we attribute to shadow effects from the arctic and antarctic ice caps. We have no measurements and no reason to show boundaries different from the Overlay Model for these signals. The Parametric Model (Figure 4-6) shows a slightly more restricted modal zone to the north and to the west of Hawaii. We have no data to determine which prediction is better. Our model for modal effects requires the propagation path to be all at night from Liberia to a location in this area. Since these paths are near 20 Mm long, the condition cannot exist for very long during each day. The practical result is that the difference between our model and the Parametric Model is of little consequence.

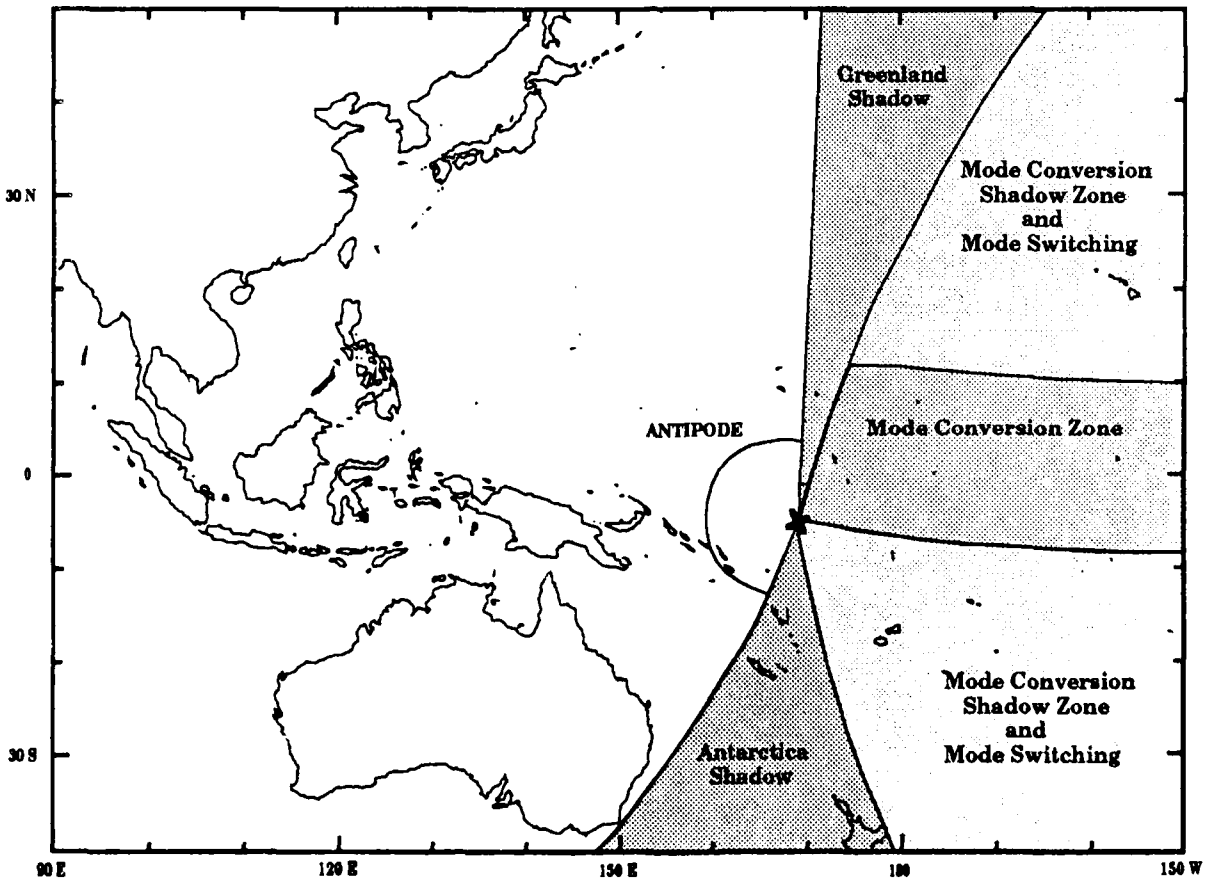

Figure 4-4. Liberia Signal Modal Zones; Analysis Model

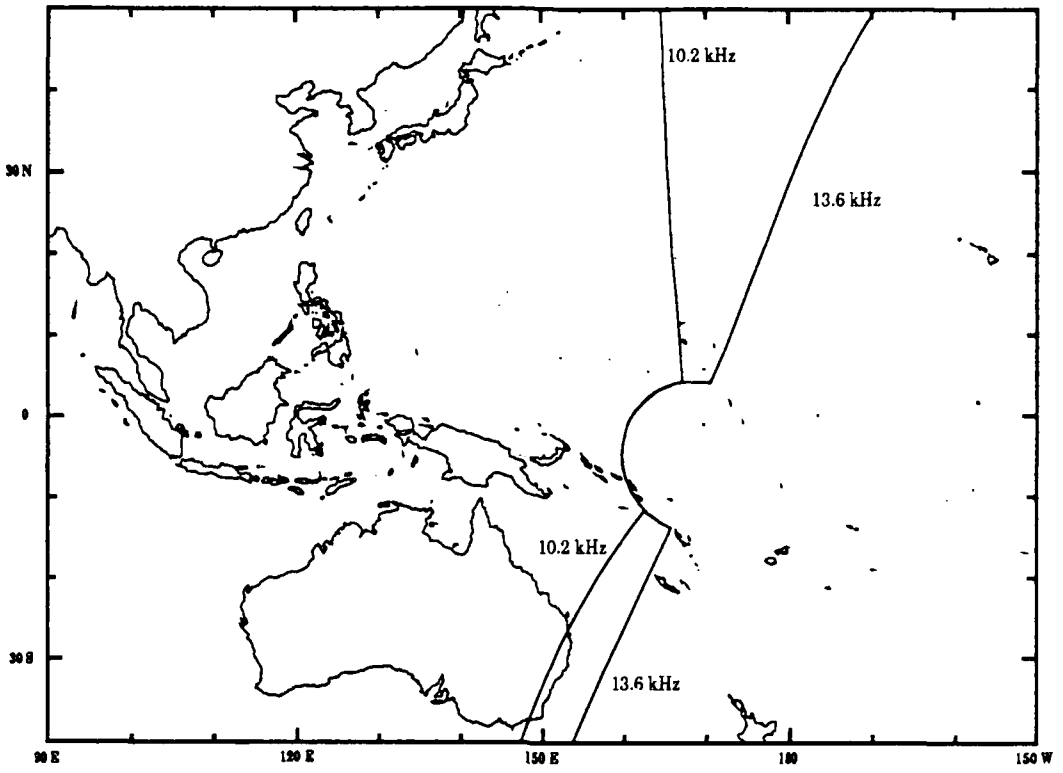

Figure 4-5. Liberia Signal Modal Zones; Overlay Model

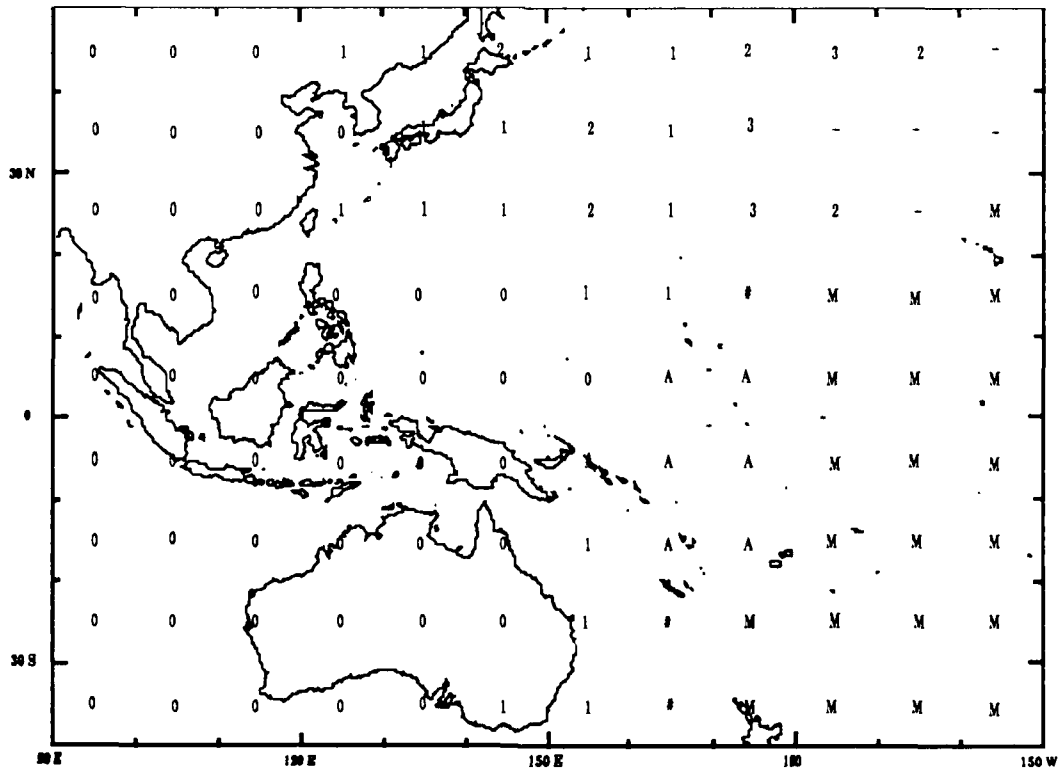

Figure 4-6. Liberia Signal Quality; Parametric Model

Not shown on any of these figures is that when the paths to the antipode from the east are mostly in daylight, much of the region east of the antipode is dominated by long-path. Also not shown, is that when this path is primarily night propagation, the long-path to the west extends as far as Brisbane. We are not aware of any models that predict the extent of the long-path this far west.

(C) HAWAII

For Hawaii the Analysis and Overlay Model predictions are largely in agreement for placement of the modal-zone boundaries (Figures 4-7 and 4-8). The Overlay Model places the 13.6 kHz near modal zone boundary further north than the Analysis Model. Also, the 10.2 kHz northern boundary slopes up to pass through Japan. Measurements at Japan support the placement of this boundary. We expect that this boundary is different from that of the equatorial mode conversion zone. We have not had the opportunity to explore the use of waveguide calculations to attempt to model this observation. In the southeast corner of the region the Overlay Model separates the boundaries for 10.2 kHz and 13.6 kHz signals. We do not see evidence for this separation in the flight data. The measurements show that this boundary needs to be placed farther east than any of the models place it. The 13.6 kHz boundary of the Overlay Model is a good estimate for all frequencies.

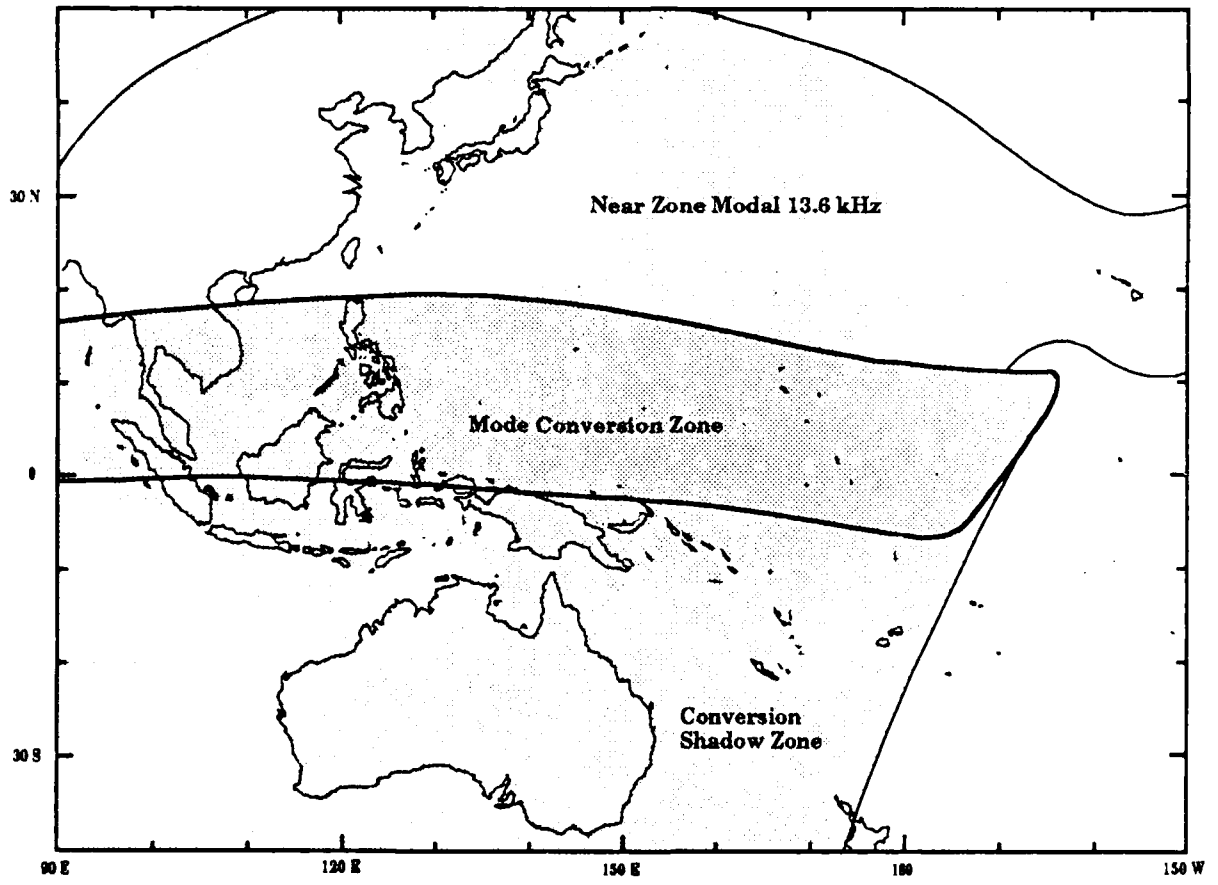

Figure 4-7. Hawaii Signal Modal Zones; Analysis Model

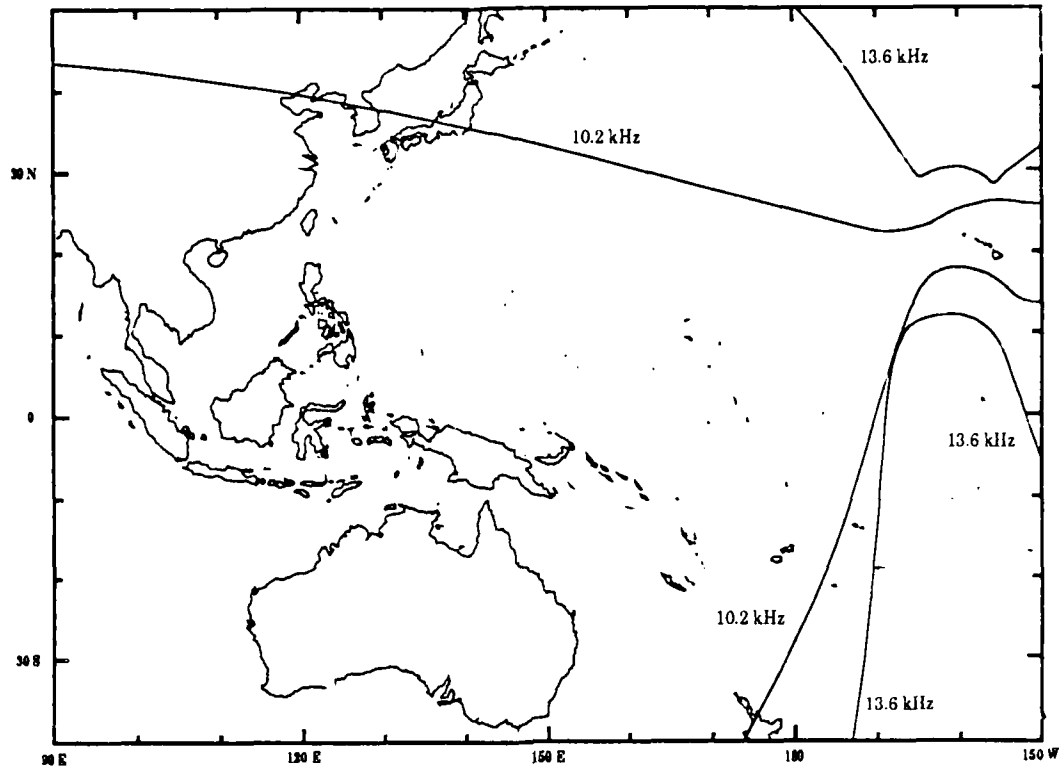

Figure 4-8. Hawaii Signal Modal Zones; Overlay Model

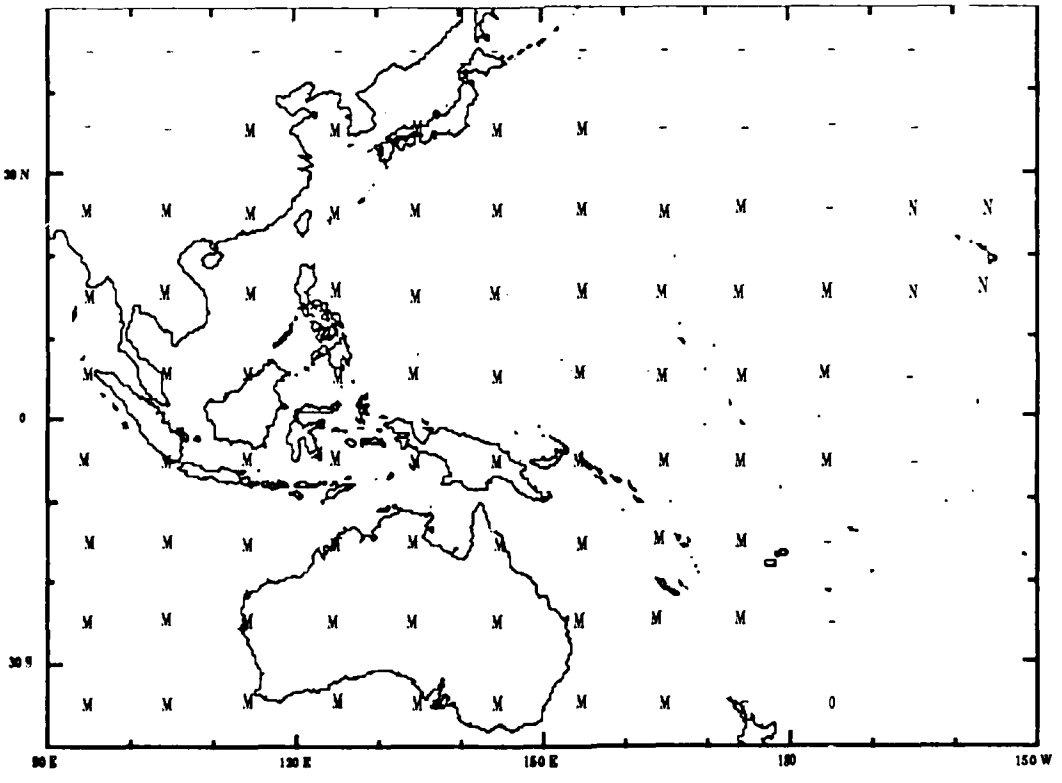

Figure 4-9. Hawaii Signal Quality; Parametric Model

The Parametric Model (Figure 4-9) being for 10.2 kHz shows a modal pattern close to the Overlay Model. Our comparison above for the 10.2 kHz signals is applicable to the Parametric Model.

We note the data suggest that the equatorial mode conversion zone boundary may vary several degrees in latitude with differing propagation conditions. We do not have sufficient data to conduct a good assessment. Until this boundary is better defined, we believe that the zone should be made a few degrees wider than presently placed in the Analysis Model.

(D) NORTH DAKOTA

With respect to North Dakota signal predictions, all three models (Figures 4-10, 4-11 and 4-12) show quite a difference in the shape and extent of the modal zones. In the Analysis Model the northern boundary of modal effects is determined by a geomagnetic boundary for the onset of conversion. We believe this boundary relationship makes physical sense and that the boundary has to be along a constant magnetic latitude, unless the model allows ionosphere parameters to vary with position. The measurements, while showing variability in the boundary, tie the boundary closely to the boundary for Hawaii, both southwest of Hawaii and west of Cubi Point. We also know from measurements that the 10.2 kHz and 13.6 kHz boundaries are close together. At times the modal effects are not as strong at 13.6 kHz as at 10.2 kHz, but we believe the boundaries are the same.

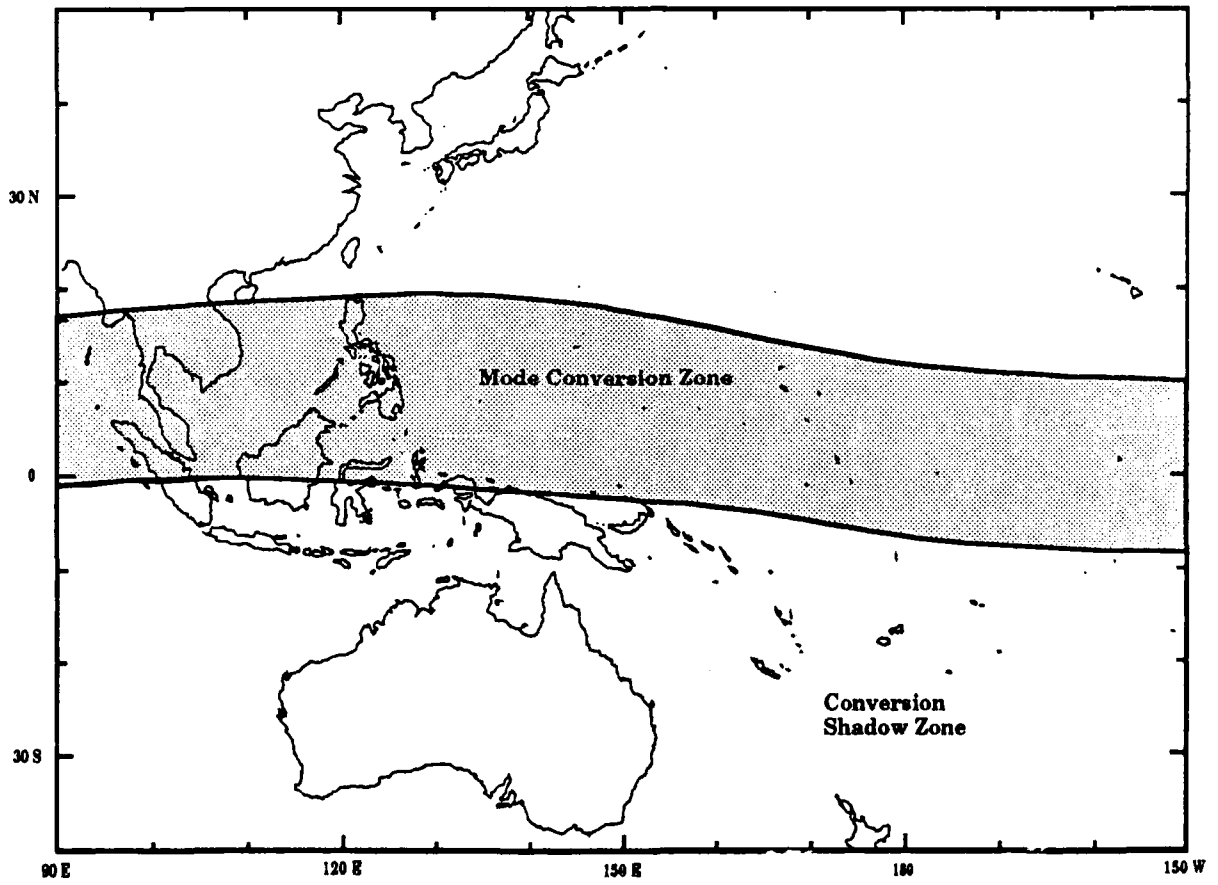

Figure 4-10. North Dakota Signal Modal Zones; Analysis Model

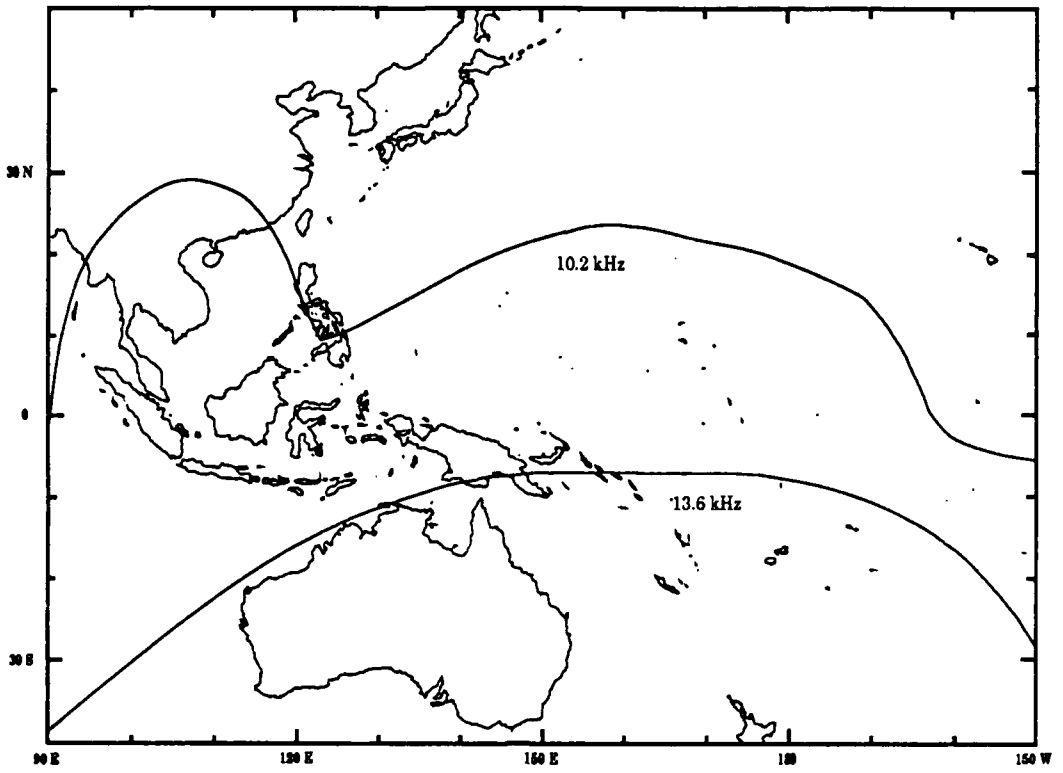

Figure 4-11. North Dakota Signal Modal Zones; Overlay Model

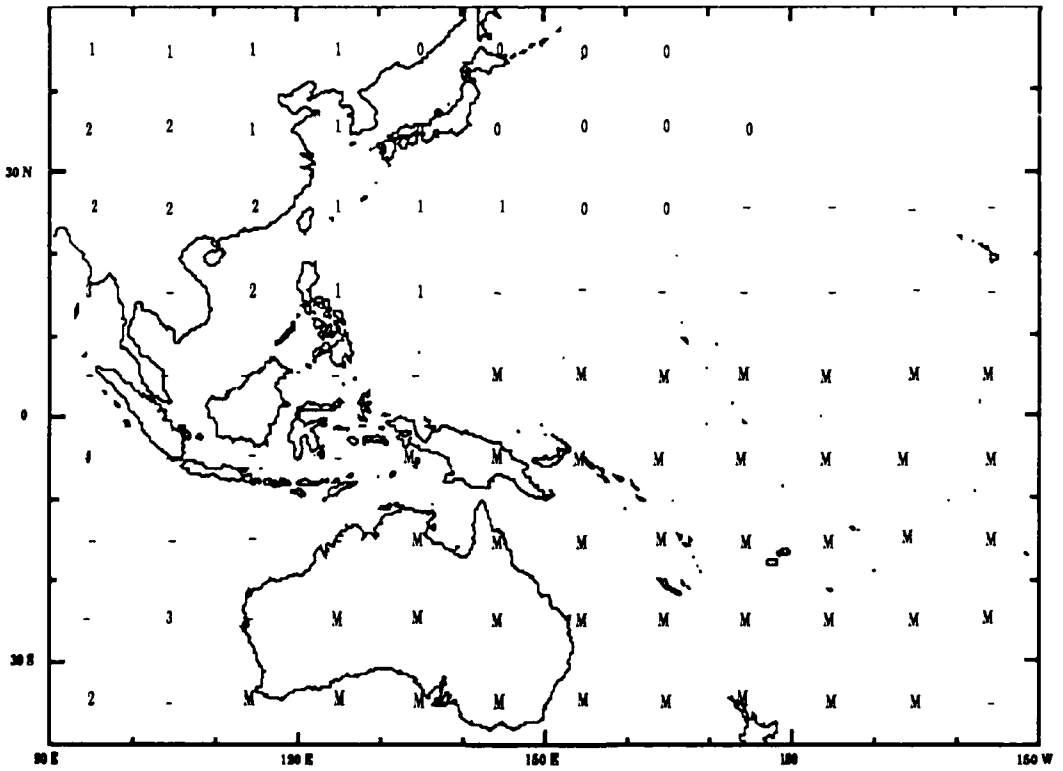

Figure 4-12. North Dakota Signal Quality; Parametric Model

The Parametric Model places the northern boundary further south than does the Analysis Model. Given that we suggest moving the boundary further north by a few degrees, we believe that this difference is significant. The Parametric Model classifies the signal as disturbed to the west of Australia. This is an area with likely strong long-path effects. During local night primarily to the east of the antipode, equatorial zone mode conversion is predicted to occur to radials west of Singapore. Our only check on this prediction is to interpret the prediction in terms of Australia. Measurements show the Australia mode conversion occurring to almost 355°.

Our long-path analysis shows Australia to be within the long-path of the North Dakota signal for about six hours (1800–2400 GMT). This prediction was not confirmed due to lack of suitable measurements.

(E) LA REUNION

Both the Analysis and Overlay Models (Figures 4-13 and 4-14) predict modal interference at 13.6 kHz to extend into the validation region. The Overlay Model predicts the boundary to be slightly further east in the vicinity of the Philippines. Our assessment is that the modal effects are not sufficient to cause excessive navigation errors within the validation zone, yet we caution that our assessment is based upon minimal measurements.

The Parametric Model (Figure 4-15) predicts no modal effects as do the other models for 10.2 kHz.

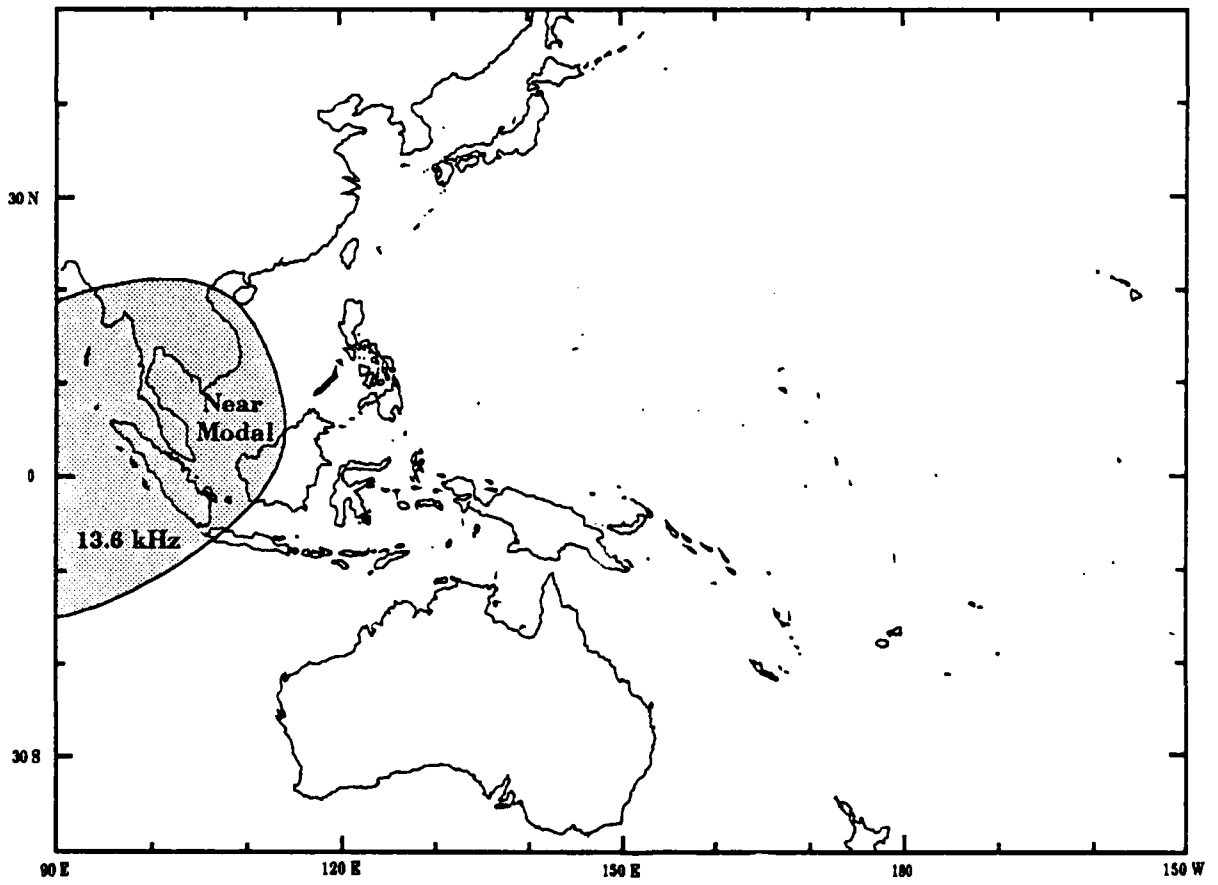

Figure 4-13. La Reunion Signal Modal Zone; Analysis Model

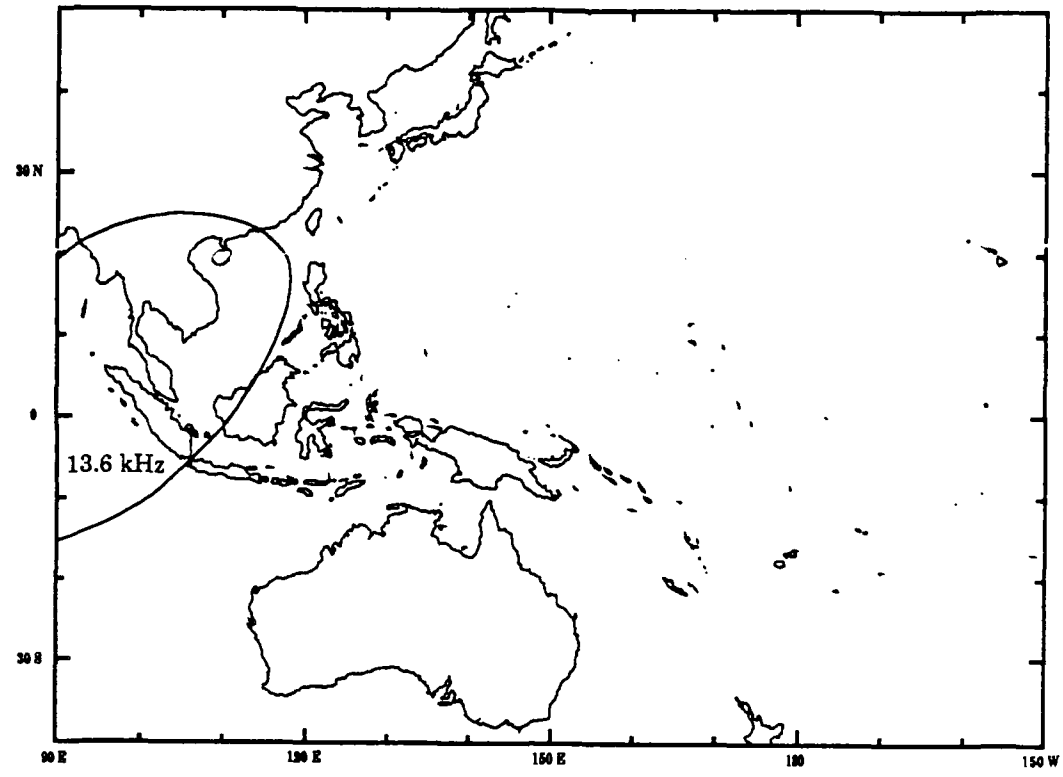

Figure 4-14. La Reunion Signal Modal Zone; Overlay Model

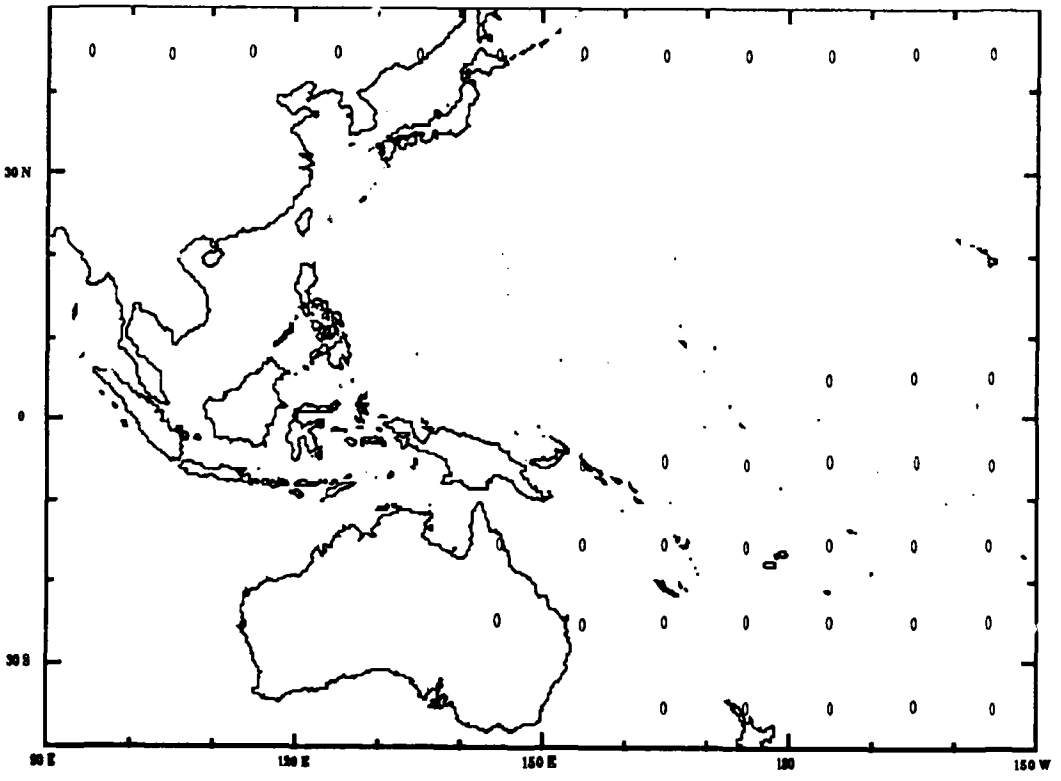

Figure 4-15. La Reunion Signal Quality; Parametric Model

(F) ARGENTINA

The boundary lines for the three prediction models, shown in Figures 4-16, 4-17 and 4-18, look quite different at first glance. However, much of the difference is due to inclusion or separation of different effects. In the Analysis Model we identify separately the different zones and do not include long-path effects. The major difference is the placement of the 10.2 kHz boundary between 150°W longitude and 120°E longitude. This is the south boundary of the equatorial mode conversion zone in the Analysis Model. The eastern edge of the boundary is close for the two models. However, the Overlay Model boundary sweeps a good 10° further north by 150°E and then curves down again almost to Darwin before arching back north to merge with the antipode zone. We suspect that this boundary includes long-path effects; otherwise we do not understand the physical phenomena involved. Some long-path effects can occur during the latter part of the sunrise transition, while night is still to the southeast of the antipode. We

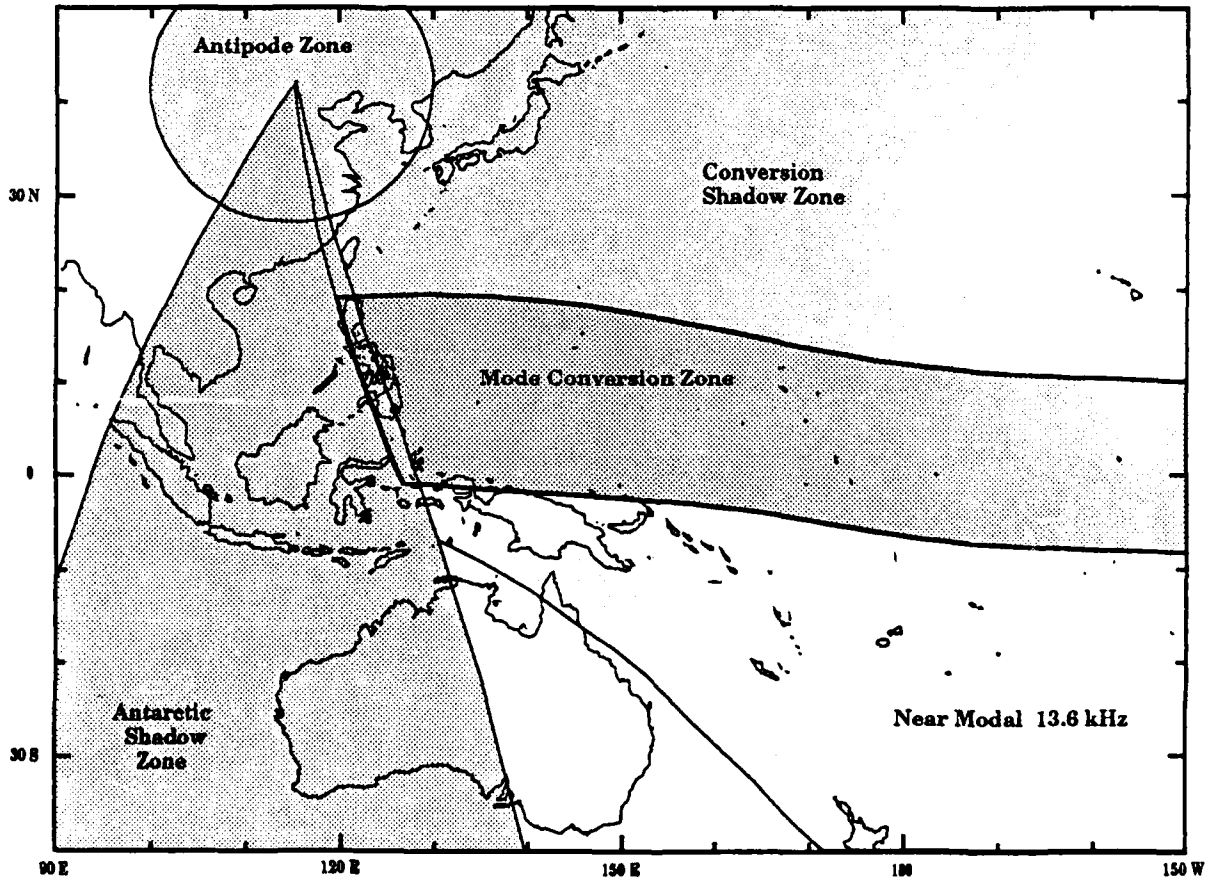

Figure 4-16. Argentina Signal Modal Zones; Analysis Model

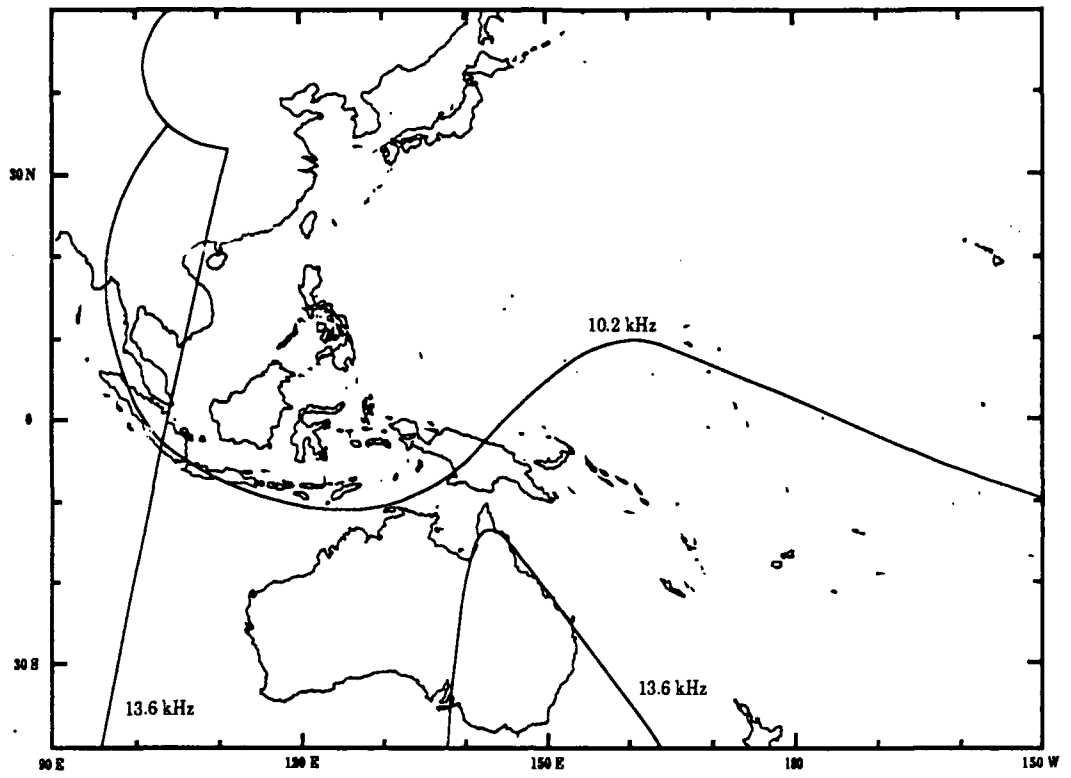

Figure 4-17. Argentina Signal Modal Zones; Overlay Model

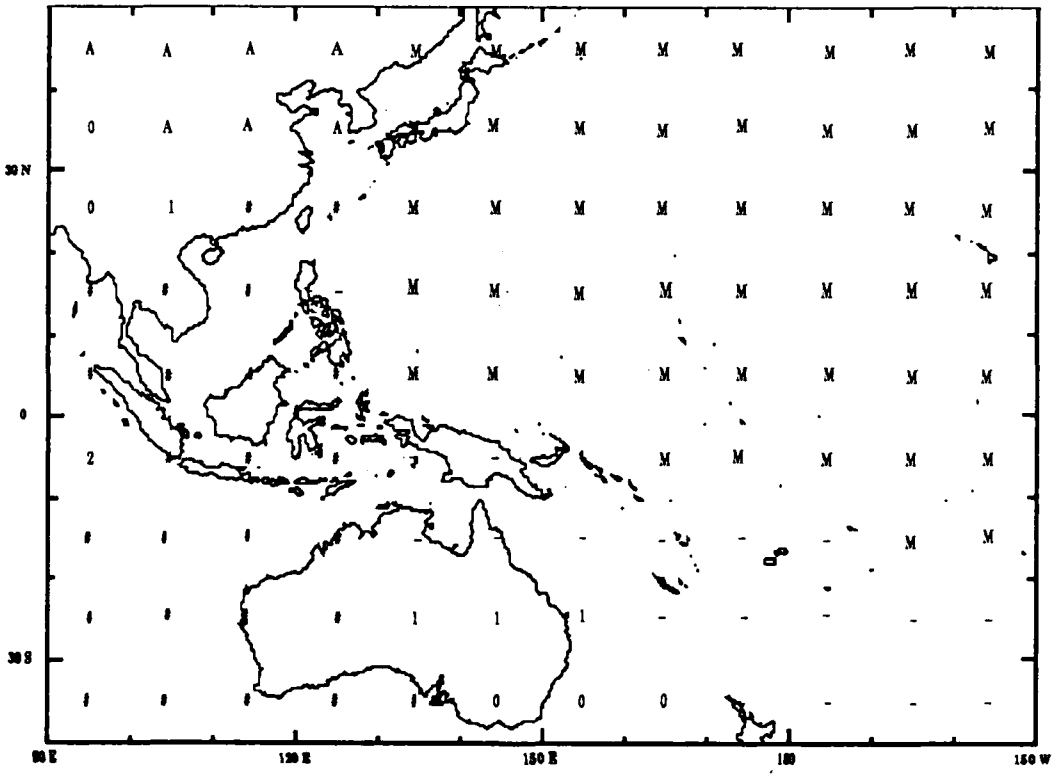

Figure 4-18. Argentina Signal Quality; Parametric Model

have almost no measurements to differentiate between these models. Most sites did not monitor Argentina when the validation data was obtained.

At 13.6 kHz we consider the Analysis and Overlay Models to be in very good agreement.

The Parametric Model is more similar to the Overlay Model, except the western modal boundary is not placed as far west. Part of the difference is the choice of symbols to label the various phenomena.

Our analysis of long-path effects predicts that the zonal boundary extends across southeast Australia just south of Brisbane and crosses near Samoa as the boundary extends eastward. We emphasize that the maximum extent of the long-path boundary varies with season. Measurements support the prediction that the boundary can reach Brisbane at its maximum extent. However, the passage of this boundary through Brisbane only occurs for about two months of the year.

(G) AUSTRALIA

The Australia self-interference consists of two mechanisms, the near zone and the equatorial mode conversion zone (Figures 4-19, 4-20 and 4-21). The near zones, the modal boundaries surrounding the transmitter, are illustrated only to compare the Analysis and Overlay Models. The two models show very similar areas for both frequencies but quite different boundary shapes. The differences in shape are worth investigating both theoretically and by measurement. None of the measurements of this validation contribute new information on these near zones.

The boundaries for the mode conversion zone, located in the upper left corner in each of these figures, have different shapes between the Analysis Model and the other models. We have difficulty defending the shape of the Analysis Model on the eastern edge from measurements. The Yap data are an important clue, Yap being near the eastern edge and in the middle, north/south, of our predicted

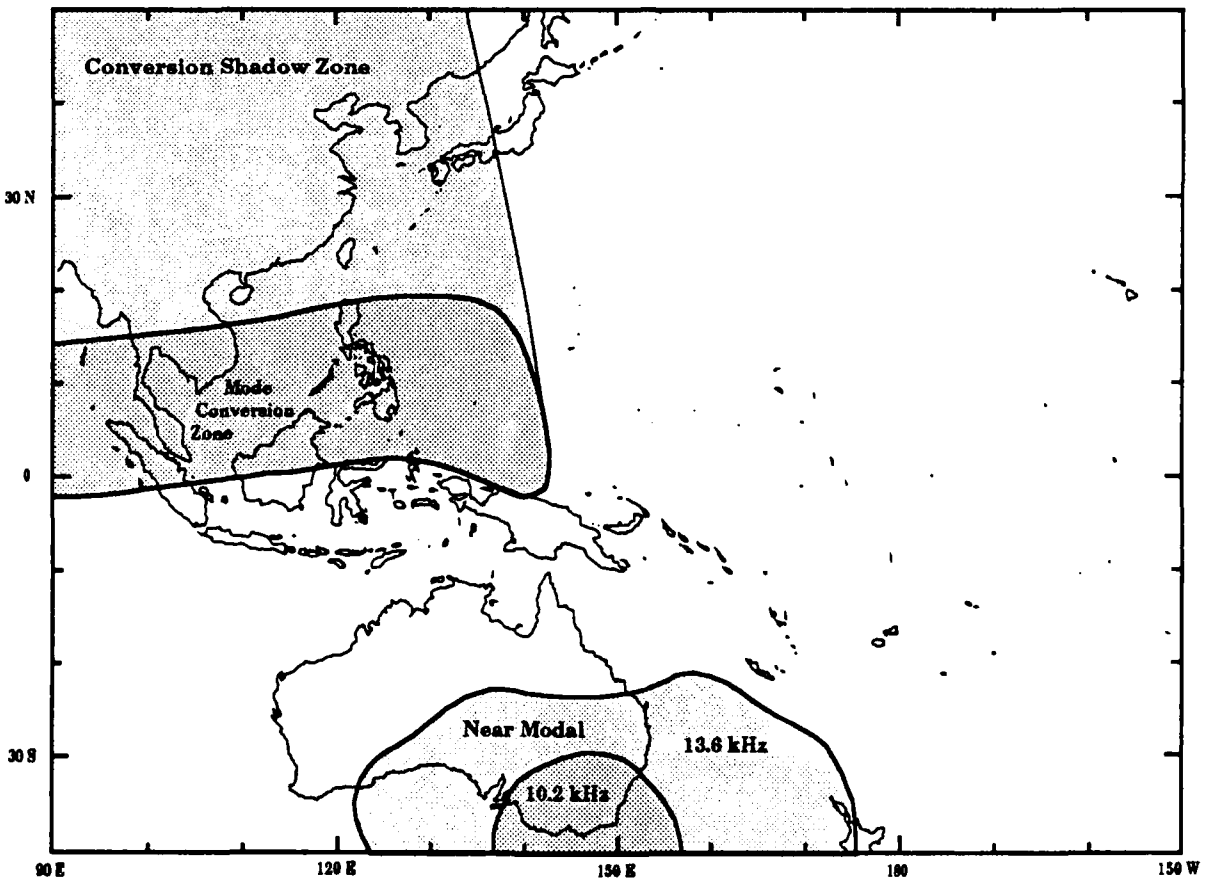

Figure 4-19. Australia Signal Modal Zones; Analysis Model

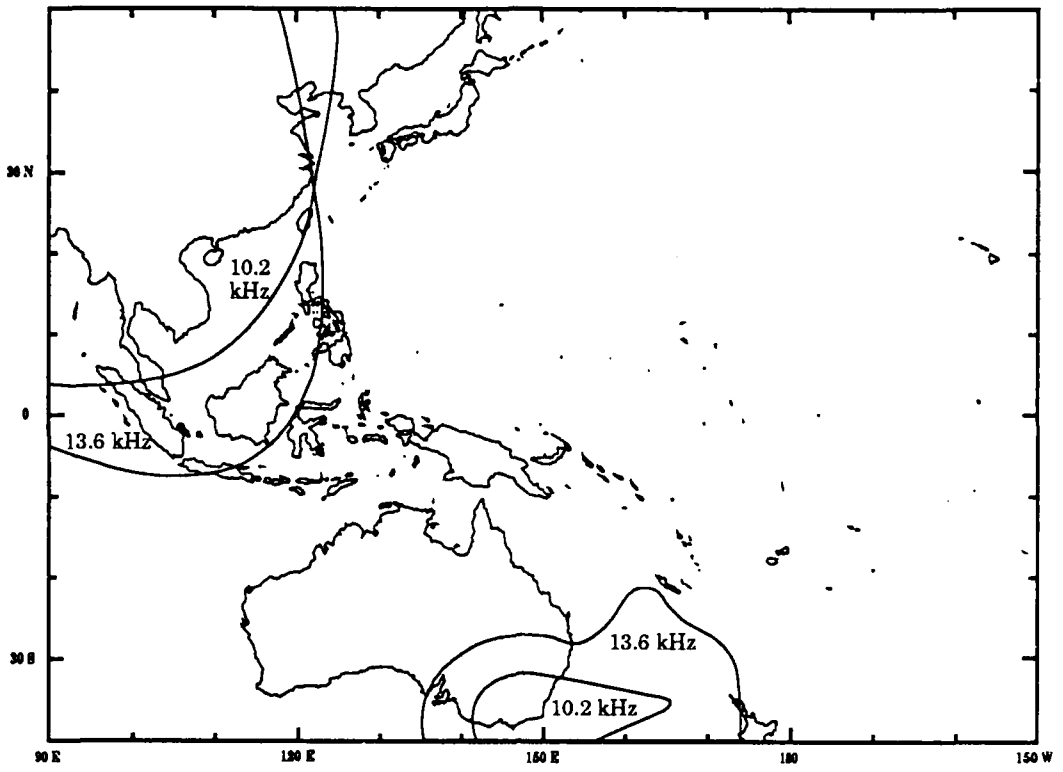

Figure 4-20. Australia Signal Modal Zones; Overlay Model

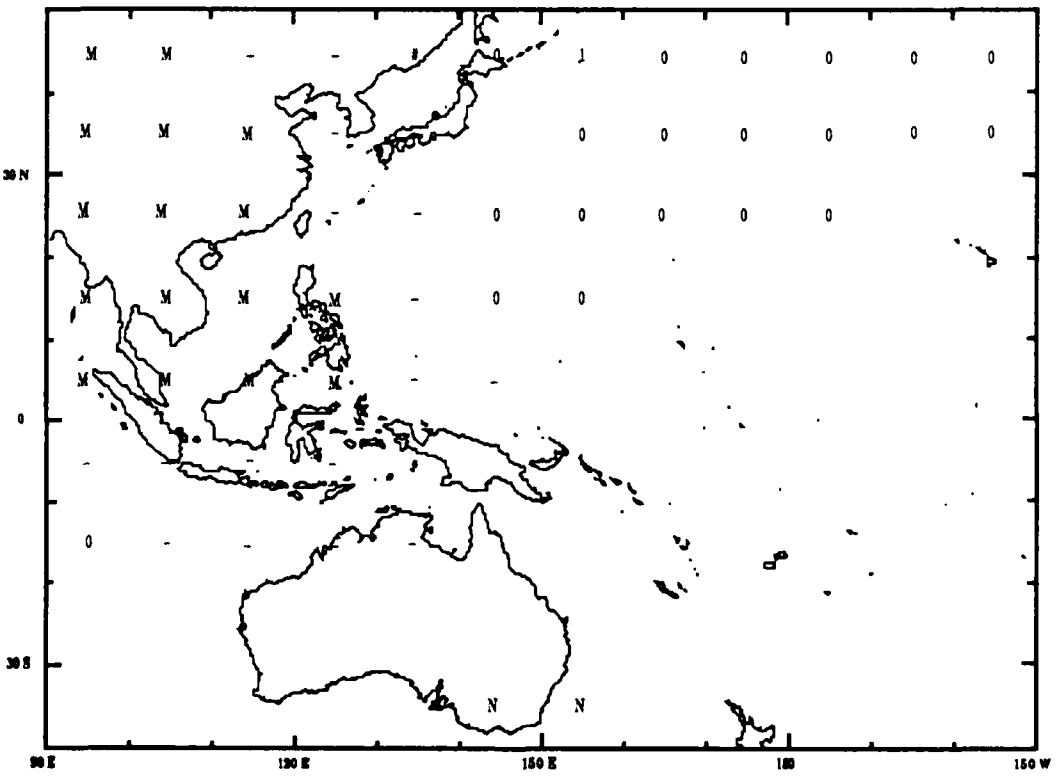

Figure 4-21. Australia Signal Quality; Parametric Model

zone. The Yap data show negligible modal effects on all frequencies. Yet, the Japan data, which measures a radial slightly to the west of Yap, clearly show modal effects. The aircraft data are not particularly helpful in establishing the shape of this boundary in this area. We suspect that the Analysis Model's predicted southward extension of this boundary towards the eastern edge needs to be modified to curve northward. A lot of work is needed, both theoretically and experimentally, to better understand the properties associated with the east and west boundaries of modal zones.

With respect to the 13.6 kHz boundary, all the evidence we have from measurements supports placing this boundary coincident with the 10.2 kHz boundary. Much of the data and calculations show the 13.6 kHz modal effects to be weaker than at 10.2 kHz. We take this information to be added support for not placing the 13.6 kHz boundary outside of the 10.2 kHz boundary. In fact, 10.2 kHz modal effects are detected at Singapore.

The Parametric Model, while more similar to the Overlay Model in the prediction of the modal area, contains a band around the modal area labeled disturbed (–). We would change most of these labels to modal (M) and change several to good (0). Particularly, we would change the bottom disturbed row of labels (crossing northern Australia), and the disturbed label above eastern New Guinea to good. We have no evidence for disturbed conditions this far south.

In every other case examined the measurements support placing the north/south boundary outside of that predicted by the Analysis Model. Also, 10.2 kHz modal effects clearly exist at Singapore. On the support of this evidence, we continue to vote for the Analysis Model, maybe with some slight adjustments.

No long-path effects are expected or observed in the validation region.

(H) JAPAN

The Analysis and Overlay Models (Figures 4-22 and 4-23) predict a modal zone boundary at 13.6 kHz (labeled near zone for the Analysis Model), extending into the southeast segment of the validation region. While each boundary is similar in extent and shape, the Overlay boundary is larger. The Parametric Model (Figure 4-24) predicts only the 10.2 kHz boundaries.

In our data analysis we attempt to test this boundary placement, but with limited success. The data show that, at least for the time of measurement, the 13.6 kHz boundary does not extend as far southeast as predicted. This finding is consistent with similar findings from the South Pacific validation on the boundary extending southeast from Hawaii and in this validation for the boundary extending northeast from La Reunion. We conclude that this boundary should be within the boundary predicted by the Analysis Model. Possibly the boundary can be moved closer to the transmitter by about 1.5 Mm.

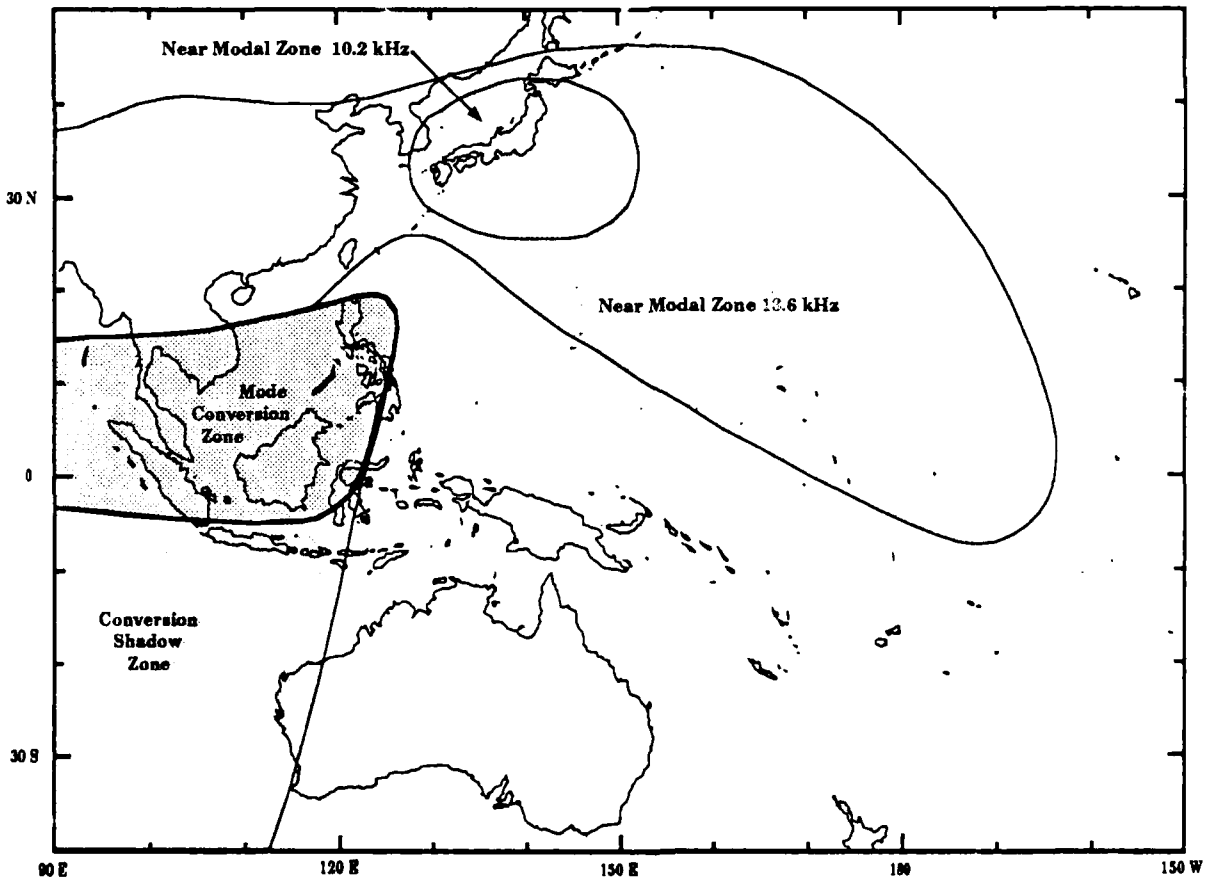

Figure 4-22. Japan Signal Modal Zones; Analysis Model

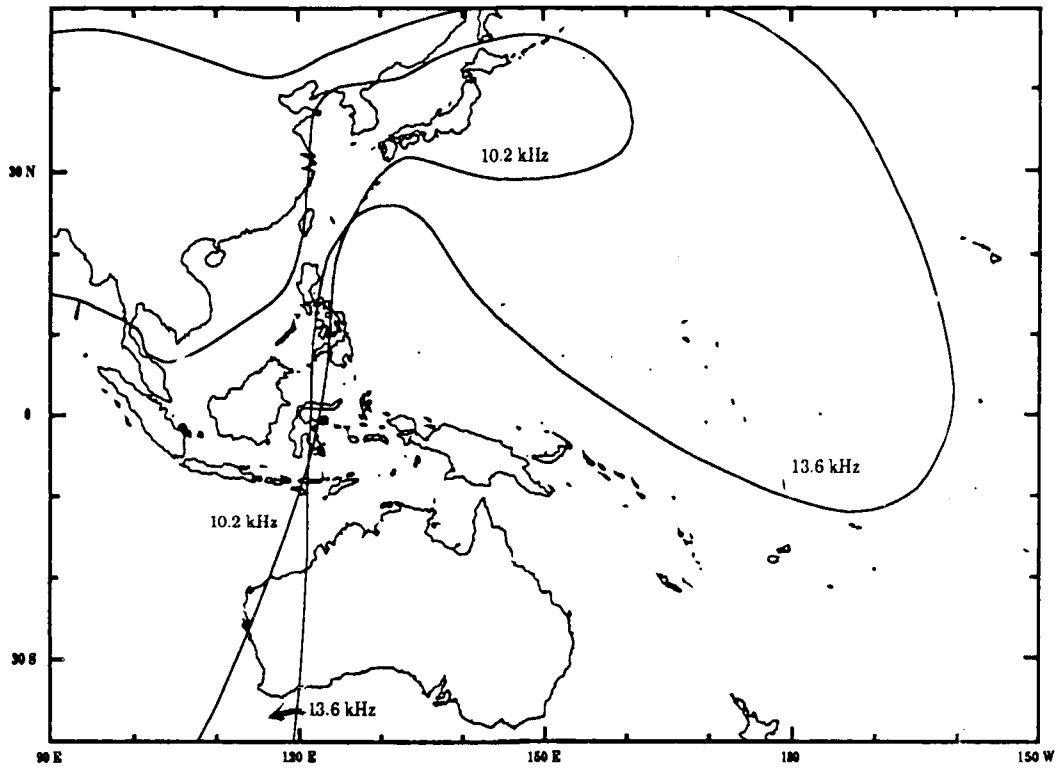

Figure 4-23. Japan Signal Modal Zones; Overlay Model

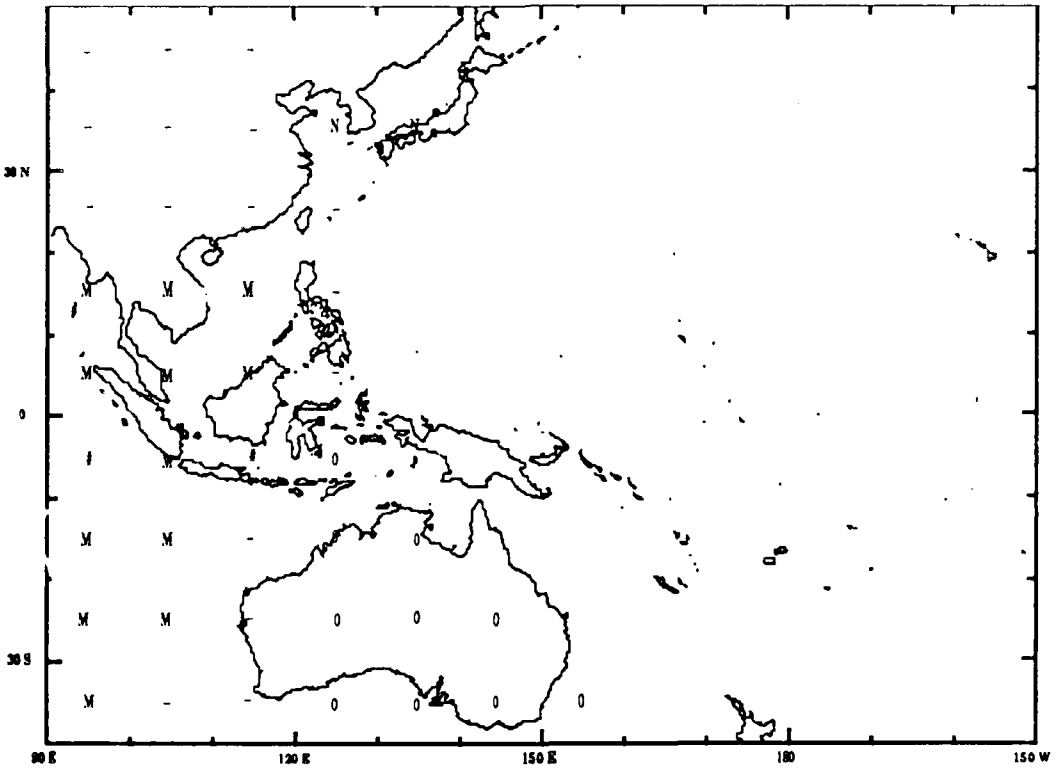

Figure 4-24. Japan Signal Quality; Parametric Model

The data support the complete separation at 10.2 kHz between the near modal zone and the conversion zone. At 13.6 kHz, the zones probably merge as shown for the Analysis Model. We have no data for comparing the placement of the 13.6 kHz near zone north boundary to the west of the transmitter.

With respect to the equatorial conversion zone, the data at Darwin clearly show some modal effects, although probably not enough to suggest switching of mode dominance. From other data and calculations we estimate that the eastern boundary of this zone should be placed along a radial just to the west of Darwin. A reasonable choice is the 187° radial, which would exit the bottom of the figure at 126°E longitude.

All models place the equatorial conversion zone and shadow zone boundaries to the west of where the data indicates it should be. We believe that the boundaries for 10.2 kHz and 13.6 kHz should be co-located.

In summary, we find small but important differences between models. We emphasize that the Analysis Model is presented only as a means for interpreting and communicating the finding of this analysis. As evidenced by the comparisons of this section, all models need refinement. Our conclusions regarding findings of this analysis will communicate recommendations for incorporating changes.

5.0 SUMMARY AND CONCLUSIONS

This section summarizes the overall validation project, places findings in perspective with goals and implementation plans, and states specifically what was found to agree or disagree with expectations and predictions.

In this section, a brief review of the overall validation is presented with emphasis on the analysis. This is followed by a comparison of the analysis results with available coverage prediction models. Following this comparison the validation conclusions are presented. Included in the conclusions are specific recommendations, both on the use of the analysis findings and on addressing unfinished business. The orientation of this report is to look for and report potential navigation problems. The emphasis on problems should not overshadow the fact that Omega works very well over the vast majority of the earth.

5.1 SUMMARY

This subsection reviews what has been presented, makes specific comparisons between expectations/predictions and analysis findings, and sets the stage for discussing conclusions by reviewing important points.

OVERVIEW

For this validation, emphasis has been placed upon establishing zones of signal self-interference. The rationale for this emphasis is that signal self-interference has proven to be a more significant problem than it was thought to be in the early stages of Omega development and operation. Signal self-interference exists on at least a few stations in all parts of the world. In this validation region, an exceptionally large number of stations exhibit self-interference problems. While weak signal levels can easily be measured and deselection made, self-interference cannot be easily measured; thus either the receiver or navigator must rely on predictions.

This Western Pacific region also has a problem of inadequate SNR coverage. Unfortunately both problems, inadequate SNR and self-interference, combine to accentuate the problems.

Over the past few years, much has been learned and information has been derived that is utilized for this validation. Some of the key knowledge and tools

available were reviewed as an introduction to this project. As is always the case, a practical plan had to be devised for data collection that coped with constraints on the resources of money, equipment, time and geography.

Validations are a particular challenge because large regions must be covered, usually over large ocean areas where very few measurement opportunities exist. The measurement phase is designed to capitalize on what was practical and to best utilize resources based upon the planners' perspectives at the time of implementation. While the collected data are not always optimal for assessing the questions at hand, much new information is derived.

In Subsection 3.3.2 ANALYTICAL GUIDANCE, a revised prediction model was devised to provide analysis guidance for data assessment. The prediction model, based on a large set of recent calculations by Gupta, defined zones of possible self-interference for each station. Composite charts were prepared (Figure 3-4 for 10.2 kHz and Figure 3-5 for 13.6 kHz) to identify areas where the greatest potential problems might occur and to assign priorities for data analysis and interpretation. The prediction model showed the existence of a region between about 0° and 15°N latitude and 95°E to 125°E longitude in which self-interference exists for many signals. This prediction is confirmed from the data analysis.

From the analysis in Subsection 3.3.4 DATA INTERPRETATION, we determine that the disturbance regions for each signal possibly are larger than our prediction model shows. Variability of propagation conditions and very limited samples for establishing boundaries prevents definitive conclusions.

Long-path signal self-interference is predicted in Subsection 3.4 LONG-PATH INTERFERENCE ASSESSMENT, to occur on three Omega signals at certain times and locations. While not fully confirmed, this interference occurs when there is redundancy of signals; thus signal deselection is a conservative safe procedure.

We found in Subsection 3.5 SIGNAL-TO-NOISE RATIO ASSESSMENT, that measured SNR and noise did not produce a good match with predictions. Signal tracking loss due to noise is a serious problem during certain time intervals, in local summer, and in the same geographic area where modal interference affects the most signals. Further, signal loss occurs on signals having otherwise good phase.

We show that by far the largest part of this validation region has good navigation coverage. Yet an area between the Philippines and Singapore (extending from 15°N to 4°S), is subjected to times of both high noise and modal effects. We estimate in Subsection 3.6 SIGNAL TIME AVAILABILITY, that at these times, not enough good signals are available for reliable navigation.

5.2 CONCLUSIONS

This subsection presents in concise form the important findings of the validation, makes recommendations regarding use of the validation findings, and identifies topics for future investigation.

The analysis confirms that good quality navigation is possible over most of the Western Pacific validation region. An exception has been identified for an area west of the Philippines. There, a combination of high atmospheric noise and equatorial zone modal effects can create time intervals when we estimate areas exist of two station coverage (Liberia [B] and La Reunion [E]) and three station coverage; the third station is Norway [A]. In these areas, the Liberia and La Reunion signals have a poor geometry relationship such that the value of using them as a pair is reduced.

For other areas where only three or four stations are predicted to have good phase quality all the time, a three station combination should be available most of the time. Seasonal noise in the vicinity of New Guinea is expected to create occasional problems.

Our analysis, because of measurement location limitations, was not able to derive definitive information to validate locations of coverage boundaries. Collectively however, the analysis findings were sufficiently supportive of the analysis model to lend reasonable credence to the model predictions and to use these predictions to guide selection of boundaries.

We conclude that the Omega signal self-interference boundaries established by the analysis model (adjusted by the measurement analysis), provide a significantly improved perspective on navigation reliability in the Western Pacific. We recommend that the information on modal boundaries resulting from this

validation be adopted in the Omega navigation model, giving due consideration for conservatism.

With respect to further possible analysis, the highest priority is to further explore the navigation consequences of the areas for predicted low or inadequate coverage. This could be partially accomplished by integrating model analysis (using fullwave prediction theory) with data interpretation. This requires more extensive data processing and iterative adjustments of propagation parameters in calculations by using trial and error techniques. We expect that important insights will be obtained. The ideal approach would be to design and conduct a special measurement campaign. We note, as discussed in Subsection 3.6 SIGNAL TIME AVAILABILITY, that the measured coverage would be significantly reduced if the noise at the time was in fact below average for this region.

Our navigation analysis demonstrates, that for the most part, accuracy is found to be within predictions, especially for mid-path day. Some evidence is derived to suggest that the low latitude ionosphere is not well characterized by the mid-latitude model traditionally used for predictions. We feel that the phase prediction model for transition times could benefit from additional calibration. We noted several examples of large variability of phase about the median. Most cases were for propagation paths with a long day/night transition.

The analysis conducted in this validation produced new insights into signal self-interference (both modal and long-path), that could be profitably applied to other geographic regions. Guidance in signal coverage conditions would be improved by applying these insights.

Determining long/short-path boundaries continues to be a problem because of the lack of a good theoretical model and definitive measurements. Addressing both aspects of the problem are straight-forward processes.

Finally, the data for near zone modal interference, predicted to extend for large distances from transmitters, are very sparse. Our attempt to assess three transmitters (Hawaii, La Reunion and Japan), provides a good example of the large areas involved and the frustrations of documenting predictions. In all cases, the zones of uncertainty remain large.

Appendix A
Generation of Geographic Plots Showing Modal Competition

The set of plots described in this appendix address the nighttime propagation modal conditions, near modal, mode conversion, modal shadow zone, and mode switching, described in Section 3.3.2 of this report. The long-path interference will be addressed in Appendix C. A geographic plot is constructed for each station where modal effects occur in the Western Pacific validation region.

The analysis of modal conditions is derived from a series of calculations for Omega signal field strength versus distance for 10.2 and 13.6 kHz produced by TASC for ONSCEN (GUPTA 1988, Ref. 23). A sample calculation is shown in Figure A-1. The legend on the right identifies each of the curves. Important features for our analysis include the relative strength of the various modes and the structure of the mode sum. In this example mode 1, marked (+), is dominant beyond 2 Mm; mode 3, marked (x), is initially dominant and remains relatively strong for

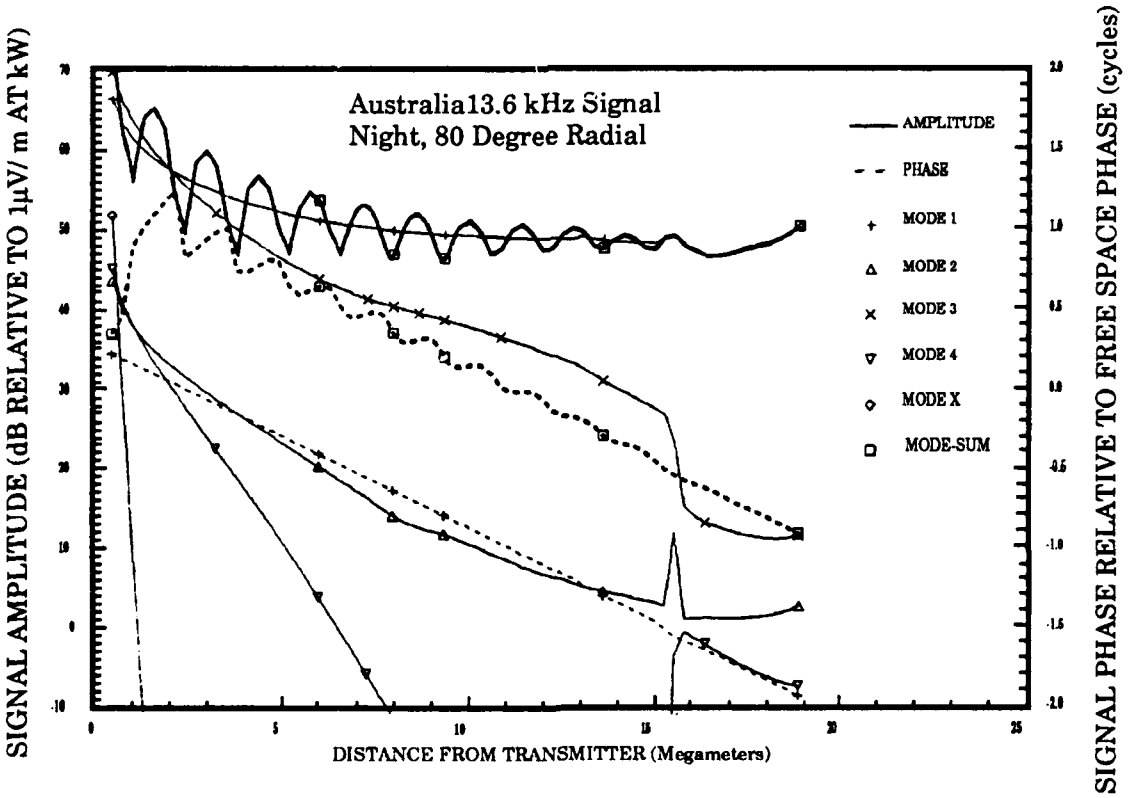

Figure A-1. Example of Omega Signal Calculation of Field Strength

a few megameters. Since the propagation velocity of mode 3 differs from mode 1, their phase values progressively change with respect to each other. The net result is that the composite signal, mode sum, undergoes amplitude fluctuations with increasing distance. It is this fluctuation observed in amplitude data that is used to identify modal effects; in our example, to identify that mode 3 is interfering with mode 2. The plot of mode 3 helps to establish where to expect modal conditions. The properties of the higher-ordered modes with distance help us determine the type of interference, such as near zone, mode conversion zone, etc. The ionospheric parameters used for calculations are shown in Table A-1. No allowance has been made for expected ionosphere variation with latitude and season. The first task is to examine the sets of calculations for each station to identify the possibility of self-interference conditions. The three most important model features useful for analysis guidance are: (1) the structure (signal fluctuation with distance) in the mode sum, (2) the modes that contribute to the mode sum, and (3) the mode that is dominant in the validation region.

Ionosphere Illumination Condition	IONOSHERE PARAMETERS	
	Reflection Height (km)	Conductivity Gradient (km^{-1})
Day	70	0.3
Night	87	0.5

Table A-1. Day and Night Ionosphere Parameters

A summary of the analysis for creating each geographic plot is presented as follows:

(A) NORWAY

No equatorial zone mode conversion is predicted to occur within the Western Pacific validation region. The phase quality of Norway signals for night propagation is predicted to be good. Possible exceptions include a few radials which propagate over the extreme northern region of either Norway and/or Eastern Russia.

The calculations show mode conversion in these radials with the higher-ordered mode dominance maintained into the validation region for both frequencies on the 30° radial and at 13.6 kHz on the 70° radial. The 50° radial shows strong modal competition at both frequencies. These predictions are very sensitive to the selected earth conductivity parameters, parameters that are not well established for these Arctic areas. A similar prediction was noted in the South Pacific validation for the 30° radial radial that crossed New Zealand. We were unable to confirm that prediction and simply noted that the calculations indicated the possibility of striations of modal switching. Figure A-2 shows the bands of possible mode switching in the Western Pacific region. Sample calculations for the Norway signal are shown in Figures A-3 and A-4 for 10.2 and 13.6 kHz respectively. Each figure shows calculations on adjacent 10° interval radials; the 60° radial showing no modal effects and the 70° radial showing mode switching. A similar relationship is predicted with the 30° and 50° radials showing modal effects and the adjacent radials showing no modal effects. Figures A-3b and

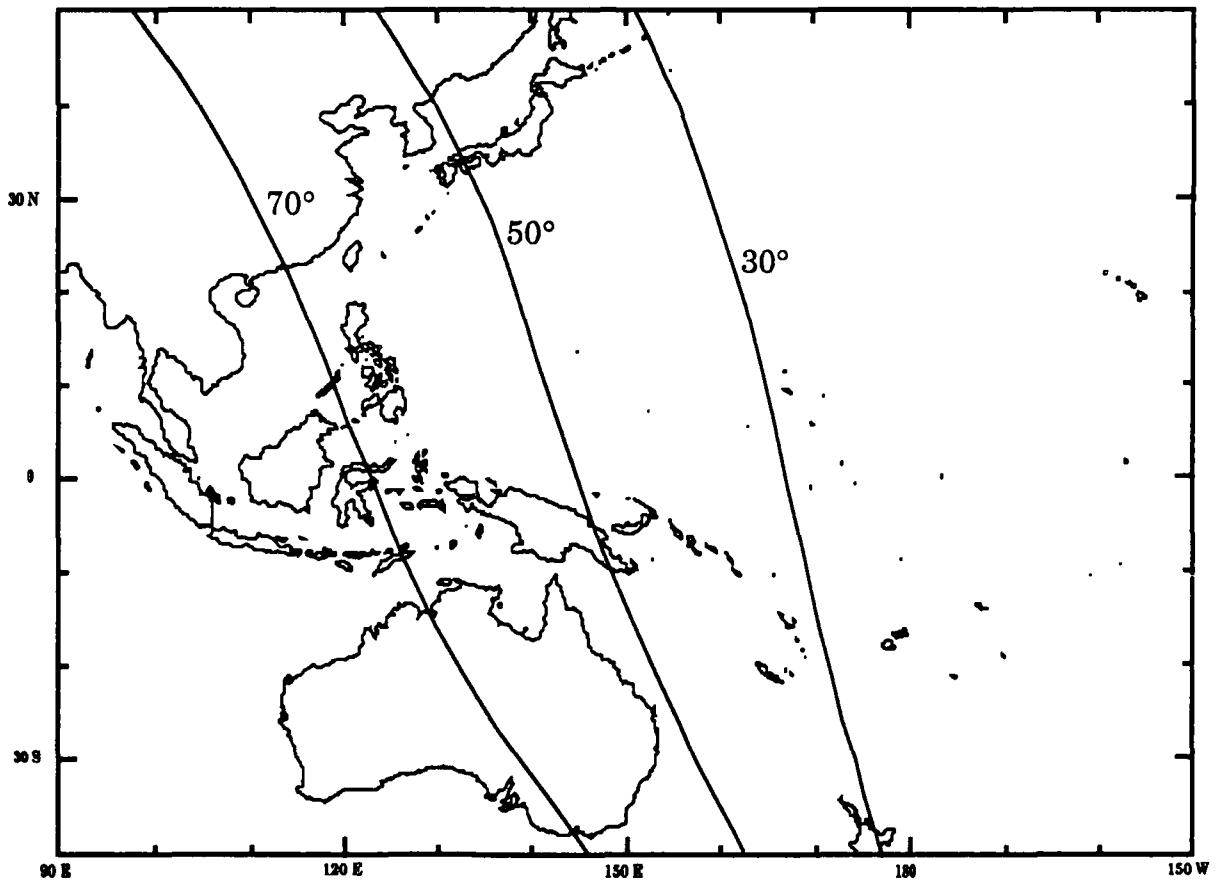

Figure A-2. Uncertain Phase Bands of the Norway Signal

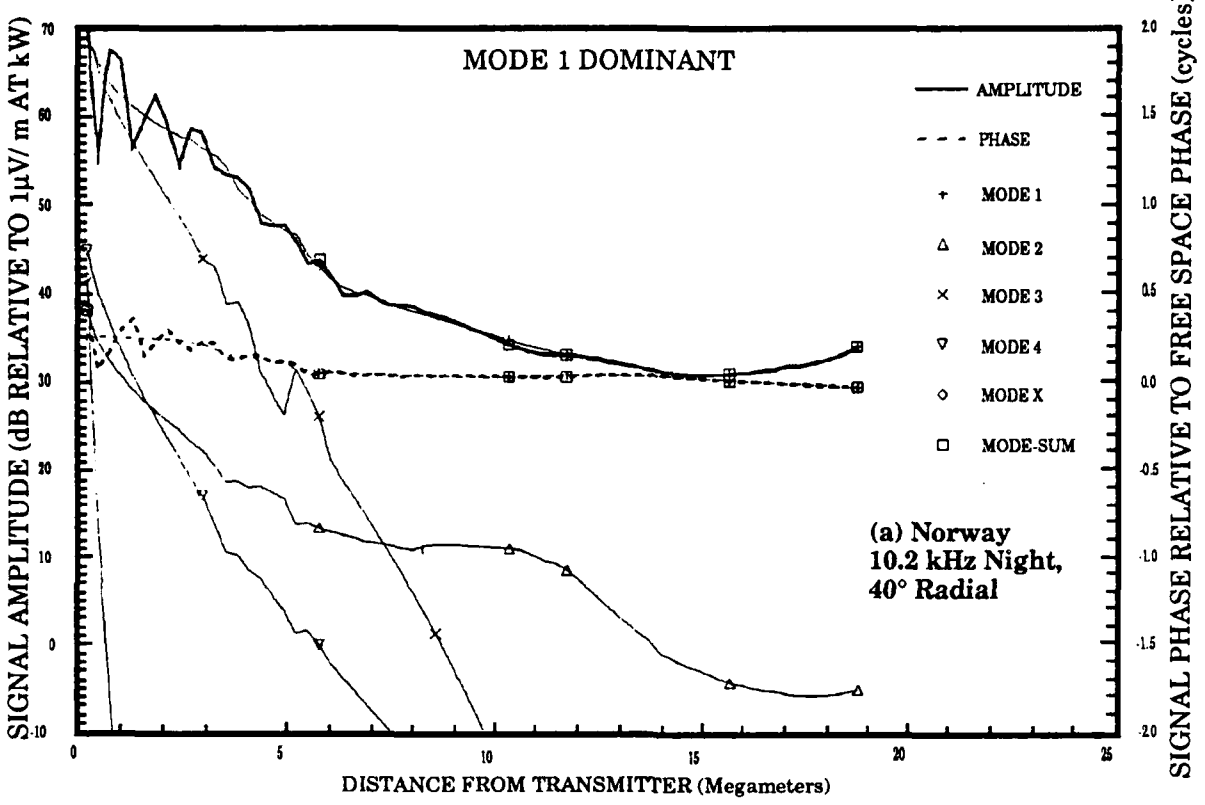

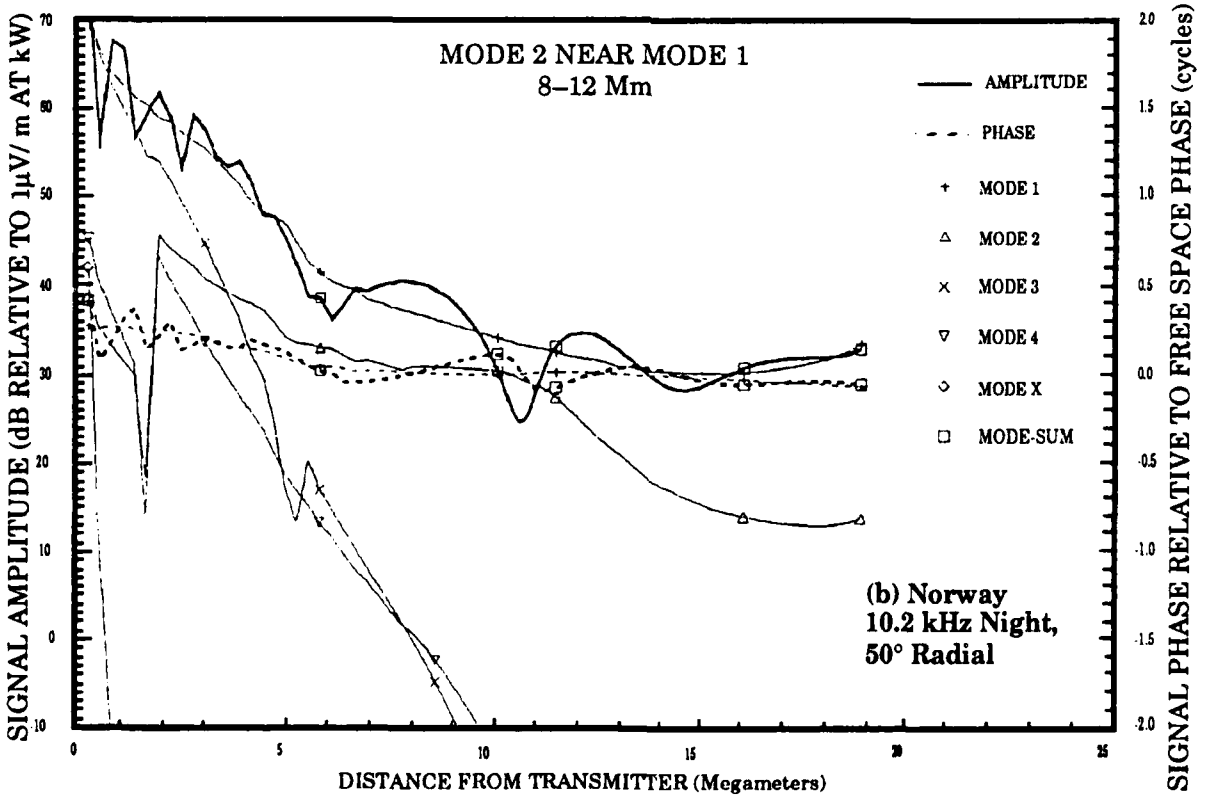

Figure A-3. Calculation of the Norway Signal Propagated at10.2 kHz

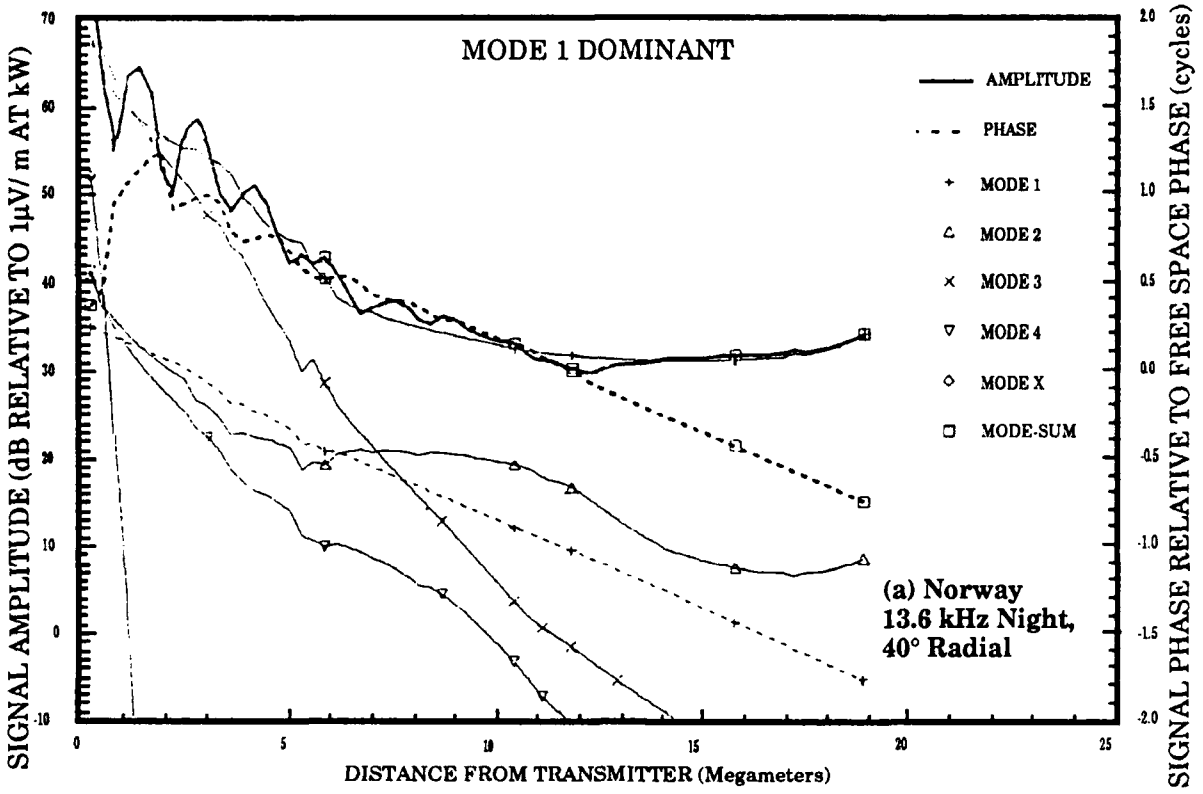

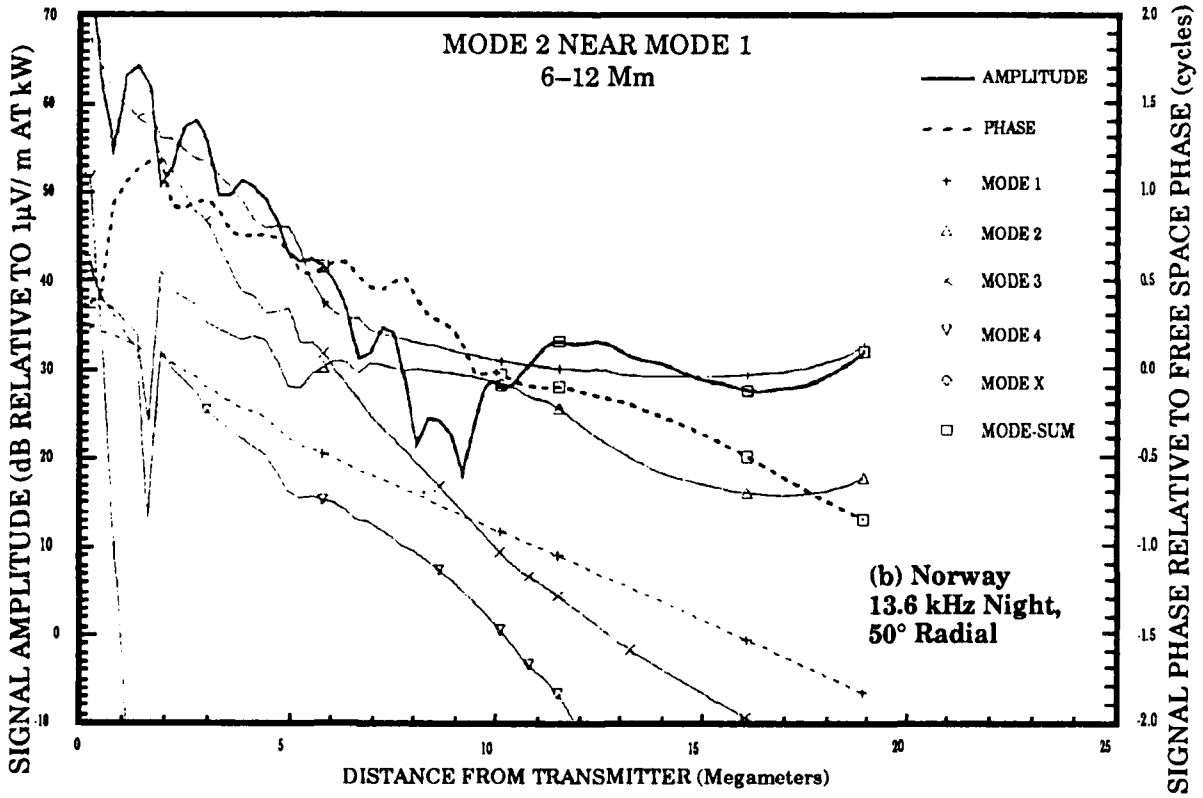

Figure A-4. Calculation of the Norway Signal Propagated at 13.6 kHz

A-4b show mode 2 close in amplitude to mode 1 over the distance interval noted in the caption. We note that, although higher mode dominance is not always predicted for 10.2 kHz, the mode competition is predicted sufficiently strong that slight variations in propagation conditions could result in dominance switching. The predicted strong mode 2 on these radials appears to be highly sensitive to the terrain conductivity features used in calculations. Since the calculations indicate that the bands are only a few degrees wide, verification of this switching between dominance and non-dominance of mode 2 would require both more radial calculations and data obtained at many locations across the zones. The calculations for night propagation paths across low conductivity terrain show a high sensitivity in cumulative phase to path parameters. This sensitivity is not nearly as pronounced for the day. Apparently this phase sensitivity is closely associated with mode conversion occurring in nighttime propagation across low conductivity terrain. We note, however, that the above prediction of modal effects has not been widely accepted in the analysis community.

We note that the Norway signal is a critical resource over segments of the Western Pacific validation region and thus both its phase quality and SNR need to be confirmed.

(B) LIBERIA

The zones for night propagation of possible poor phase on Liberia signals in the Western Pacific are shown in Figure A-5. The Liberia station is inside the equatorial mode conversion zone; near the northern edge. Consequently, shadow zones lie on both sides of the mode conversion zone. Also, propagation path segments traversing the conversion zone tend to be longer. The paths to the central eastern part of the Western Pacific validation region have segments within this zone as much as 20 Mm long. Within the mode conversion zone, the signals show highly complex conversion. Upon exiting into the shadow zone, all signals are predicted to be mode 2 dominant. The calculations show that the relative strength of the modes leaving the equatorial zone can vary greatly with azimuth. Within the mode switching zone, large modal structure is predicted on some radials, while on others very little structure is predicted. Figures A-6 and A-7 show representative calculations of the Liberia signal showing mode conversion. Along a 260° radial of propagation, Figures A-6a and A-6b for 10.2 kHz and 13.6 kHz respectively, the path is within the mode conversion zone out to a distance of 13

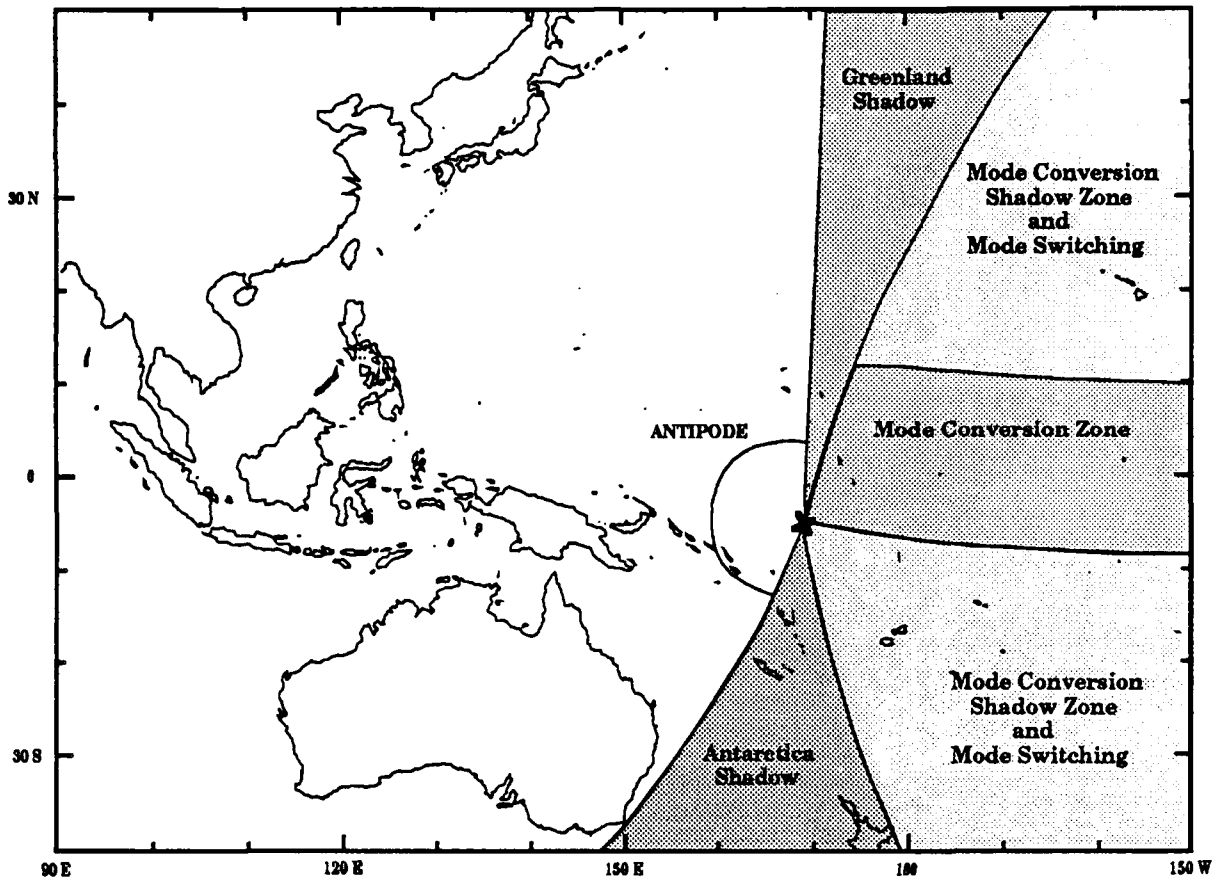

Figure A-5. Modal Zones for the Liberia Signal

Mm. We note that the propagation predictions are so complex that the details are uninterpretable. We simply conclude that the signal is unpredictable for navigation purposes. Along a 310° radial of propagation, Figures A-7a and A-7b for 10.2 kHz and 13.6 kHz respectively, the path crosses near Hawaii. On this path the mode conversion is within the first two megameters from the transmitter. At both frequencies, the 2nd mode emerges dominant from the conversion zone and remains dominant to the antipode. In the vicinity of Hawaii, a radial distance near 15 Mm, mode 2 is predicted 25 dB stronger than mode 1 at both frequencies.

The paths from Liberia to the eastern side of the Western Pacific validation region are all very long, greater than 14 Mm. Consequently, the all night condition only occurs for short periods of time, or not at all during some seasons on some paths.

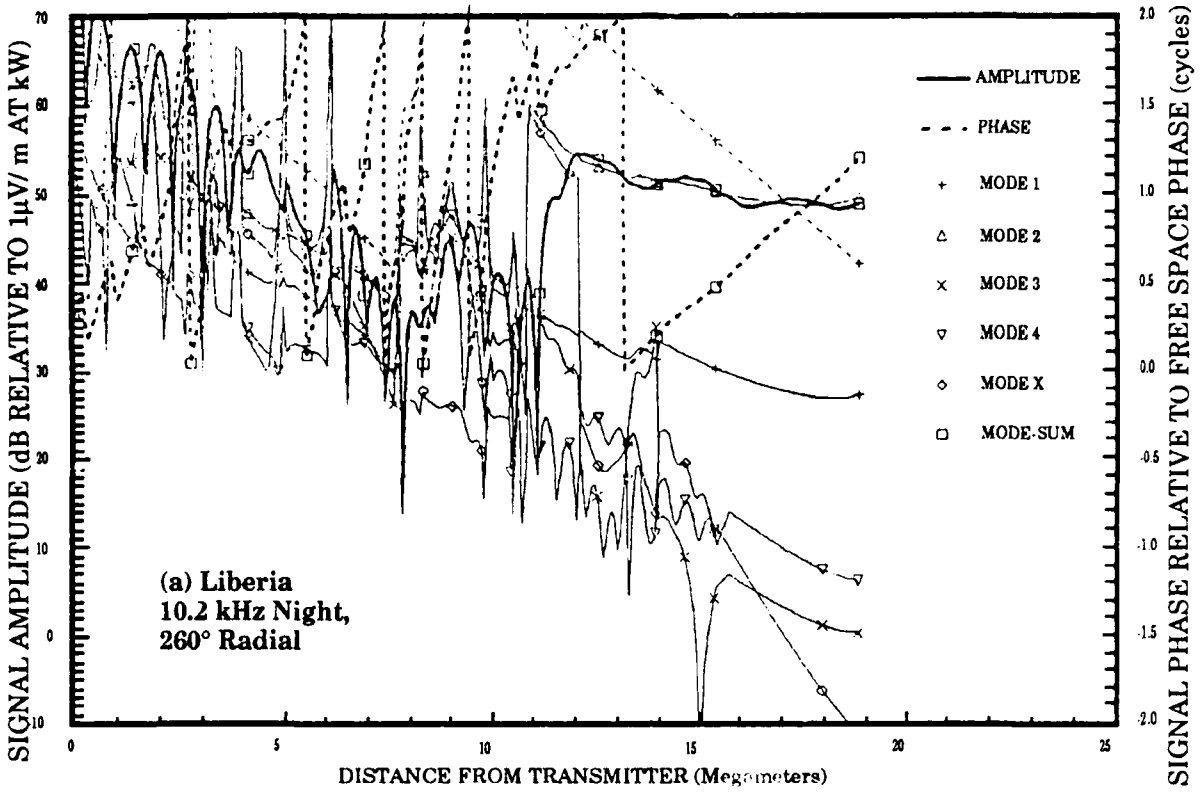

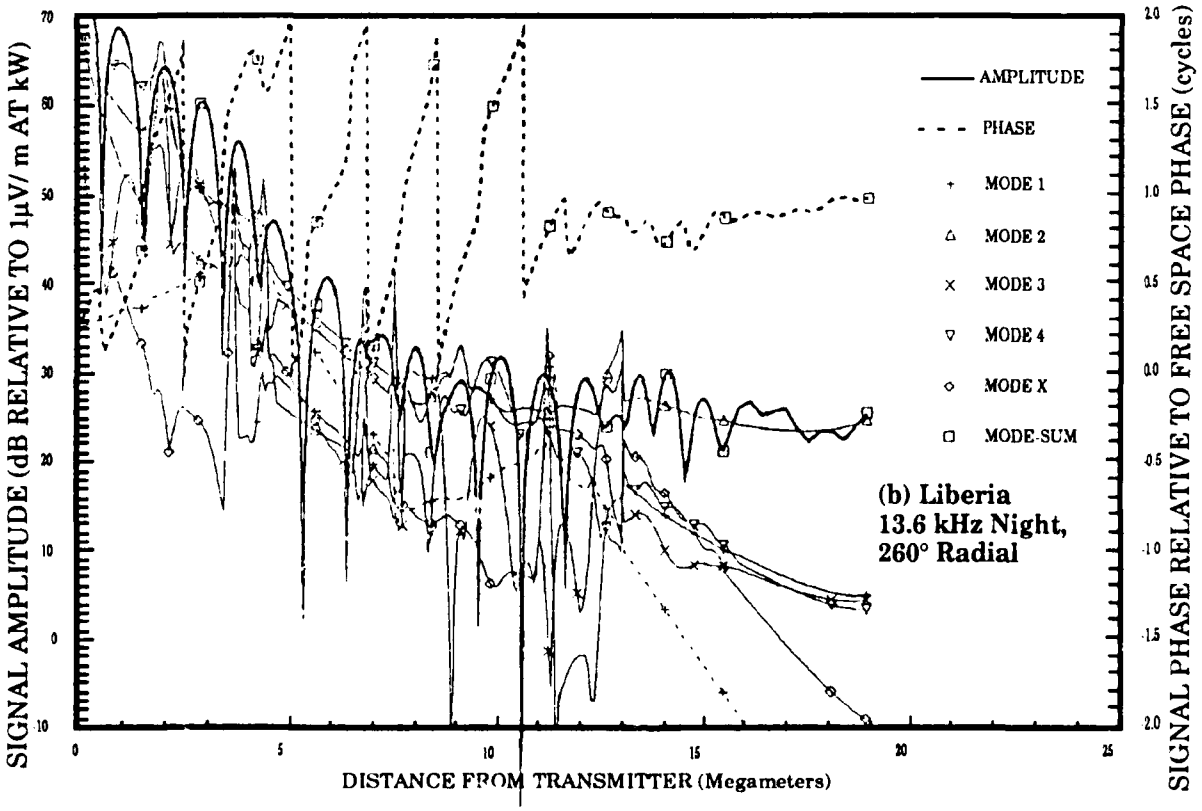

Figure A-6. Calculations of the Liberia Signal Propagated on the 260° Radial

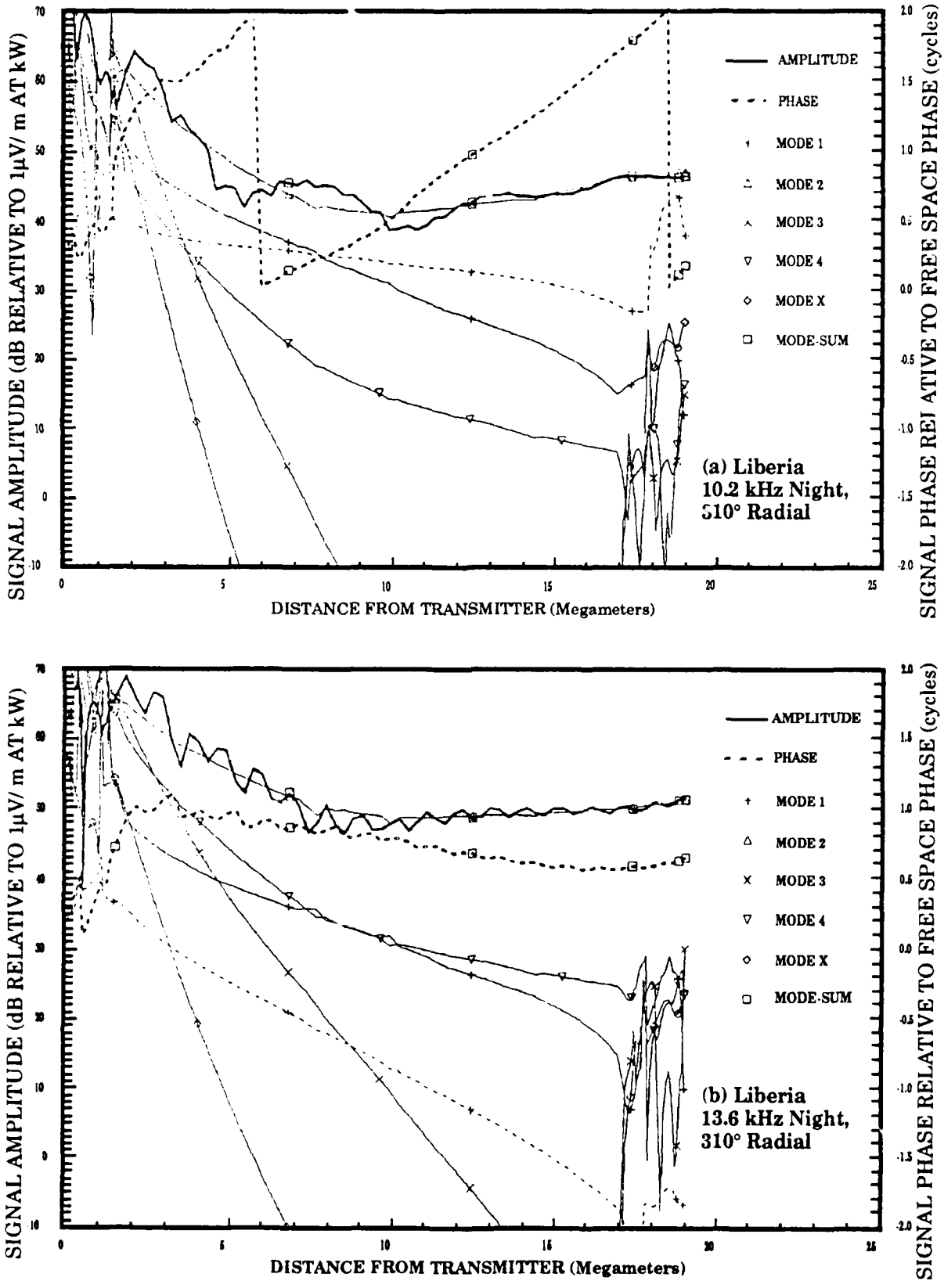

Figure A-7. Calculations of the Liberia Signal Propagated on the 310° Radial

(C) HAWAII

For Hawaii, the possible extent of unreliable phase is shown in Figure A-8. For radial bearings between 200° and about 250°, mode conversion is the dominant factor in determining the area of unreliable signal. This conversion occurs as the

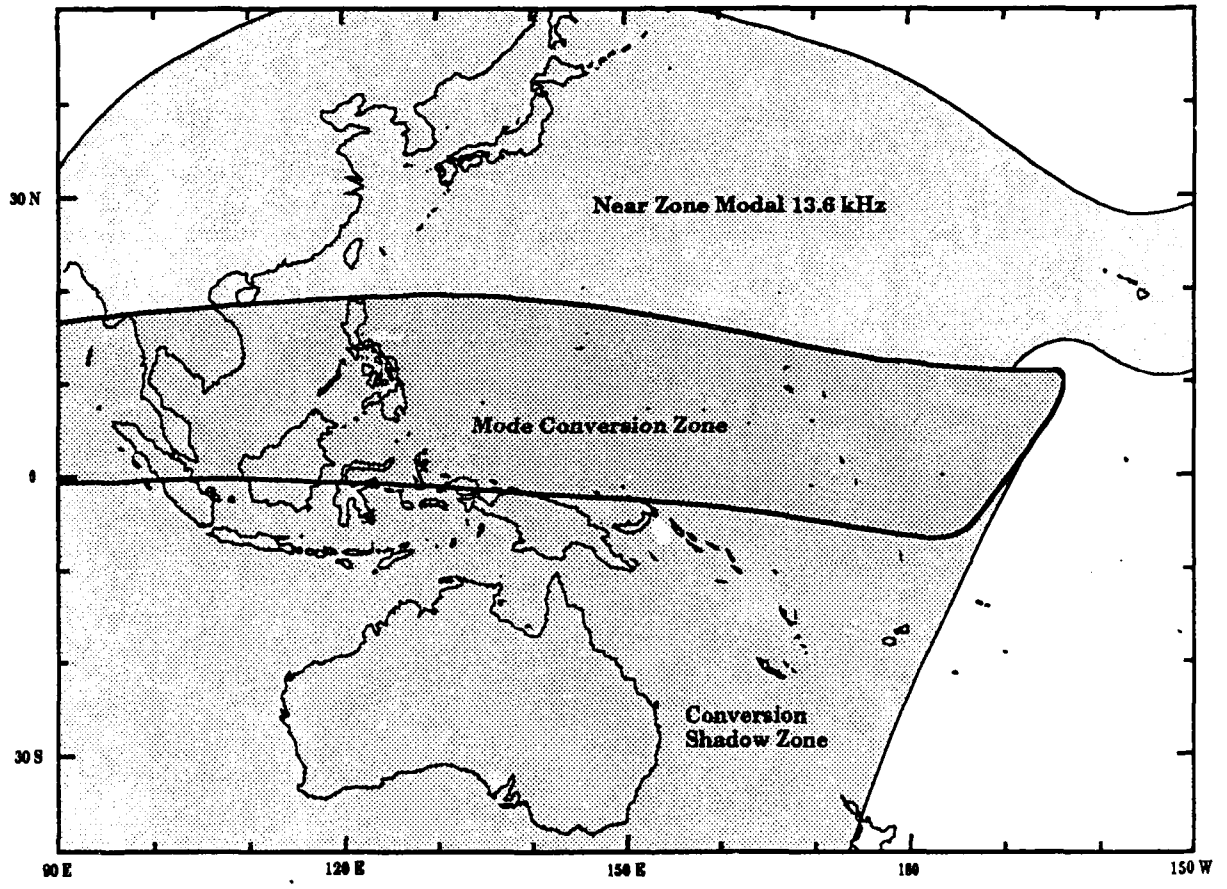

Figure A-8. Modal Zones for the Hawaii Signal

signal propagates across the equatorial zone. The onset of mode conversion occurs within a very short change in radial bearing. This is illustrated in Figure A-9, which shows the calculated signals at two bearings, 200° and 205° for 10.2 and 13.6 kHz respectively. The equatorial zone lies approximately between 2.5 and 3.8 Mm. A small amount of mode conversion is noted at the 200° heading by a slight increase in the level of modes 2 and 4 in the transequatorial region. At the 205° heading, mode conversion has become very strong with, at 10.2 kHz, mode 2 being the dominant mode beyond the conversion region. At 13.6 kHz, mode 1 exits the region slightly dominant. By a radial bearing of 210°, mode 2 is

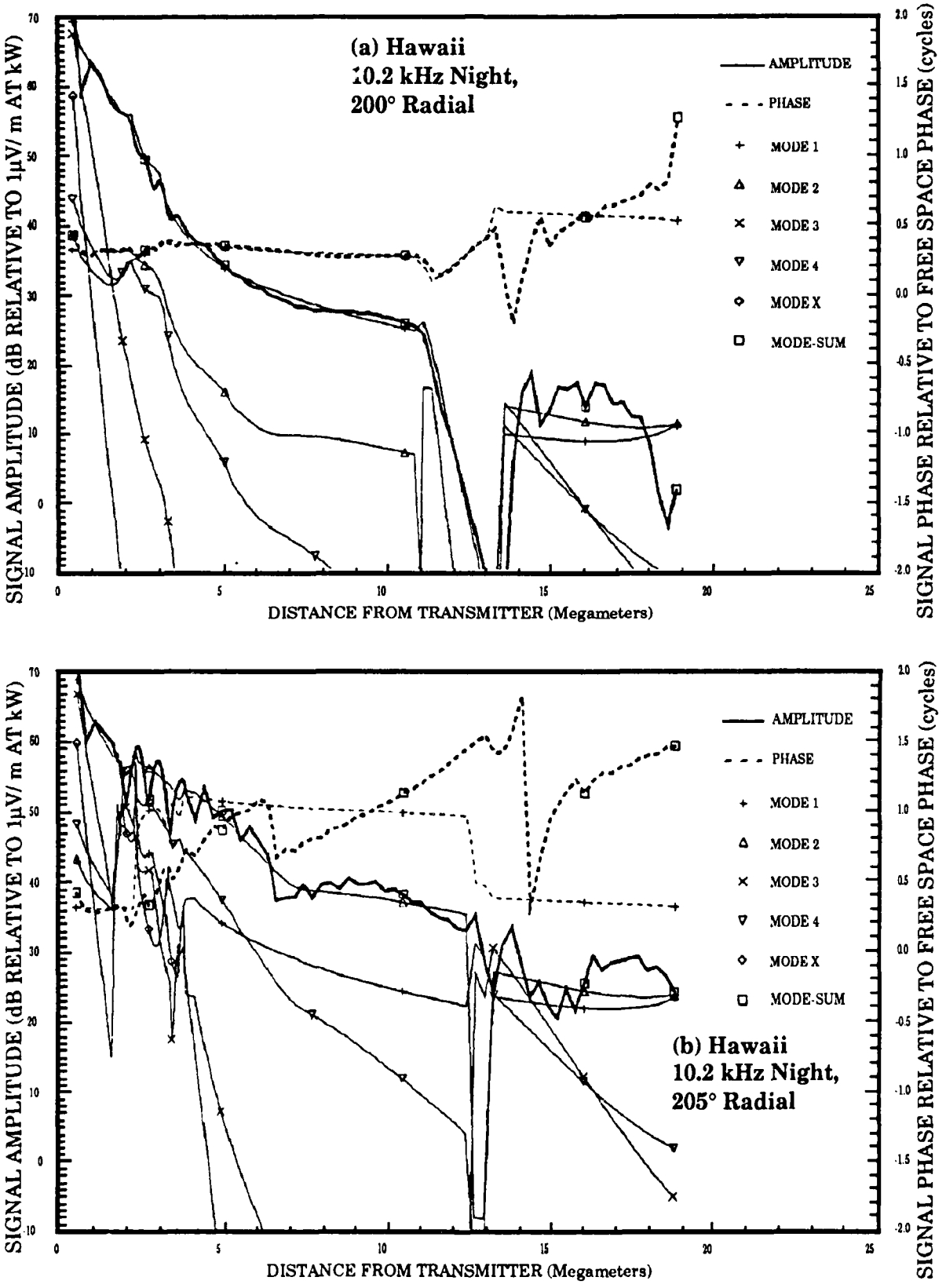

Figure A-9ab. Calculations of the Hawaii Signal Propagated on the 200° and 205° Radial at 10.2 kHz

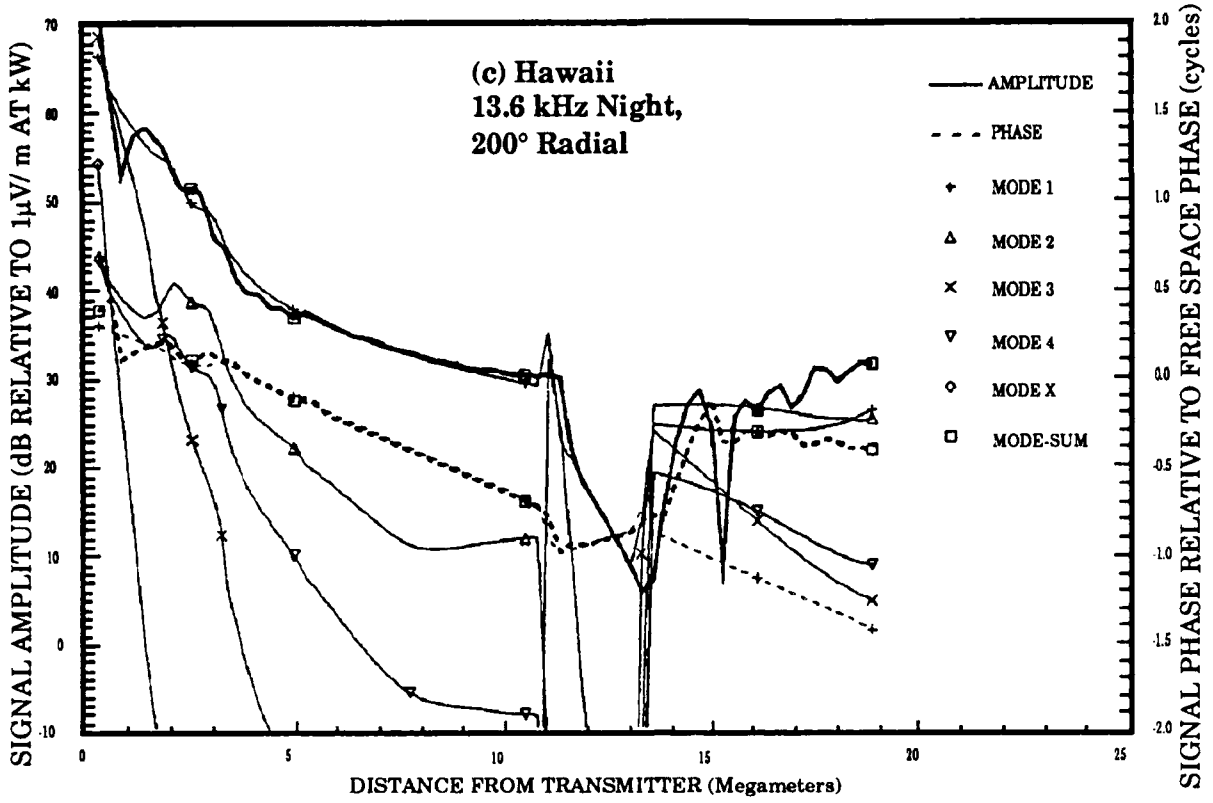

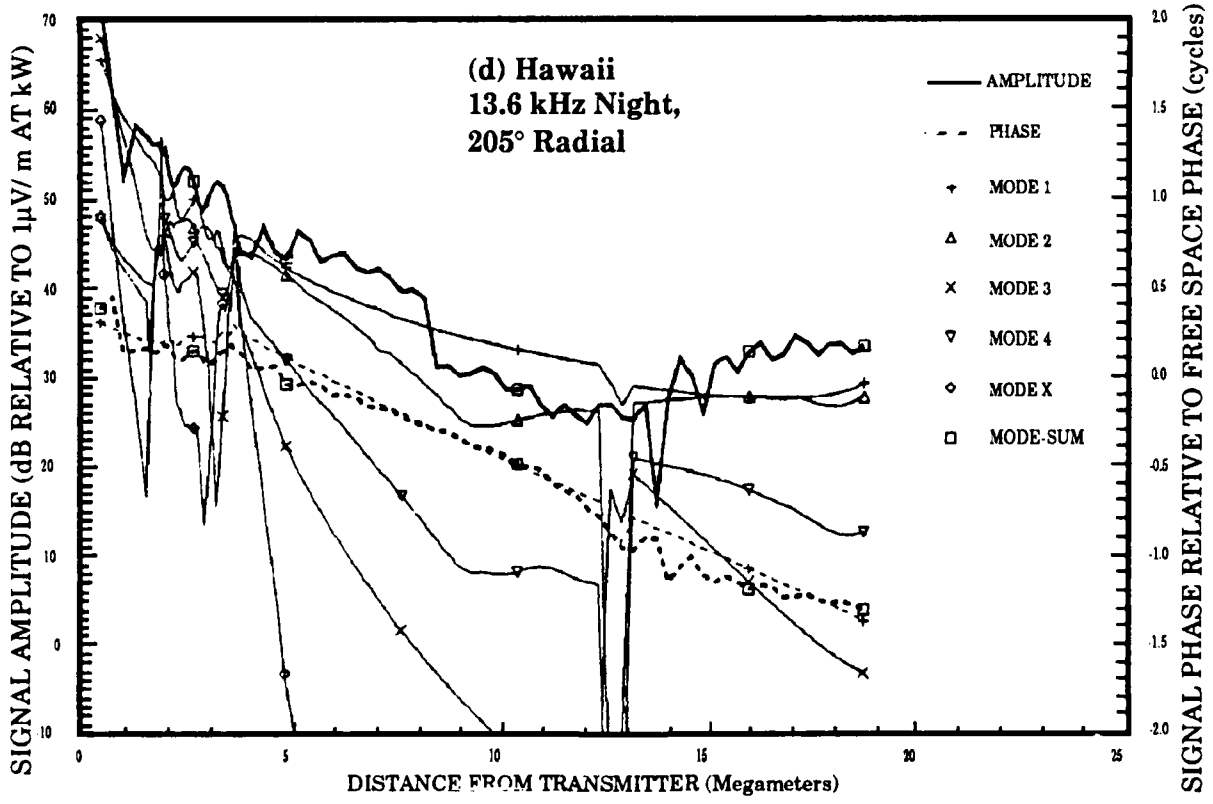

Figure A-9cd. Calculations of the Hawaii Signal Propagated on the 200° and 205° Radial at 13.6 kHz

dominant to 7.4 Mm. Beyond the equatorial zone, mode competition may or may not exist, depending upon the relative level of the modes exiting this zone. The calculations show that the modal levels are quite sensitive to radial bearing. It is possible that the modal levels would also be quite sensitive to ionospheric parameters. The sensitivity to ionospheric parameters could lead to a seasonal effect, a possibility we have not investigated.

For 10.2 kHz, mode 1 is predicted to remain dominant between the transmitter and the mode conversion zone for all bearings. The margin of dominance is small over much of the path as is shown in Figure A-10.

For 13.6 kHz, beginning at a radial of about 210°, mode 3 begins to acquire a dominant position between the transmitter and the onset of mode conversion. Mode 2 becomes stronger with increasing bearing and by 270°, mode 2 crosses mode 3, thus becoming dominant for part of the distance to the onset of mode conversion. After the 300° radial, mode 1 competes with mode 2 to about 330°. Beyond 330°, mode 1 is dominant within the Western Pacific validation region except for the near zone modal dominance by mode 3.

Figure A-10 shows the calculated 10.2 kHz and 13.6 kHz signals for the 280° radial. At 10.2 kHz, the largest margin of dominance at 5 dB occurs at 2 Mm. At 13.6 kHz, mode 1 is 5 dB below the dominant mode to 3.4 Mm, the distance where mode dominance switches from mode 3 to mode 2. Beyond 3.4 Mm, the margin of mode 2 over mode 1 increases with distance, reaching 12 dB by 7 Mm. On a radial to Japan, approximately 300°, the 10.2 kHz mode 1 component of the signal is dominant by about 6 dB at 7 Mm, and at 13.6 kHz modes 1 and 2 are about equal.

Our interpretation is that, given expected propagation variability, the modal effects in a sector bounded by the 270° and 310° radials can evidence modal effects on all Omega frequencies. The most pronounced effects would be at 13.6 kHz. Modal effects would also occur more frequently at 13.6 kHz.

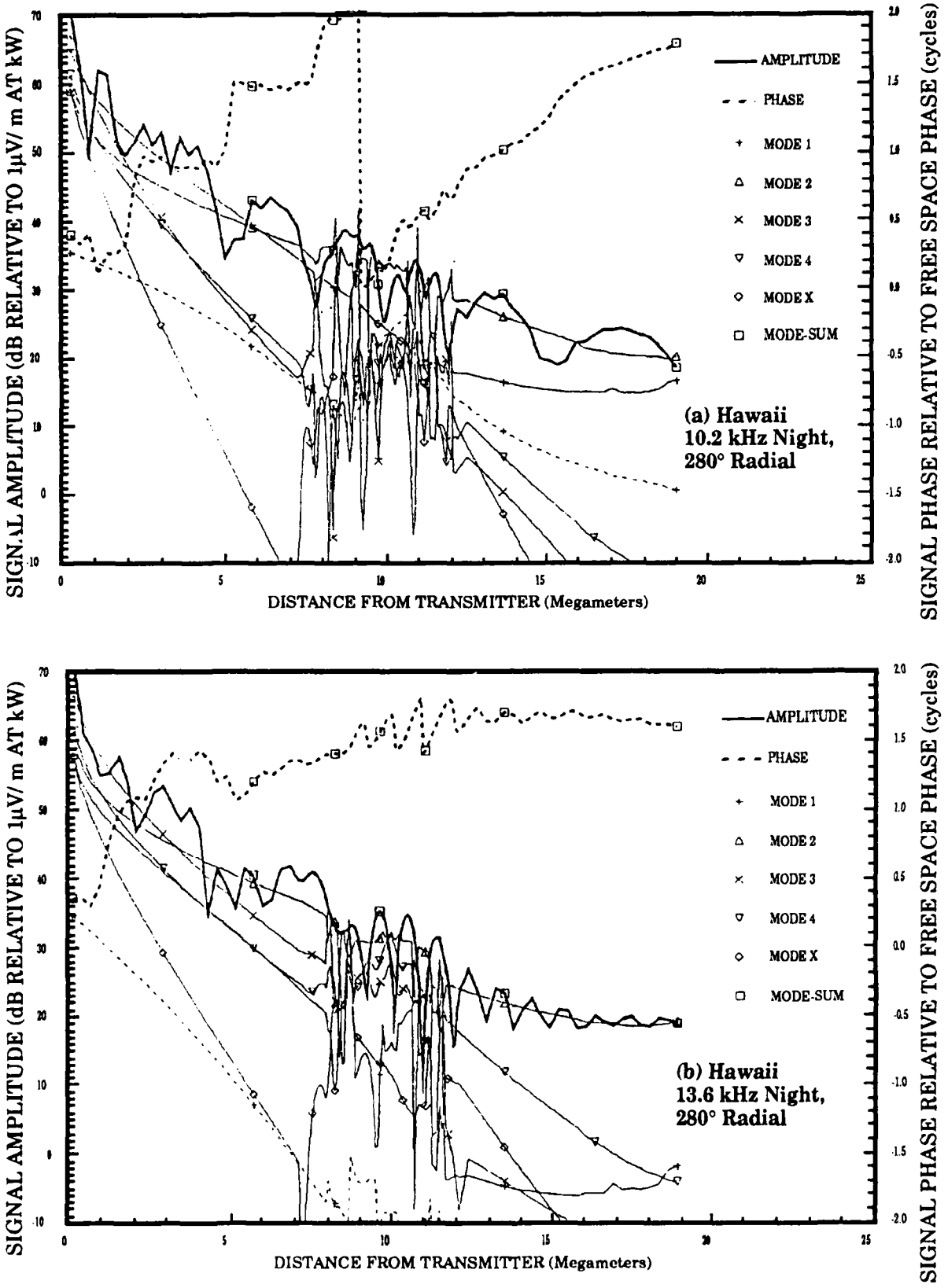

Figure A-10. Calculations of the Hawaii Signal Propagated on the 280° Radial

(D) NORTH DAKOTA

The zones for nighttime propagation of possible poor phase on North Dakota signals in the Western Pacific are shown in Figure A-11. The signal from North Dakota incurs modal conversion in propagation in the equatorial zone at headings greater than 205°. The signal enters the lower right corner of the validation region along a radial of 223°. A sample calculation showing the equatorial zone effects is shown in Figure A-12 for a radial of 300°. Yap lies close to this path at a distance of about 11.7 Mm, well within the mode conversion zone. For both 10.2 and 13.6 kHz, mode 1 is dominant before the mode conversion zone and mode 2 is dominant exiting this zone. The northern boundary moves northward with more westward propagation, as does the magnetic equator. As with Hawaii, the buildup of modal conversion occurs very quickly as the signal's direction of propagation increases beyond 200°. The modal interference structure and its magnitude in the zone below the equator varies in a complex manner in relation

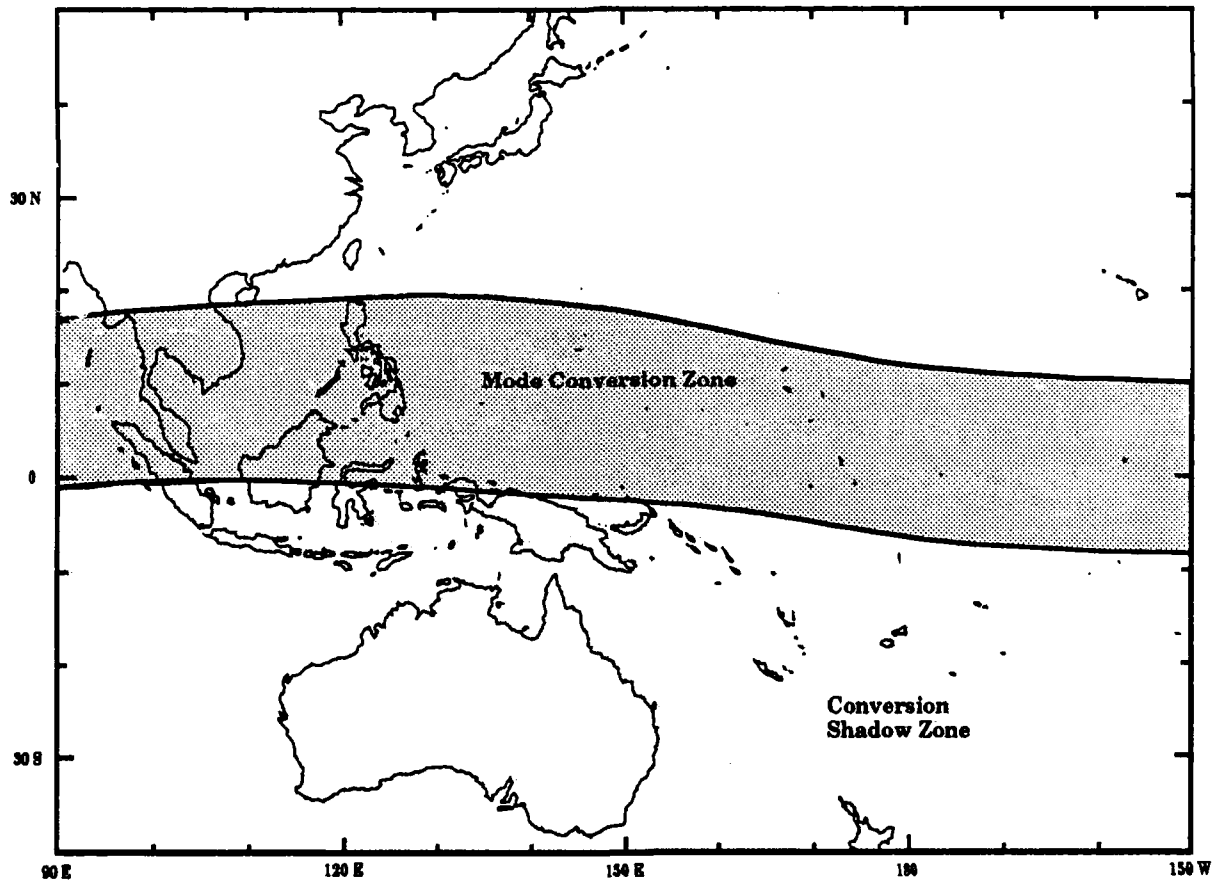

Figure A-11. Modal Zones for the North Dakota Signal

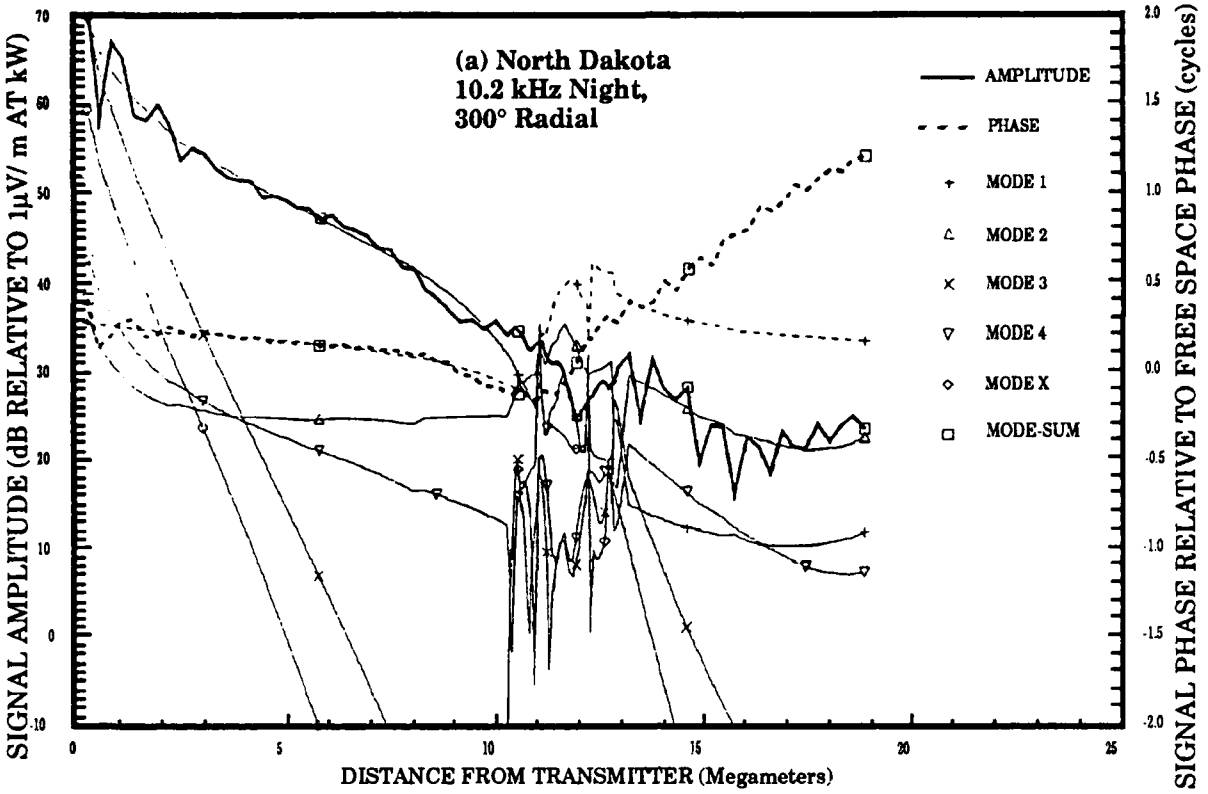

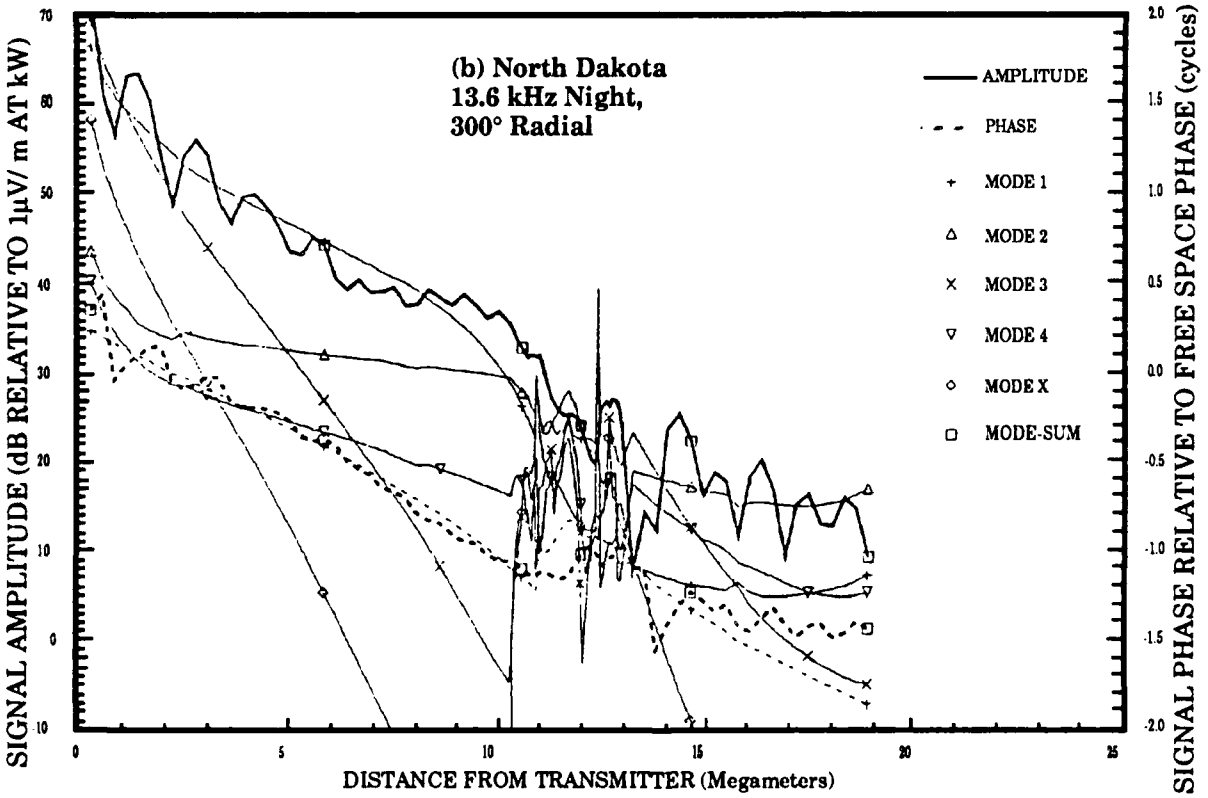

Figure A-12. Calculations of the North Dakota Signal Propagated on the 300° Radial

to frequency and direction of propagation. Because of phase uncertainty, the North Dakota signal is not considered useful for navigation at night below the northern boundary of the mode conversion zone. For all daytime propagation no modal signal self-interference is expected.

(E) LA REUNION

The La Reunion signal is predicted to have good phase quality throughout almost all of the Western Pacific validation region. The calculations for 13.6 kHz (Figure A-13), show that in a broad sector to the south-of-east, the initially dominant mode 3 extends a short distance into the validation region. The 70° radial crossing Singapore, has the largest extent of modal competition. Figure A-14 shows the computed signals for 10.2 and 13.6 kHz on this radial. The crossover for mode 1 dominance occurs at 1.8 Mm for 10.2 kHz and 4.1 Mm for 13.6 kHz. The farthest possible extent of this crossover at 13.6 kHz is estimated to be about 7 Mm. Singapore is about 5.8 Mm from the station.

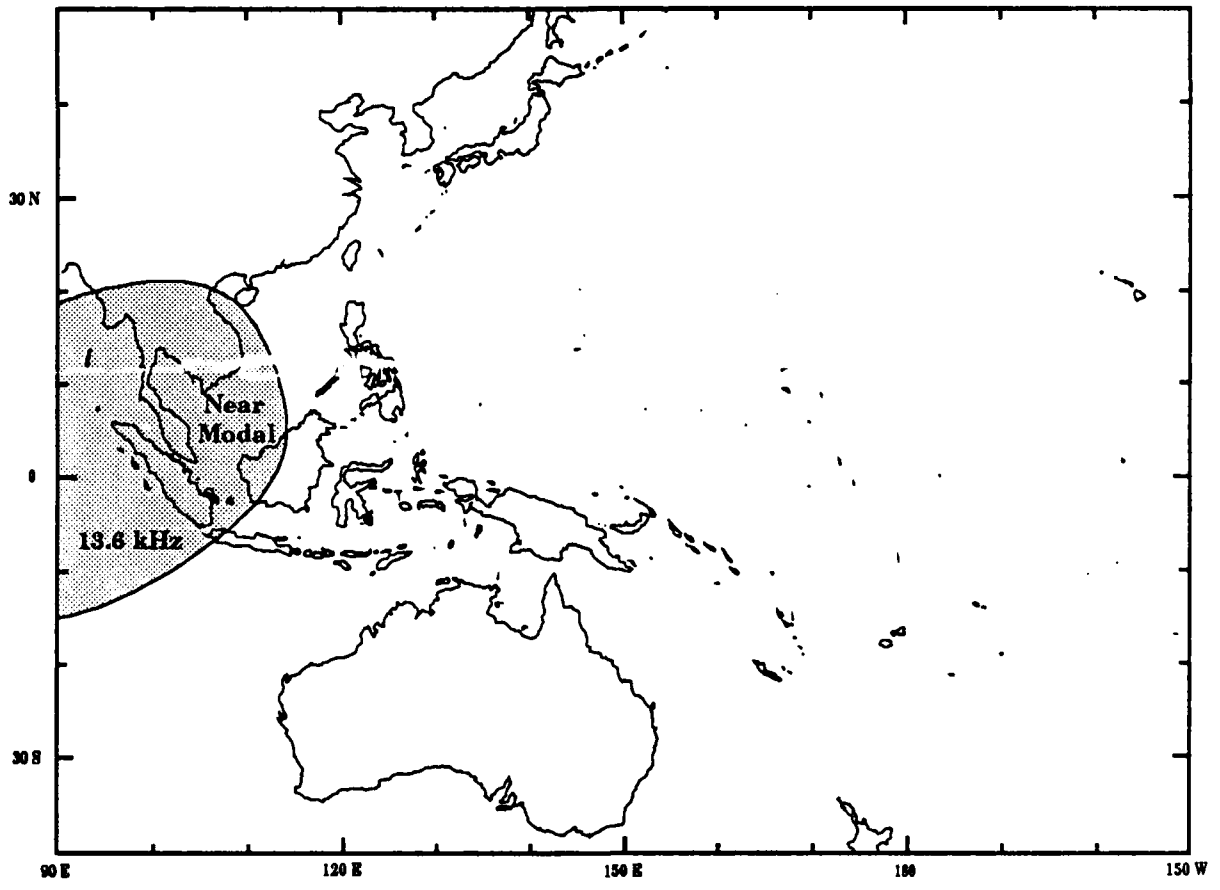

Figure A-13. Modal Zone for the La Reunion Signal

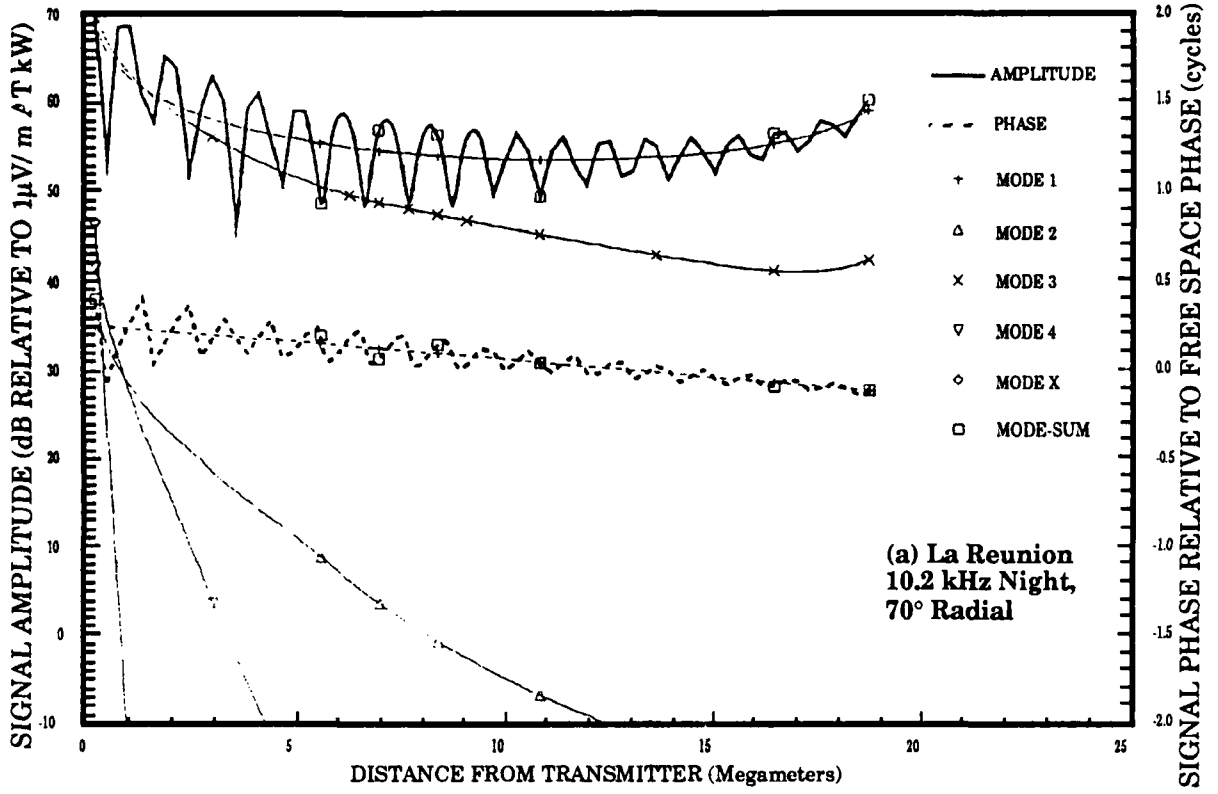

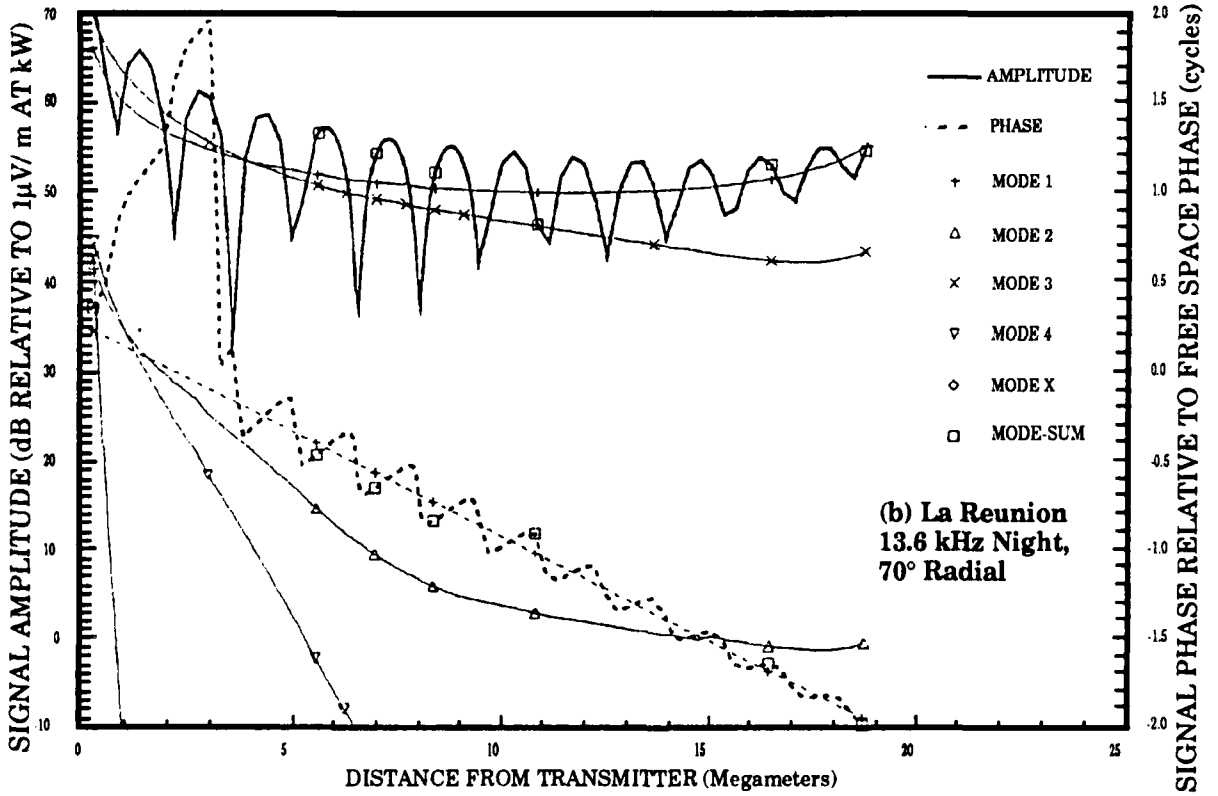

Figure A-14. Calculations of the La Reunion Signal Propagated on the 70° Radial

(F) ARGENTINA

The zones of possible poor phase on Argentina signals in the Western Pacific are shown in Figure A-15. Five zones are depicted: near modal, mode conversion, conversion shadow, antarctic shadow and the antipode. The 10.2 and 13.6 kHz signals have different envelopes of near modal with only the 13.6 kHz near modal extending into the validation region. At 13.6 kHz, many modes are excited efficiently. In the validation region, mode 2 becomes dominant for radials greater than 240°. The near modal zone for 13.6 kHz is probably highly dependent upon propagation conditions, and thus the mode conditions are expected to vary from time to time. A sample calculation showing the mode interaction effects is shown in Figure A-16.

The mode conversion zone starts on the left along a propagation path radial of 195° and extends eastward with increasing bearing. The conversion zone extends to near the 350° radial. This radial is incident on the antipode from a bearing of

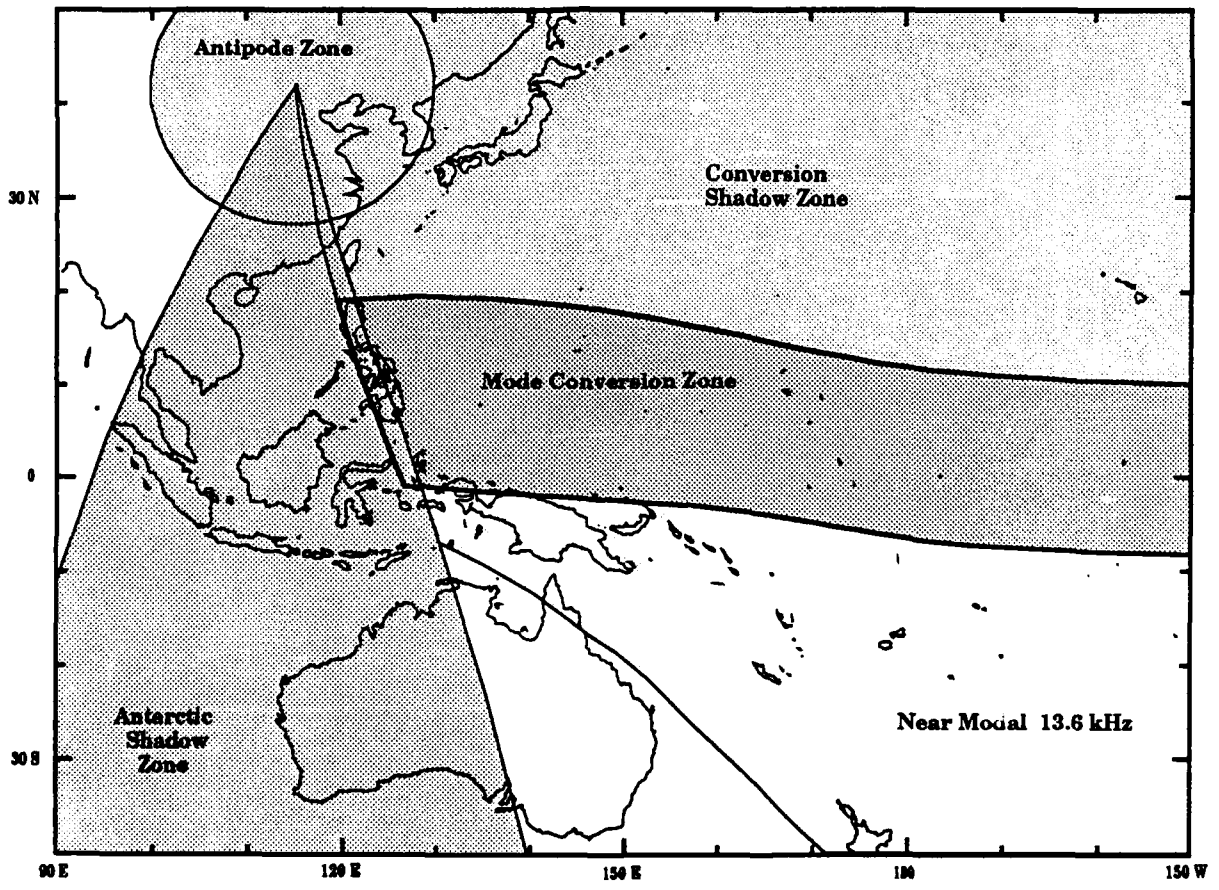

Figure A-15. Modal Zones for the Argentina Signal

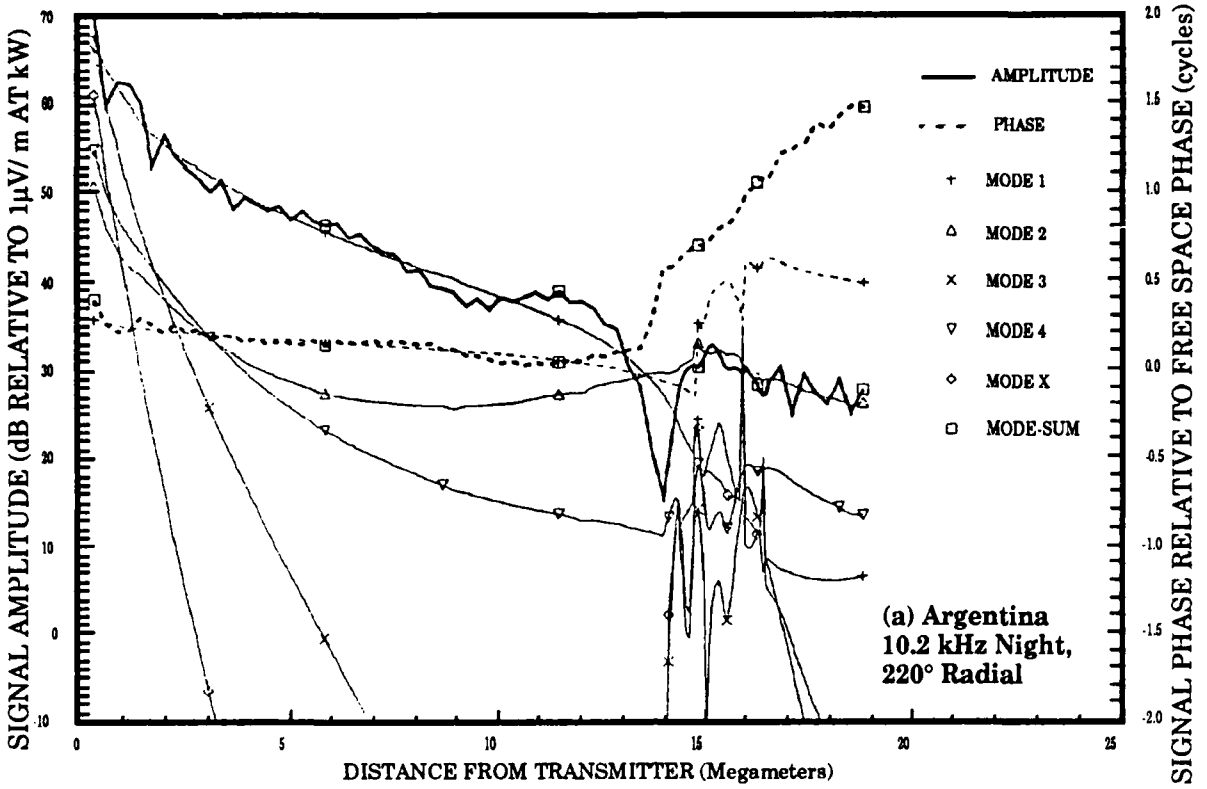

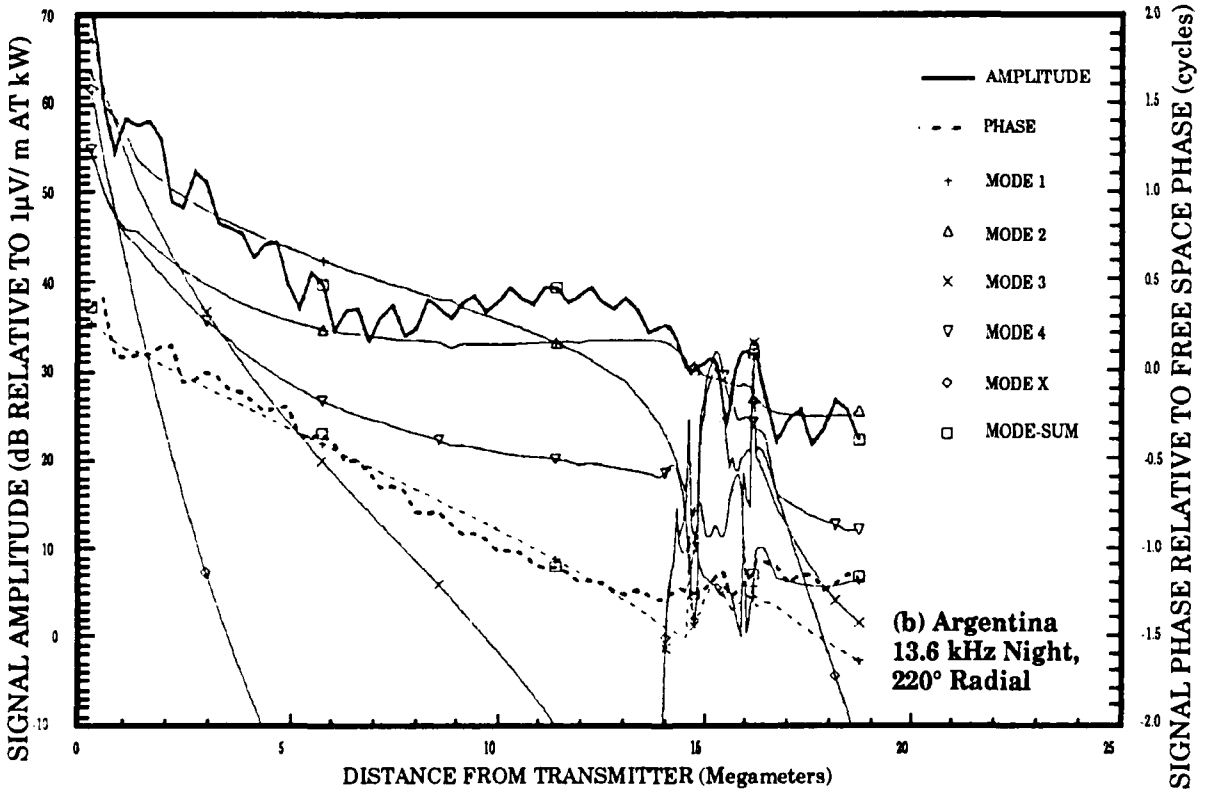

Figure A-16. Calculations of the Argentina Signal Propagated on the 220° Radial

10°. Once the equatorial zone is reached, rapid mode conversion takes place with many modes switching around. Mode 2 dominance occurs after exiting the equatorial mode conversion zone.

The shadow zone is predicted to be dominant mode 2 throughout the area. Received phase is not predictable because of the earlier unpredictable mode conversion effects.

The antarctic shadow zone is along the western side of the validation region. This zone extends to the antipode (20.97°N, 114.81°E). Due to propagation across the Antarctic during daylight, the signals are expected to be very weak during austral summer. During parts of winter the signal in this zone could be either mode 1, 2 or 3, depending on the radial and distance.

A standard guard zone is depicted for the antipode region.

We note that the Argentina signal is useful at night only in two very small areas within this validation region.

(G) AUSTRALIA

For Australia (Figure A-17), the zones of possible unusable phase are the near modal around the transmitter, the equatorial mode conversion zone, and the shadow zone. For 10.2 kHz, the near modal zone extends to 0.6 Mm north, 0.9 Mm east, 0.7 Mm south and 0.7 Mm west. For 13.6 kHz, this zone extends 1.1 Mm north, 2.4 Mm east (100° and 110° radial), 1.4 Mm south and 1.9 Mm west. This near modal zone was examined in the South Pacific validation.

The nighttime equatorial mode conversion zone lies mostly above the geographic equator. This is because the magnetic equator is offset northward. The onset of equatorial mode conversion occurs on the far side of the world on a propagation path heading greater than 180°. The bearing of mode conversion onset is masked by the effects of trans-antartic propagation. By the time that the propagation path is near tangent to Antarctica, 210° bearing, the equatorial conversion is evident in the calculations. This path traverses east of Africa, crossing the equator about 47°E longitude. The equatorial mode conversion zone extends from 47°E, eastward to near 142°E longitude. The eastern part of this zone is in

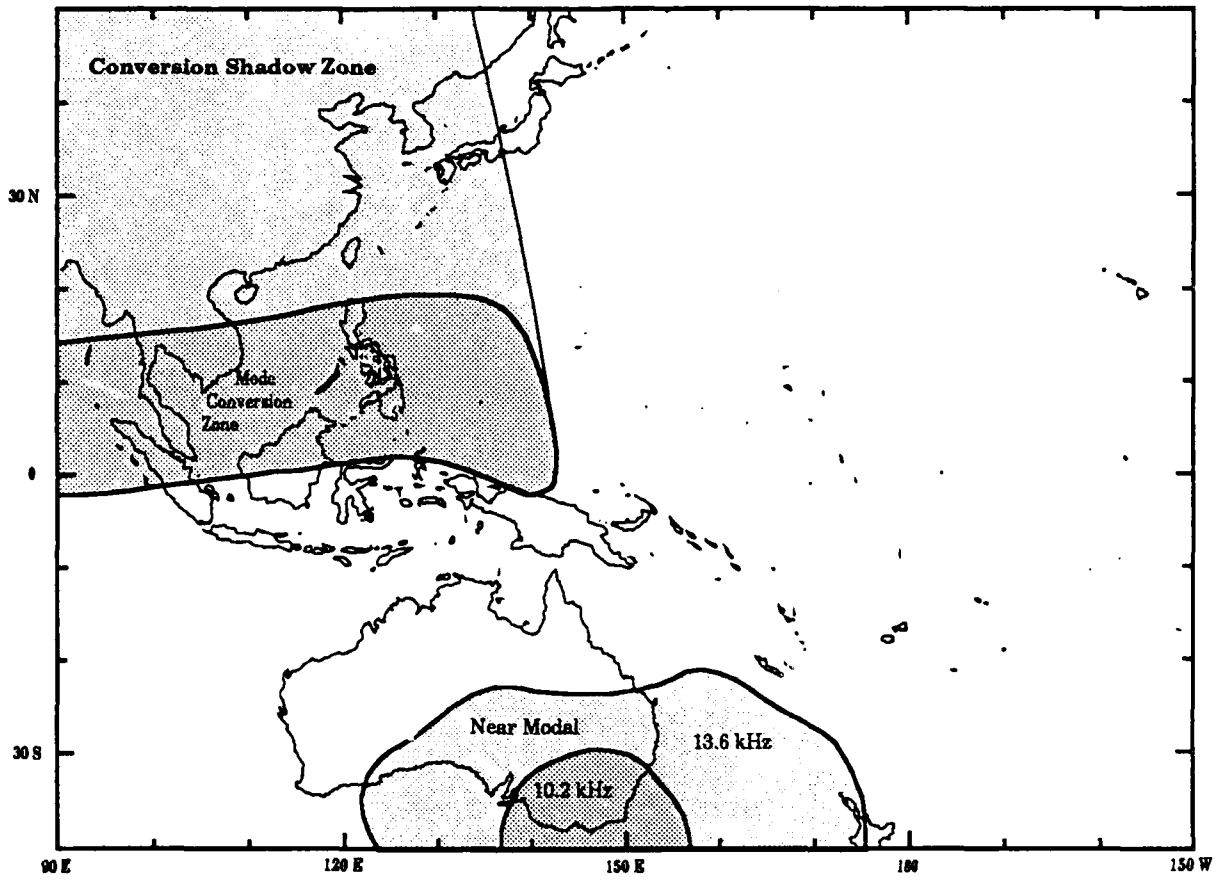

Figure A-17. Modal Zones for the Australia Signal

this validation region. The calculations predict the boundary to be between the 350° and 353° radials.

The shadow zone from equatorial mode conversion extends northward with the eastern boundary predicted to cross Japan near Nagoya.

In Figures A-18 and A-19 we show field strength versus distance calculations at 10.2 and 13.6 kHz for the 330° and 350° propagation path radials respectively. The 330° radial crosses the Philippines near the Cubi monitoring site, which is near 6.7 Mm on the path. The 350° radial crosses Japan just west of Nagoya, which is near 8.3 Mm on the path. These calculations show the predicted complexity of mode conversion within the equatorial mode conversion zone and the resultant effects on mode dominance within the shadow zone. We note that Cubi is in a strong mode conversion area and that Nagoya lies on a path with less pronounced equatorial zone mode conversion effects. While the mode dominance at Cubi is unpredictable, at Nagoya both the 10.2 kHz and 13.6 kHz signals are

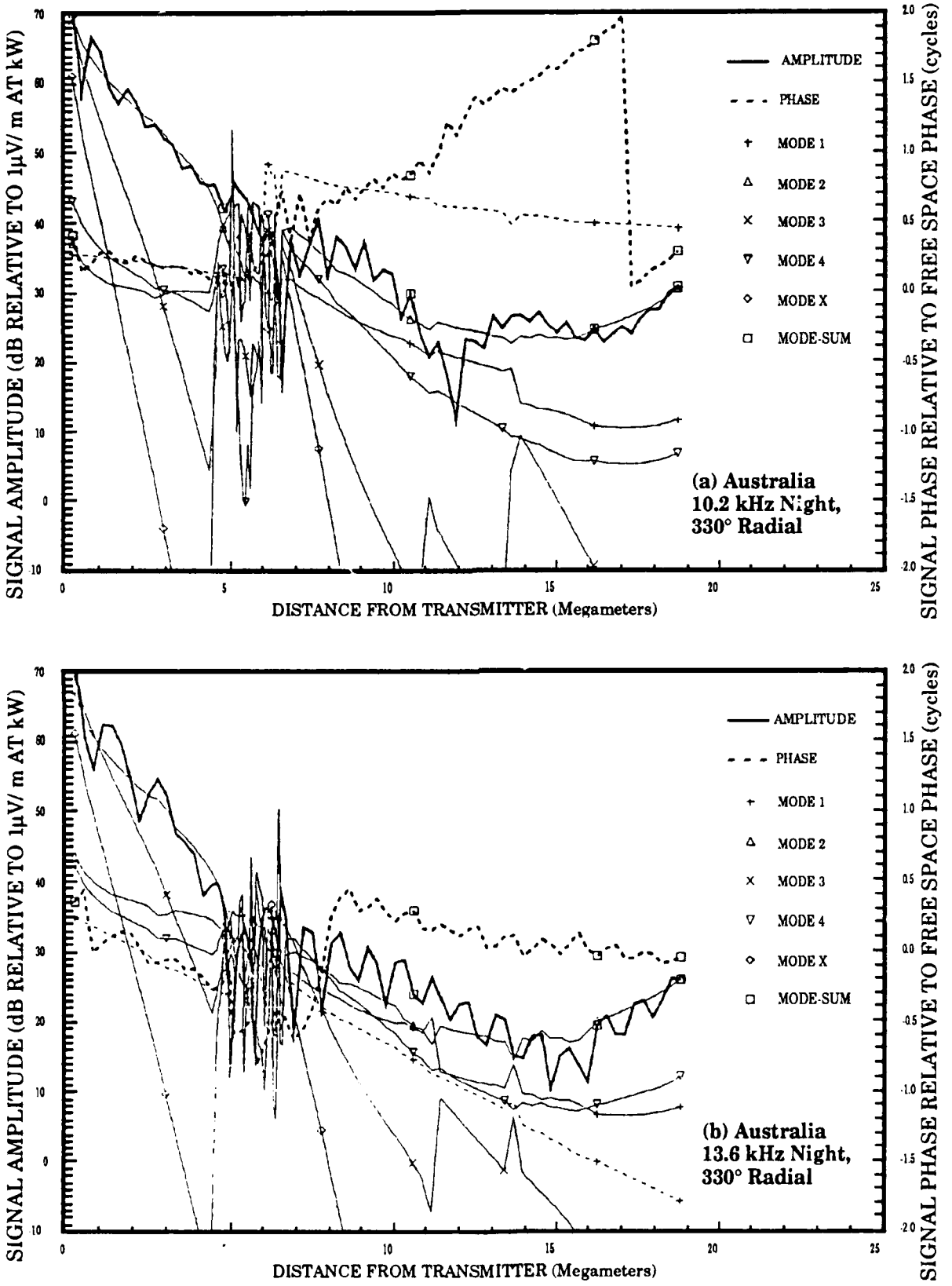

Figure A-18. Calculations of the Australia Signal Propagated on the 330° Radial

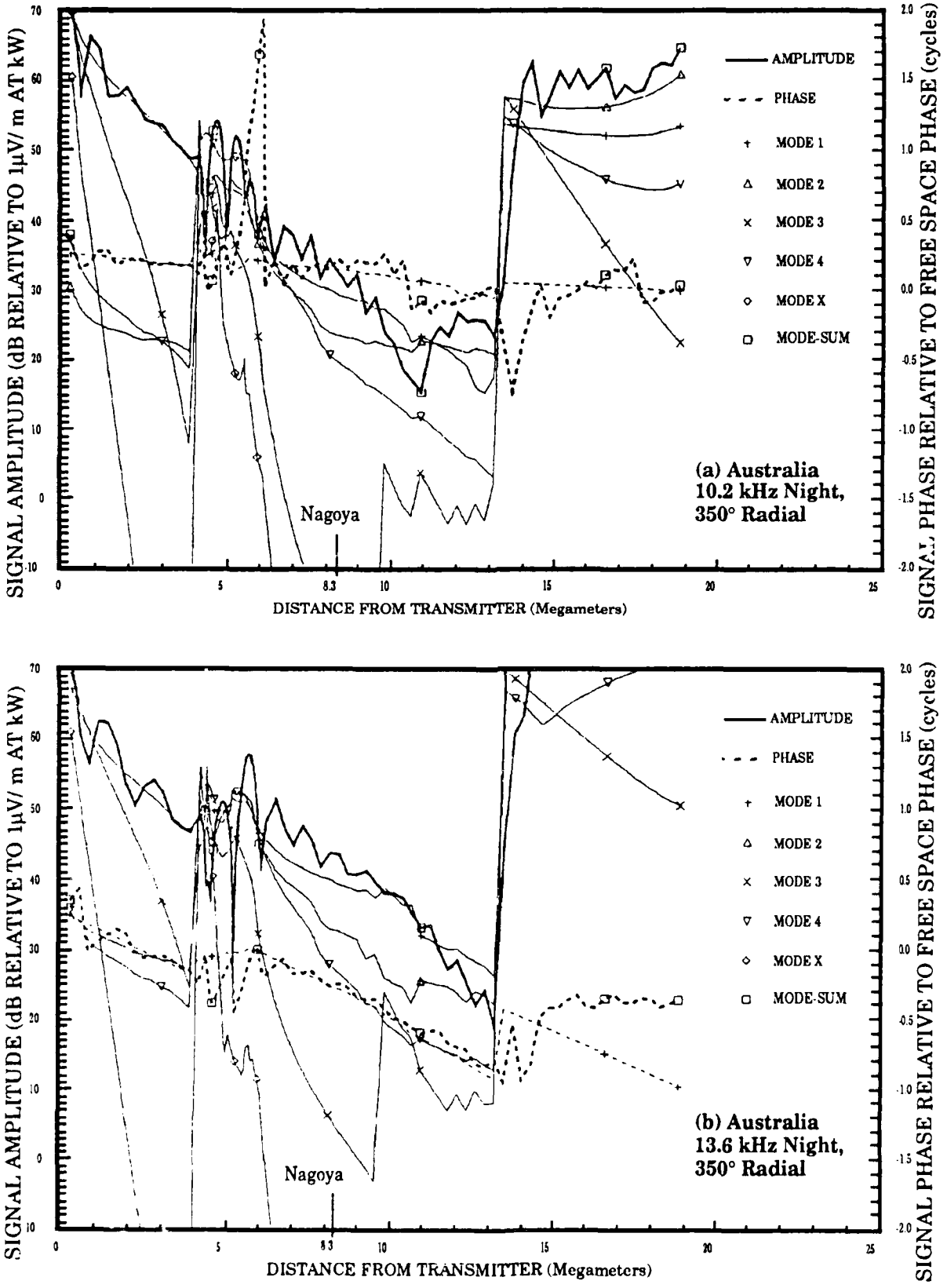

Figure A-19. Calculations of the Australia Signal Propagated on the 350° Radial

predicted mode 1. The mode 2 signal component is predicted to be about 6 dB below the mode 1 signal. However, the shadow zone prediction, for the 330° radial, is for mode 2 to be dominant. Our assessment is that the mode dominance predictions for the shadow zones are too sensitive to the chosen calculation parameters to be reliable for prediction testing.

(H) JAPAN

The zones of possible poor phase on Japan signals in the Western Pacific are shown in Figure A-20. The predictions show possible near modal zone competition extending into the eastern side of the validation region. This zone for 13.6 kHz was examined in the South Pacific validation where we concluded that the zone did not extend as far as predicted by calculations. However, we felt that the data were too limited to establish a definite conclusion and further assessment was needed. The reader is referred to the South Pacific validation report for our

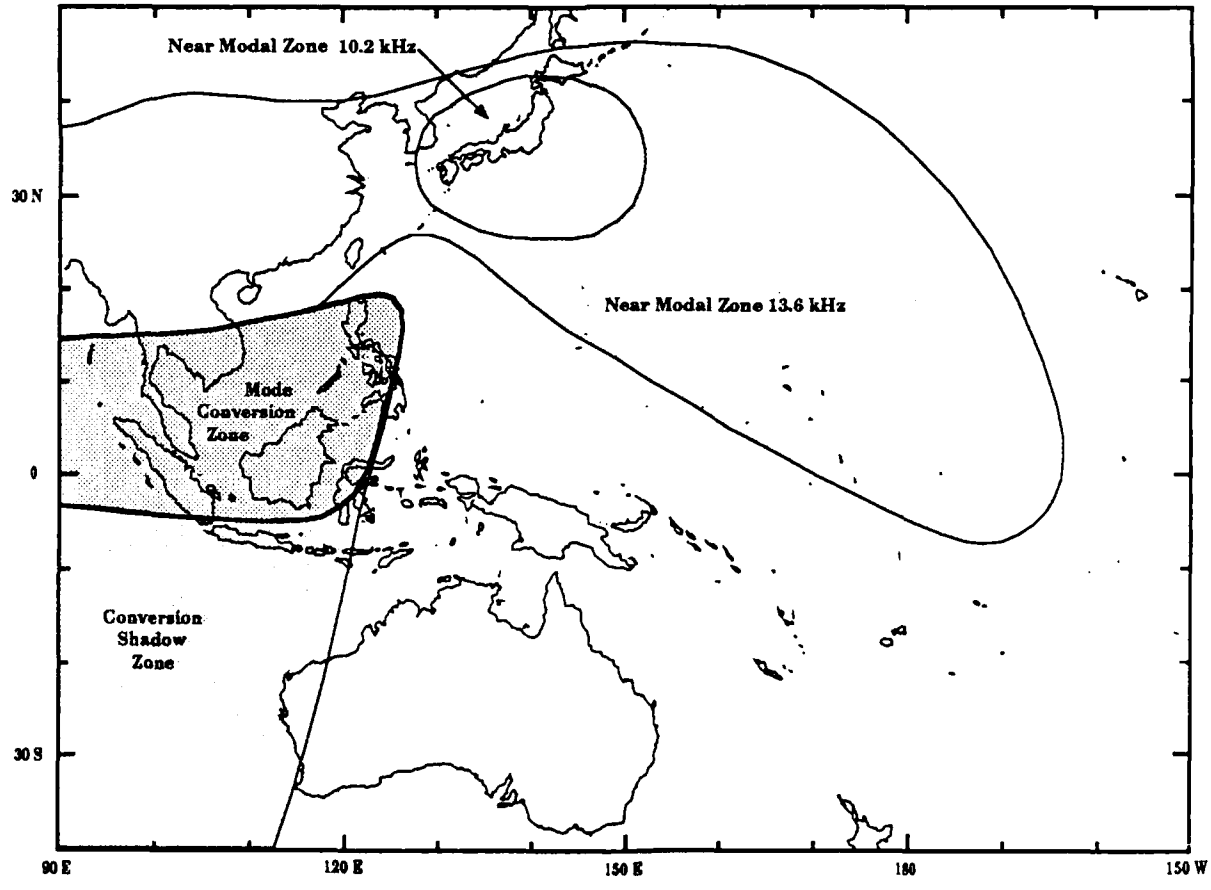

Figure A-20. Modal Zones for the Japan Signal

rationale in suggesting adjustments to this boundary. Here we use the calculation predictions and conduct an independent assessment of boundary placement. A sample calculation showing the mode competition effects of the near zone at 13.6 kHz is shown in Figure A-21 for the 110° radial. For 10.2 kHz predicted boundary, the maximum possible extent of mode 2 dominance is about 2.4 Mm which occurs on the 90° radial. For 13.6 kHz, we have plotted the predicted maximum extent of the modal interference. We estimate this distance in Figure A-21 to be 8 Mm. At this distance the mode 3 is predicted to be less than 2 dB below the dominant mode 1. Near the crossover line the slope of mode 3 compared to mode 1 is only about 1 dB per Mm greater. Thus, this boundary line distance would vary quite a bit with expected variations in propagation conditions.

The predicted equatorial mode conversion zone starts between the 190° and 200° radial from the station as shown for the 10.2 kHz signal in Figure A-22. Note the mode plots at about a distance of 3 Mm. We chose the 190° radial for our plot in Figure A-22 in order to be conservative in allowing for phase deselection.

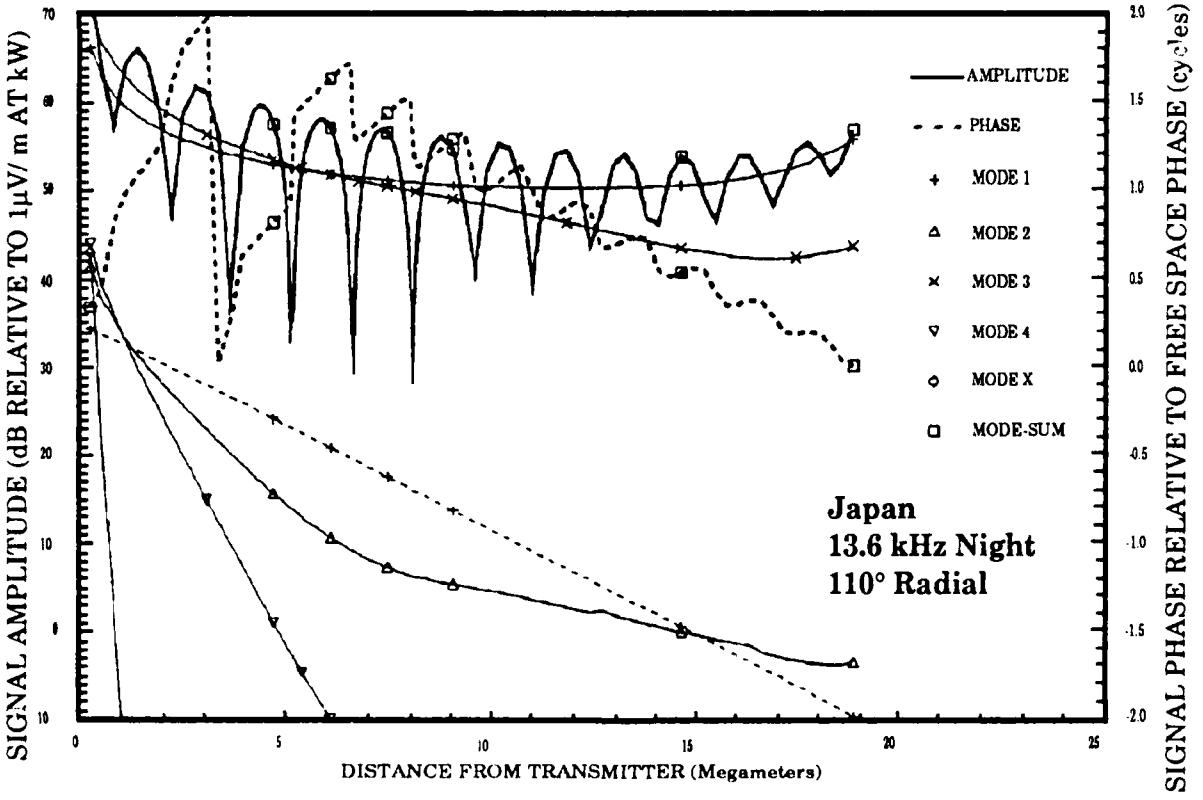

Figure A-21. Calculations of the Japan Signal Propagated on the 110° Radial at 13.6 kHz

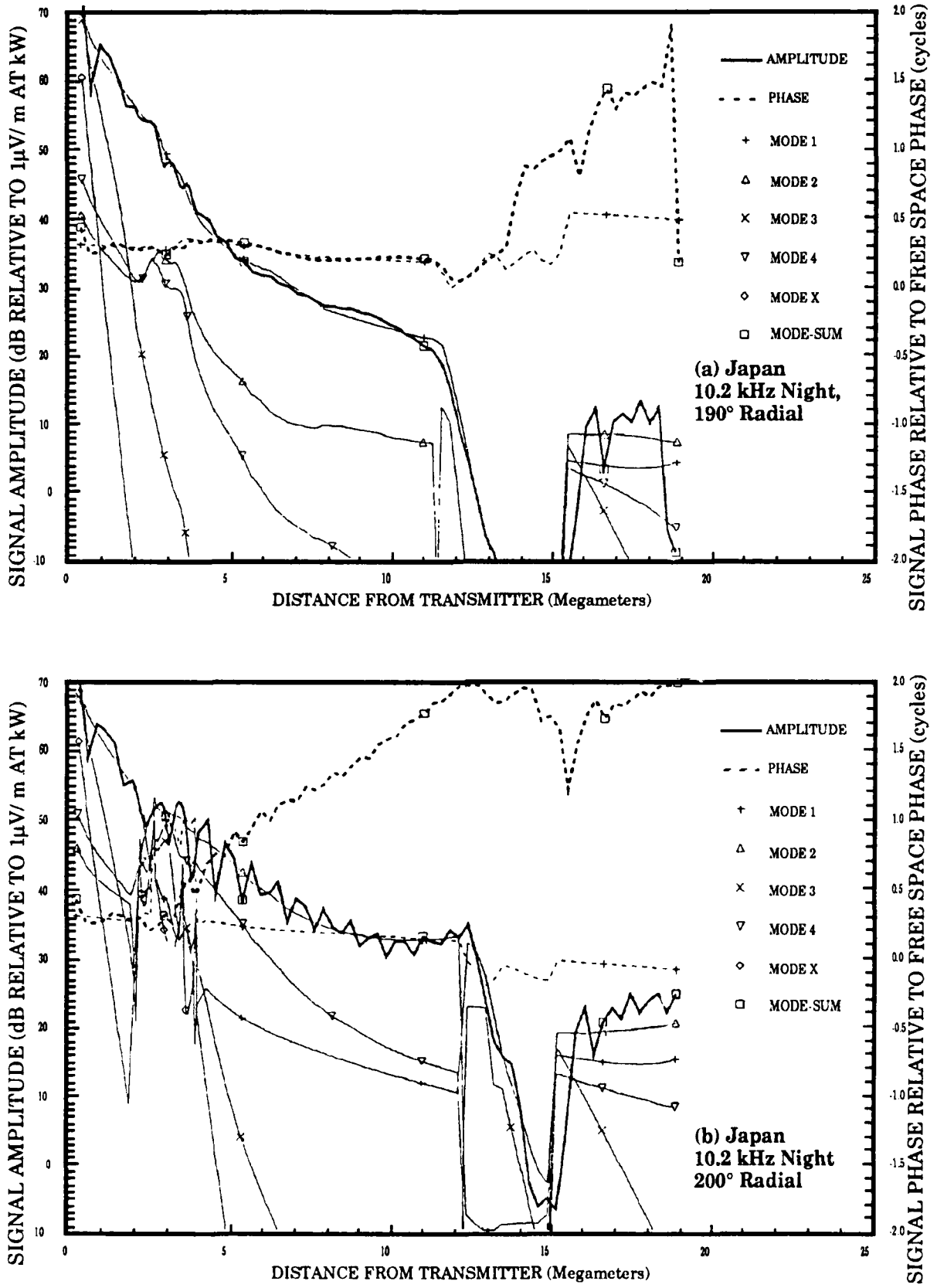

Figure A-22. Calculations of the Japan Signal Propagated at 10.2 kHz

The eastern edge of the conversion shadow zone extends across the western edge of Australia crossing close to Perth. We note from Figure A-22 that the 10.2 kHz signal on the 200° radial is predicted mode 2 dominant in this shadow zone. As cited earlier, the situation appears very sensitive to selected parameters. This is illustrated by the calculations of Figure A-23, which shows the 10.2 and 13.6 kHz signals on a 206° radial. This figure shows a different modal structure in the shadow zone, i.e. beyond 5 Mm distance.

SUMMARY

The propagation predictions from calculations of this section are used in this validation as guidance for data analysis assessment and as a model for extending interpretation of measurements from selected locations to the total Western Pacific validation region. It should be emphasized that these charts are for nighttime propagation on each signal path and thus are time static. This means they do not take into account the diurnal variability of the zones of unusable phase. They are also seasonally static. Variations in solar illumination at the poles are not integrated into the analysis. While these charts are considered a good model for validation data assessment, further interpretation is needed to derive navigation guidance.

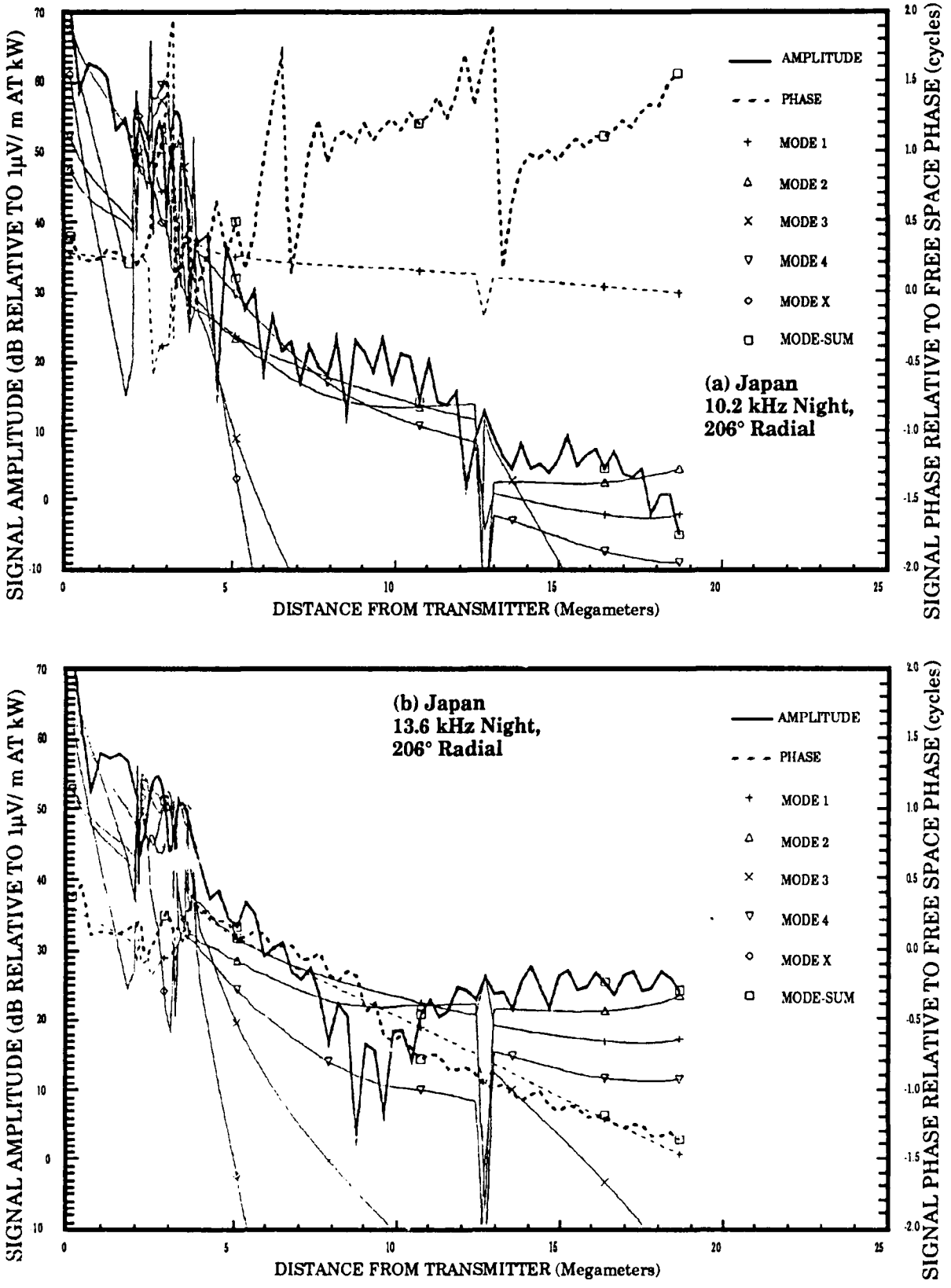

Figure A-23. Calculations of the Japan Signal Propagated on the 206° Radial

THIS PAGE INTENTIONALLY LEFT BLANK

Appendix B

Modal Interference Data Analysis

GENERAL OVERVIEW

The procedure we use for data interpretation is to work across the validation region from east to west, generally following the sequence of flights. We group the analysis into four geographic areas: (1) Hawaii to Guam, (2) Guam to, but not including, Cubi Point in the Philippines, (3) Japan vicinity, and (4) west of Cubi Point to Singapore. These areas form natural divisions because of predicted phenomena and available data. The first area, west of Hawaii, includes the onset of equatorial zone mode conversion for the Hawaii signals and the predicted long extent of the 13.6 kHz near modal zone for the Japan signal. Equatorial mode conversion zones for North Dakota and Argentina, which start east of Hawaii, also extend clear across this area, as well as most of the validation region. The second area, Guam to the Philippines, includes the predicted eastern edge of the Australia equatorial mode conversion zone. It also includes the conversion zones from the first area. The third area, in the vicinity of Japan, is selected because of the special interest in checking the Japan transmitter and because of the concentration of traffic around Japan. The fourth area, the Philippines to the western edge of the region, includes the eastern edge of the Japan signal equatorial mode conversion zone as well as the continuation of conversion zones for Hawaii, North Dakota, Argentina, and Australia. This area is predicted to be very difficult for navigation because of modal effects and high atmospheric noise levels.

The process for each geographic segment is (1) for each Omega station, to determine the predictions, from calculations, of the dominant mode and signal amplitude structure in the general area and specifically for locations where data are available, (2) to compare flight amplitude data with calculations, (3) to examine available fixed-site phase data for possible modal effects, and (4) to examine shipboard phase-error or phase-difference data, if available, for clues of modal effects. To assist our interpretation of modal phenomena, we depend heavily on comparisons of the amplitude and phase patterns across the band of Omega frequencies and upon the dynamics of propagation diurnally and from day-to-day. The analysis techniques we use were devised for the South Pacific validation, but with several important differences that we describe in this section.

In this validation, we conduct an even more integrated examination of aircraft amplitude, fixed-site phase, and shipboard phase-difference data then that of the South Pacific validation. In addition to finding the cross-comparison of the different data types valuable, we benefit significantly from the experience gained from the South Pacific analysis. In this validation, we also find the propagation conditions quite variable from day-to-day and thus have to make use of all opportunities to piece together a coherent regional picture. Each of the data sets (flight data, fixed-site data and shipboard data), has special processing and interpretation requirements.

As with the South Pacific analysis, we are unable to extract meaningful phase data from the flights. This is due to large reference oscillator frequency offsets and to sample intervals that are too long to measure the phase drift. The amplitude data require much processing and careful interpretation due to many kinds of interference, such as local aircraft noise and precipitation static. The expertise of Carl Kugel at NOSC proved invaluable for establishing confidence in flight data interpretation.

Each flight was along a propagation radial from a selected Omega transmitter. For all other signals, the propagation path varied in azimuth from the transmitters with flight time. For the South Pacific validation, we constructed predicted signal levels across the radials as intersected by the flight path. Since the distance from the transmitter generally was large, the available radials (usually calculated at ten-degree intervals) produced rather sparse prediction values along the flight paths. This sparseness was a problem as the computed signals often changed markedly between radials. We found that the agreement between predictions and flight data were poor, and the effort provided minimal value for coverage interpretation. Consequently, we now rely more heavily on predicting boundaries for modal zones and/or signal levels and assessing evidence for their existence in the data. These modal zones are derived in Appendix A.

An important difference for the fixed-site data, with respect to the South Pacific validation, is that none of the received phase is referenced to an atomic frequency standard. Reference frequency drifts are often quite large and occasionally change quickly in unpredictable ways. Consequently, the techniques for mitigating the effects of phase drift, devised in the South Pacific validation, had

to be greatly refined for this analysis. Otherwise the database would not be sufficient to conduct the modal effects assessment.

As in the South Pacific, we encounter large areas of high interest for modal analysis where no fixed monitoring sites existed. Fortunately, the Aids to Navigation Research Vessel, Tsushima, operated by the Japanese Maritime Safety Agency, collected navigation data in several key locations and used a stable reference oscillator that allowed direct measurement of phase for each signal. We are able to integrate the Tsushima data with the flight and fixed-site data to derive a more comprehensive assessment of modal boundaries. The Tsushima data are particularly important for modal assessment west of Cubi and Darwin, because data from Singapore, the only more westerly fixed site, is generally unsatisfactory.

Our assessment of modal occurrence is subjective. Also, the techniques for interpreting data from each of the recording platforms, aircraft, fixed site and shipboard, differ somewhat. Thus, to aid the reader, we will present an overview of the data features considered important to assessing modal effects.

OVERVIEW OF ANALYSIS TECHNIQUES

The purpose of this data analysis is to determine where modal self-interference occurs. The steps are (1) first to determine if the recorded signals are composed of more than one mode, (2) to interpret the likely mechanisms for producing the higher-ordered modes from the geographic pattern of modal interference, and (3) to compare the interpretations with the calculation predictions derived in Appendix A. Data and analysis samples are presented throughout this appendix to support our interpretation. Here we present a model and show representative data to illustrate our interpretation of non-modal and modal effects for the different sets of data used.

We make use of the fact that each mode propagates with a unique velocity and attenuation rate that varies with frequency and propagation conditions. A model to represent this propagation in idealized form is represented in Figure B-1. First we start with a model of pure single-mode signal to produce the diurnal amplitude and phase curve shown in part (a). The characteristics of this curve are (1) daytime stable and repeatable amplitude and phase segments, (2) a sunset transition with a slight dip in amplitude and phase retardation, (3) stable

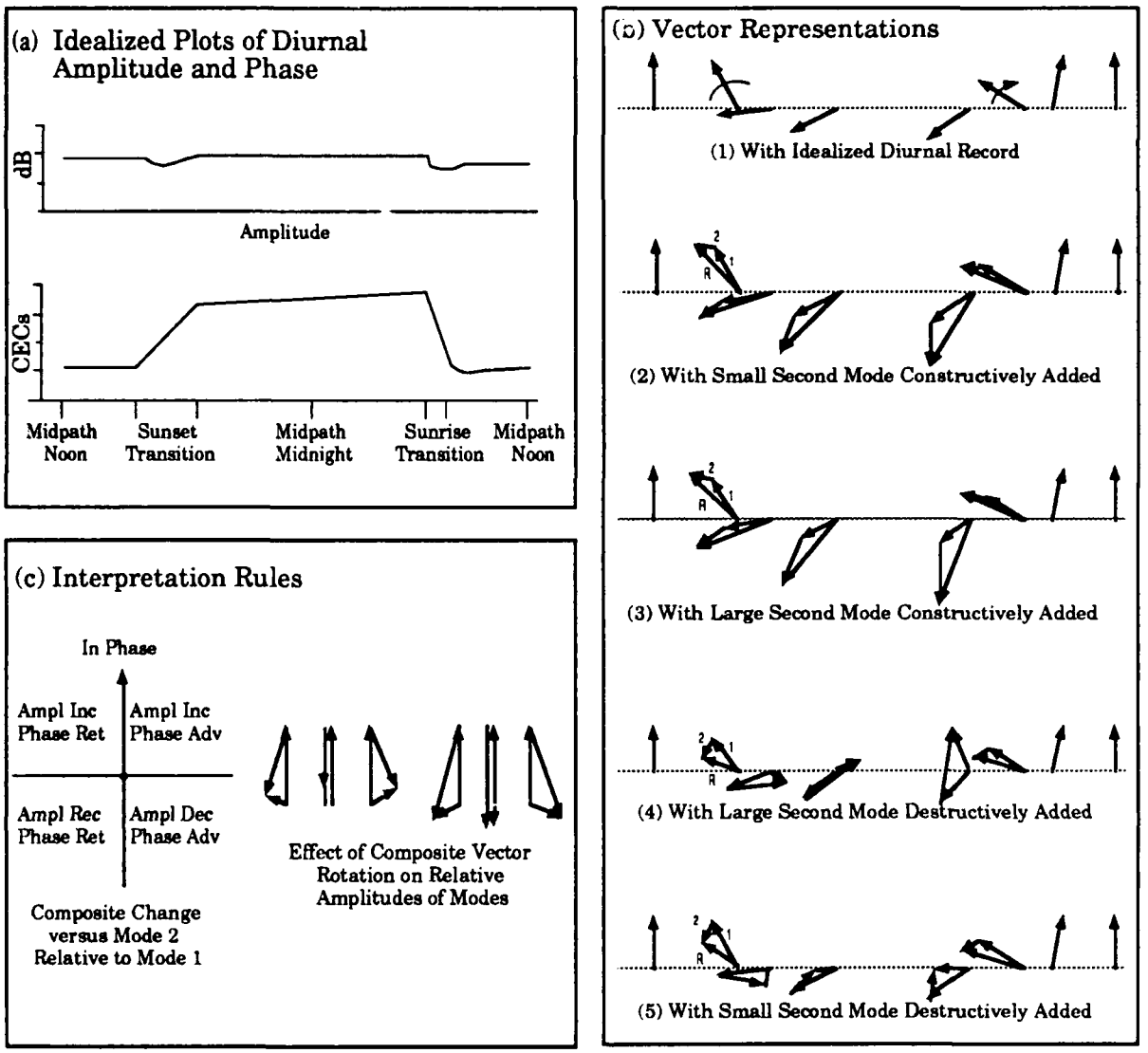

Figure B-1. Model for Modal Component Analysis

nighttime amplitude and a slight further retardation of phase throughout the night, and (4) a sunrise transition with a slight dip and a phase advance that may overshoot slightly into the early morning period. This single-mode model is also shown in vector form as the first line of part (b). When a higher-ordered mode appears during sunset on the path, the vectorial relationship to the first mode is dependent upon position and propagation conditions. If the added mode is small and phased as shown in the second line of part (b), the resultant signal amplitude is greater and the phase will undergo a larger diurnal change. If the added mode is strongly dominant, but with the same phase relationships, the conditions are as shown in line three. The resultant signal will show the same

trends as line two, but more pronounced; that is, a greater amplitude and larger diurnal phase change. However, when the added mode is strong and its phase rotates past phase opposition to mode 1 (line four), the resultant signal will incur reduced amplitude and a large phase change. In the sample shown, the amplitude is decreased to one-third and from noon to presunrise, the phase change is 220° more than for only mode 1. When, as shown on line five, the added mode is small and similar in phase pattern to line four, the composite signal will incur reduced amplitude and undergo a reversal in phase rotation. For our example, this reversal occurs between the third and fifth vector set. The rules for estimating the mode relationships from the measured signal are summarized in part (c). Vector diagrams are also shown for the signal and its modal components when the components are passing through phase opposition.

A key factor for assessing signal modal content is that the modal components have a systematic relationship with frequency for a given site and propagation conditions. This relationship has a frequency dependence for both amplitude and phase that, in principle, provides a great deal of information on the propagation conditions. For example, a specific situation outside the equatorial zone may produce a diurnal pattern that at 10.2 kHz is similar to line two and at 13.6 kHz is similar to line four of Figure B-1. The 11.3 kHz signal would have a composition that is somewhere in between. In another situation, involving propagation in the equatorial zone, the relationship would be reversed; 10.2 kHz similar to line four and 13.6 kHz similar to line two. The interpretation can get quite complex when the relative modal strengths and phases are changing. As an example, consider the fifth vector set of line four. At the time of just before or early in the sunrise transition, if the higher-ordered mode component should decrease from being dominant to being smaller than the first mode, the composite phase would rotate further. Then when the higher-ordered mode disappears during sunrise, a complete cycle slip would occur. The opposite, a cycle advance, could take place from the condition of the fifth vector set in line five. Here the higher-ordered mode would have to become larger than the first mode and remain so until the sunrise transition would cause its phase to rotate back past its phase opposition to mode 1. However, changing conditions provide the dynamics that make assessment of modal conditions easier.

INTERPRETATION OF AIRCRAFT DATA

In using aircraft data, we are dependent on the signal amplitude spatial patterns to assess modal content. If only one mode is present, the signal will vary monotonically with changing distance from a station. When additional modes are strong, the components successively add constructively and destructively. The ratios of maxima to minima (or fade depths) along the path provide a measure of the amplitude ratios of the components. One threshold used to identify potential for unreliable navigation is for the fade to equal or exceed 20 dB. This ratio equates to a higher-ordered mode being within 1.5 dB of the first mode. However, if the higher-ordered mode is more than 1.5 dB above the first mode the ratio of maxima to minima will be less than this criteria. If the ratio of mode amplitudes is changing rapidly with distance, the two modes may not be within this ratio at the location of phase opposition. Thus, interpretation by fade depth has to be exercised with caution.

We find that the modal competition created within the equatorial mode conversion zone creates a very different fade pattern from that observed on mid-latitude propagation paths. The equatorial fade pattern can have a much shorter fade interval and be much more irregular with distance and across frequency. At times this fade pattern is very difficult to distinguish from noise, especially precipitation static when received on electric antennas (whips). We will show several examples of data that we interpret as evidence of modal competition in our first analysis segment, this being flights from Hawaii. One of the strongest claims we can make for the observed fades evidencing modal competition is that the pattern is consistent and uniquely related to paths with propagation in the equatorial zone. We have now seen enough evidence of this relationship to have high confidence in our interpretation. We show extra examples in this analysis to make this case for the reader.

INTERPRETATION OF FIXED-SITE DATA

For fixed-site data we use the diurnal curves of phase data to compare the phase effects between the three frequencies. We have not yet worked out a method for using amplitude data because of non-linearities in the amplitude measurements. These non-linearities produce low sensitivities to amplitude change over much of the receiver sensitivity range.

Because an atomic frequency reference was not available, we use two processing methods for assessing phase effects, a phase drift removal process and a phase difference measurement. In the first method, the reference oscillator drift rate is incrementally subtracted from all measurements. The ideal result is a nearly stable diurnal phase curve for each measured signal. In most cases, the reference oscillator frequency offset was reasonably constant over a 24-hour period. Thus, the correction process makes possible phase plots from which signal self-interference can easily be evaluated.

The procedure used to reduce reference frequency drift effects is as follows. First, a 13.6 kHz Omega signal is selected for reference based upon expected signal quality and propagation stability. The received phase offset of this reference signal over a 24-hour period is determined by counting the cycles of phase change between times of mid-path noon. Assuming that the received phase at mid-path noon is the same value for successive days, the phase offset versus time (drift rate) is subtracted from the phase data by distributing the offset over the 24-hour period. The error caused by variation of phase from day-to-day, while possibly large for navigation purposes, is generally not significant when checking for modal effect patterns. The drift rate is then subtracted from all other signals. Proportional adjustments are made for the other frequencies. The drift rate is adjusted as needed when progressing through a sequence of days.

In the second method, we examine data of measured phase-difference between two received stations. In using phase-difference data, an attempt is made to use a strong signal containing only a first mode as a reference. Those signals suspected of having modal interference can then be easily evaluated. For some data, this second method has the additional complication that the data contain Propagation Prediction Correction (PPC) calculations that are applied to each frequency. Since the errors of the PPCs may differ for each frequency, the conclusions regarding evidence of modal effects are more complex and thus less certain.

Several examples of diurnal-phase data are presented to illustrate the information content in the data. In Figure B-2, an example is given of a set of received signals where mode 1 is strongly dominant. This data show the Japan signals recorded at 6 minute intervals on Hawaii. Several characteristics are very evident. The diurnal phase pattern follows a very representative shape with the following properties: (1) different day and night reflection heights with

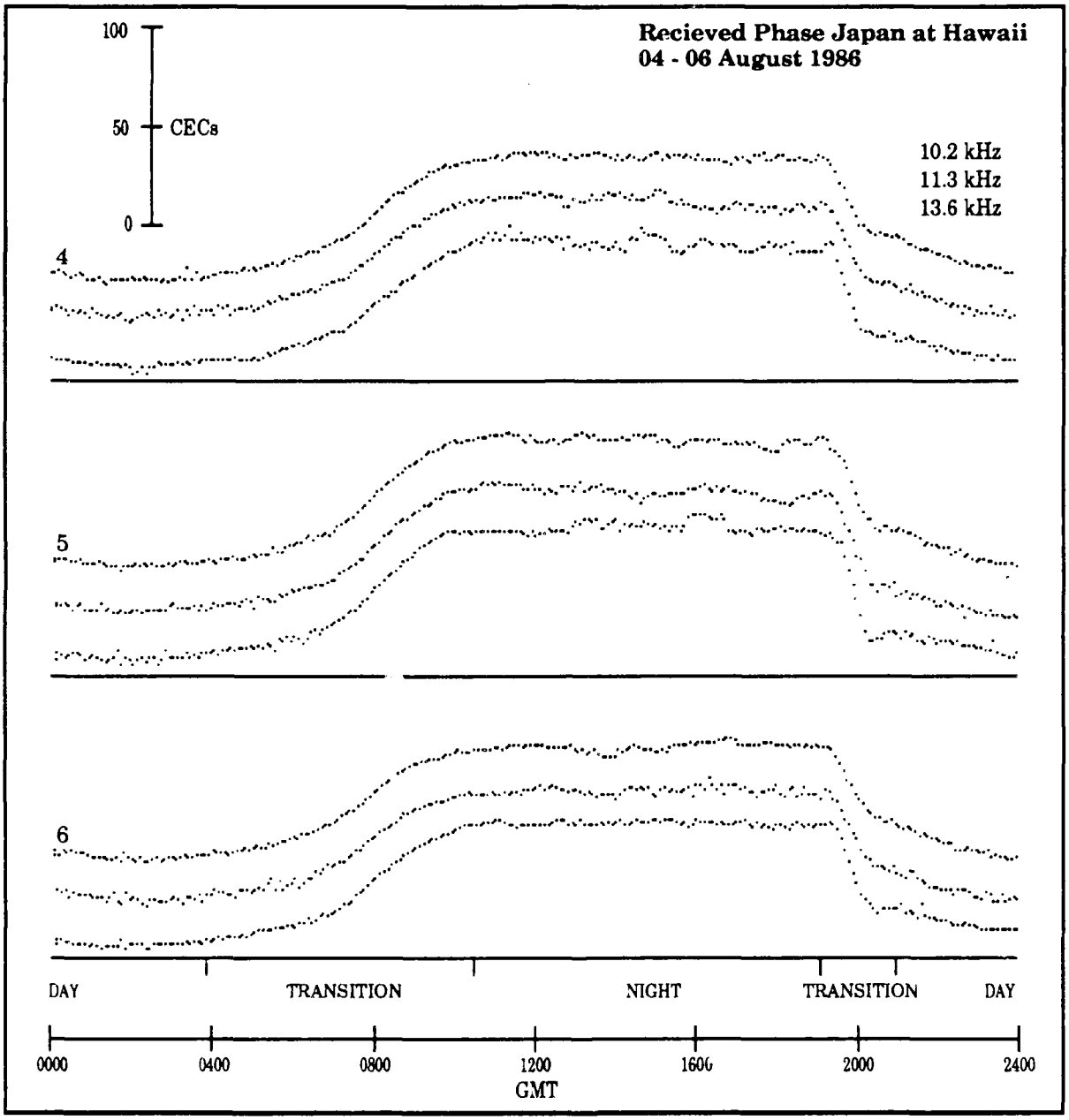

Figure B-2. Example of Clean Mode 1 Signals

smooth transitions between, (2) the expected solar zenith angle effect during daylight, and (3) often some continuing relaxation of the ionosphere throughout the night. When fluctuations due to varying propagation conditions do occur, the phase response at all frequencies is very similar when mode 1 is clearly dominant. This is the case shown in Figure B-3. This data for Japan, recorded on hourly intervals at Brisbane, show different phase patterns for different days as a result of different propagation conditions. Even though the daily phase

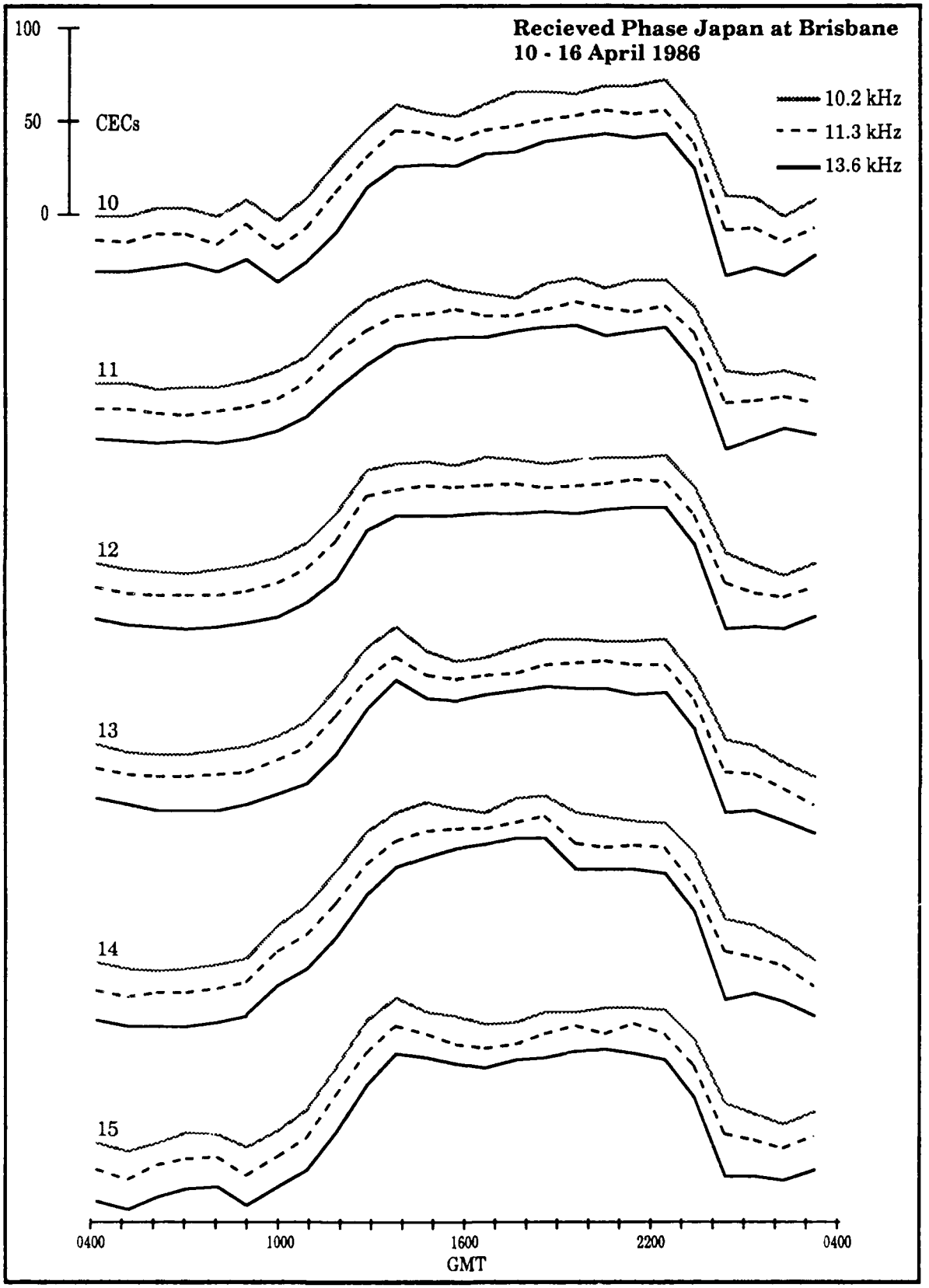

Figure B-3. Example of Propagation Variability; Mode 1 Signals

patterns differ, the phase records for each frequency within a day show nearly the same trend. Many variations within hours and between days are observed in the data, yet these variations across the set of frequencies are similar.

When modal competition is present, there is much less similarity between phase records across frequency and from day-to-day. Many data samples from the Western Pacific monitoring sites show the presence of multiple modes. Pronounced modal effects are almost always evident on the Hawaii signal received at Brisbane, as illustrated in Figure B-4. This figure is an excellent example of the type of phase data obtained for modal competition conditions. This figure shows phase records of 24-hour periods at the three frequencies for six consecutive days. Our objective is to show the marked difference in the records between Figures B-3 and B-4. We note that the comparison accentuates the variability, evident in Figure B-4, of the individual frequency records. This is most evident when comparing different days and different frequencies on a given day. None of the phase records in Figure B-4 have the characteristic diurnal shape of a single mode signal shown in Figure B-3.

There are many characteristics evidenced in phase records that provide clues about the propagation conditions. The most dramatic is the cycle jump of 100 CECs. This occurs frequently in Figure B-4, at both 10.2 kHz and 11.3 kHz. These jumps occur most frequently during the sunrise and/or sunset transitions but can occur at any time during the night. In Figure B-4, the 10.2 kHz signal shows a large phase change near the middle of the night for all of the days shown. This phase change does not occur on the 11.3 kHz and 13.6 kHz frequencies. We interpret the modal effects to be strongest at 10.2 kHz, strong at 11.3 kHz, and evident but not strong at 13.6 kHz. The added mode causes the composite day-to-night phase change at Brisbane generally to be (1) less at 13.6 kHz, (2) greater at 11.3 kHz, and (3) uncertain relative to a single-mode condition at 10.2 kHz. A problem at 10.2 kHz is that during the hourly sample interval, the phase often changes more than 50 CECs. Thus, the phase could be interpreted as going either positive or negative. Other characteristics of phase data will be introduced as specific interpretations of data are presented.

One challenge is to select good illustrations from the Western Pacific validation set. Many factors contribute to making the data less than ideal for illustrating its information content. These factors include reference oscillator drift, local

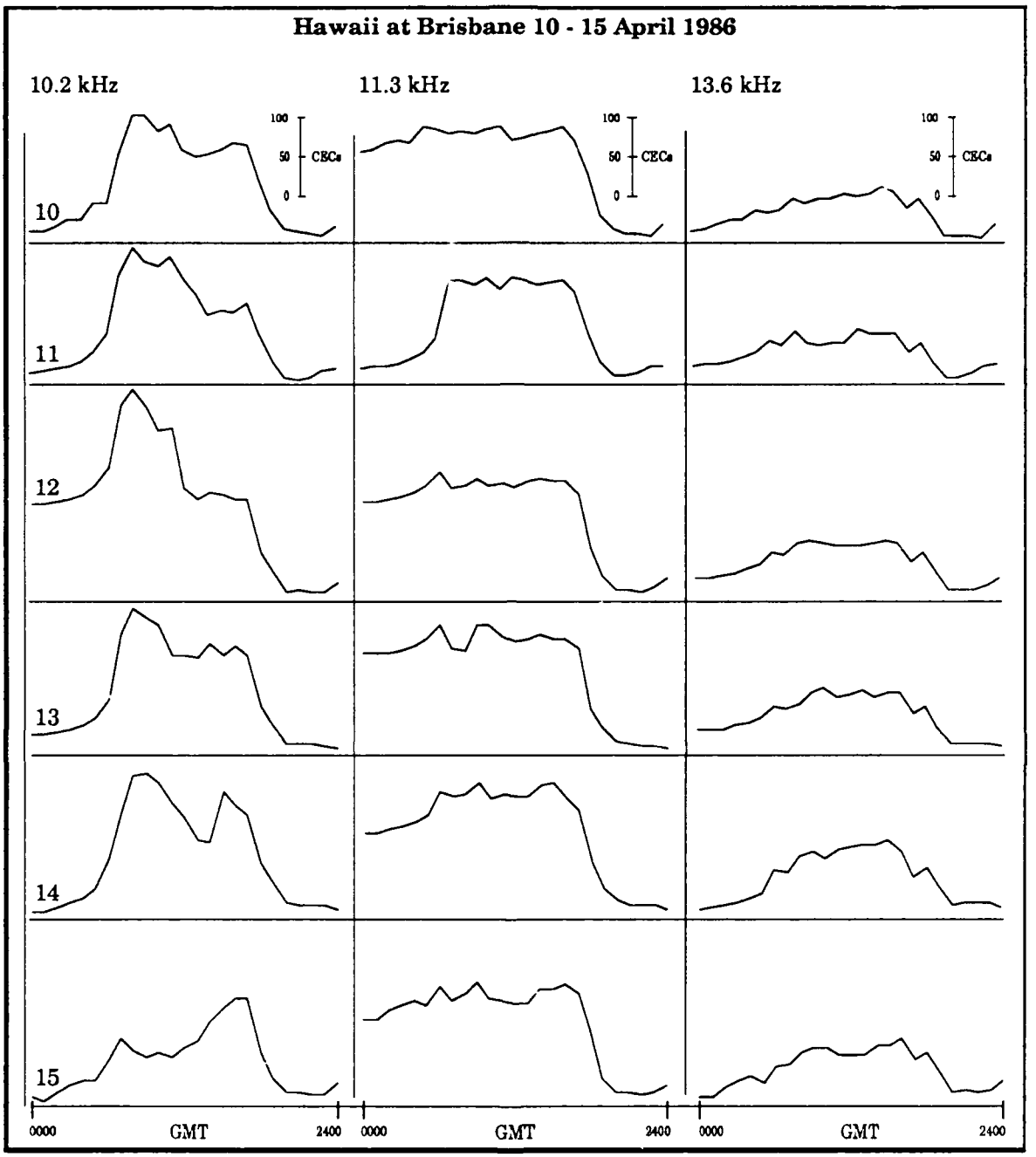

Figure B-4. Example of Received Multimode Signals

interference, signal tracking loss, very strong modal effects, and in the case of Brisbane, long sample intervals. A more detailed account of the techniques for interpreting modal effects, as well as better data samples, was presented in the South Pacific Validation report.

Interpreting the nature of modal effects once they have been detected can be a significant challenge. Often the best that can be done is to compare the observations with expectations from predictions. To illustrate, we use the Hawaii signals of Figure B-4 and the calculations of Hawaii signal levels versus distance shown in Figures B-5 and B-6. Brisbane is on a 226° radial from Hawaii and thus between the radial calculations at 220° and 230°. For 10.2 kHz, the calculations predict mode 2 to dominate at Brisbane by about 8 to 10 dB. For 13.6 kHz, mode 2 is only 2.5 dB above mode 1 at 220°, but is 8 dB above at 230°. The observed marked tendency for cycle jumps during the day/night and night/day transitions at 10.2 kHz is consistent with switching from daytime mode 1 dominance to nighttime mode 2 dominance. However, the 10.2 kHz cycle jumps in the middle of the night evidence that modal competition is much stronger than would occur with the predicted 8 dB separation. Since both modes 1 and 4 are candidates to compete with mode 2 at the distance of Brisbane, the vector sum of these modes must be near the magnitude of mode 2 when cycle jumps occur. We believe that the large variation in phase signifies that the modal components are near phase opposition. The lack of large phase fluctuations at 13.6 kHz at any time indicates that the modal competition is quite different. Since the diurnal phase curve differs from single-mode propagation, a higher mode is present. We estimate the diurnal phase change for the fifth curve to reach 50 CECs more than the predicted single-mode value. Several possibilities could be invoked to explain this measurement, but all require the involvement of a mode other than mode 1. The lack of cycle jumps could be a result of the specific location of the receiver for these particular propagation conditions.

Our interpretation for this example is that all three frequencies incur modal competition. At 10.2 kHz, no mode dominates the competition by more than a few dB. At 11.3 kHz, mode switching on all days at sunrise clearly demonstrates that the nighttime mode differs from the daytime mode. Here a higher mode must be dominant. We rule out mode conversion at the terminator because of the lack of mode switching at 13.6 kHz. At 13.6 kHz, the lack of mode switching and the large phase deviation from the single-mode diurnal curve makes for a complex and uncertain situation. Modal competition has to be present, but we cannot be certain if a higher-ordered mode ever becomes dominant. To take the interpretation farther would require scenario calculations that attempt to create the composite signal conditions as measured.

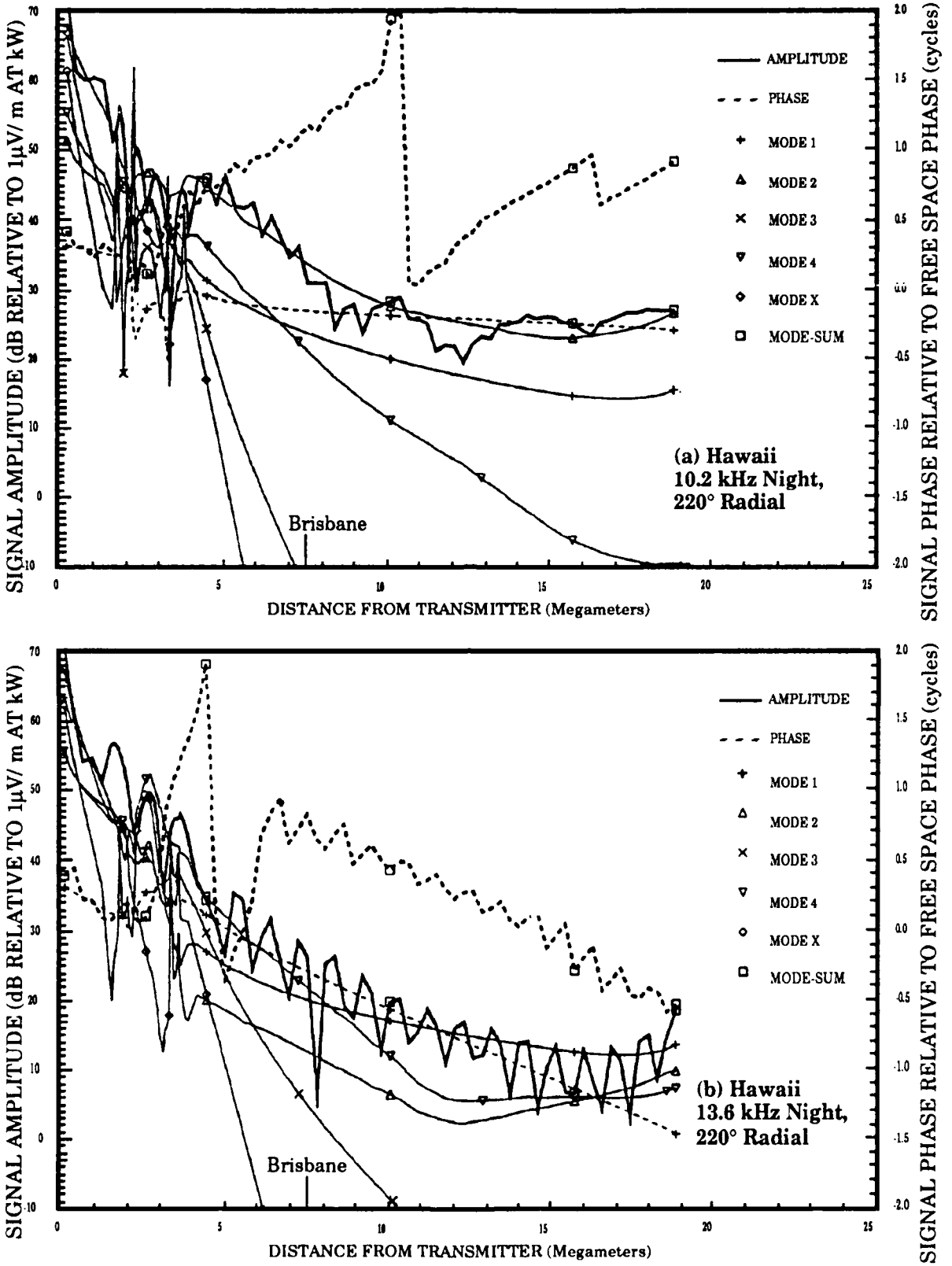

Figure B-5. Calculations Showing Predicted Modes; Hawaii Signal to South of Brisbane

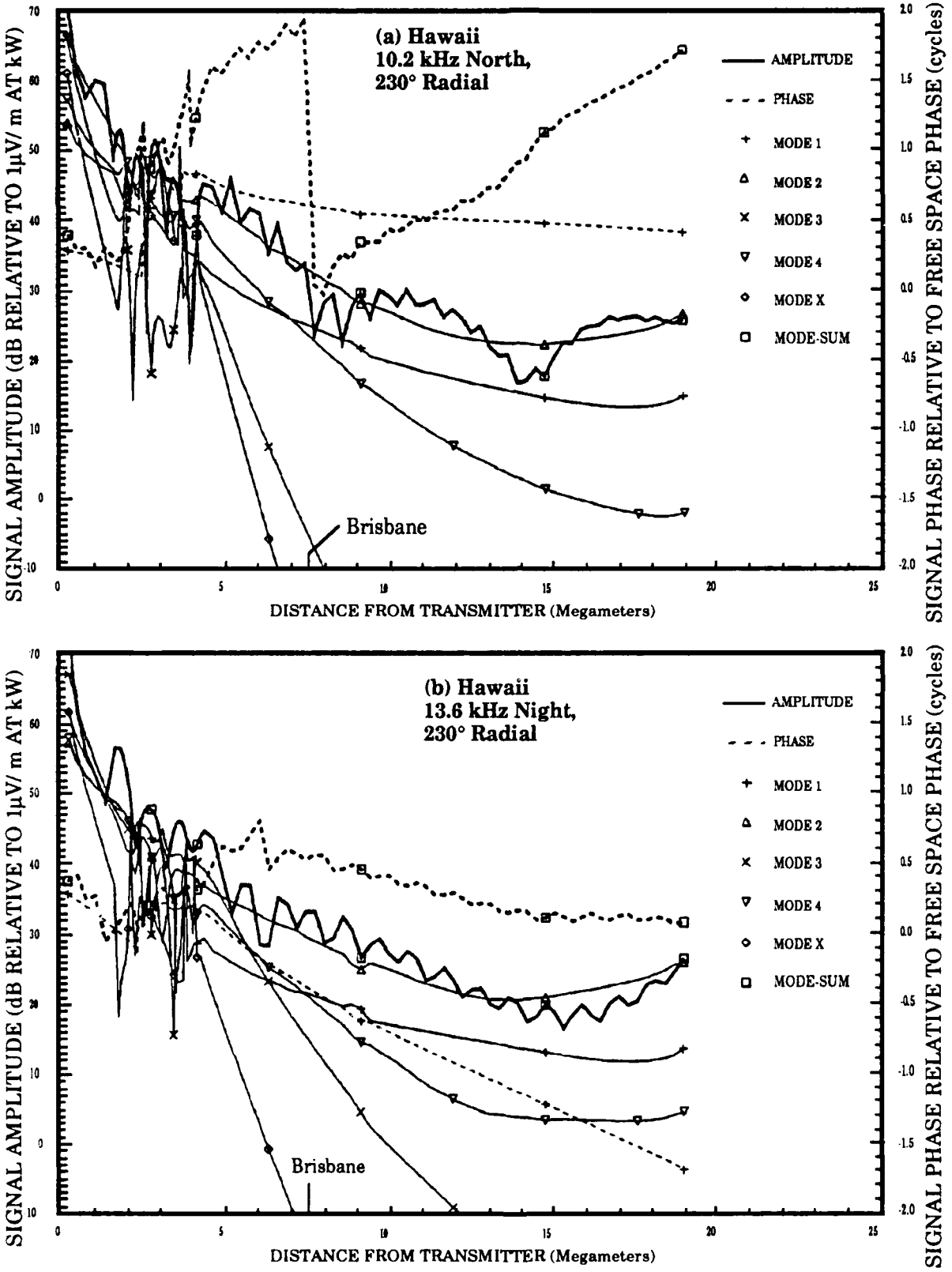

Figure B-6. Calculations Showing Predicted Modes; Hawaii Signal to North of Brisbane

We again note that it is generally easier to recognize the existence of modal competition in the presence of normal propagation variability by comparing the diurnal phase data between multiple frequencies. The occurrence of a cycle jump, as seen in some of the above examples, makes identification of multimode easy even without additional frequency data.

The recorded phase data of a single signal are much easier to interpret for phase quality than the phase-difference data that include propagation effects of two signals. The signal phase data facilitate comparison of modal effects between frequencies, a condition particularly difficult to interpret using phase-difference data. For this reason, extra effort is devoted to obtaining the phase records from the Western Pacific sites, none of which had atomic frequency references. We found that we could remove enough of the frequency offset from the data so that the diurnal phase patterns could be recognized. The quality of the processed data vary quite a bit from site-to-site and at a site over time.

The reference oscillators at some monitor sites were reasonably stable, while other oscillators were much less stable. We found that we had to separately estimate and remove the reference oscillator drift from data on almost every day. Local interference was a significant problem at almost all of the fixed sites, particularly at 10.2 kHz. In some cases we were able to assess signal phase quality in the presence of interference, while in others we had to discard short segments of data. In the case of Singapore, we found much of the data essentially useless in that large blocks of every day were bad. Under these conditions we were unable to establish reasonable frequency drift corrections.

INTERPRETATION OF SHIPBOARD DATA

The shipboard data provided to us are grouped in time segments that coincided with periods of independent satellite navigation fixes obtained on the ship. These periods occurred daily and were typically for an eight-hour interval of a day. The data were recorded using an atomic frequency standard. The ship motion was largely removed from the data before being provided to us. This was done by applying Propagation Phase Correction (PPC) calculations based upon the determined ship's position. If the ship's position and prediction corrections are accurate, the deviation of the data from a horizontal line is a measure of the propagation variation. It took some time for us to intuitively become comfortable

with this data because we did not have the familiar diurnal curve to use for reference. Another problem is that the breaks in data usually are for the night, the period we are most interested in. However, at least some portion of the night, usually an early night period, is available for analysis. We compare the data using the three frequencies for indications of modal effects much like we do for the fixed-site data. As we note later, the reference phase evidently lost lock with the atomic standard, with the result that the phase-error data could not be interpreted.

We are fortunate that the phase-error data were referenced to an atomic frequency standard because the data have many step functions, often not of a full cycle and not coincident between frequencies. Judgement is required as to when these jumps are caused by instrumentation. As a doublecheck, we use the SNR data which were jump-free to assist in determining when to remove a phase jump. Phase jumps are removed only when the jump is between adjacent data values and no evidence is detected of ongoing propagation dynamics. Here we show three short examples of data to illustrate important features. The data in Figure B-7 show the phase error and SNR for a time period where the corrections were very accurate, propagation was stable and very close to predicted. The phase-error data show a cyclic offset on all frequencies that is attributed to local interference. This interference, which is frequently present in the data, masks some of the modal effects. Figure B-8 shows a sample where the propagation was less stable and where some modal effects occur. During sunset, near 1500 GMT on the first two dates, the 11.3 kHz and 13.6 kHz signals have a phase oscillation and an amplitude dip that do not occur on the 10.2 kHz signal. We attribute this pattern to modal competition occurring at this time. Figure B-9 is a sample where the modal effects are strongly evident. The first sample (Figure B-7) serves to show that both the phase error and SNR curves are very close to straight lines when the ship position is accurately determined and propagation is as predicted. This sample provides a reference for comparing the other samples. The second sample (Figure B-8) shows what variable propagation looks like. When no modal competition exists, both the phase error and SNR data of the three frequencies, while undergoing change with time, have very similar characteristics. The third sample (Figure B-9) shows the effects of exceptionally strong modal competition. We note that for many time intervals, the records between frequencies are very different. Later we show other examples where the

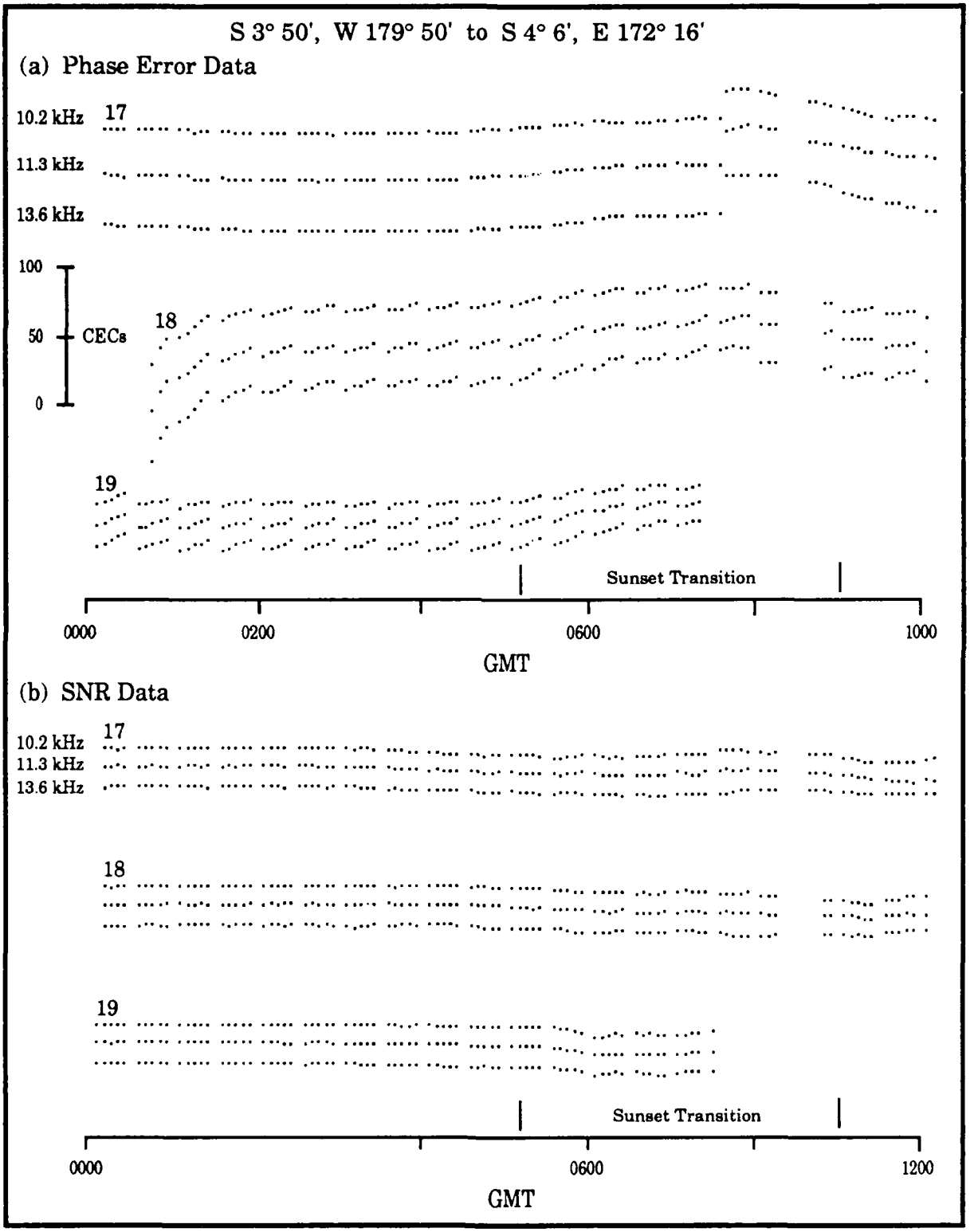

Figure B-7. Shipboard Data; Japan Signal 17-19 February 1987

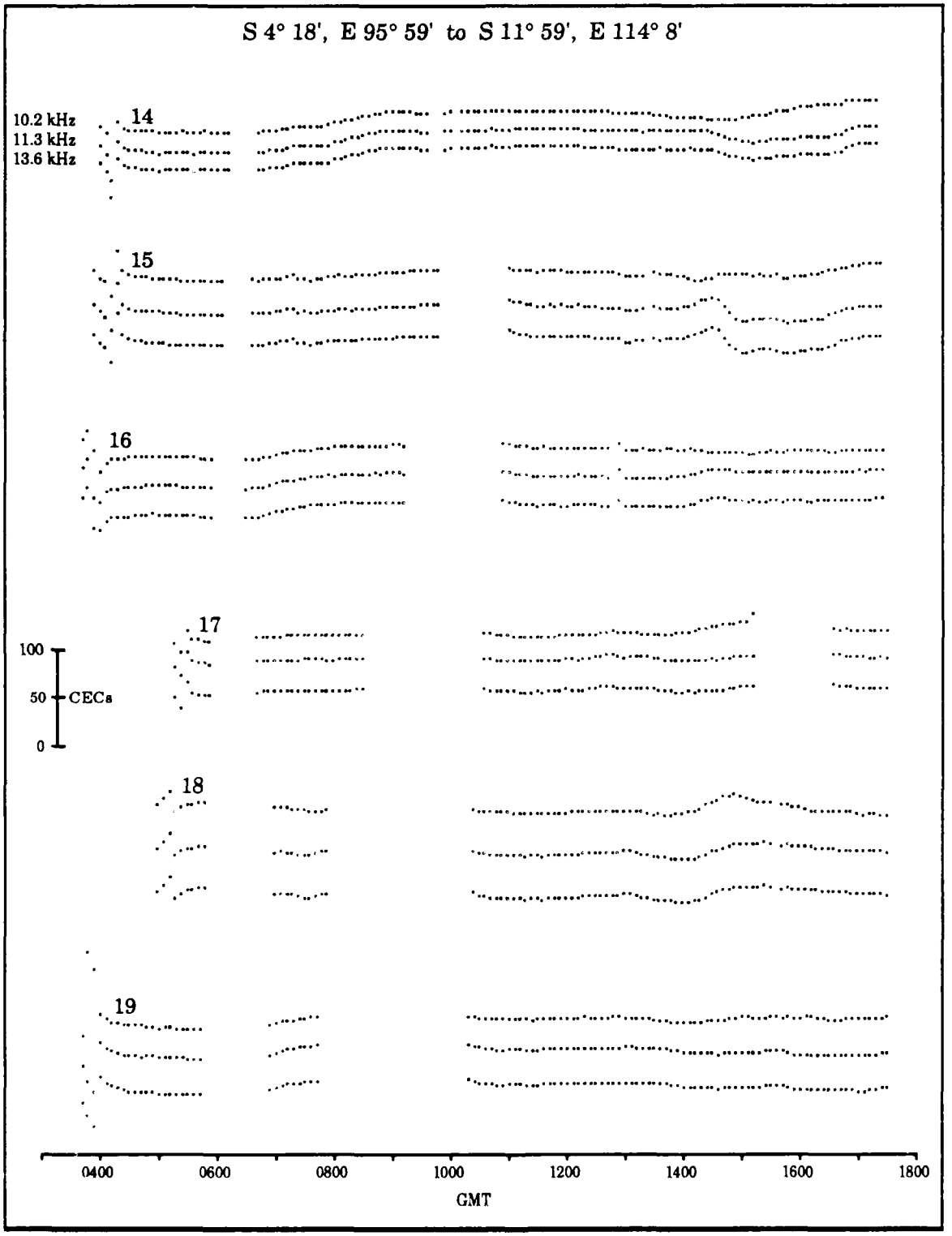

Figure B-8a. Shipboard Phase Error Data; La Reunion Signal 14-19 August 1986

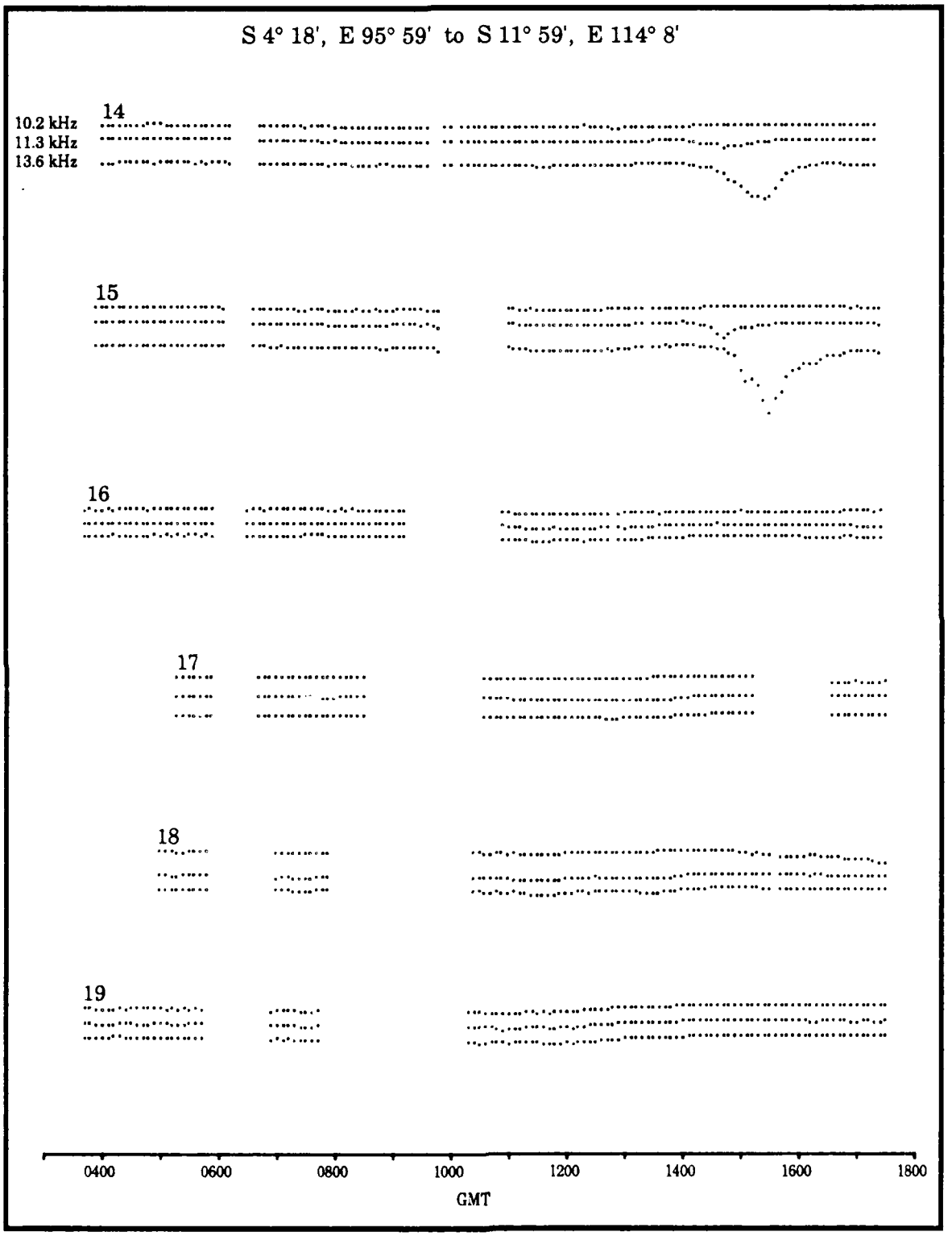

Figure B-8b. Shipboard SNR Data; La Reunion Signal 14-19 August 1986

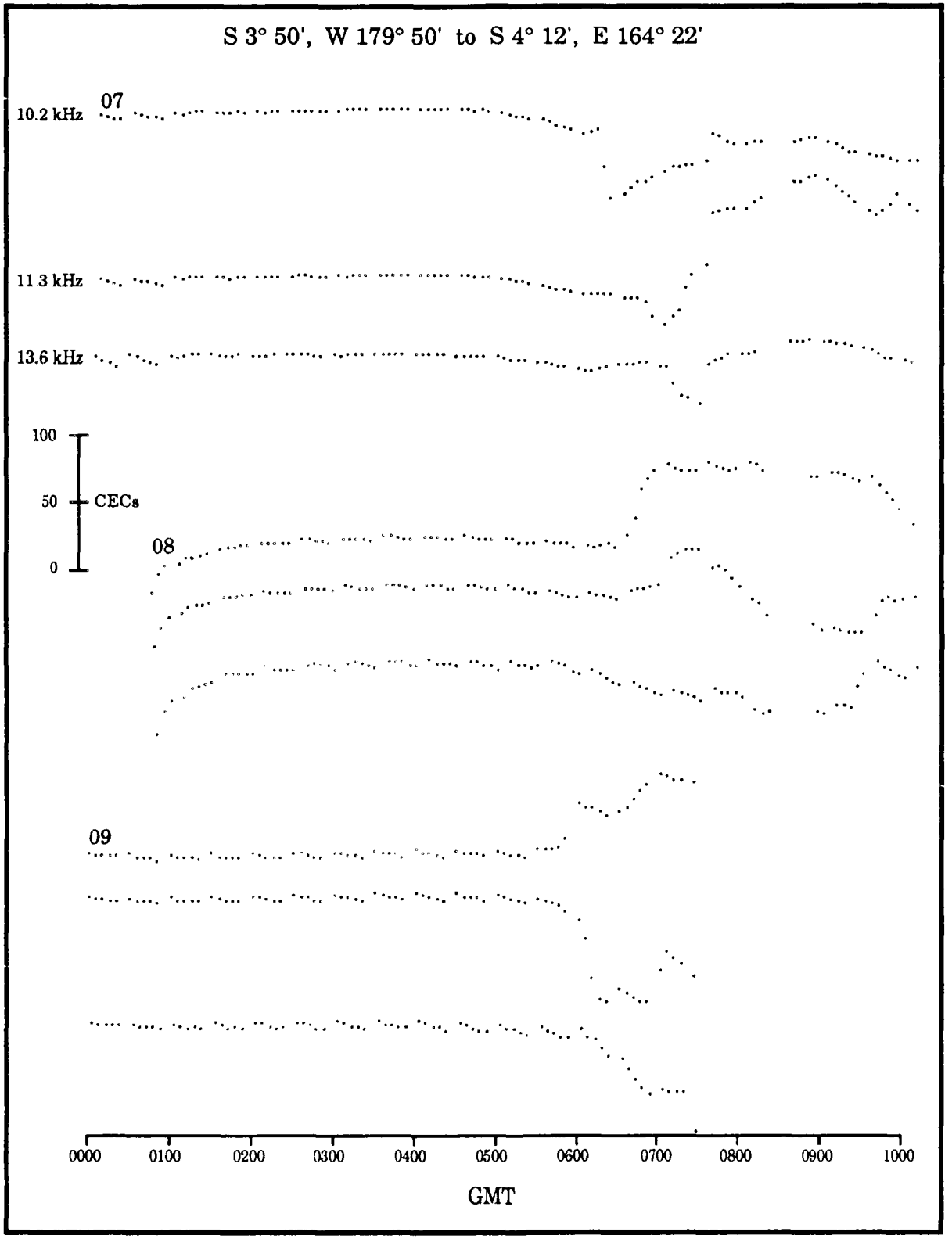

Figure B-9a. Shipboard Phase Error Data; Hawaii Signal 7-9 February 1986

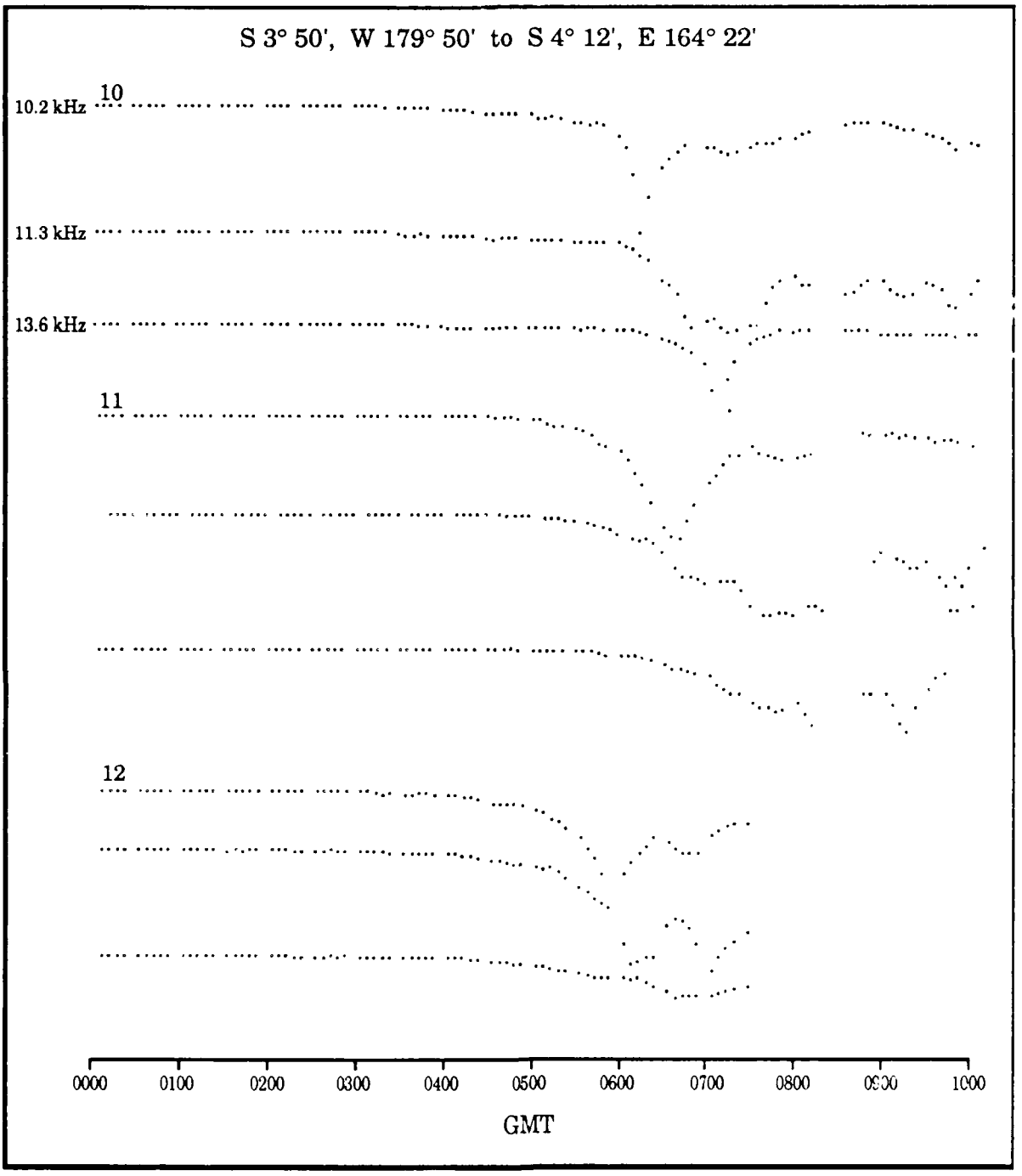

Figure B-9b. Shipboard SNR Data; Hawaii Signal 10-12 February 1986

modal effects are much less pronounced. Even in these other cases, the modal competition is easily identified. We find the SNR data a good indicator of modal effects. When modal competition is present, the same frequency that shows a phase deviation also shows an amplitude deviation. In fact, because of interference effects on the phase-error data, the modal effects are often easier to identify using the SNR data.

As stated earlier, the ship data allow us to assess modal effects in areas not covered by other data. This data certainly are a very valuable addition to this analysis.

GENERAL COMMENTS ON SHIPBOARD ANALYSIS

In summary, while each of the three categories of data requires somewhat different processing, they provide complementary information on modal effects. In this analysis we further extend the integration of data devised in the South Pacific analysis to include more effective use of the shipboard data. We note that the integrated multifrequency phase and SNR data provide effective clues for the presence of modal interference. These clues could be processed with some future receiver for automatic station deselection. We also focus more on case studies as contrasted to statistical analysis. Our reasoning is that for both the South Pacific and this analysis, we found significant propagation variability which suggested that the size of our database was insufficient to produce reliable statistics.

MODAL ANALYSIS SUMMARY; AIRCRAFT, FIXED SITE AND SHIP

We find that the analysis is more definitive when it is possible to examine a grouping of data from an area. Usually a group consists of several aircraft flights and a fixed site, with the fixed site being a hub for the flights. Not all flights fit into a convenient group. When ship operations are within the vicinity of a group, these data are also included. For each group we compare observations with predictions, testing for signals with predicted good phase and for predicted phase problems.

We summarize the analysis by grouping the assessment into areas within the Western Pacific region. This method is more operationally oriented than keying

on flights and supports the presentation of a more coherent picture of navigation conditions. Generally we identify the area with an easily recognized landmark. However, we make the bounds for any given area vague. The reader is referred to Appendix A for maps showing predictions of phase quality for each of the signals.

WEST OF HAWAII TO GUAM (Hawaii, Flights 1 and 2, and Southeast Ship Transits): This area is characterized by having three stations predicted always good (Norway, La Reunion and Australia), and five stations predicted to have some nighttime modal problems at some locations within the area. Most modal problems occur because of equatorial zone mode conversion. Specific predicted phase problems are noted in the following commentary for each station. The data consist of measurements on (1) Oahu Hawaii, (2) flights from Hawaii to Kwajelein and from Kwajelein to Guam, and (3) the Tsushima ship transit from Japan to Hawaii and then a loop south to the equator and back to Japan. The data for the flight from Hawaii to Guam were from along the extended 254° radial of Hawaii through Kwajelein (see Section 3, Figure 3-2) and then a dogleg to Guam. A summary of predictions and observations by stations is as follows:

(A) Norway: Good coverage is predicted to the east of Kwajelein and north of Guam at all times with mode 1 being dominant everywhere. The signal at Hawaii was above noise for about 6 hours each day, generally between 1400 and 1800 GMT. This period approximately coincides with the greatest amount of night on the path and with the decrease in noise sources from the western rim of the Pacific. The flight data collected on the Hawaii to Kwajelein segment have inadequate SNR. The Kwajelein to Guam record, while noisy is consistent with a mode 1 signal. The ship data show tracking south of Hawaii to the equator with the phase being good at all measured times.

Conclusion: The data suggest that signal-to-noise ratio is close to marginal during local afternoon. This condition can last well into the local night.

(B) Liberia: The antipode of Liberia is south of Kwajelein at (S 6° 31', E 169° 20'). The signals to the east of Kwajelein are predicted either equatorial zone modal and/or long-path. This prediction is confirmed by the Hawaii and shipboard data. The flight data collected on the Hawaii to Kwajelein segment have too much interference to determine phase quality. West of Kwajelein, the flight data are consistent with a mode 1 signal.

Conclusion: Modal effects are as predicted. The phase quality is poor east of Kwajelein when local night is in the vicinity of this area.

(C) Hawaii: This area contains the eastern boundary of the predicted equatorial mode conversion zone. Emphasis is given to exploring the position of this boundary using both aircraft and shipboard data. For this purpose we include flight data from the South Pacific analysis (Figures B-10 and B-11), for comparison with data obtained on the Hawaii to Kwajelein flight (Figure B-12). The flight paths are shown in Figure B-13. The signal amplitude records for these flights are noisy. We interpret the noise to result from modal effects, first near zone and later equatorial zone. The calculations predict that on the 202° radial, at 10.2 kHz, the modal interference should rapidly decrease to a negligible level. We do not see this happening. This is because other modes, while not predicted dominant, do not decrease nearly as rapidly. On the other radials at 10.2 kHz, observable effects could be produced to the distance of intersection with the equatorial zone. The calculations predict that at 13.6 kHz the near modal zone should also rapidly decrease for the 202° radial (Figure B-10), but for the 244° and 254° radials (Figures B-11 and B-12) should extend to the equatorial zone. The data show that modal effects extend on all radials and frequencies to the equatorial zone. For the 202° radial, the TASC calculations pre-

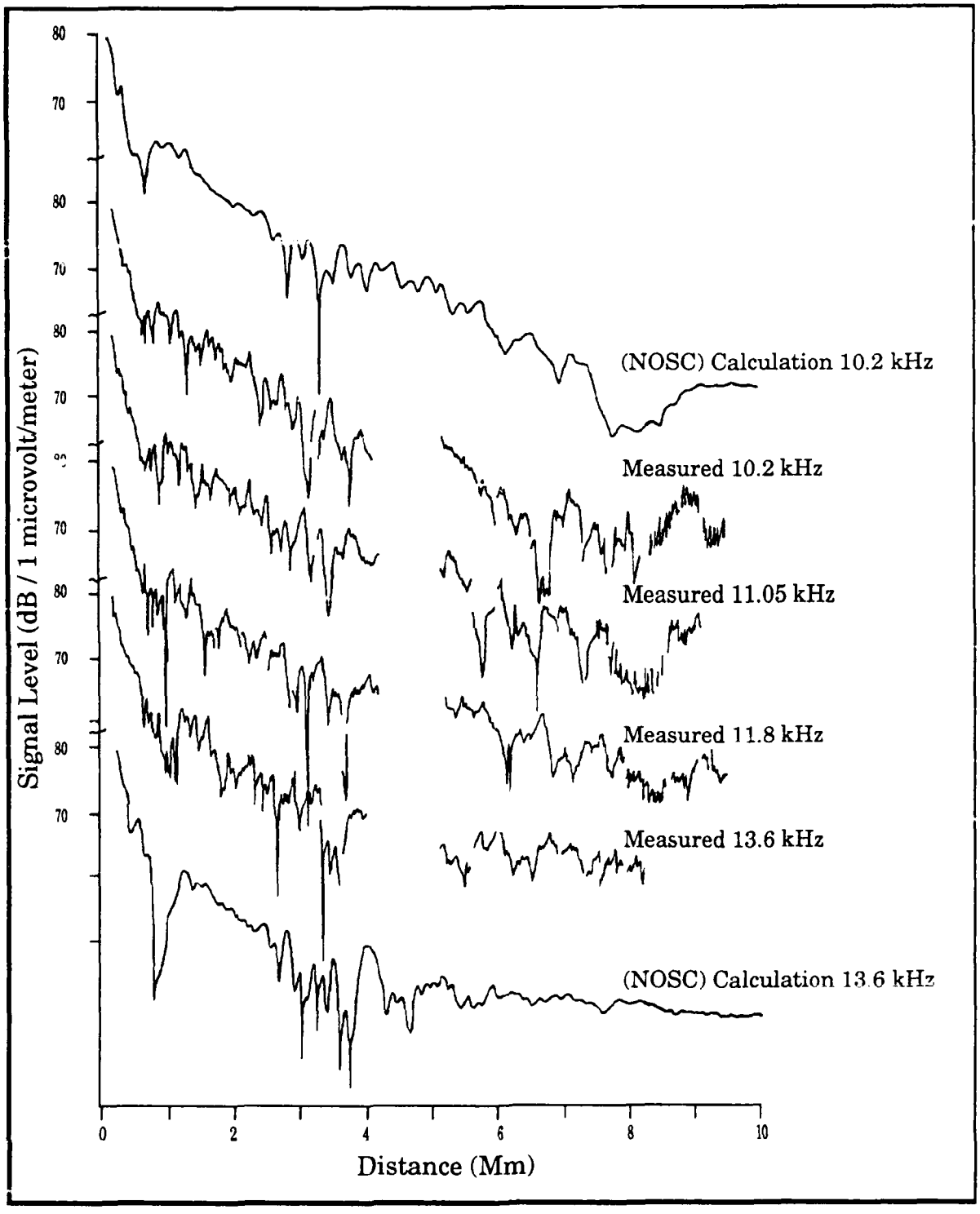

Figure B-10. Measured and Calculated Hawaii Signals, 202° Radial

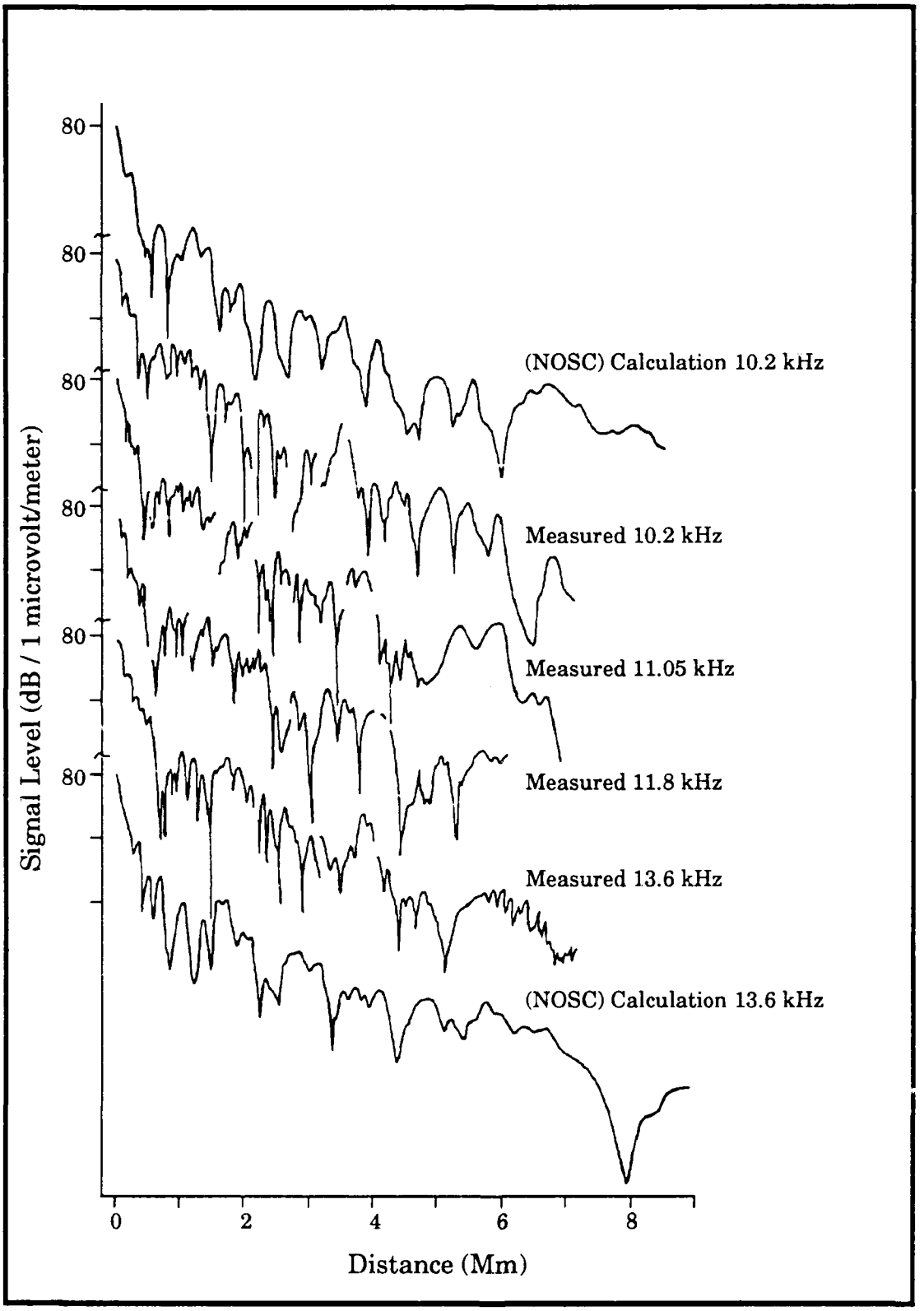

Figure B-11. Measured and Calculated Hawaii Signals, 244° Radial

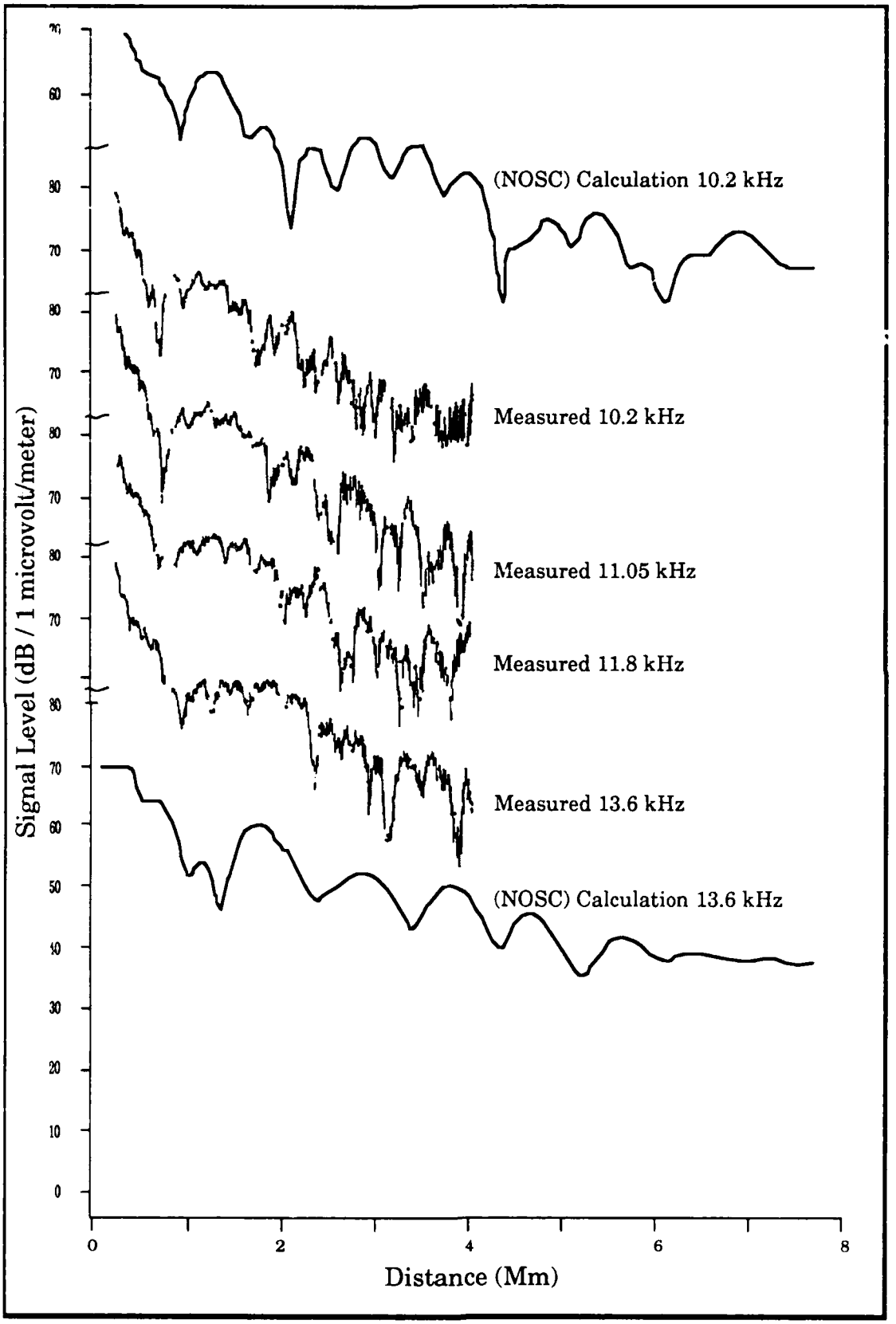

Figure B-12. Measured and Calculated Hawaii Signals, 254° Radial

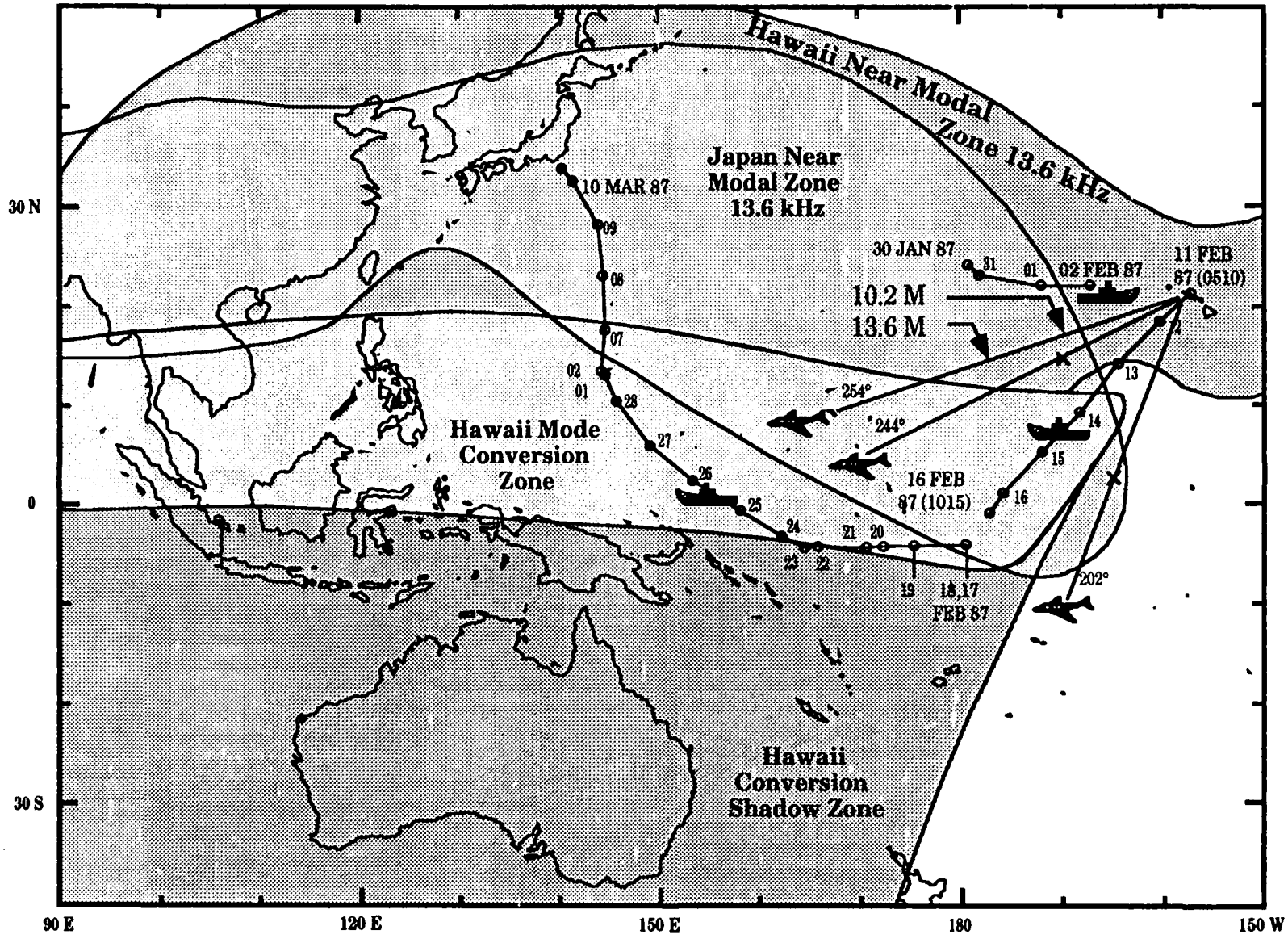

Figure B-13. Flight and Ship Transits in Western Pacific

dict the boundary of the equatorial zone is just to the west; the NOSC calculations show modal effects. The data show strong modal fades beginning near the middle of the predicted north/south extent of the zone (marked on Figure B-13). This radial could be very close to the eastern edge of the zone. For the 244° radial, the equatorial-zone boundary is difficult to define; our estimate is at about 1.5 Mm. We note from the mark on this radial that this position is about 2° latitude north of the predicted zone. For the 254° radial, we interpret the onset location of the equatorial zone mode conversion to vary with frequency. Two marks, for onset at 10.2 kHz and 13.6 kHz respectively, are shown in Figure B-13. The 10.2 kHz boundary mark lies about 4° north of the predicted boundary; the 13.6 kHz, 3° north.

The 11–16 February shipboard data are shown in Figure B-14 with the track plotted in Figure B-13. During sunset on 11 February, the ship was close to Hawaii and the propagation phase corrections removed most of the variability from the record. During sunset on 12 February, the ship was beyond the near modal zone for 10.2 and 11.3 kHz but within this zone for 13.6 kHz. The record shows that the 13.6 kHz phase deviated from the predicted phase. On 13 February, the ship was north of the equatorial mode conversion zone, but we expected modal effects at 13.6 kHz. No effects were observed. By sunset on 14 February, the ship was inside the predicted zone yet minimal deviations of phase are noted. By 15 February propagation during the transition period is becoming more variable and modal effects are easily noted at 11.3 kHz, starting after 0600 GMT. The SNR perturbation is not pronounced until an hour later. The early night of 16 February shows strong modal effects at 10.2 kHz and 13.6 kHz starting near 0600 GMT. The onset is much easier to see in the SNR data, but can be found in the phase-error

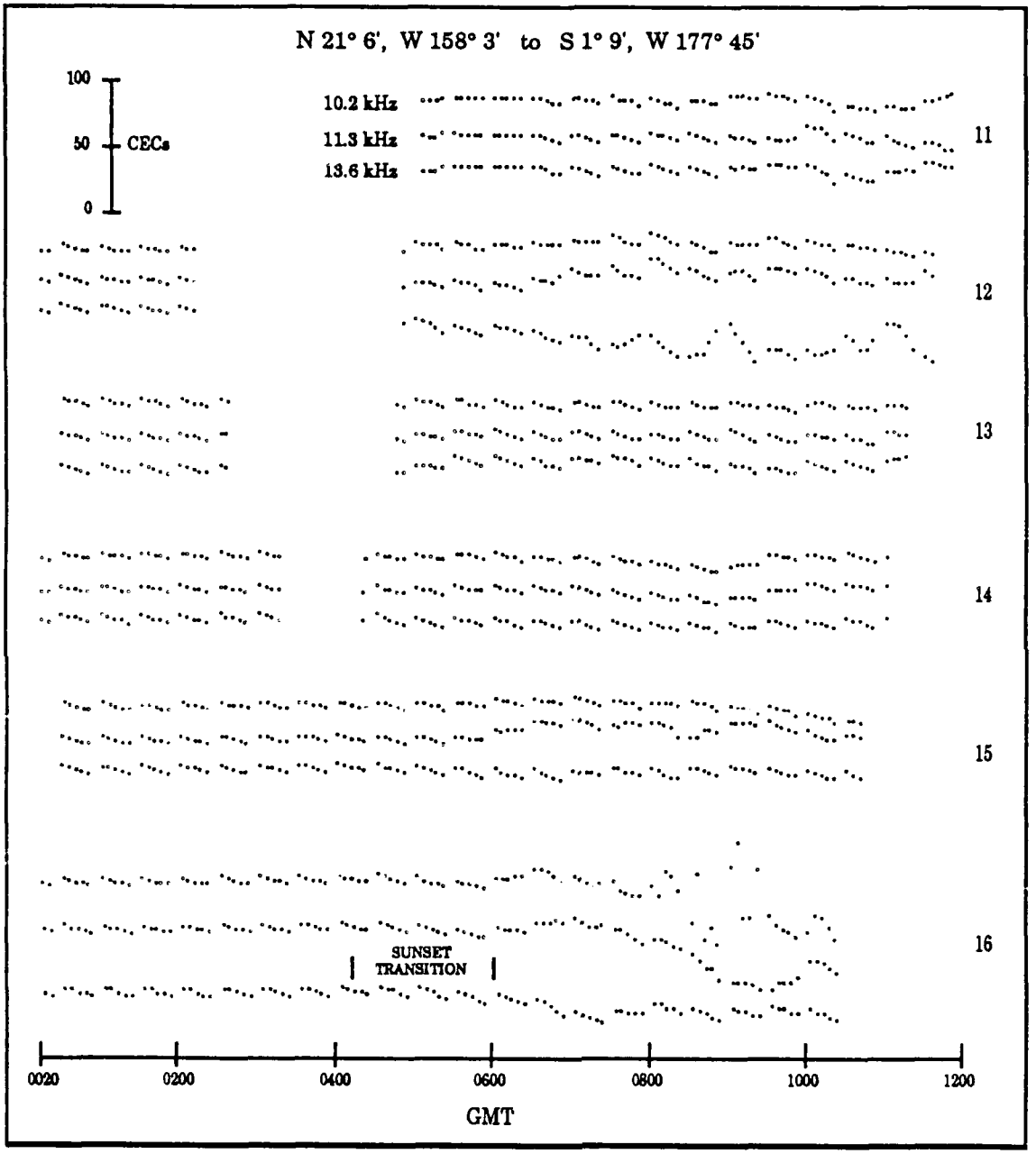

Figure B-14a. Shipboard Phase Error Data; Hawaii Signal 11-16 February 1987

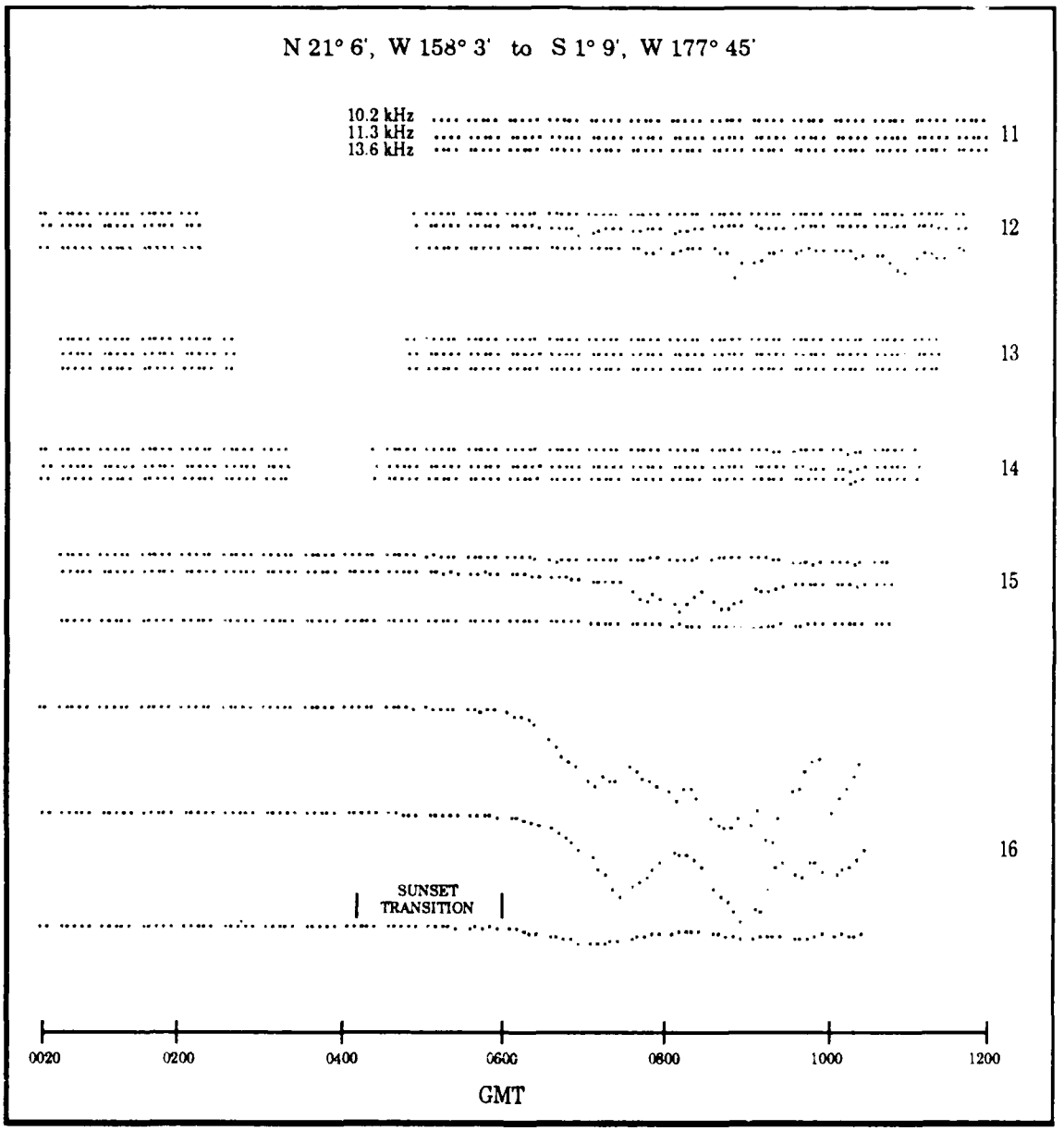

Figure B-14b. Shipboard SNR Data; Hawaii Signal 11-16 February 1987

data. We find that looking at the data from a highly oblique angle in the direction of increasing time, helps in recognizing the locations of perturbation onsets.

The ship transit from 17 to 20 February shows early nighttime modal effects for each date. The ship moved westward from about 180° to 163°E, roughly parallel to and 3° above the southern zone boundary, so that by 20 February the period of early evening data is quite short.

The flight on the extended radial from Kwajelein show continuation of the modal effects to the end of the radial.

Modal effects are strong in all the Brisbane data, as shown with the example in Figure B-4. Unfortunately, we do not have data for overlapping dates.

Conclusion: The aircraft and ship data show quite different locations for onset of the equatorial zone modal effects, the difference being almost 10° in latitude. We do not have an explanation. We know from other measurements that the time of modal onset varies, sometimes not starting until later in the night. In this case, the ship's records would end before onset. The aircraft data are the greatest concern because they suggest that the boundary needs to move north. We think that more investigation is required before a suitable boundary can be determined.

The Brisbane data show that, once equatorial zone mode conversion occurs, the effects can extend far beyond the zone.

(D) N. Dakota: Calculations show mode 1 for both frequencies north of the equatorial mode conversion zone. Within and to the south of the conversion zone the signals are predicted modal. The aircraft data from Hawaii to Kwajelein are not useful for analysis due to editing out interference. Beyond Kwajelein the data show modal effects.

The Tsushima ship transit from Hawaii on 11 through 16 February was along a radial common to the propagation of the Hawaii and North Dakota signals. We find comparison of data from these stations very interesting (see Figures B-14 and B-15). We note strong similarities at the times of phase effects. These include the close tracking across frequencies on 11 and 13 February, the deviation in the 13.6 kHz signal in early evening on 12 February, the 11.3 kHz deviation on 15 February and the strong deviations of 10.2 kHz and 11.3 kHz on 16 February.

The exception from strong correlation is the slightly different SNR and phase tracks between stations on 14 February. The details of modal effects on the phase records are expected to differ because ionosphere reflection is occurring at different locations in the conversion zone. We take the similar occurrence of conversion effects to give strong credence to the conversion theory.

Conclusion: The prediction of mode conversion in the equatorial conversion zone is supported by the small sample of data. The similarity between North Dakota and Hawaii data for the initial detection of modal effects strengthen this interpretation.

(E) La Reunion: Calculations show that the signals are strong mode 1 at all times throughout this area. Except for Hawaii, all measurements were at times when large segments of daylight occurred on the path.

Conclusion: While not confirmed, we expect that the La Reunion signals are very reliable east of Guam to Hawaii.

(F) Argentina: Calculations show mode conversion within the equatorial zone, higher mode dominance in the shadow zone and mode 3 dominating this area south of the equatorial zone. The phase measurements at Hawaii show nightly mode

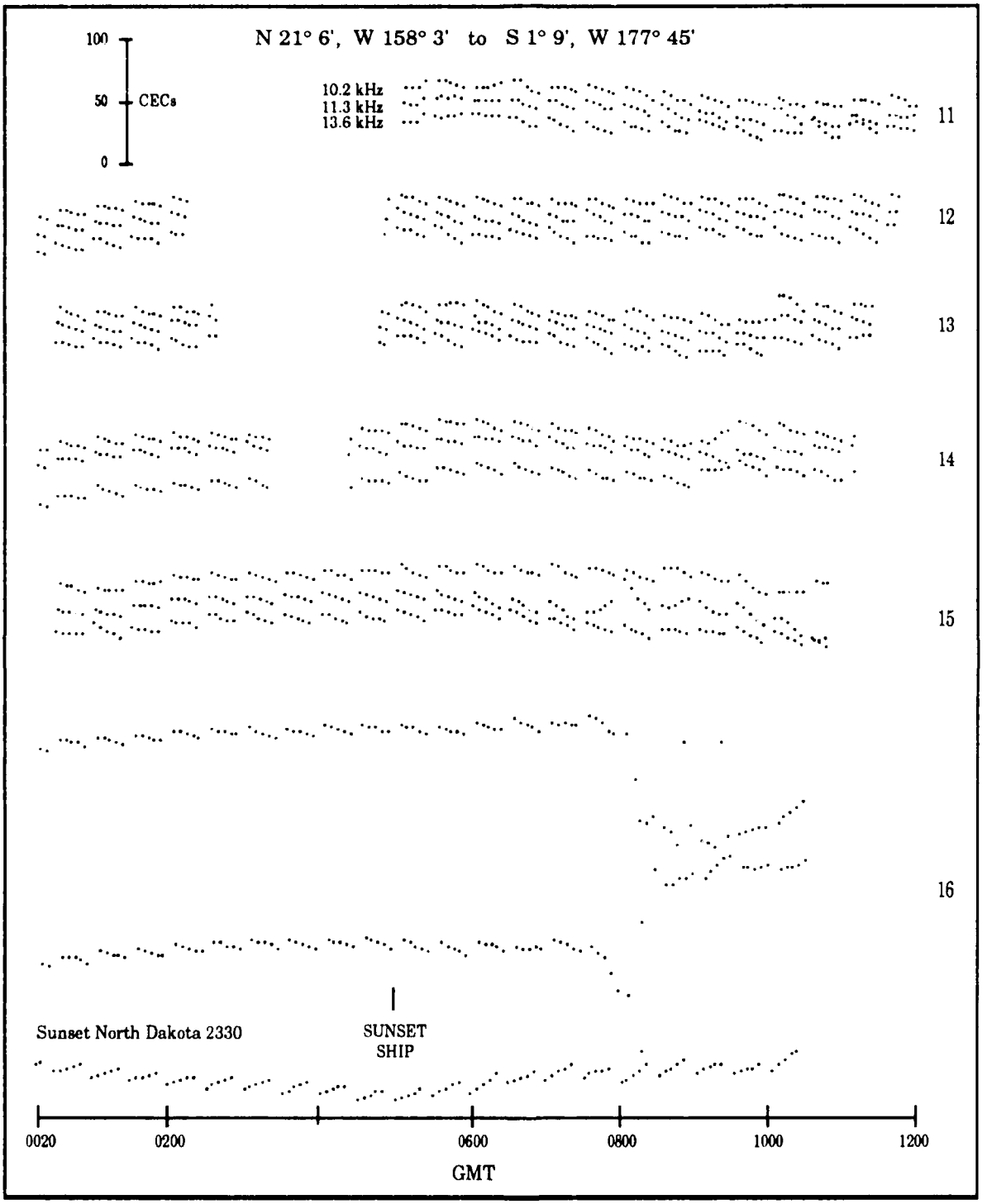

Figure B-15a. Shipboard Phase Error Data; North Dakota Signal 11-16 February 1987

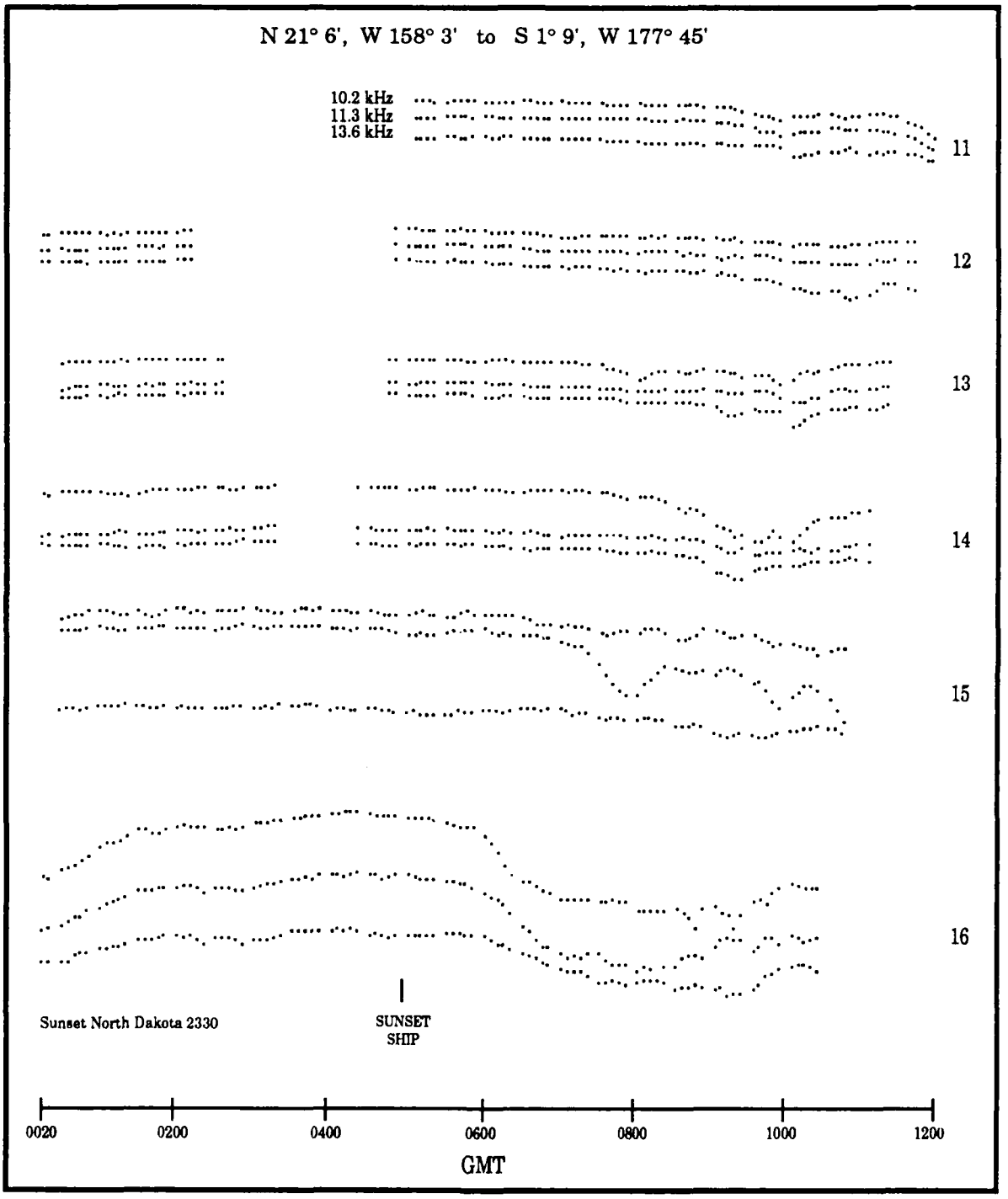

Figure B-15b. Shipboard SNR Data; North Dakota Signal 11-16 February 1987

conversion effects. Our sample size, one month, was too small to obtain reliable statistics.

The Tsushima ship transit from Hawaii on 11 through 16 February, Figure B-16, is interesting in that the data contribute to the pattern established for Hawaii and North Dakota. Propagation is from the southeast rather than northeast. The entire record is for times of sunset transition or early evening on the propagation path. Sunset starts at Argentina about 2330 GMT, before the record begins. We note that most of the large phase deviations occur before sunset at the ship. Our particular interest is in the post sunset (after 0600 GMT), records for 12, 13 and 14 February. We note that while the data change quite a bit with time, the three frequencies track each other reasonably closely. We take this to indicate that the mode conversion conditions were not strong during this time. Unfortunately the data gap on these dates covers a very interesting time interval, one that could provide important clues on the transition effects.

Conclusion: The measured modal self-interference supports predictions. The findings are consistent with conclusions of the South Pacific validation.

(G) Australia: The calculations predict the Australia signal to be strongly mode 1 dominant at all times. No significant modal effects were observed or expected. The flight data from Hawaii to Kwajelein were obscured by interference. Beyond Kwajelein, the data are consistent with a dominant mode 1. The phase records at Hawaii occasionally show slight indications that some modal component is still present in the signal. We estimate the modal content at 13.6 kHz to be slightly stronger than the calculations predict.

Conclusion: Mode 1 dominance occurs as predicted.

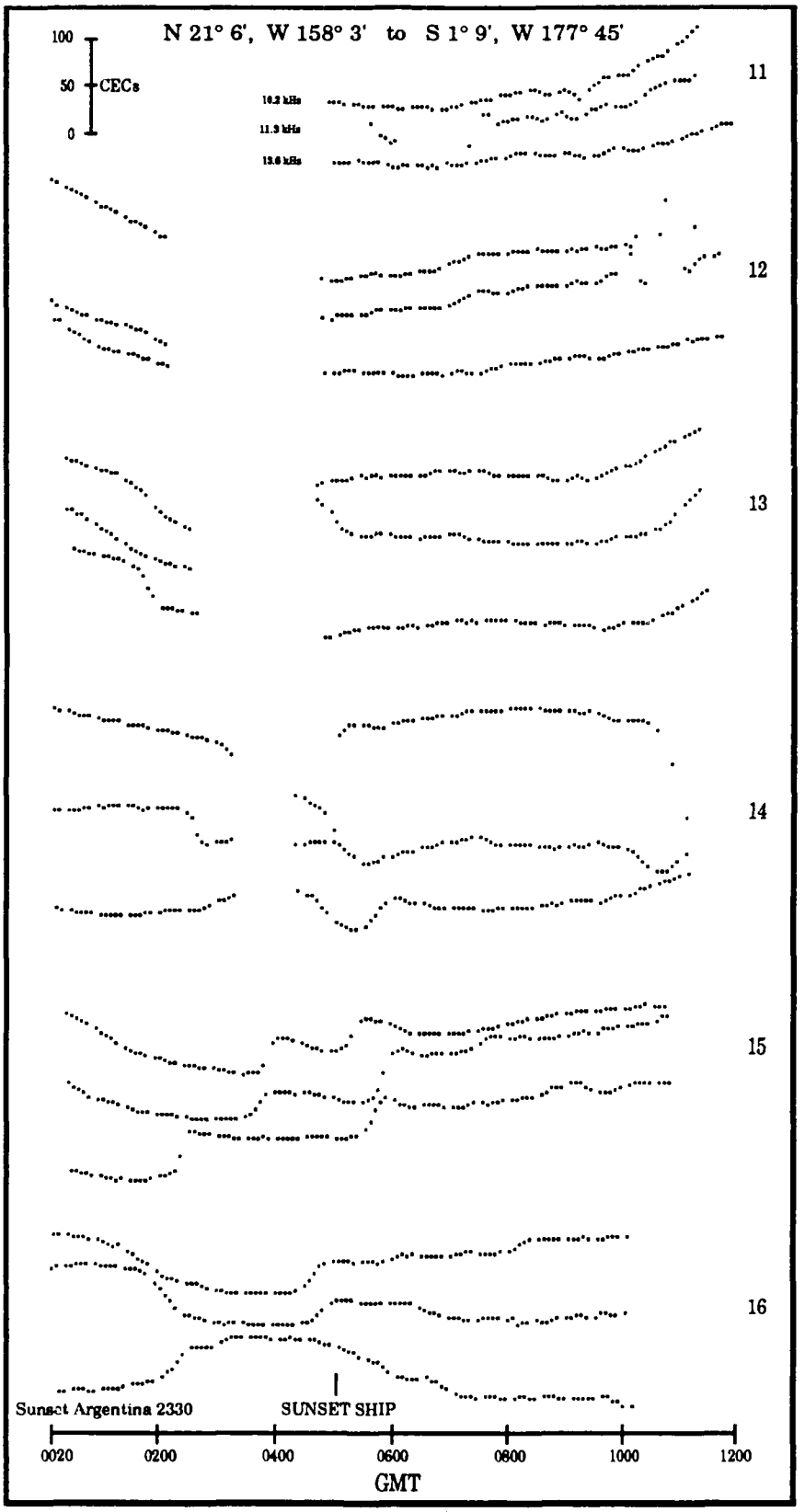

Figure B-16a. Shipboard Phase Error Data; Argentina Signal 11-16 February 1987

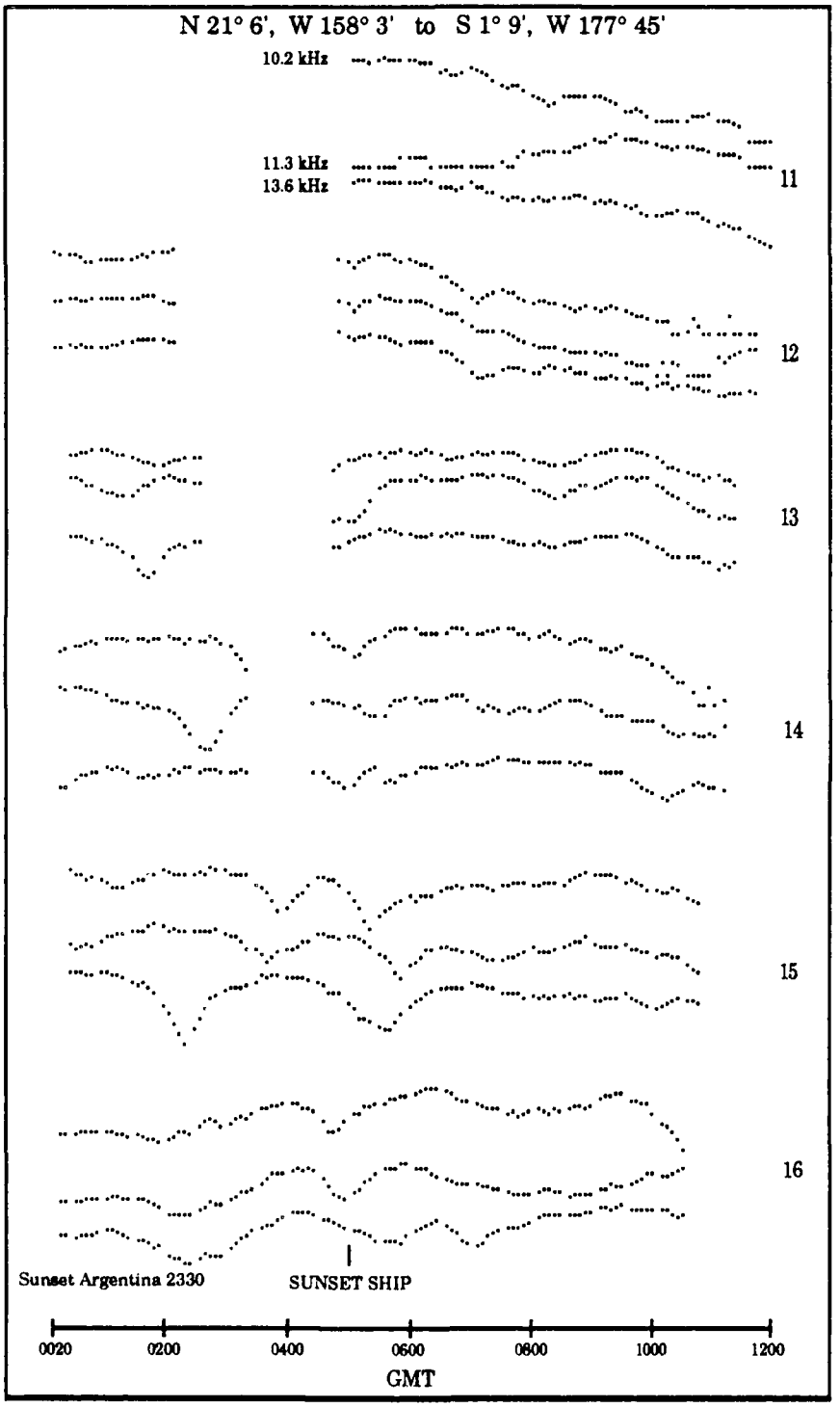

Figure B-16b. Shipboard SNR Data; Argentina Signal 11-16 February 1987

(H) Japan: The calculations show that mode 1 is dominant at all times at Hawaii, but that influence of the third mode at 13.6 kHz could extend to the vicinity of 8°S, 165°W. We are particularly interested in testing this prediction because similar extensions of the nighttime third mode are predicted for Hawaii and La Reunion. For Hawaii, which was part of the South Pacific analysis, this predicted extension is in a direction where no data were obtained. The flight data again were obscured by interference. For the ship data we have three transits. For the first, 19 January to 5 February 1987 from Japan to Hawaii, the records are all for either daytime or early sunset transition periods. We were unable to detect any modal effects. However, since sunset was not established at Japan, we believe the third-ordered mode excitation was too low. For the 11 to 16 February transit from Hawaii to the equator, the ship would have entered the very edge of the predicted third mode zone only on the 16th. No modal effects were observed on this transit. For the transit from 17 February to 5 March, which was along the equator moving west and then up to Japan, the data again were collected for time periods when Japan was in daylight. Thus again, we really have no data to test the extent of the predicted dominance of the third mode along south-easterly radials.

Conclusion: Mode 1 dominance occurs as predicted. The prediction of the third-ordered mode dominance could not be tested.

West of Hawaii to Guam; Overall Summary: The data confirm the existence and approximate boundaries of the predicted nighttime equatorial modal conversion zones for Hawaii, North Dakota and Argentina. The Liberia signal east of Kwajelein, at nighttime, is mostly long-path. The La Reunion and Australia signals are good at all times. Norway has good phase but could not be received at all times in Hawaii. The ship reception of Norway was evidently good; this being in mostly daytime when noise is highest. The Japan 10.2 kHz signal is predicted

good at all times, while the 13.6 kHz phase quality may be questionable between Japan and Kwajelein.

The data suggest that the equatorial modal zone boundaries may fluctuate several degrees latitude with variations in propagation conditions. However the data set is too small to provide more than a suggestion.

SOUTH CENTRAL AREA; GUAM TO 130° EAST LONGITUDE (Flights [3 & 4], 12, 13, [15 & 16 &17], Yap, and Darwin; excluding the vicinity of Japan): This area is characterized by having four stations predicted always good (Norway, Liberia, La Reunion and Japan), and four stations predicted to have some nighttime modal problems at some locations within the area. Modal problems occur because of equatorial zone mode conversion. The eastern edge of the predicted equatorial mode conversion zone for Australia signals is within this area (see Appendix A, Figure A-18). The data consist of measurements on Yap, flights on two radials from Australia (Flights [3 & 4] and [12 & 13]) and on two radials from Japan (Flights [15 & 16 &17] and [12 & 13]). The analysis summary by stations is as follows:

(A) Norway: All radials, 10.2 kHz and 13.6 kHz, are predicted mode 1. The overlay model for 0600 GMT during February predicts coverage loss over much of the area due to insufficient SNR. All flights are at times when Norway is in daylight. The day/night transition is however, at high latitudes. On flight 4 the signal on leaving Guam going north is very weak and noisy. The data show some hint that the amplitude pattern for 13.6 kHz differs to a small degree from the 10.2 kHz and 11.3 kHz patterns.

For flight 12, all signals have good SNR and are consistent with clean mode 1. For flight 13, the SNR at 10.2 kHz is very poor, the signal level being about 22 dB. At 11.3 kHz and 13.6 kHz, the signal levels are nearly the same but the noise is less. The signal levels for flight 13 are only about 2 dB less than for flight 12, but due to noise the signal quality is much different.

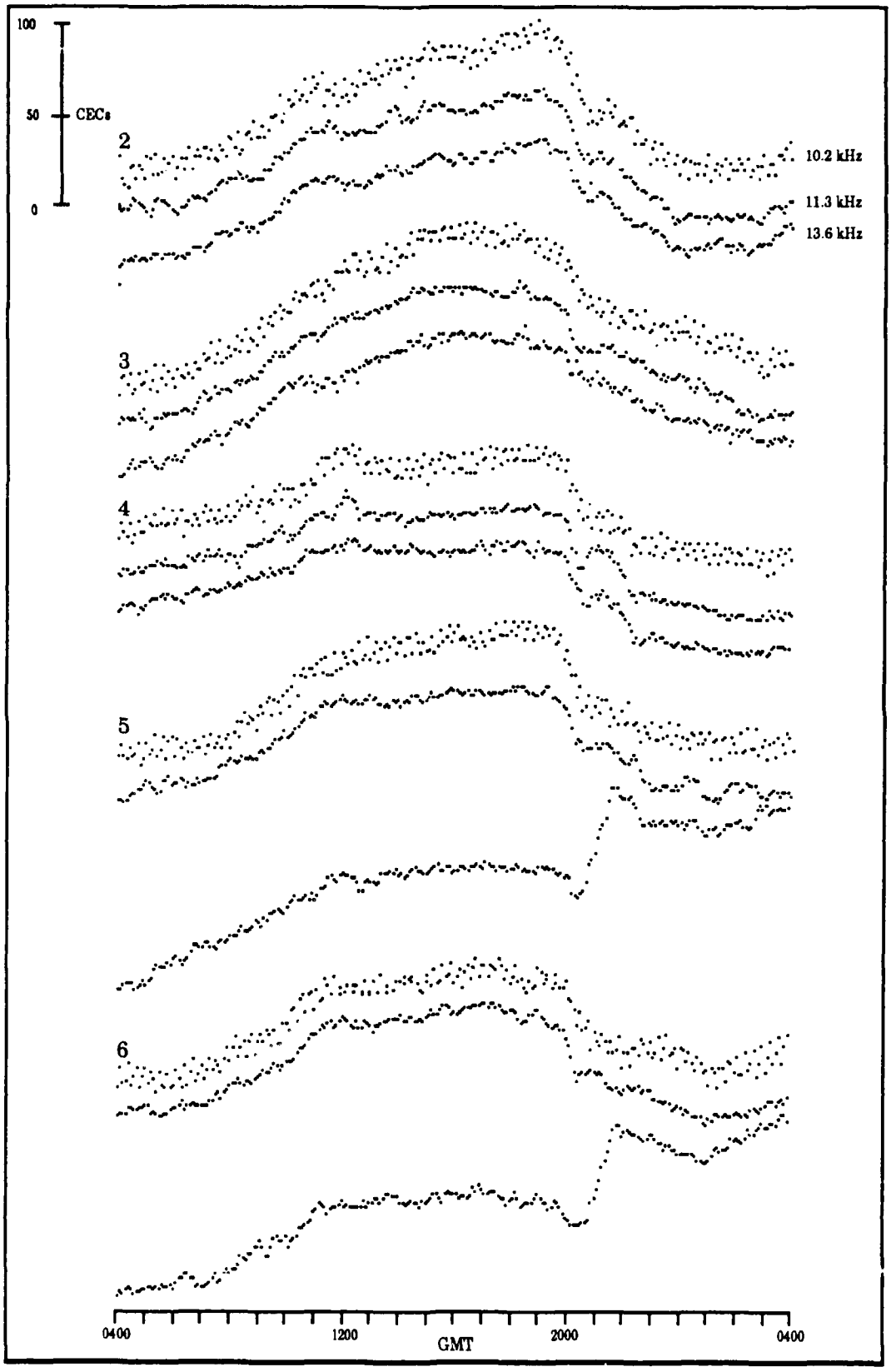

Figure B-17. Norway Received Phase at Yap; 2-7 May 1986

At Yap the Norway signal is very noisy and mostly mode 1 at all times. On occasion we note a phase jump at 13.6 kHz during sunrise as shown in Figure B-17. Interestingly, in the samples we have examined in detail, we do not see evidence of multiple modes prior to the onset of the jump. Evidently the modal-like condition is confined to sunrise, which for the time of our data is confined to about one hour. We suspect tracking loss.

At Darwin, the phase records are very complex. For May 1986, the period we examine in the most detail, the phase track is regularly lost soon after 0600 GMT due to weak signal in high atmospheric noise. The signals generally recover, sometime after 1500 GMT, when the regional thunderstorm activity has decreased and most of the path is in darkness. Sunset does not occur at Norway until about 2000 GMT. By 2100 GMT, sunrise starts at Darwin. Signal phase tracking generally is lost during sunrise on the low latitude portion of the propagation path. Tracking loss can last up to two hours. After this time the phase transition is essentially complete. Sunrise at Norway occurs near 0030 GMT. For the periods of this data, night never really gets well established in the Arctic region where mode conversion at night is predicted.

Conclusion: The data are consistent with the predictions. Coverage just south of Yap may be a problem because of SNR. At Darwin signal loss at all frequencies occurs regularly for two periods of time. The outage times are typically 0600 to 1500 GMT and 2100 to 2300 GMT for a total of 11 hours.

(B) Liberia: The coverage models predict good phase quality except when SNR is inadequate. Unreliable tracking is predicted south of Yap in February at 0600 GMT. Throughout flight 4, all three signals were weak (about 22 dB above a micro-

volt/meter) and very noisy. The data are consistent with a mode 1 signal.

The flights in the vicinity of Japan show a weak signal level and a very noisy 10.2 kHz signal.

For flight 12, the 10.2 kHz signal is very weak and noisy during the first one-third of the flight, as is the 11.3 kHz signal for the first one-sixth. For flight 13 the signal quality is very good on all frequencies. The data for both flights are consistent with mode 1 signals.

For Yap, the Liberia signal is good quality mode 1 at all times. The phase records show a definite increase in noise during the afternoon and early evening. The phase quality is better than for Norway.

For Darwin, the Liberia signal has good phase quality and adequate SNR. We found no instances of modal effects or signal loss.

Conclusion: The Liberia signal is mode 1 at all times. SNR could be a problem at times of very high atmospheric noise, particularly storms occurring in the Philippines and/or New Guinea.

(C) Hawaii: Guam is within the equatorial mode conversion zone for the Hawaii signal. The calculations predict the northern border to lie about 4° north of Guam. North of this zone, the 13.6 kHz signal is predicted mode 3 dominant. Flight 4 is almost perpendicular to the Hawaii radials. The data show definite modal structure at 10.2 kHz and possible modal structure at 11.3 kHz and 13.6 kHz for about the first third of the flight. We estimate the northern boundary to be near 22° north latitude, or about 2° north of predicted.

For flight 12, modal effects can be detected (primarily on 11.3 kHz) about one halfway along the flight. For flight 13, all three signals undergo large amplitude changes. The total distance increase is about 1.6 Mm, yet in the first quarter of the flight, the 10.2 kHz signal amplitude decreases by almost 20 dB. After going through a minimum lasting about 40 minutes, the signal increases again by nearly 10 dB. Similar changes are noted at the other frequencies, with the large changes occurring about the same time. Since the changes occur together, something other than multiple mode interference must be contributing.

For flight 15, which is an approximate extension of flights 2 and 3, pronounced modal effects are observed on all frequencies. These effects are much stronger at 10.2 kHz and 11.3 kHz than at higher frequencies.

At Yap, the Hawaii signals are strongly modal throughout the night and the transition periods on all three frequencies. We noted modal effects on every night we examined.

At Darwin, we note strong modal effects on all days. At 10.2 kHz and 11.3 kHz, phase tracking is frequently lost at times of cycle jumps. At 13.6 kHz cycle jumps are common, but tracking seems to be maintained.

Conclusion: The Hawaii signal is clearly modal within the predicted mode conversion zone. The flight data do not give us a clear indication of the northern modal boundary. A possible reason is that the flights were nearly perpendicular to the radials. Flight 15 shows that modal effects extend into the shadow zone.

(D) N. Dakota: Guam is within the equatorial mode conversion zone for the North Dakota signal. The calculations predict the northern border to lie about 4° north of Guam. North of

this zone all frequencies are predicted mode 1 dominant. Sunrise at North Dakota occurs after 1.5 hours of flight time. No modal effects could be detected prior to this time.

For flight 12, modal effects can be detected close to half-way along the flight. The effects are not strong. For flight 13, the signal level is too low to measure for most of the flight.

At Yap, the North Dakota signals are strongly modal on all nights and all frequencies. We note that the North Dakota signal propagation path to Yap has less than one-half the distance within the conversion zone that the Hawaii signal has. The magnitudes of the modal effects are about equal, though the time histories are quite different.

At Darwin, the signals are very weak and strongly modal. At 10.2 kHz phase tracking is typical maintained for only about five hours, starting near 2300 GMT.

Conclusion: As predicted, the North Dakota signal is mode 1 above the mode conversion zone and modal within the zone. The flight data do not provide information on the modal boundary.

(E) La Reunion: This signal is predicted clean mode 1 within the area. The data from flight 4 are consistent with a dominant first mode on all frequencies. The data from flights in the vicinity of Japan also support the signals being clean mode 1.

For flights 12 and 13, all signals are strong, near 40 dB above a microvolt per meter. The data are consistent with good phase quality.

At Yap, the La Reunion signals are clean mode 1 at all times. The phase quality is very good on all records we examined.

At Darwin, the signals are clean mode at all times with good SNR.

Conclusion: La Reunion is a reliable navigation signal in this area.

(F) Argentina: Guam is within the equatorial mode conversion zone for the Argentina signal. The calculations predict the northern border of this zone to lie about 4° north of Guam. North of this zone, all frequencies are in the shadow zone. No measurements were made on flights in this area.

At Yap, this channel was used for station calibration.

At Darwin, the path crosses the edge of Antarctica. The data cover time periods when the path segment crossing Antarctica is night at all times. The calculations show strong mode competition beyond Antarctica for nighttime propagation. The data show that the phases of all three frequencies track very closely, except for periods of tracking loss. We assume the signals are mode 1 since no mode switching is detected. The diurnal phase pattern is almost completely controlled by day/night conditions on the Australia side. Tracking loss is most likely to occur during sunrise over Australia. Tracking loss can also occur during the period of maximum daylight on the Argentina side of the path.

Conclusion: We were unable to test any predictions of equitorial modal conversion effects because no data were obtained. From other measurements we infer that the modal effects in this area are as predicted. Below the equatorial zone, the Darwin measurements show that mode 1 dominates. Tracking loss occurs on most days during sunrise on the Darwin side.

(G) Australia: The TASC calculations predict the eastern boundary of the equatorial mode conversion zone to be about 3° west of

Guam. On the 353° radial the higher-ordered modes peak at a distance of 5 Mm, but are at least 12 dB below mode 1. The NOSC calculations show modal effects at 10.2 kHz on the 357° radial, which crosses Guam, starting at 5.8 Mm. Guam is also about 5.8 Mm from the Australia station. We note modal effects on the flight 3 and 4 data, starting near 4.6 Mm distance from Australia and continuing to the end of the flight at 8 Mm distance (Figure B-18). We interpret the amplitude variations having a long period of 100 to 500 Km to be modal effects on all four frequencies.

For flight 12, modal effects start one-fifth of the way along the flight, 8 Mm from the station. The 10.2 kHz signal incurs a 10 dB decrease in about 10 minutes and becomes very noisy. The 11.3 kHz signal also is very weak, but somewhat less noisy. At 13.6 kHz the amplitude decrease is about 4 dB. After about two hours the signal levels start increasing, reaching the starting values after six hours. Modal effects are evident until the end of the flight at Yap, a distance of 5.4 Mm. For flight 13, modal effects are noted to about 4.5 Mm from the station.

At Yap, slight modal effects are detected at 10.2 kHz and 11.3 kHz for about 20 percent of the nights. We looked at several months' worth of data and could not discern more than negligible modal effects. The navigation quality is observed satisfactory at Yap on all frequencies.

At Darwin, all signals are excellent phase quality and high SNR.

Conclusion: Modal effects occur north of Yap. South of Yap the phase quality is good on all frequencies. These observations are in conflict with our prediction that places Yap in the middle of the north/south span of the equatorial mode conversion zone.

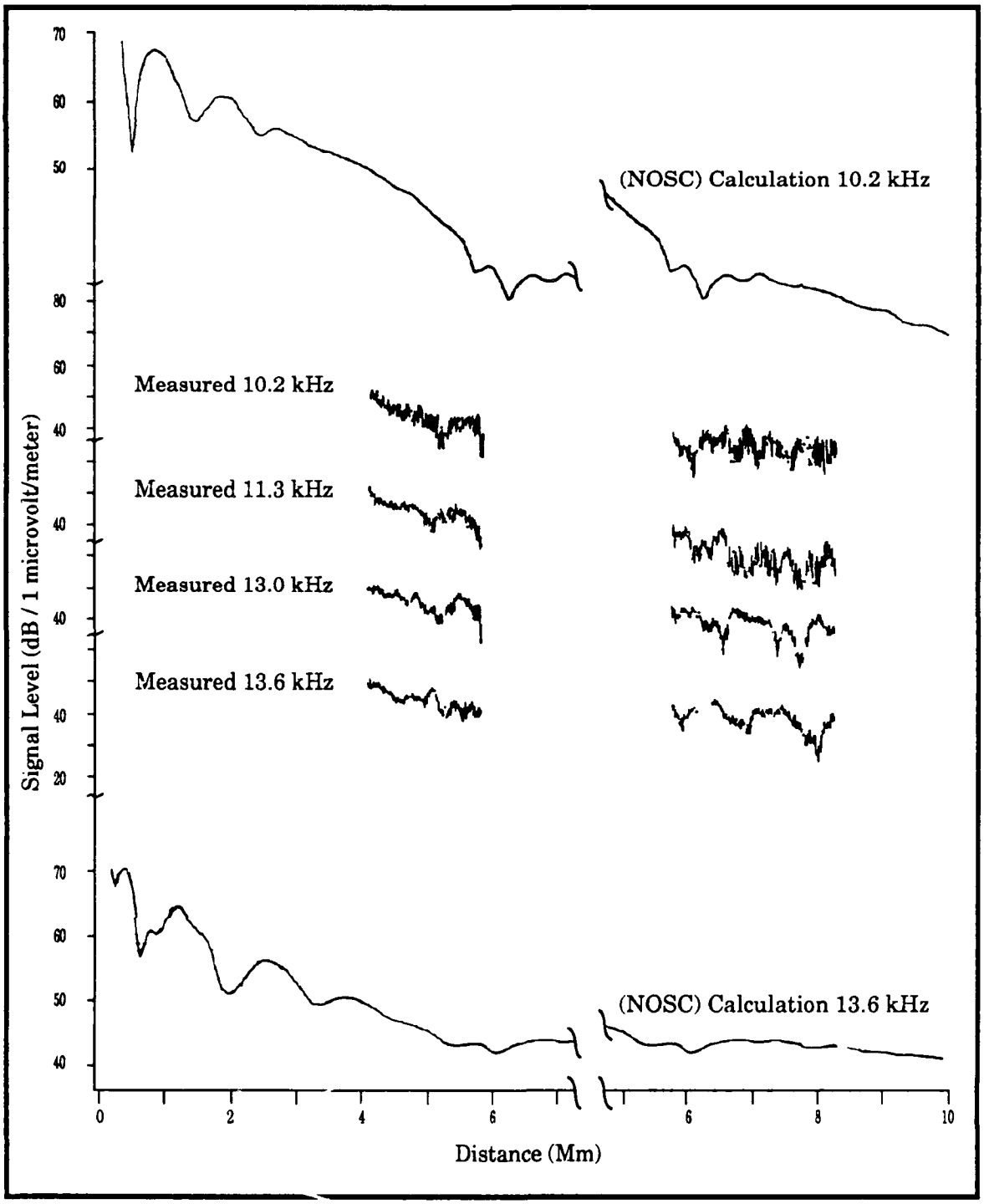

Figure B-18. Measured and Calculated Australia Signals, 357° Radial

(H) Japan: The Japan signals are predicted good quality mode 1 for the entire area beyond 2 Mm from the transmitter. This prediction is supported by the flight data for both of the radials. Samples of flight data are presented in the discussion of the Japan area.

The Yap, data also clearly show the signals to be clean mode 1 at all times.

At Darwin, we frequently note slight modal effects. Occurrence of modal effects may vary seasonally. In May 1986 only minor effects are detected, and then for about half of the nights. During June the modal effects are more evident and frequent, being detectable on almost all nights. While only a few cycle jumps are noted, on some other nights the effects were close to the level we believe could result in jumps. We show an example of six days' data in Figure B-19 that we consider representative of the data set. The record for the first day, 05- 06 June, shows what we consider relatively strong modal effects for this location and station. Effects this strong occur less than ten percent of the time.

Conclusion: The Japan signals are of good navigation quality throughout this area. The Darwin data indicate that the eastern equatorial modal zone boundary for Japan is slightly to the east of our prediction. We expect that on radials just to the west of Darwin the modal effects are sufficient to dictate signal deselection.

South Central Area; Overall Summary: The equatorial modal effects noted to the east for the Hawaii, North Dakota, and Argentina signals were predicted and observed for this area. Our prediction is for the equatorial mode conversion zone for the Australia signals to begin west of Guam and extend westward to the edge of the validation region. Modal effects are detected on flight data for locations north of Yap. Modal effects are only weakly evident at Yap. Thus the data only partially support the Australia modal prediction. The Norway signal, while

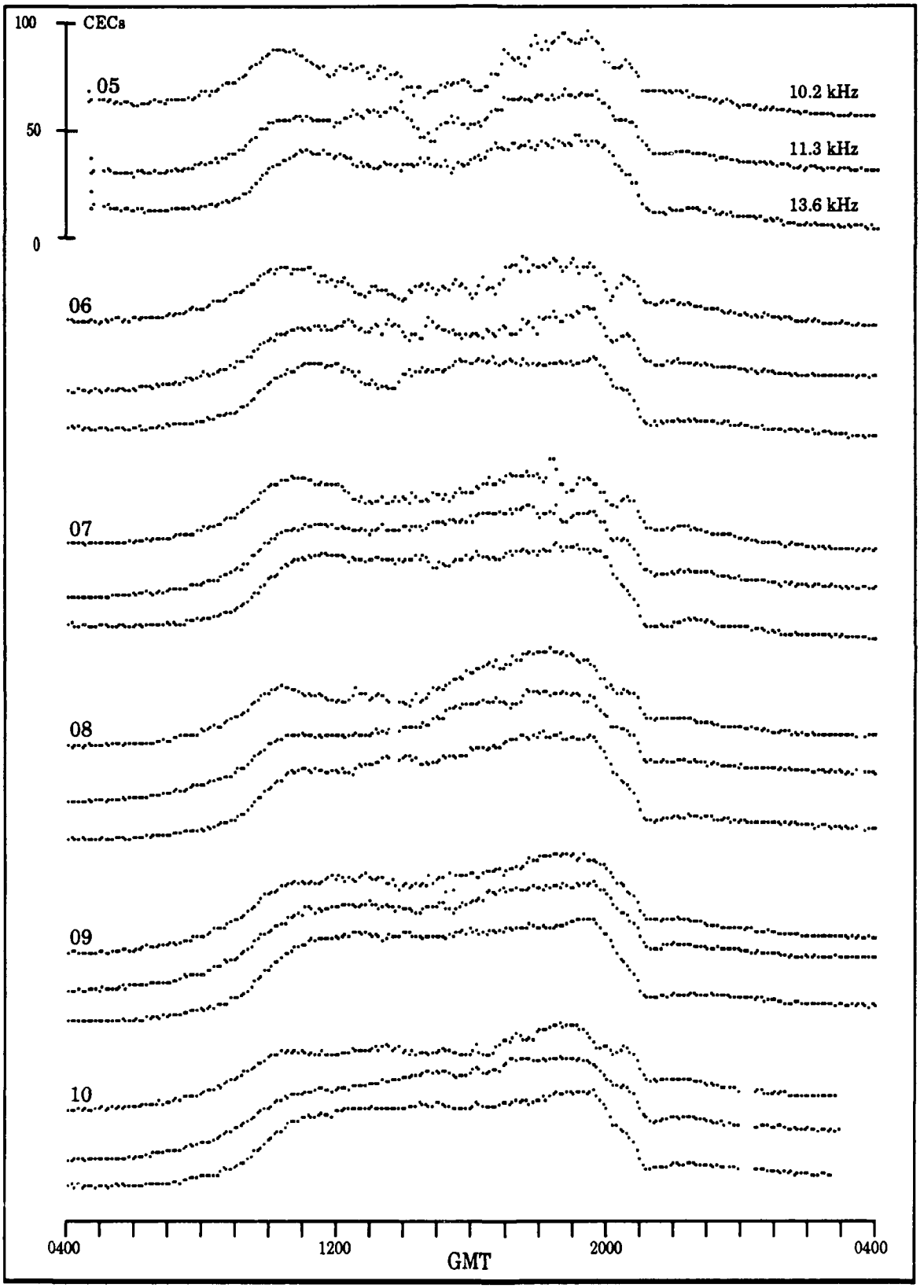

Figure B-19. Japan Received Phase at Darwin; 5-11 June 1986

weak, has good phase quality. Japan signals are good at all times and locations. The aircraft data only weakly support placement of modal boundaries.

We conclude that Norway, Liberia, La Reunion and Japan provide good signals throughout the area. We note that the Japan signal radial to Darwin probably delineates the eastern edge of its equatorial mode conversion zone. The Australia signals are good below their mode conversion zone. The North Dakota signals are good above their mode conversion zone.

NORTH CENTRAL AREA; JAPAN AND VICINITY FLIGHTS (Overflight radials of Japan transmitter and Japan fixed site): This area is selected to give focus to the documentation of the near modal zone of the Japan Omega station and to assess navigation capability in the high traffic area of Japan. Because the Japan signal has no diurnal phase change, the reference oscillator drift can be very accurately measured and removed from all other station records. The analysis summary by stations is as follows:

(A) Norway: The predictions show the Norway signal to be generally mode 1 and reliable in this area. One of the TASC computed radials (50° bearing), with a predicted competitive mode 2 component at 13.6 kHz, passes just to the east of the Japan monitoring site.

The flights in the vicinity of Japan show a good signal level (30 dB) and good amplitude tracking between frequencies.

At Japan, we find all three signals mode 1 at all times. We cannot detect even a trace of a higher mode competing. During local summer, July, the noise frequently gets very strong in the afternoon and early evening. On several days the phase track is lost during this time interval. We cannot determine that thunderstorm noise is the primary cause, but it seems quite plausible.

Conclusion: The Norway signals have good quality phase at all times. Atmosphere noise may create reception problems a small percentage of the time.

(B) Liberia: Liberia signals are predicted clean mode 1 at all times. Liberia should be very reliable for navigation.

All the flight data support the prediction of a good quality navigation signal.

At Japan, the signal quality is good at all times. Noise is relatively low and the phases of all signals track each other closely.

Conclusion: The Liberia signals are of good navigation quality at all times.

(C) Hawaii: Predictions for Hawaii signals in the vicinity of Japan show the 10.2 kHz signal to be mode 1 dominant, with mode 2 being 4 dB below mode 1 on the 290° radial and 7 dB below on the 300° radial. Japan is on the 299° radial. At 13.6 kHz mode 2 is predicted dominant by 5 dB on the 290° radial, and equal to mode 1 on the 300° radial.

The flights in the vicinity of Japan show a good signal level until sunrise starts at Hawaii. Following sunrise in Hawaii, 1600 GMT, the signals gradually decrease by about 20 dB by 2000 GMT. Prior to 1600 GMT no modal structure was detected.

At Japan we find the modal conditions quite variable from day-to-day. Most of the time the signals indicate clean mode 1 on all frequencies. Part of the time, about 25 percent, we detect evidence of modal effects at 13.6 kHz. Occasionally, nearly 10 percent of the time, we observe marked modal effects on all frequencies.

We show examples of all conditions in Figure B-20 for the measurement period 20 April to 01 May 1986. The phase records for the last five days, 26 through 30 April, show no modal effects. The phase records of all three frequencies track very closely for the entire period.

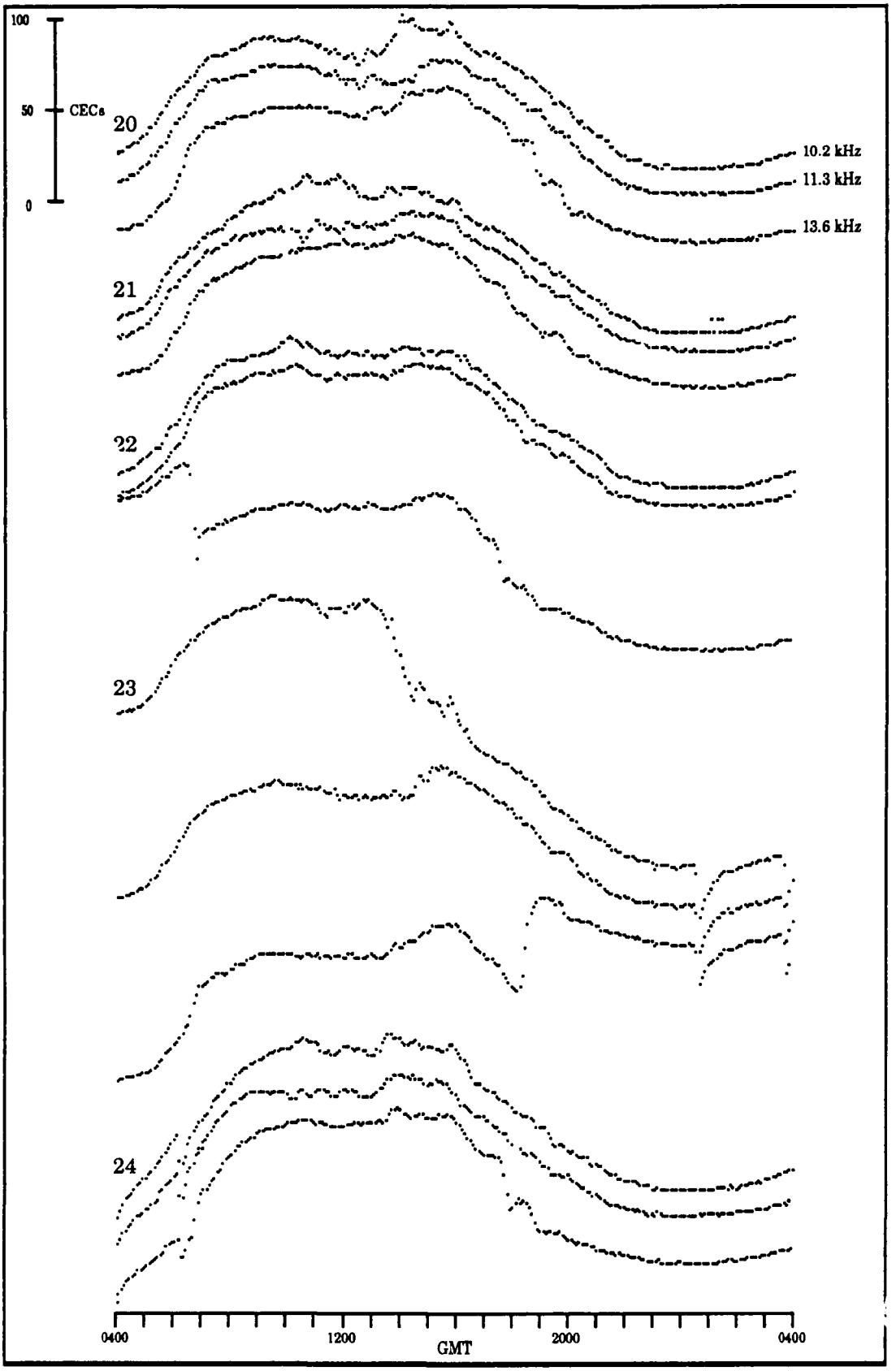

Figure B-20a. Hawaii Received Phase at Japan; 20-25 April 1986

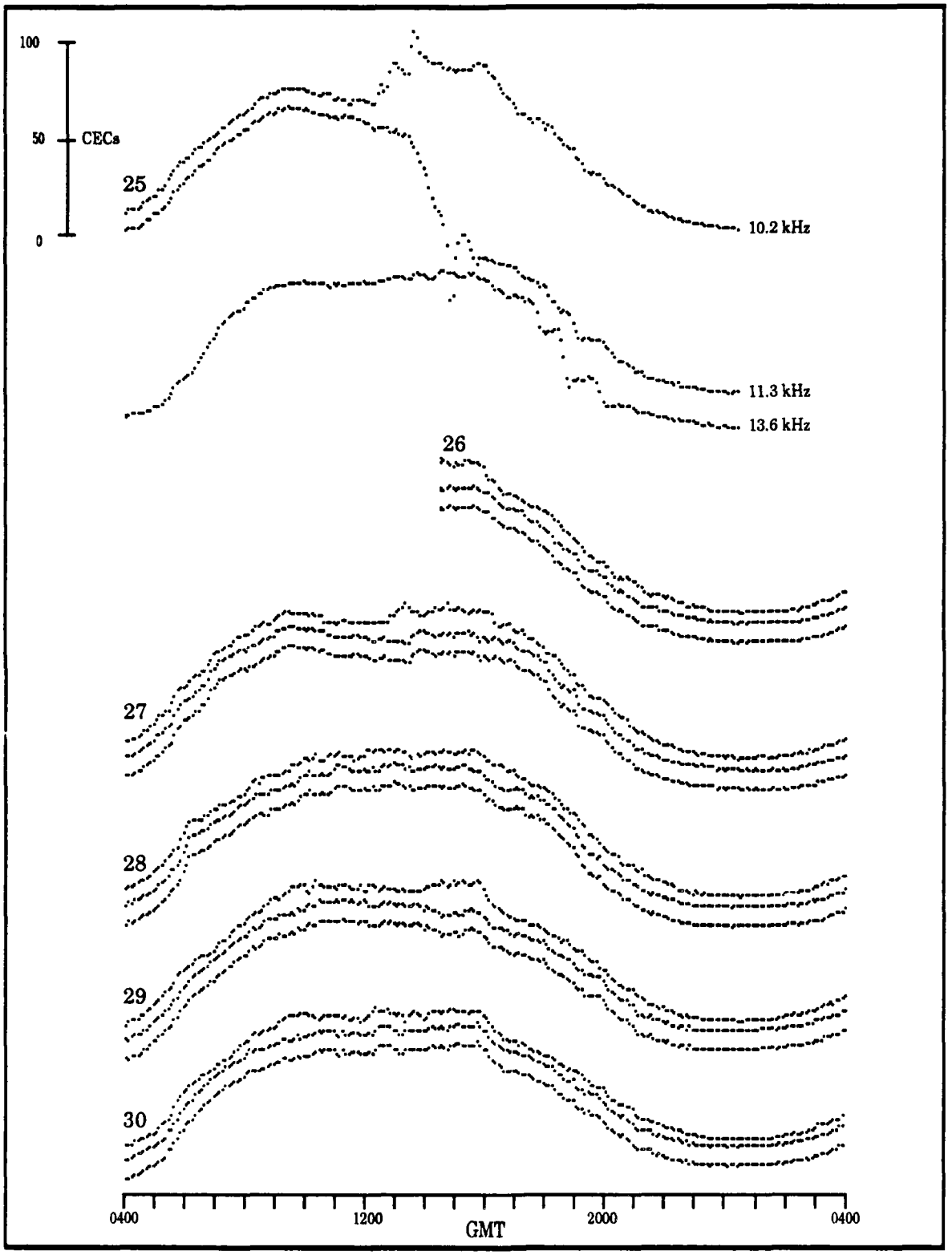

Figure B-20b. Hawaii Received Phase at Japan; 25 April-01 May 1986

On some dates minor disturbances occur; the dates of 20, 21 and 24 April are good examples. For 20 April we note two effects: (1) a propagation disturbance after midpath midnight, where each frequency has a slightly different phase perturbation, and (2) the sunrise and sunset transitions of 13.6 kHz, about halfway through the transition time, where the phase slope is very steep. For 21 April a small disturbance occurs before midnight where each of the phases has a different time history. The 22 April record is a good example of sunrise/sunset transition effects on 13.6 kHz. At both transitions the 13.6 kHz phase undergoes a sharp step, the sunset step resulting in a jump. The 24 April record also shows the 13.6 kHz phase steps, but with a solar flare somewhat masking the sunset step.

Examples of strong modal effects are noted in the 23 and 25 April, phase records. When strong modal effects occur, they seem to be most often associated with a disturbance onset after midpath midnight. Cycle jumps can occur at any time during the period of evident modal effects. For 23 April the large phase transition for 10.2 kHz occurs at the beginning of the detected modal effects. For 13.6 kHz, the cycle jump occurs in the opposite sense during the sunrise period. For the 25 April record, a cycle jump occurs only at 11.3 kHz beginning at about one hour after onset of modal effects, onset being near midpath midnight.

The planned flight 18 from Tokyo to Midway was cancelled. This flight would have been valuable in testing the modal structure of the Hawaii signal in the vicinity of Japan.

Conclusion: Modal effects can occur on all frequencies in the vicinity of Japan. From the magnitude of phase perturbations when cycle jumps do occur, we suspect that on

some nights, when no jumps are recorded, jumps would occur at other locations.

(D) N. Dakota: The North Dakota signals are predicted clean mode 1 at all times to as far south as the equatorial zone. The calculations show that on the 320° radial through Japan, the attenuation rate for mode 1 begins to increase at 9.6 Mm, the distance of Japan.

The flights in the vicinity of Japan show a weak signal level but no modal effects.

At Japan, the signals show nearly the same time histories, except for about one hour at the end of the sunrise period. At this time each frequency typically shows a slightly different phase trace. On a few records a cycle jump is recorded, similar to the example in Figure B-21. This figure shows the small modal effect at the end of sunrise occurring on 21 and 22 April, and a cycle jump during the same time interval on 24 April. While this modal effect is generally negligible at Japan, we suspect that it is more pronounced further south. Because of the predicted increased attenuation rate of mode 1 south of Japan, we estimate that cycle jumps occur in front of our predicted conversion zone during this late sunrise period.

Conclusion: The North Dakota signals, while weak, provide acceptable navigation quality signals in the vicinity of Japan. On infrequent occasions a short segment less than two hours at late sunrise could be modal.

(E) La Reunion: The predictions are for good quality navigation signals at all times in this area.

The flight data are consistent with strong mode 1 dominant signal.

At Japan, the phase records for this station show clean mode 1 with good SNR at all times at all frequencies.

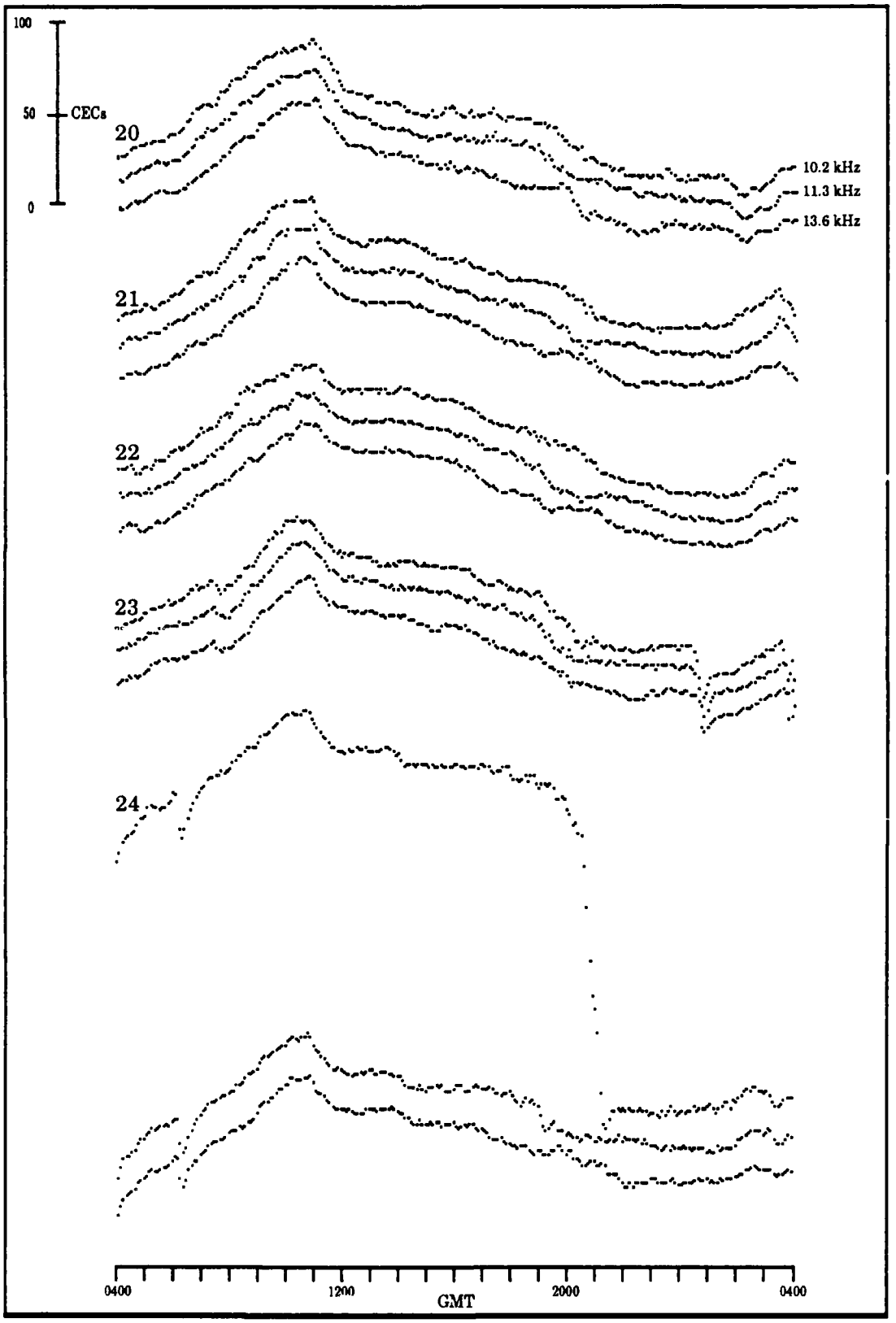

Figure B-21. North Dakota Received Phase at Japan; 20-25 April 1986

Conclusion: The data support the prediction that the La Reunion signals provide high quality navigation at all times.

(F) Argentina: The Argentina nighttime signals are predicted to be long-path dominated. Also the short-path is in the equatorial mode conversion zone shadow.

No flight or fixed-site data were recorded for this validation.

Conclusion: The Argentina signals are probably unusable at nighttime in the vicinity of Japan.

(G) Australia: The predictions for the Australia signals place the eastern boundary of the equatorial mode conversion zone to the east of the propagation path to the Japan monitoring site. This propagation path lies about 1° longitude west of Yap. This prediction places the monitoring site in the conversion shadow zone where we assign an uncertain rating to phase. The TASC calculations for the 345° radial show mode 2 at Japan dominant by about 12 dB at 10.2 kHz and show modes 1 and 2 equal at 13.6 kHz.

In the vicinity of Japan, on the last leg of flight 4, the 10.2 kHz signal is very weak and noisy; the 11.3 kHz signal is also weak but less noisy. Although they may be questionable, we believe we can detect modal effects in the data.

At Japan, the 10.2 kHz and 11.3 kHz signals consistently show pronounced modal effects, while the 13.6 kHz signal shows negligible effects. A typical data set example is shown in Figure B-22. Cycle jumps occur almost every night on either 10.2 kHz or 11.3 kHz or both. While jumps can occur at any time during the night, we note frequent occurrences near midpath midnight. With few exceptions

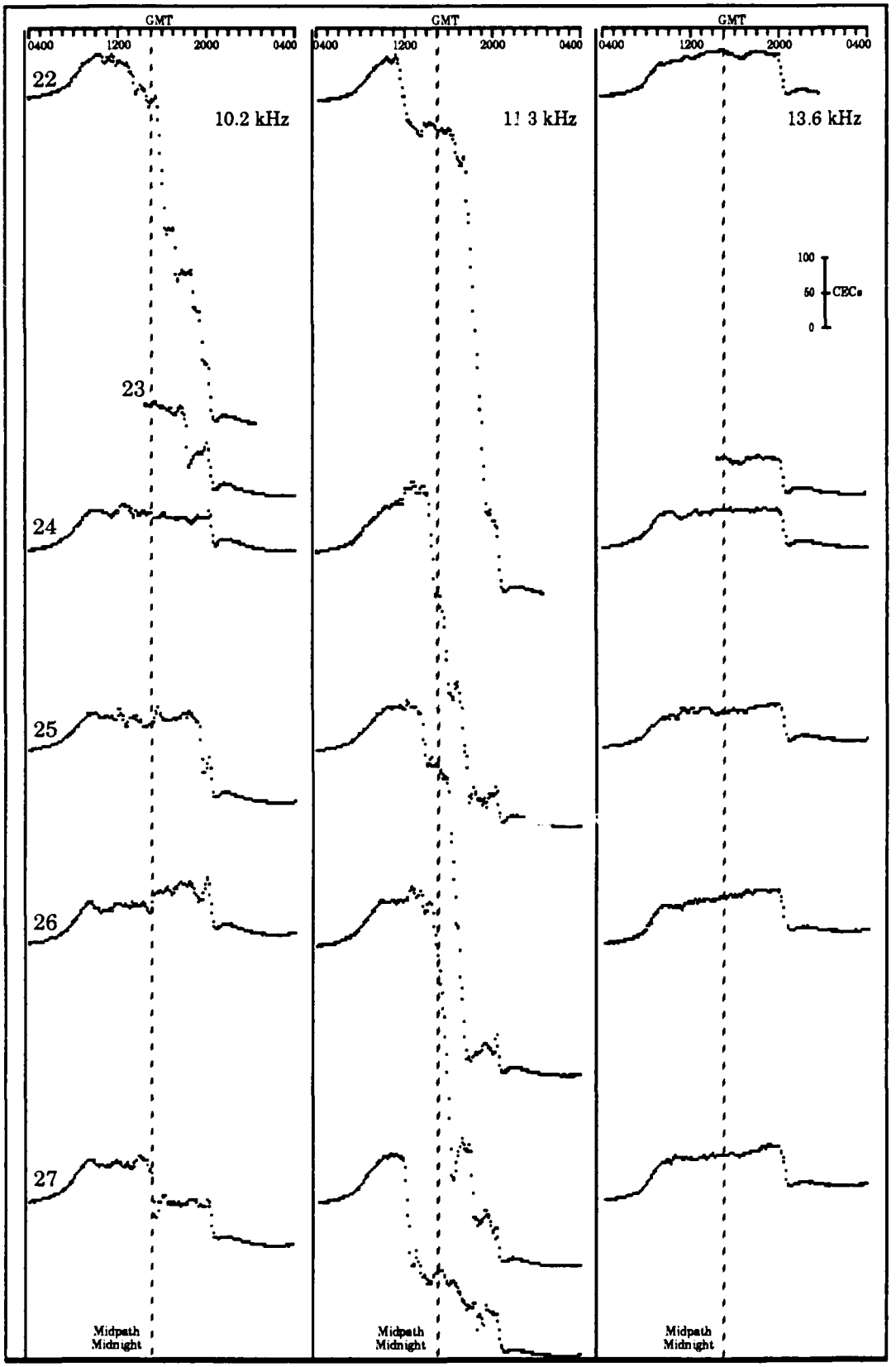

Figure B-22. Australia Received Phase at Japan; 22-28 April 1986

we do not detect the onset of modal effects until after the sunset transition period.

Conclusion: The fact that modal effects are pronounced at 10.2 kHz and 11.3 kHz and not at 13.6 kHz suggests that the mode 2 content is less than the calculations predict. We consider the strong modal effects at Japan and the negligible effects at Yap as evidence suggesting that more understanding is required in order to make good predictions.

(H) Japan: The calculations predict the normal zones of near modal effects around the Japan transmitter. As with Hawaii and La Reunion, a large area with mode 3 dominant is predicted to extend at night to the southeast of the transmitter. Four flight radials were measured to document the near zone modal parameters of the Japan signals. We present composite data from all flights on a given radial for continuity, even though the data are included in other areas.

The data for the 81° flight radial (segments of flights 4 and 5) are shown in Figure B-23, along with field strength calculations. The NOSC calculations predict strong modal interference at 10.2 kHz to 2.5 Mm and at 13.6 kHz to 5 Mm. The measurements extend to 1.3 Mm. While the data cover only a short distance, it is evident that the signal strength patterns are very different than those predicted. A key feature of the data not predicted by the calculations is the broad minima occurring at each frequency beyond the first large narrow minima.

The data for the 141° flight radial (flights 17, 16 and part of 15) are shown along with NOSC field strength calculations in Figure B-24. Here the calculations are more similar to the measurements. We again note a signal component at all frequencies that produces a broad mini-

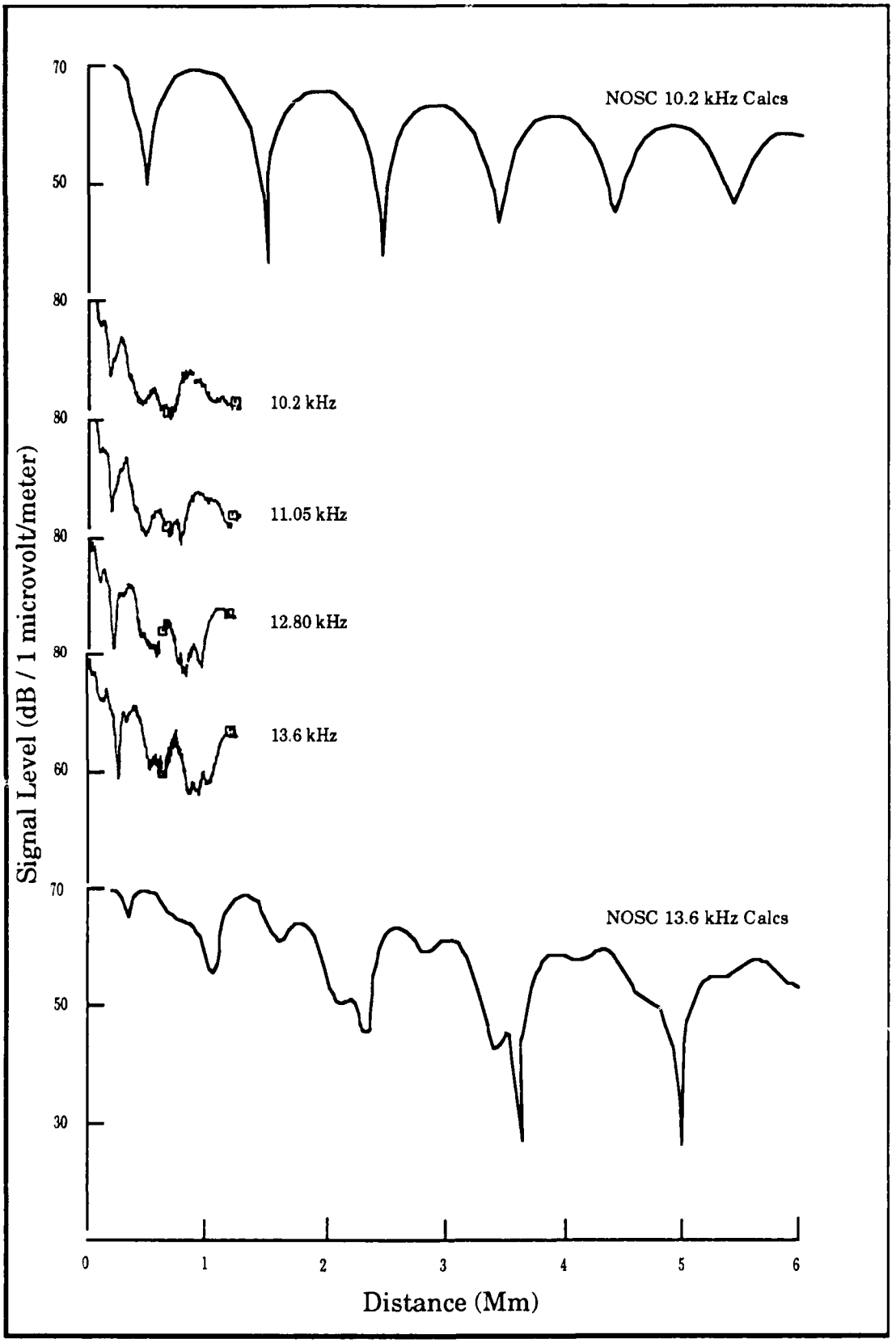

Figure B-23. Measured and Calculated Signals; Japan 81° Radial

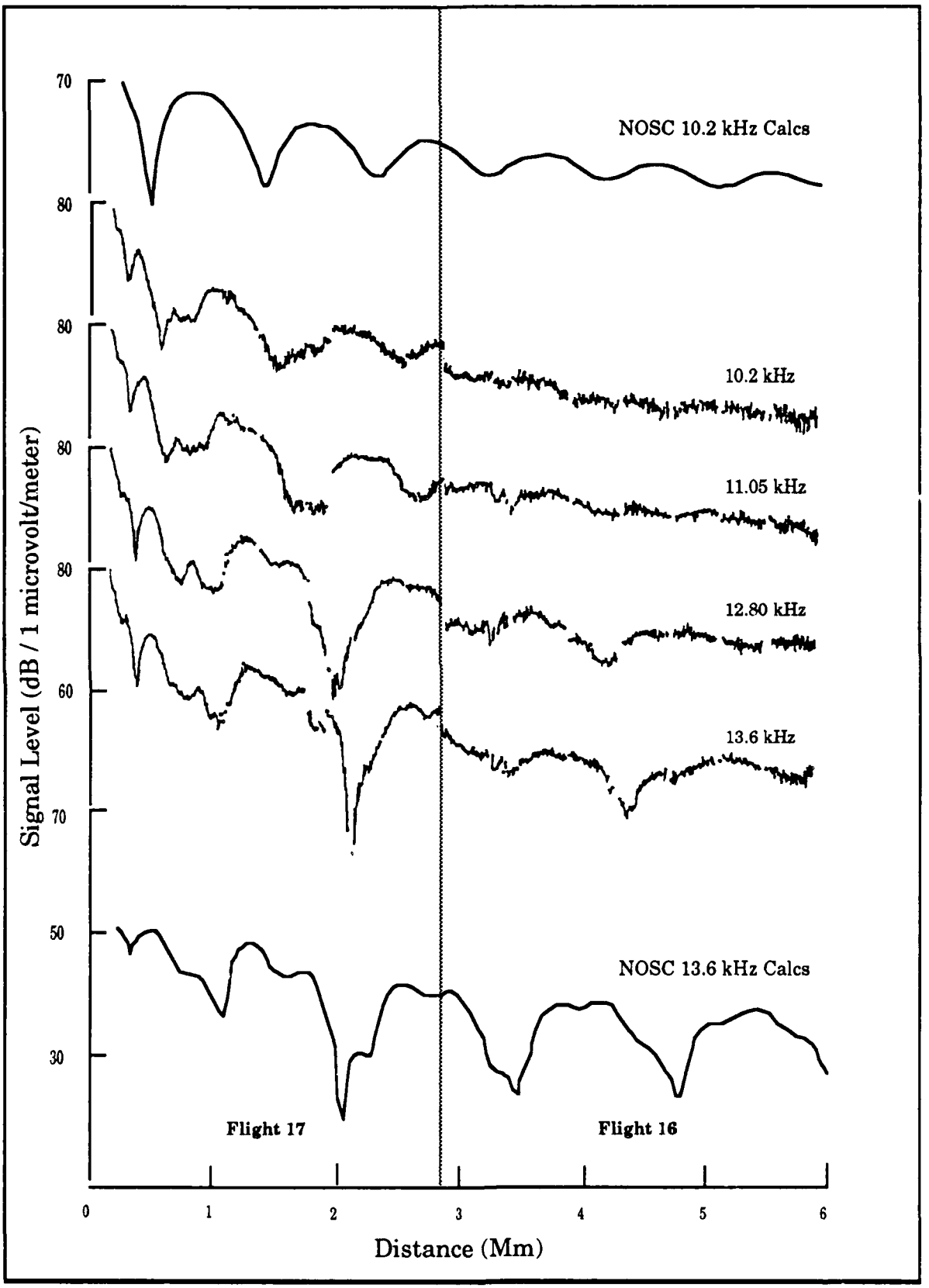

Figure B-24. Measured and Calculated Signals; Japan 141° Radial

mum. This minimum moves from 0.7 Mm at 10.2 kHz to 0.9 Mm at 13.6 kHz. We believe this component to be the same as observed on the 81° radial. The two flights incurred different propagation parameters. Flight 16, on the right side, shows less modal structure than we would expect if the conditions of flight 17 had existed. The data for flight 16 show quite a bit less mode structure than the calculations predict. We estimate that the propagation parameters for fight 17 would also produce less structure in the 3 to 6 Mm distance interval. The measured signal levels at 6 Mm are lower than predicted by about 8 dB. The data show that mode 1 is dominant beyond 1 Mm at 10.2 kHz and 2 Mm at 13.6 kHz. This supports our above analysis for the area west of Guam.

The data for the 166° flight radial (flights 12 and 13) are shown along with NOSC field strength calculations in Figure B-25. The agreement between predictions and measurements continues to improve. The simpler mode structure on this radial may contribute to the improved prediction. The predicted distances of the signal nulls at both 10.2 kHz and 13.6 kHz are very close to that measured, indicating a good prediction of the ionosphere reflection height. Propagation loss continues to be higher than predicted, in this case by about 7 dB at 6 Mm. The data show that mode 1 is dominant beyond 0.75 Mm at 10.2 kHz and safely beyond 2 Mm at 13.6 kHz. This near zone boundary supports our above analysis of the area in the vicinity of Yap.

The data for the 205° flight radial (flights 5 and 6) are shown along with NOSC field strength calculations in Figure B-26. In our estimation the agreement between predictions and measurements is very good. Features of the calculations which are noted in the data include (1) the signal null location inside 1 Mm, (2) the segment with

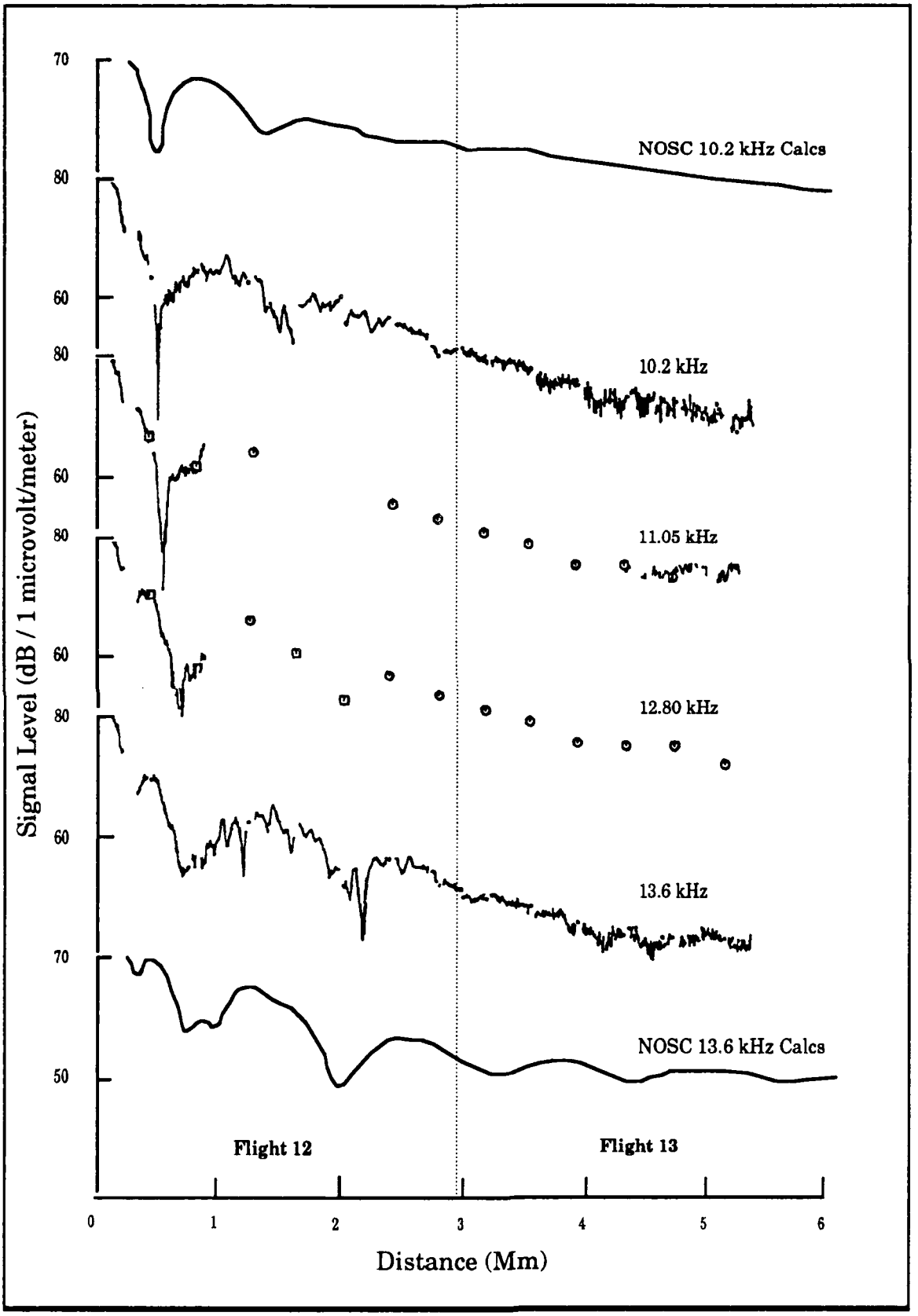

Figure B-25. Measured and Calculated Signals; Japan 166° Radial

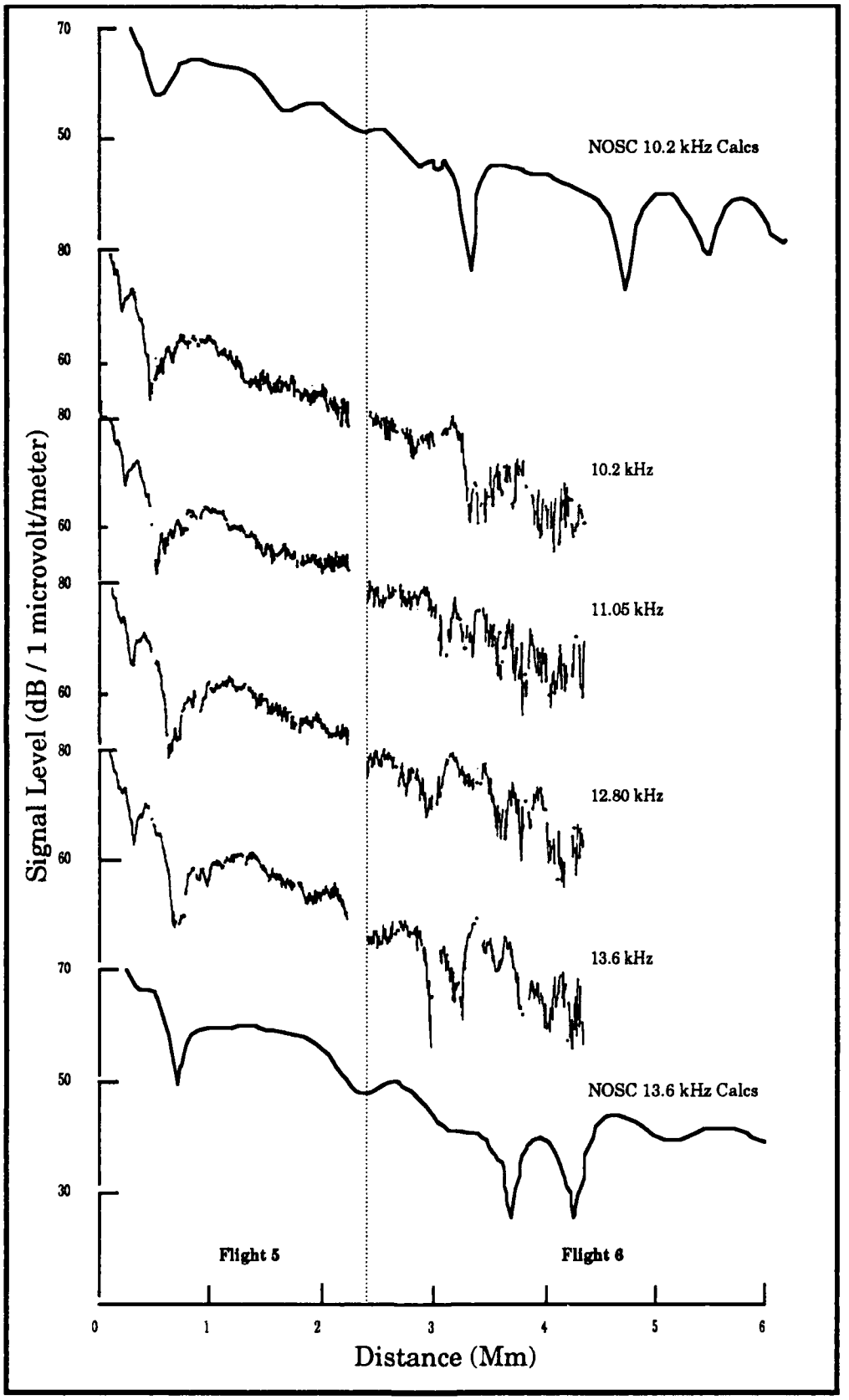

Figure B-26. Measured and Calculated Signals; Japan 205° Radial

little evidence of nulls to a distance near 3 Mm, and (3) the double nulls beyond 3 Mm. The predicted signal nulls beyond 3 Mm and the measured signal fluctuations are due to modal conversion. The data show mode conversion starting just inside 3 Mm about 500 Km south of Cubi Pt.

The data for the 221° flight radial (flights 11 and 9) are shown along with NOSC field strength calculations in Figure B-27. The main signal features of the calculations are reflected in the data, but somewhat subdued and masked in noise. We note that at 10.2 kHz two modes combine to produce a deeper and narrower null than predicted and the modal structure to 3.5 Mm is negligible. The stronger structure around 4 Mm is somewhat reflected in the data. At 13.6 kHz the measured signal null inside 1 Mm is not as deep and is more spread out. The broad maximum to 2 Mm seen at all frequencies is reflected in both calculations. The two minima predicted between 2 and 4 Mm can be detected in the data with careful observation. Data taken with other instrumentation on this flight show much stronger modal structure. It is tempting to edit out this structure as noise, but we believe from the distance patterns between frequencies that the data are real. The stronger structure is in closer agreement with predictions. The onset of mode conversion is difficult to estimate from both the calculations and the measurements. We place the boundary at 3 Mm, which is 15°N latitude.

Conclusion: The flight radials and calculations show that to the south (140° to 220° radials), the near zone is within 1 Mm at 10.2 kHz and safely within 2 Mm at 13.6 kHz. The agreement of predictions with measurements confirms the suitability of using predictions to establish the near zone boundary over this southern sector. To the east and southeast, where a large projection of the near modal

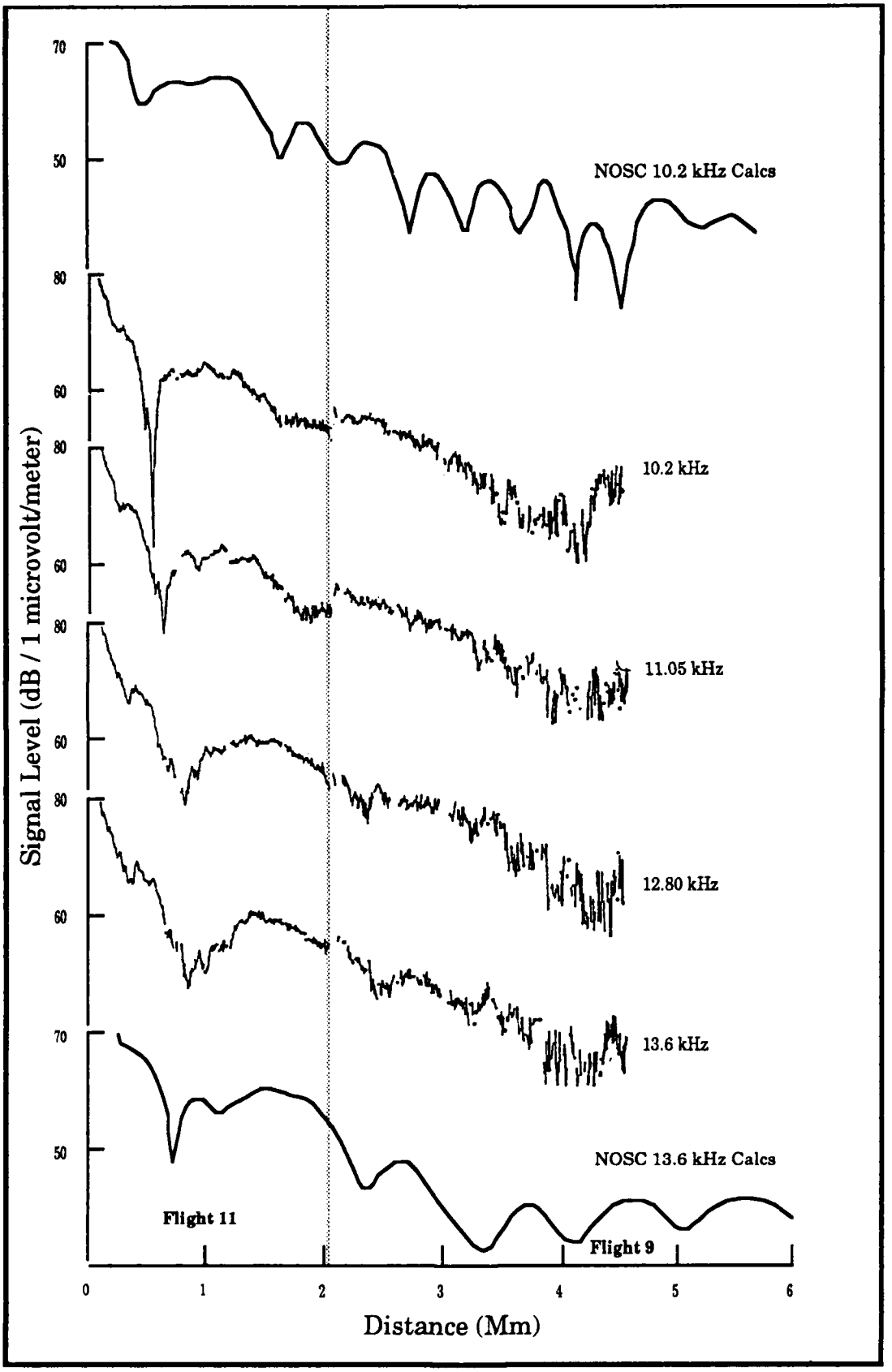

Figure B-27. Measured and Calculated Signals; Japan 221° Radial

zone is predicted at 13.6 kHz, we have no measurements. Here the calculations (81° and 141° radials) do not agree with measurements sufficiently to give high faith in the predictions. Hints are that the modal content is less than predicted.

North Central Area; Overall Summary: The combined flight and monitor site data generally support the predictions for modal effects. Good signals in the vicinity of Japan are: Norway, Liberia, North Dakota and La Reunion. We note that Norway SNR can be marginal when thunderstorm activity is high in a broad area around Japan. The North Dakota signal is weak. Thus, closer to noise sources, such as at Taiwan and Hong Kong, this signal may not be trackable. The Hawaii signal has good phase quality at Japan most of the time, but we detected significant modal effects on about ten percent of the days. We have no data on the Argentina signals; they are predicted not usable in this area. The Australia signal shows strong evidence of being in the shadow zone of the equatorial zone mode conversion. Modal interference is strong at night on 10.2 kHz and 11.3 kHz. The 13.6 kHz signal produced a characteristic mode 1 diurnal phase curve on almost all days.

We conclude that in this area navigation is adequate but not particularly redundant.

WESTERN AREA; PHILIPPINES TO THE WESTERN REGIONAL BOUNDARY (Flights 6, 7, 8, 9, 10, and 14; the fixed sites, Cubi and Singapore; and the Tsushima SW transit): This area is predicted to be the most difficult for navigation in the Western Pacific validation region. Here the Japan equatorial mode conversion zone is added to the other zones. As noted in Figure 3-4 the nighttime good signals at 10.2 kHz are limited to Norway, Liberia and La Reunion for most of the area. For 13.6 kHz (Section 3, Figure 3-5), La Reunion may be modal over part of the area, leaving Norway and Liberia the only good signals at night. We note later in SNR analysis that Norway coverage is unreliable at both 10.2 kHz and 13.6 kHz, at least in the eastern part of this area.

With respect to the database and its quality, the sample size west of Cubi is very sparse. The Cubi data, while requiring an extensive amount of processing work, generally provided good results. For Singapore, the only other fixed site in this

area, data interruption occurred essentially daily. In most cases we cannot remove reference oscillator drift effects. For the aircraft data, noise problems are more severe. We believe the aircraft noise problems are due to both generally higher atmospheric noise and in several cases weaker signals. For the Tsushima ship, the phase records are highly inconsistent. In most cases we are unable to establish systematic reference oscillator drift trends and thus are not able to decipher data of individual station phase. For the ship data we resort to interpretation of SNR and phase-difference data. In this section we show some SNR data to illustrate findings. However, the findings for each case are based upon assessment of all available data.

The analysis summary by stations is as follows:

(A) Norway: The Norway signals are predicted mode 1 at all times. Coverage is predicted marginal for late afternoon and early night.

For flight 6, the amplitude records are very noisy with very frequent dropouts occurring. Signals are in the range of 20 to 22 dB. The flight starts with most of the path in daylight and ends with the night terminator close to Norway. The data are consistent with a mode 1 signal.

For flight 7, the amplitude increases along the flight, from about 27 to 38 dB at 10.2 kHz. The flight times are the same as for flight 6.

For flight 8, the signals are near a constant level throughout the flight, ranging from near 34 dB at 10.2 kHz to near 31 dB at 13.6 kHz. The data are consistent with mode 1 propagation.

For flight 9, the signals are weak and noisy until daylight is confined to the high latitude portion of the path. During all night on the path, the signal is of good quality. At sunrise along the flight the signals gradually decrease, almost 18 dB at 10.2 kHz.

For the Cubi site, the Norway data for the January 1987 period show good phase tracking between frequencies and adequate SNR.

For the Singapore site, using mostly August data, we find many days where phase tracking is lost. The times of lost track coincide with expected afternoon buildup of thunderstorm activity and near local midnight decrease in activity. When phase is reliably tracked, the signals are mode 1.

Conclusion: We find the Norway signals are mode 1 throughout this area. SNR is a problem for phase monitoring at all locations.

(B) Liberia: Excellent coverage is predicted throughout this area. Signal levels are predicted very strong.

For flight 6, the signals appear clean mode 1. Signal levels are near 33 dB.

For flight 7, good clean signals are measured. The signal levels range from 33 to 40 dB.

For flight 8, this signal is in sunset transition. Sunset occurs at Liberia as the flight terminates. The signals are strong and have mode 1 characteristics.

For flight 9, we estimate good quality navigation signals at all times.

For the Cubi site, the Liberia data show good SNR and phase tracking between frequencies at all times.

For the Singapore site, the Liberia signals are good quality.

Conclusion: All measurements confirm that the quality of the Liberia signal is very good.

(C) Hawaii: In this area the Hawaii signal is within its equatorial mode conversion zone, or in the shadow zone just below.

For flight 6, the signals clearly show modal effects on all frequencies throughout the flight.

For flight 7, the signals clearly show modal effects on all frequencies throughout the night portion of the flight. After sunrise at Hawaii the signal gets very weak. By then the flight is nearing Bangkok.

For flight 8, the signals are very weak and noisy, especially at 10.2 kHz and 11.3 kHz. Modal effects are observed in the noise throughout the flight.

For flight 9, the 10.2 kHz and 11.3 kHz signals are in the noise, and the 13.6 kHz signal shows modal effects.

For the Cubi site, the Hawaii data show very strong modal effects on all nights and all frequencies. Cycle jumps can occur throughout the night, especially on 10.2 kHz and 11.3 kHz. The data are very similar in general to other examples of strong modal effects; see for example Figure B-22.

For the Singapore site, we find the Hawaii signals very weak and highly modal at night. Signal tracking was frequently lost, but the times of loss do not fit to the expected diurnal noise pattern.

The Tsushima data show strong modal effects for all measurements south of the predicted equatorial mode conversion zone.

Conclusion: The Hawaii signals are very weak and at night are highly modal. This signal is not suitable for navigation in this area most of the time.

(D) N. Dakota: Calculations show mode 1 for both frequencies with no modal structure.

For flight 6, most of the flight data were recorded after sunrise at North Dakota. The signal levels are in the noise.

For flights 7 and 8, no data were recorded.

For flight 9, the signals are in the noise for the entire flight.

For the Cubi site, the North Dakota data show modal effects on all nights and all frequencies. Cycle jumps can occur throughout the night, but are much more frequent during sunrise. The cycle jumps are also most frequent at 10.2 kHz, slightly less frequent at 11.2 kHz, and still less at 13.6 kHz.

For the Singapore site, no data are analyzed.

The Tsushima data show strong modal effects at night for all measurements within the predicted equatorial mode conversion zone.

Conclusion: We consider the North Dakota station unreliable for navigation in this area during periods of local night because of modal effects. The signals also have poor or inadequate SNR over much of this area during local afternoon and early night.

(E) La Reunion: The 10.2 kHz signal is predicted to be strong and clean mode 1. The 13.6 kHz signal is predicted to have a significant mode 3 component extending as far east as 110°E.

For flight 6, which is to the east of the predicted 13.6 kHz near modal zone, no modal effects are noted. The signal levels are near 45 dB at both 10.2 kHz and 13.6 kHz.

For flight 7, which is predicted within the 13.6 kHz near modal zone, no modal effects are observed. The signal levels at about 50 dB for 10.2 kHz and 43 dB for 13.6 kHz.

For flight 8, the measurements start when the sunset terminator is near the middle of the path. After sunset at La Reunion, the data consist of short intermittent samples. The data are not suitable for modal assessment.

For flight 9, the data are consistent with a clean mode 1 signal at all frequencies.

For the Cubi site, the La Reunion data show high SNR at all frequencies and good phase tracking between frequencies at all times.

For the Singapore site, we find the SNR excellent and the phase quality generally quite good. More work is needed to search for near zone modal effects at 13.6 kHz.

For the Tsushima ship, we search for 13.6 kHz modal effects during the ship transit west of Singapore and then back to the southeast, south of Sumatra. We are able to detect some modal effects as shown in Figure B-28. This data of measured SNR show some dates where the 13.6 kHz signal goes through an amplitude dip during the sunset transition. We note in particular the dates of 12 through 15 August. Since the 13.6 kHz SNR trace differs markedly from the other two traces and the amplitude pattern follows that expected for two modes going through phase opposition, we interpret the data to show the predicted near zone modal effects.

Conclusion: We believe that the La Reunion signals are generally of very good quality throughout this area. The predicted near zone modal interference for the 13.6 kHz signal is detected in some of the Tsushima data. When this interference occurs within this area, we believe that

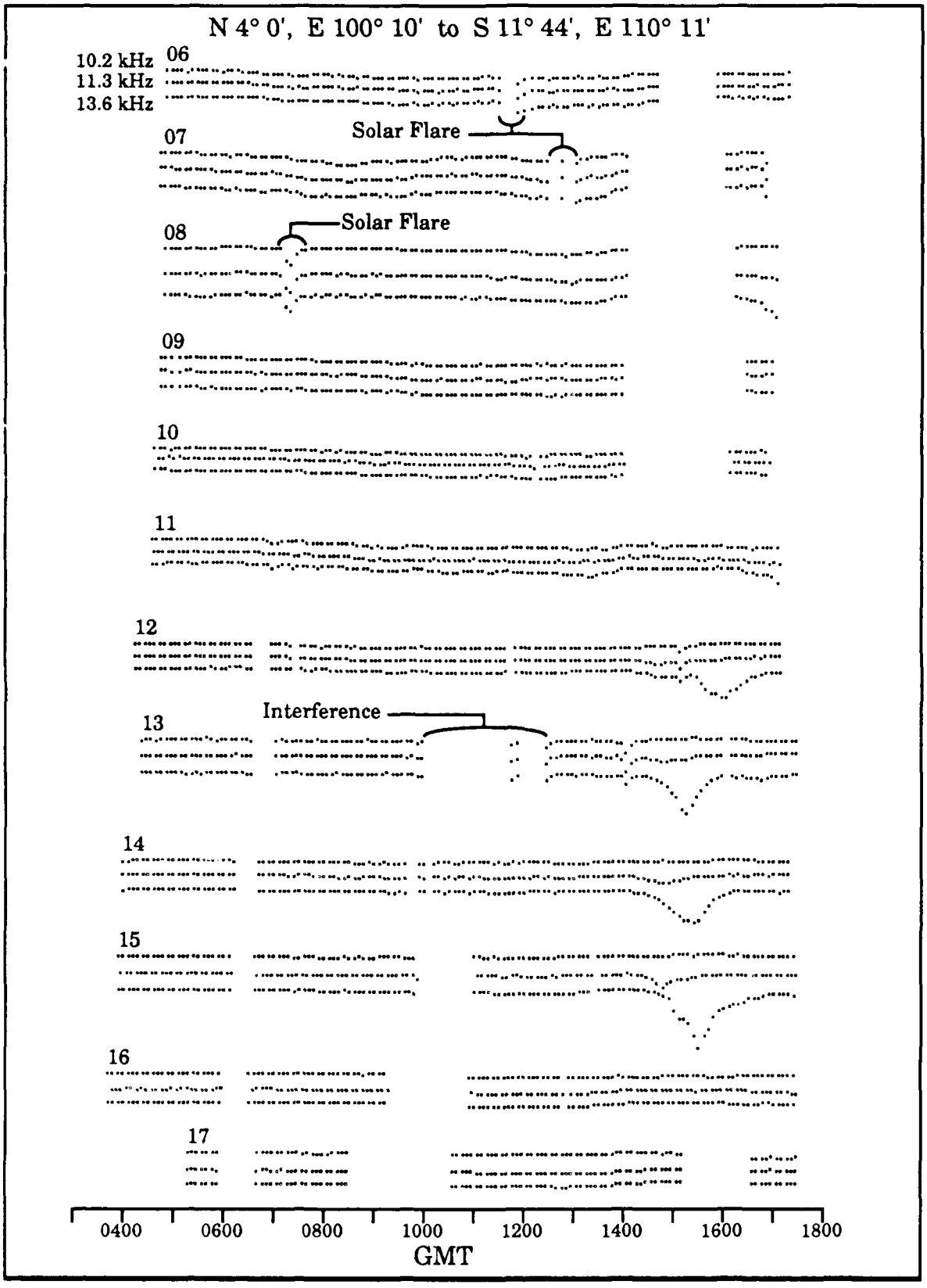

Figure B-28. Shipboard SNR Data; La Reunion Signal, 6-17 August 1986

the effect is marginal with respect to negating use for navigation.

(F) Argentina: These signals are in the shadow zone of Antarctica. Antarctica is in continuous night during May. The signals are predicted mixed mode in this shadow.

For flight 6, no data are available.

For flight 7, the Argentina portion of the path is in daylight during the flight. The received signals are in the noise until near 1700 GMT. After that the record is too short to assess modal conditions.

For flight 8, sunrise occurs at Argentina at the beginning of the flight. The 10.2 kHz and 11.3 kHz signals are in the noise for the first 2 hours and the last hour. Between 1400 and 1600 GMT the amplitudes of all three signals track closely, indicating mode 1 propagation.

For flight 9, no data are available.

For the Cubi site, the Argentina channel was used for system calibration.

For the Singapore site, we find both frequent periods of tracking loss and what we interpret to be good evidence of modal effects. We do not have a sufficient sample size to reliably estimate trends.

Conclusion: We do not have a good assessment of the Argentina signals in this area. We expect that the signals are poor quality for most of the time.

(G) Australia: The south boundary of the equatorial mode conversion zone is predicted to be near the equator, possibly a few degrees south. The north boundary is predicted to slope from the northern tip of the Philippines on the east edge of this area down to about 14°N at 90°E longitude. Below

the conversion zone the Australia signals are predicted safe mode 1 in the measurement area. North of the conversion zone boundary, the signals in this area are in the conversion shadow zone.

For flight 6, the end of model effects occurs at about one-third of the flight distance; this is near 7°N latitude.

For flight 7, the start of model effects occurs at just inside 7 Mm. This is at 5°N latitude, near 100°E longitude. The indicator is a gradual 20 dB decrease in the signal level, only on the 10.2 kHz signal.

For flight 8, the measurements span the distance interval from 5.9 to 7.1 Mm. Modal effects are noted on 10.2 kHz, 11.05 kHz, 13.0 kHz and 13.6 kHz. The flight covers from 5°N to 5°S latitude. We estimate that modal effects occur over the full flight.

For flight 9, we estimate that modal effects start at least by 5°N latitude. The effects get more pronounced as the aircraft moves north. The effects are strongest at 10.2 kHz, intermediate at 11.2 kHz, and smallest at 13.6 kHz.

For flight 10, on a radial 327°, we have data covering a round trip flight. This data, shown in Figure B-29, show modal effects on both flight legs on all three frequencies. Important features of this data are (1) the magnitude of the modal effects with frequency, (2) the similarity in geographic location between flight legs, and (3) the changes in modal effects between the flight legs. As is typical with much of the data, the modal effects get smaller as the frequency increases. The geographic position of the model effects is similar, but the effects are definitely stronger on the later flight leg. This flight gives us a good clue regarding the time history of modal effects.

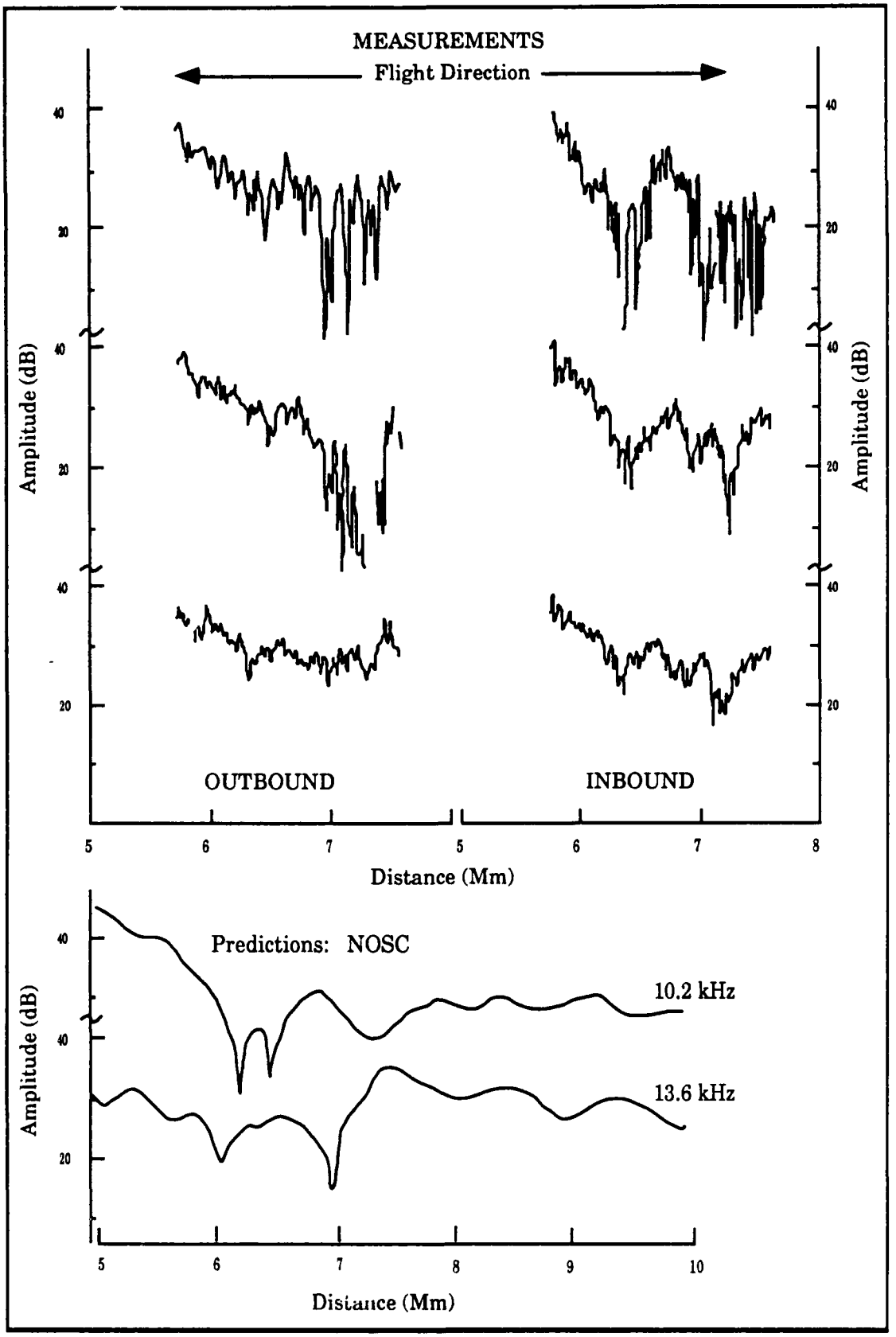

Figure B-29. Australia Signal Modal Effects; Flight Data

For the Cubi site, the Australia data show very strong modal effects on all nights and all frequencies. As shown by the example in Figure B-30, any characteristic described previously for modal effects can be found in the Australia data. Cycle jumps can occur throughout the night, but are far more likely to occur during the transition times, especially on 10.2 kHz and 11.3 kHz. We interpret the data to indicate that on most nights at 10.2 kHz and 11.3 kHz switching to a higher-ordered mode occurs at sunset. This mode remains dominant until sunrise. At 13.6 kHz the higher-ordered mode is not as strong, and switching may or may not occur. Switching is also more likely to occur at times other than the day/night transition periods.

For the Singapore site the data show evidence of the site being on the edge of the equatorial mode conversion zone. Modal effects are definitely detected but are usually minor. Because of some frequently occurring equipment failure mode that appears differently on each channel, we are often unsure to what we should attribute to modal effects. We believe that further analysis may yield a more definitive interpretation.

The Tsushima data show modal effects along the equator as shown in Figure B-31 for the dates of 01 through 05 August 1986. These SNR data indicate that modal effects, which start during sunset transition, become much stronger in the night.

Conclusion: The data do not facilitate a good determination of the equatorial modal zone southern boundary for Australia, because of conflicting results. The collection of data suggest that the best choice is to place the boundary as predicted. Certainly on many nights the boundary is further north, but some data indicate that the boundary can be as far south as we predict. In this area reliable signals for navigation can only be assured below 3°S longitude.

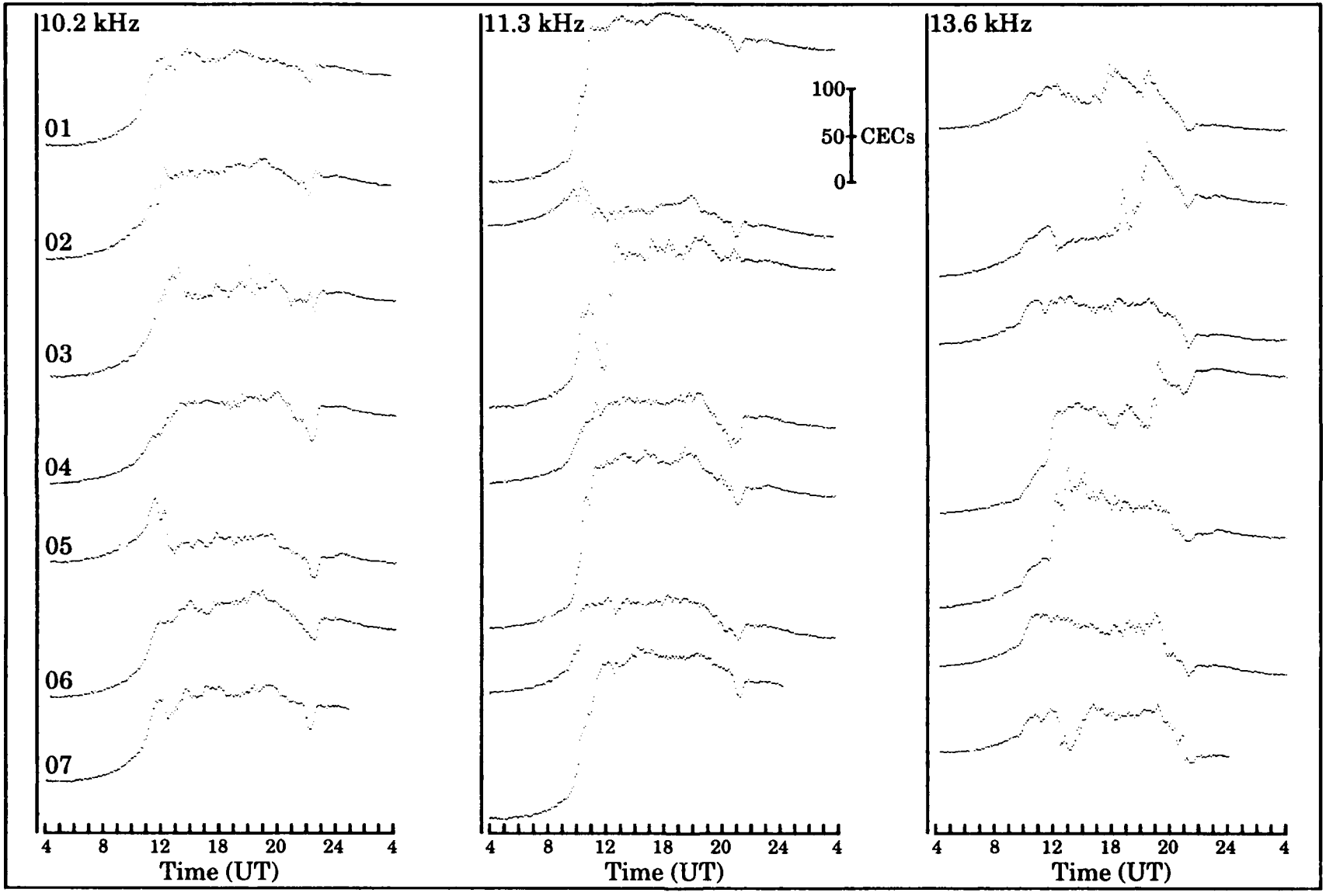

Figure B-30. Australia Received Phase at Cubi Point; 01-08 January 1987

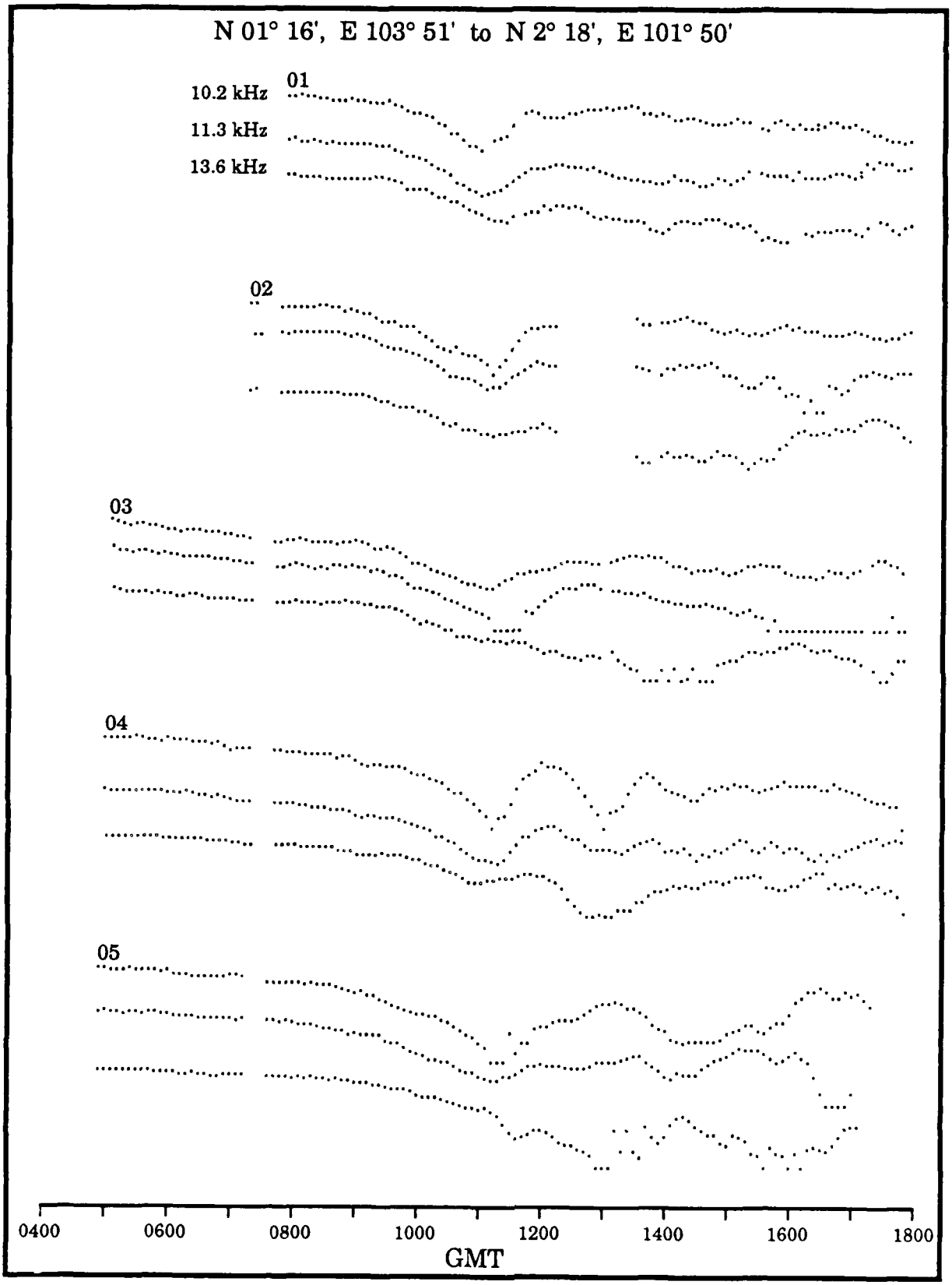

Figure B-31. Shipboard SNR Data; Japan Signal 01-05 August 1986

(H) Japan: The north boundary of the equatorial mode conversion zone is predicted to slope from the northern tip of the Philippines on the east edge of this area down to about 14°N at 90°E longitude. The south boundary is predicted to be about 4° south of the equator. Above the conversion zone the Japan signals are predicted safe mode 1 in the measurement area. South of the conversion zone boundary, the signals in this area are in the conversion shadow zone. We predict the eastern edge of the zone to be about 4° longitude east of Cubi Point, on the 200° radial from Japan.

For flight 6, the data are shown in Figure B-26. We found the mode conversion starting about 500 Km south of Cubi Point at a latitude of 10°N.

For flight 7, which starts at the south eastern corner of the mode conversion zone, the initial modal effects are slight. As the flight progresses into the conversion zone, the modal effects become more pronounced and are evident until flight termination at Bangkok.

For flight 8, modal effects are noted on all frequencies throughout the flight. The first half of the flight is in the predicted conversion zone and the last half in the predicted shadow zone.

For flight 9, the data (shown in Figure B-27), show modal effects to a latitude of 15°N.

For the Cubi site, the Japan data show modal effects on many nights and all frequencies. While the modal effects are often quite evident, cycle jumps are very rare. An example of typical data is shown in Figure B-32. Interestingly the 13.6 kHz signal shows modal effects that are very similar to the other frequencies. This is in contrast to several other observations where the 13.6 kHz signal tends to show lesser effects. We find the occurrence of

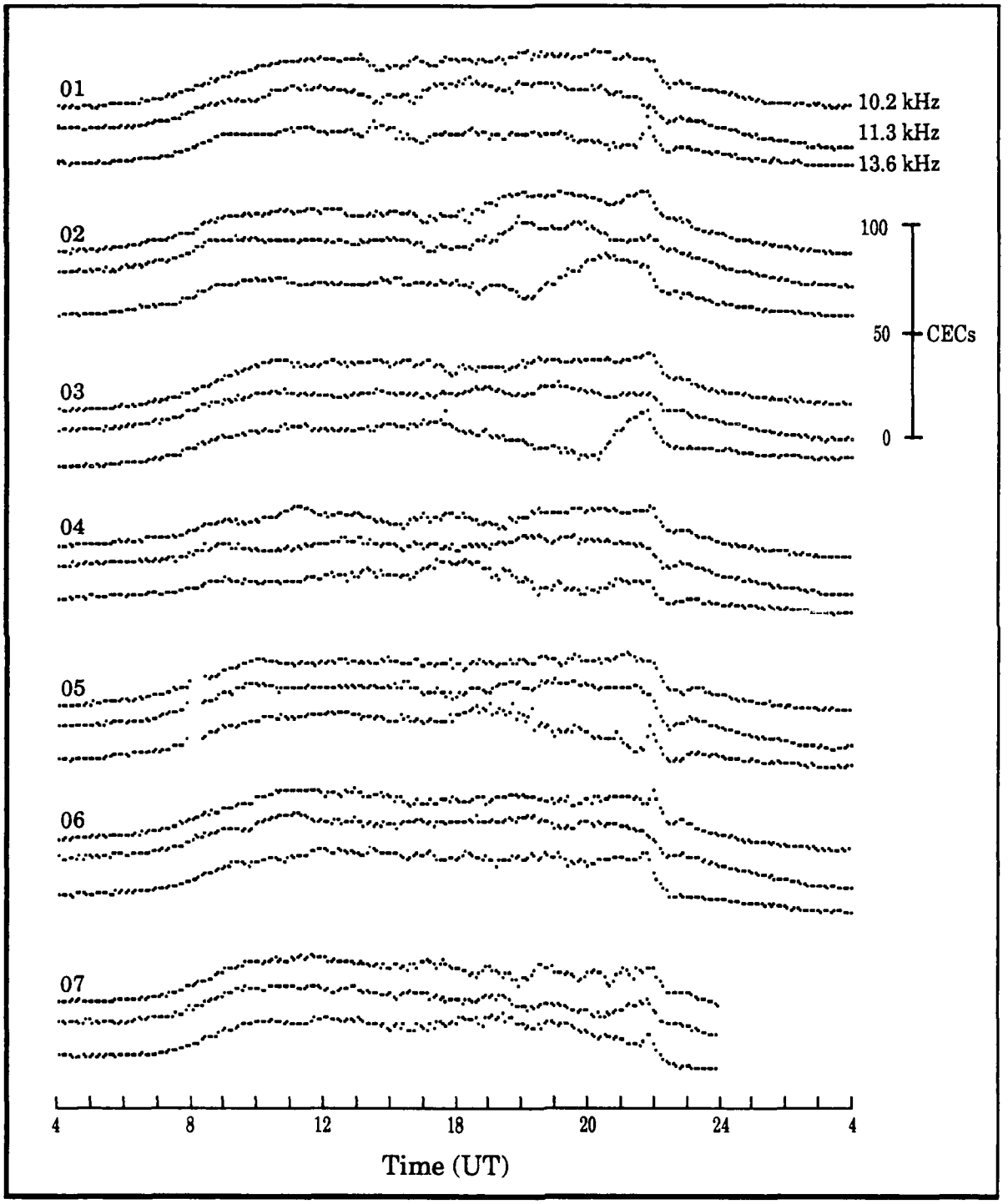

Figure B-32. Japan Received Phase at Cubi Point; 01-08 January 1987

modal conditions quite variable, with periods of days with no detectable effects and then periods of days with lots of modal activity.

For the Singapore site, the data show evidence of strong modal interference on all nights and all frequencies. The modal effects become evident near completion of the sunset transition and last into the sunrise transition. Cycle jumps occur on many days, most frequently at transition times.

The Tsushima data show the onset of modal effects in the southwest transit from Japan to Singapore. Figure B-33 contains SNR data showing the detection of modal effects after sunset on 25 July. At this time the ship was crossing 20°N latitude.

Conclusion: The data do not facilitate a good determination of the equatorial modal zone northern boundary for Japan, because of conflicting results. The collection of data suggest that the best choice is to place the boundary where predicted on the eastern edge and slightly north of predicted on the west side of this area. The aircraft data indicate that the boundary can be farther south than we predict. In this area reliable signals for navigation can only be assured above 20°N longitude.

Western Area; Overall Summary: The combined flight, monitor site, and shipboard data generally support the predictions for modal effects. Good signals in this area are Liberia and La Reunion. We note that Norway SNR can be insufficient when thunderstorm activity is high within this area. The North Dakota signal is very weak and modal. At times this signal may not be trackable. The Hawaii signal has bad phase quality at night all of the time below 20°N latitude. The Argentina signal is weak and shows some modal effects where measured in this area. The Australia signal shows strong effects above the equator. The Japan signal shows strong modal effects below about 20°N

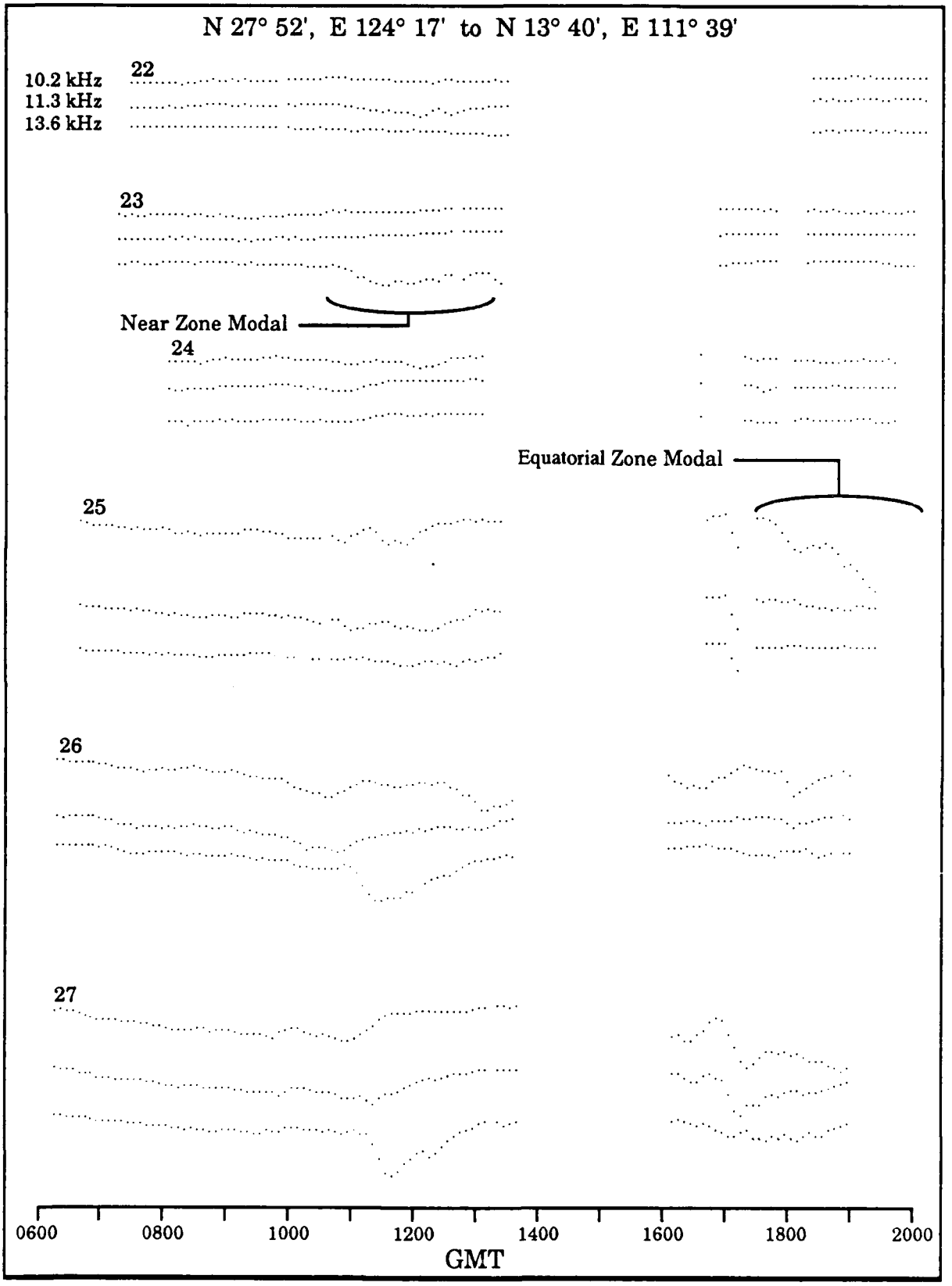

Figure B-33. Shipboard SNR Data; Japan Signal 22-27 July 1986

latitude. The data show that signal coverage, addressed in Subsection 3.5, may be inadequate on many stations during daytime propagation conditions.

We conclude that in this area navigation support is not adequate during local nighttime, especially during high noise months.

THIS PAGE INTENTIONALLY LEFT BLANK

Appendix C

Presentation of Predicted Long-path Interference Boundaries for Signals in the Western Pacific Validation Region

OVERVIEW

In this appendix we describe our predictions of long-path interference occurrence in the Western Pacific. Long-path interference is the signal self-interference resulting from the dominant signal propagating more than halfway around the world, more than 20 megameters (Mm). The mechanism for long-path interference is described in Section 3.4.1. The model we describe here was developed as part of the South Pacific Validation. The reader is referred to Appendix C of that validation report for a detailed description of the model development. Here we summarize the features of the model that are applicable to the Western Pacific predictions. We showed in the South Pacific Validation that under certain conditions, the dominant signals propagate well beyond 20 Mm; i.e., the received signal is a long-path signal. These long-path signals are not normally considered suitable for navigation. For this region, some long-path interference is predicted for three stations, Liberia, North Dakota and Argentina. A geographic plot of the long-path/short-path boundary is constructed for each of these stations.

MODEL DEVELOPMENT

To summarize from the South Pacific Validation, the model of long-path interference conditions was derived from a series of Omega field strength calculations produced by TASC for ONSCEN (GUPTA 1988, Ref. 23). This set of calculations is described in Appendix A. The calculations are for two frequencies, 10.2 and 13.6 kHz, and two propagation conditions, either all day or all night on the path. These calculations were made for each station, generally on 10° radial intervals and to a radial distance of 19 Mm. The antipode, being halfway around the world, is 20 Mm from each station. The prediction of field strengths beyond 19 Mm are made using an extension to these calculations which is derived for this analysis and is described here.

The analysis procedure used for each station is (1) first to determine if long-path is likely to exist in the validation region, (2) if it is likely, to select the radials that best represent the long-path effects in the region, (3) to determine the greatest extension of the long-path on each selected radial, and (4) to estimate the time history of the long-path/short-path boundary location along the radial. Important factors for locating the boundary between long- and short-path propagation include (1) location of each station antipode, (2) relative field strength of signals at the antipode incident from opposite radials, (3) propagation beyond the antipode, and (4) the effect on propagation of relative solar illumination of the long and short propagation paths.

The locations and antipodes of the Omega stations having long-path effects in this region are listed in Table C-1. Only Liberia, North Dakota, and Argentina are of concern for this region.

STATION	LOCATION		ANTIPODE	
	Lat	Long	Lat	Long
A Norway	66.42 N	13.15 E	66.42 S	166.85 W
B Liberia	6.31 N	10.66 W	6.31 S	169.34 E
C Hawaii	21.41 N	157.83 W	21.41 S	22.17 E
D North Dakota	46.37 N	98.34 W	46.37 S	81.66 E
E La Reunion	20.97 S	55.29 E	20.97 N	124.71 W
F Argentina	43.05 S	65.19 W	43.05 N	114.81 E
G Australia	38.48 S	146.93 E	38.48 N	33.07 W
H Japan	34.61 N	129.45 E	34.61 S	50.55 W

Table C-1. Omega Station Antipodes

The incident signal levels at the maximum distance calculated (19 Mm), from the Liberia, North Dakota, and Argentina transmitters, are shown in Figures C-1 through C-3. These figures show both day and night propagation for both 10.2 kHz (part a) and 13.6 kHz (part b). For these plots, the horizontal ordinates, which are bearing scales for day and night propagation, are the bearings of the radials from the transmitter. These scales are offset 180° from each other.

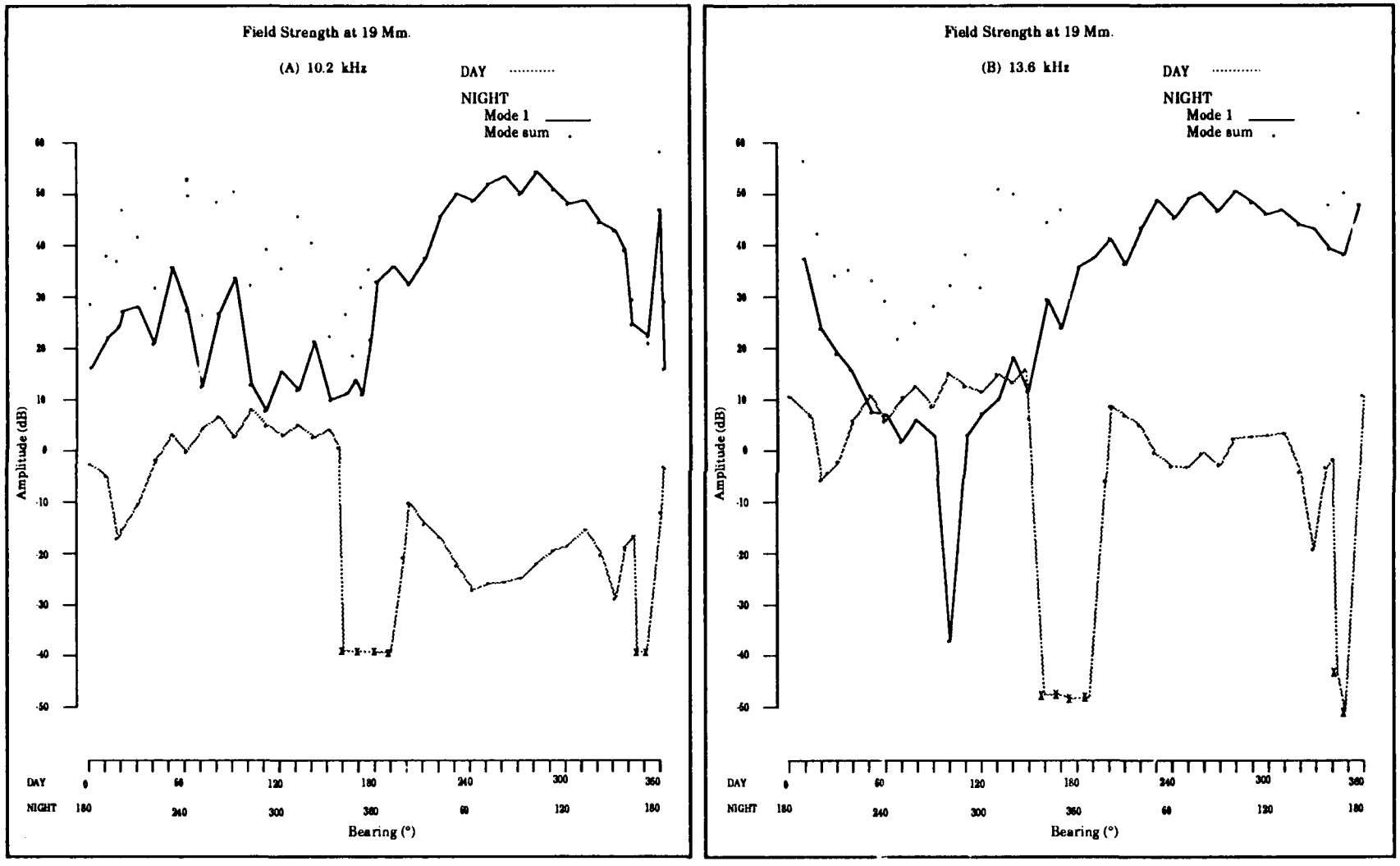

Figure C-1. Predicted Liberia Signal Levels

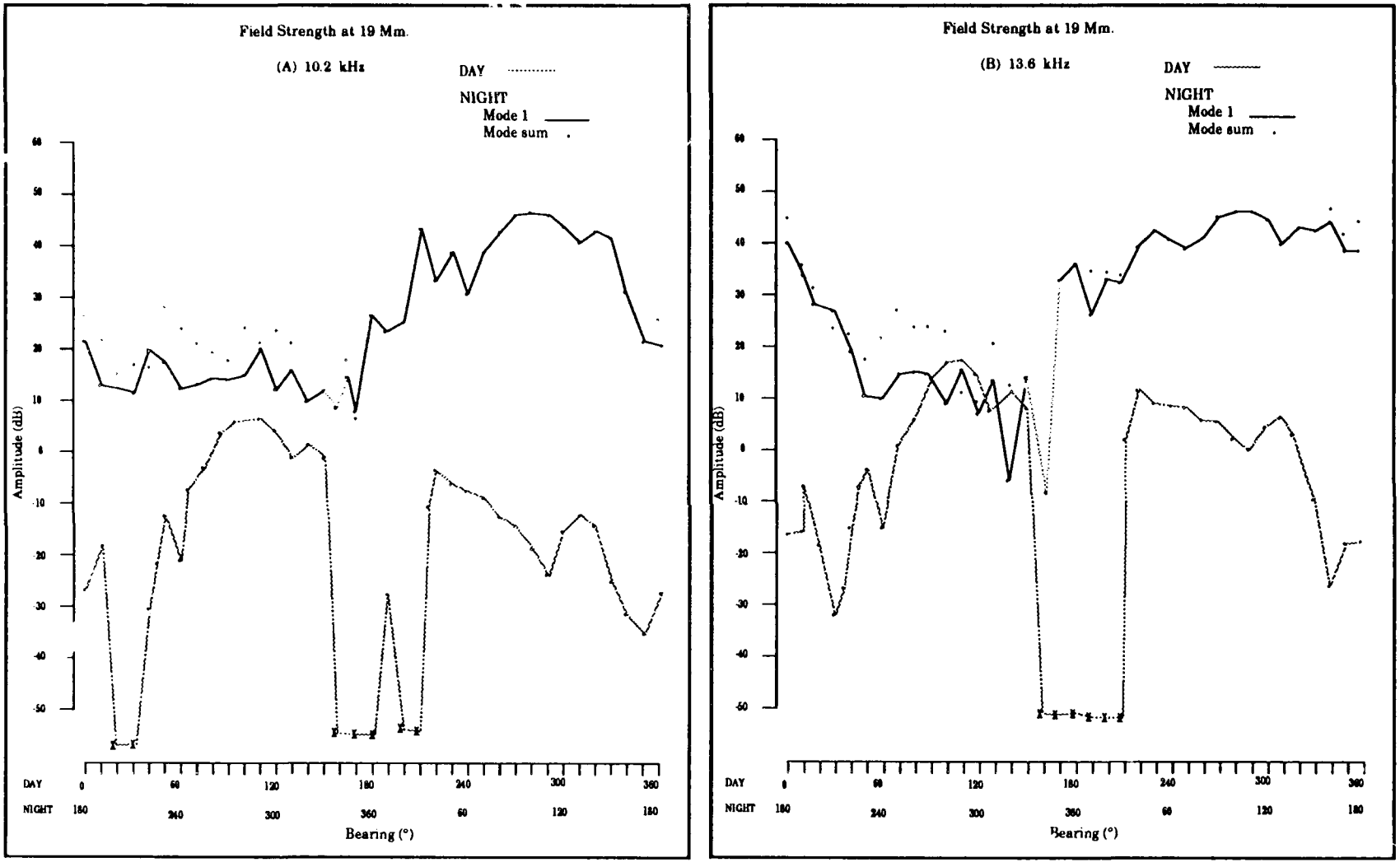

Figure C-2. Predicted North Dakota Signal Levels

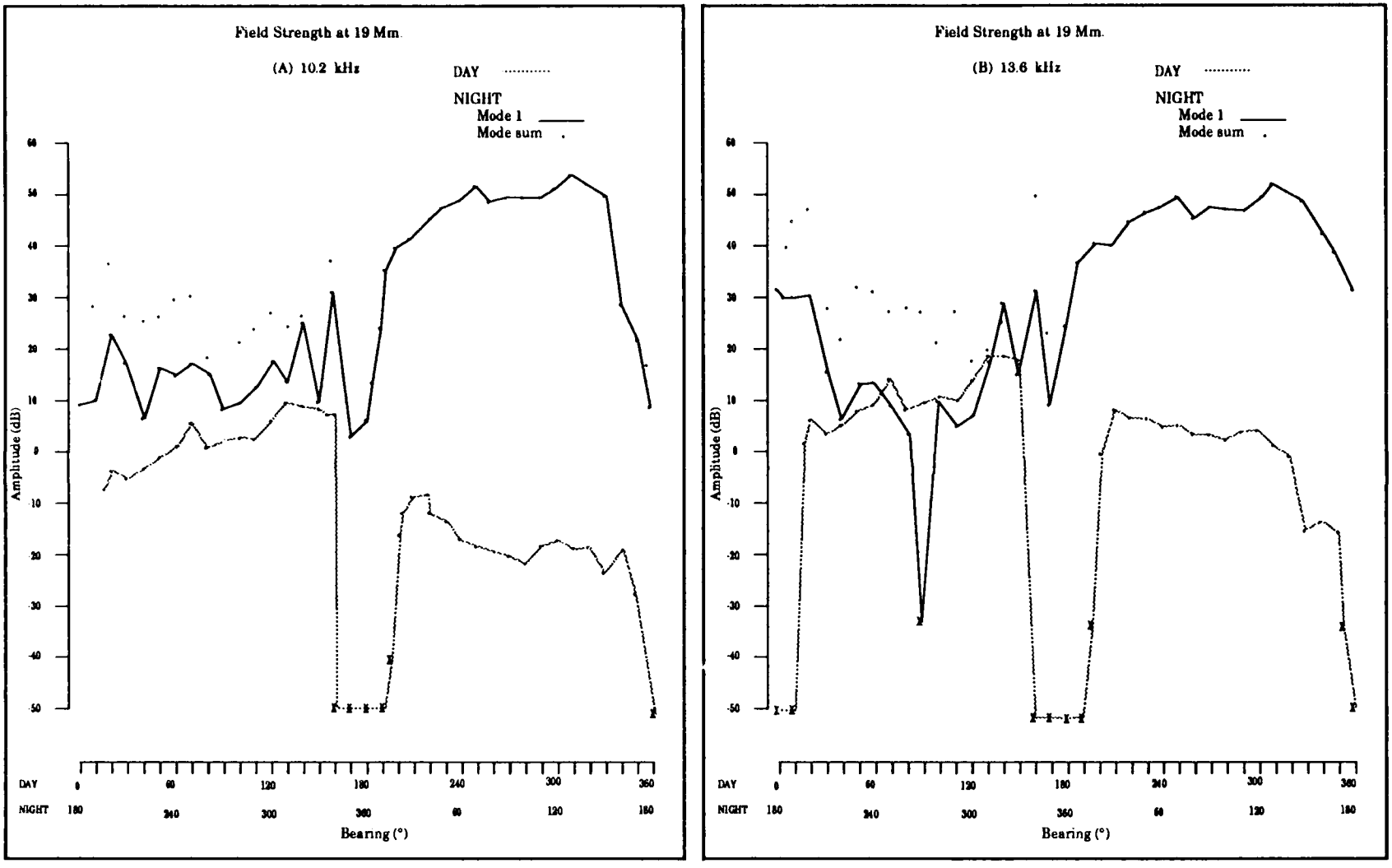

Figure C-3. Predicted Argentina Signal Levels

This was done to allow direct comparison between the relative strengths of signals incident from opposite directions. The arrival angle at the antipode for each radial is 360° minus the plotted angle. For night propagation, both total fields and mode 1 fields are plotted where their levels are significantly different.

These plots show that:

(1) The field strength for all daytime propagation at 19 Mm is almost always less than or equal to the field strength for all nighttime propagation in the opposite direction;

(2) The signal propagating at nighttime in a broad sector to the east of the transmitter (30° to 140° for Liberia in Figure C-1a) arrives at the antipode with a much higher signal level than when propagating to the west;

(3) When a signal propagates over a low conductivity region during daytime (150° to 190° for Argentina in Figure C-3a), the signal arriving at the antipode is much weaker than otherwise;

(4) The combined effects on propagation result in complex variations of field strength with bearing change; and

(5) The mode 1 level in propagation to the west at nighttime is often much lower than the total field, i.e. mode sum (for an example see Liberia Figure C-1 180° to 330°). The low level of mode 1 relative to the total field is often strongly associated with signals having incurred mode conversion in propagation through the equatorial zone.

The conditions depicted in Figures C-1 through C-3 are useful for determining if long-path interference is likely to occur and along what radials. These plots also show how the maximum extent of the long-path/short-path boundary will change with radial bearing and frequency. The actual determination of the boundary position is done by extending the propagation calculations produced by TASC using the following technique.

Since creation of a computational model is not considered practical within the time and resource constraints of this validation, a first-order model for determining long-path/short-path boundaries is devised from the TASC field strength calculations previously described. The technique involves extending the field strength predictions beyond the 19 Mm by attaching "mirrored" segments of calculations that represent the predicted propagation conditions. The process, described in the South Pacific Validation report, consists of three operations:

(1) The signal levels versus distance for propagation in opposite directions and for both day and night are plotted. The plot is created by breaking the great circle path at the transmitter and transforming the circle to a straight line so that the transmitter is located at both ends of the plot. The antipode, 20 Mm from the transmitter, is placed in the middle of the graph at an equal distance from each representation of the source. This first or reference plot places the day/night terminator at the transmitter and the antipode. Each of the paths is either in all daylight or all night.

(2) The paths are extended in either direction beyond the antipode by joining appropriate segments of the propagation curves. For example, the nighttime propagation curve is extended beyond 20 Mm using the slope and shape of the nighttime curve inside 20 Mm.

(3) "Real" propagation situations are represented by joining appropriate segments of day or night propagation curves at the distance where the terminator intersects the propagation paths. The intersection of this daytime extension with the curve of daytime propagation establishes the long-path/short-path boundary for the time when the terminator crosses the transmitter and the antipode. The positions of crossover for the dominant fields that are propagating in opposite directions (i.e. long-path/ short-path boundaries) are obtained for representative solar positions. The variation in position along a radial establishes the time history of the boundary location. A set of these positions for different radials establishes the geographic boundaries.

When a daytime segment is attached to a nighttime segment, the attachment is made to the mode 1 component of the nighttime signal when this field differs significantly from the mode sum. The mode 1 component is joined because this component is expected to be the primary source for the daylight path. The higher-ordered modes are rapidly attenuated in the daylight side of the terminator. The procedure used does not account for mode conversion across the terminator. We do not know what errors may be incurred by not accounting for mode conversion. The best way to assess errors will be to compare the derived predictions with measurements of both modal boundaries and times when boundaries cross measurement sites.

Geographic plots showing the maximum extent of the long-path/short-path boundaries in the validation region at 10.2 kHz on 22 February are presented in

Figures C-4 through C-6 for the Liberia, North Dakota, and Argentina stations respectively. The general shape shown in these boundaries is more significant than the shape detail because the construction was generated using data from relatively few radials. More insights regarding the boundary shape between the radials used can be derived from examination of the relevant signal levels at the antipode, shown in Figure C-1, C-2 or C-3. The long-path/short-path boundaries at 13.6 kHz lie inside the 10.2 kHz boundaries, i.e. towards the antipode.

A general feature of this prediction is that the greatest extent of a boundary away from the antipode occurs when the short path to the boundary is in total daylight. The boundary reaches this greatest extent on any given radial approximately when the sunrise terminator reaches the same location and remains there until approximately sunset over the transmitter. Thus, the farther away from the antipode the boundary moves, the longer it remains at its farthest extent. The westernmost extent of the boundary seldom goes much beyond the broad area typically defined as the antipode zone. The boundary dwell time at this western end is usually quite short, from a few minutes to an hour or so. The rate at which the boundary moves along a radial increases as the angle the terminator forms with a radial decreases. The rate is slowest when the terminator is nearly parallel to the equator and can be very high (almost instantaneous in time) over many megameters in those rare situations when the terminator is nearly parallel to the radial for some distance.

The reader is referred to the South Pacific Validation report for additional background information and more illustrations of long-path interference phenomena.

Specific comments regarding analysis results for the long-path conditions predicted for this Western Pacific region are as follows:

Liberia: The propagation at low latitudes incurs a strong nonreciprocal west/east and day/night effect. The Liberia signal long-path/short-path boundary shown in Figure C-4 extends far beyond the validation region, as much as 12.8 Mm to the east of the antipode. The boundary on the 250° radial is at its easternmost position between 1120 and 1840 GMT on 22 February, a period over seven hours. This boundary location results from a combination of the maximum eastward propagating signal strength and a relatively weak westward propagating signal. The 13.6 kHz signal does not

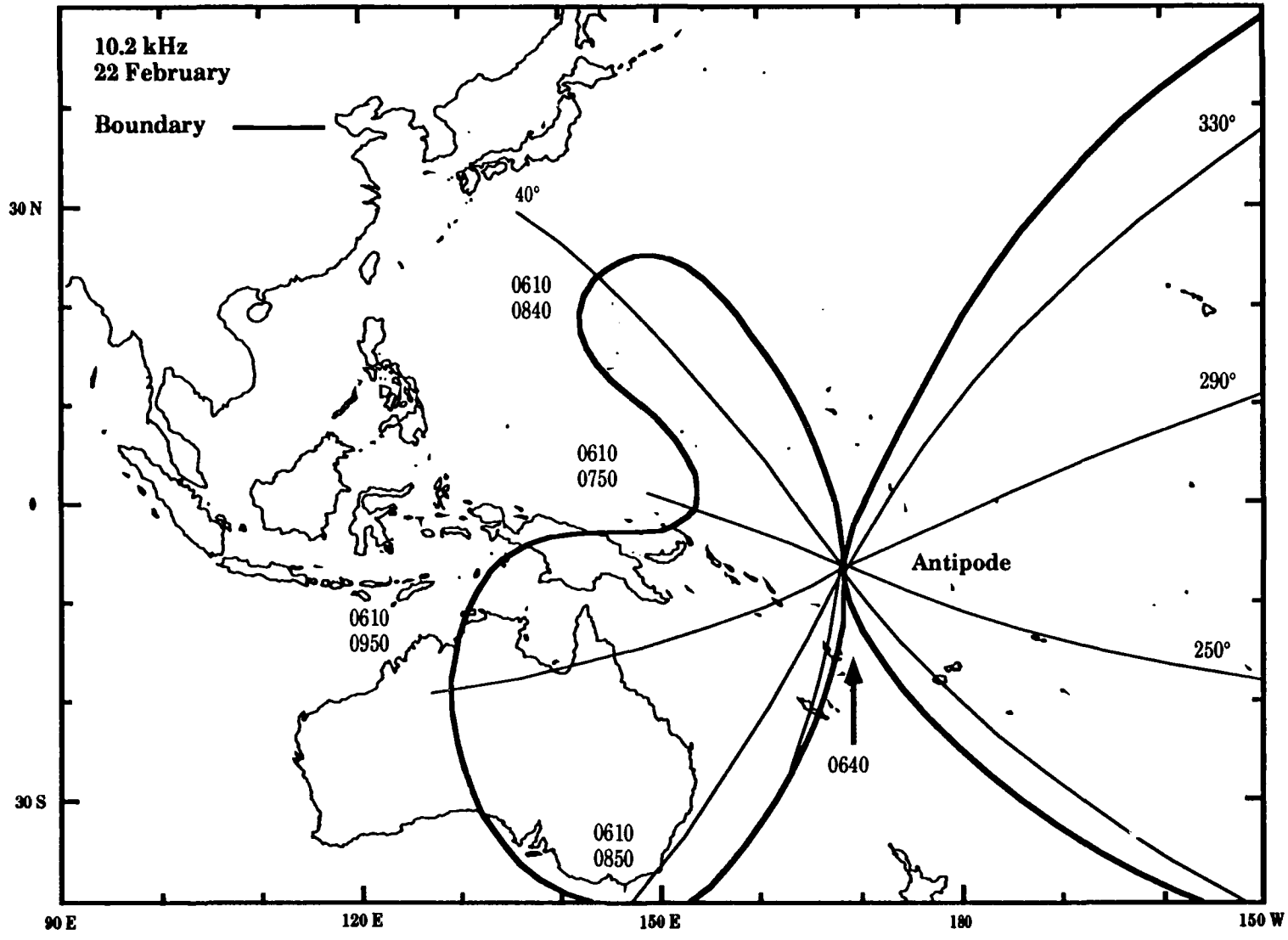

Figure C-4. Liberia Signal Long-path Maximum Extent

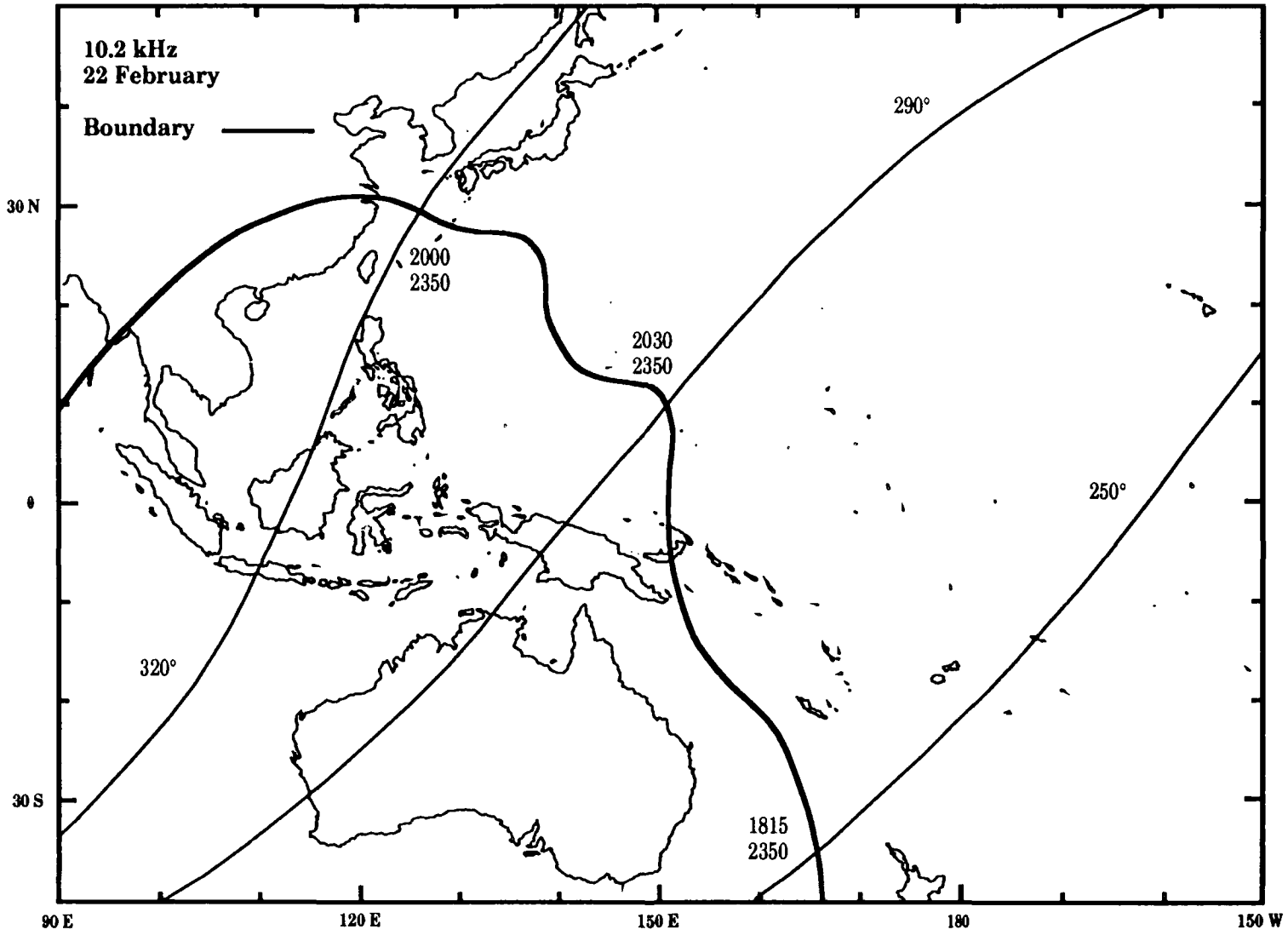

Figure C-5. North Dakota Long-path Maximum Extent

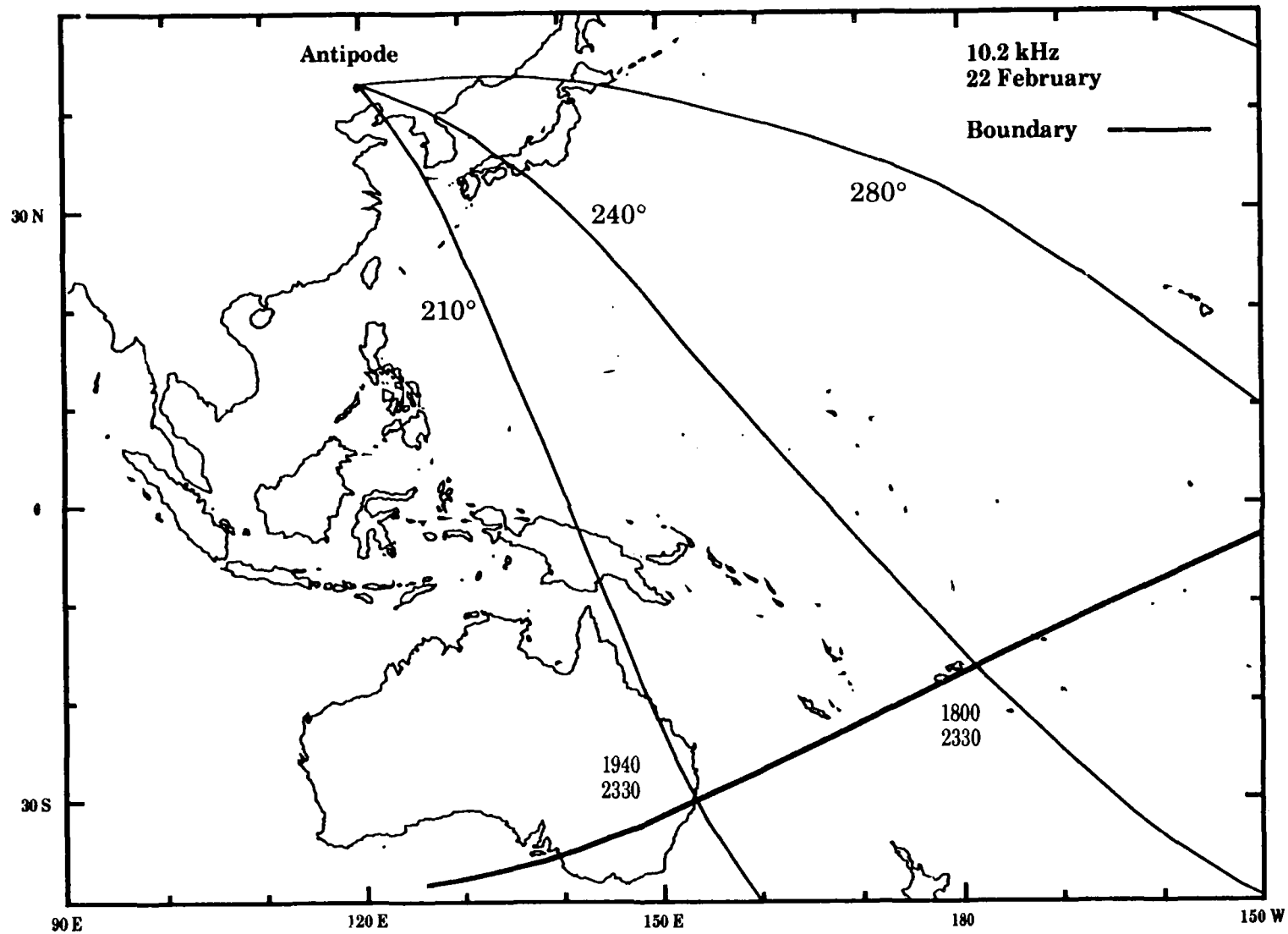

Figure C-6. Argentina Signal Long-path Maximum Extent

incur as much attenuation difference, 54 versus 78 dB, as is noted by comparing the curves of Figures C-1a and C-1b. Thus the 13.6 kHz boundary at maximum extent will be several megameters to the west of the 10.2 kHz boundary. Of all the signals, the Liberia signal showed the farthest boundary movement to the west of the antipode. The position of this boundary is expected to be quite sensitive to the relative composition of day and night components. The consequence for the Western Pacific is that the long-path signal to the east is both very strong and lasts for many hours. We estimate about 9 hours at Hawaii.

The predictions for Liberia result in an unusually large westward extent of the long-path. These lobes to the west are much larger than for any other station. We are not confident that these lobes are as large as predicted and consider it important to test for this feature.

North Dakota: As shown in Figure C-5, the predicted eastern extension of the long-path/short-path boundary lies to the east of Australia and New Guinea, and north of Taiwan, Hong Kong, and Rangoon. The boundary is at its eastern most extent, east of Australia, for almost six hours; from near 1800 to near 2400 GMT. The field strength curves, Figure C-2, show that the boundary shape can be quite complex. We predict the 13.6 kHz boundary to be inside the shown 10.2 kHz boundary by about 1.5 Mm.

Argentina: As shown in Figure C-6, the 10.2 kHz long-path/short-path boundary makes a broad diagonal sweep across the validation zone. The boundary enters the eastern edge from the vicinity of Samoa, crosses just south of Brisbane and merges with the signal Antarctic shadow about midway across Australia. The dwell time at the easternmost extent is predicted to vary with radial, being near four hours at Brisbane and increasing east of the validation region to about ten hours in the central United States.

MODEL ASSESSMENT

We feel that this analysis technique provides a good start for assessing/validating long-path effects. This is a model that needs calibration with additional measurements and could benefit from calculations beyond 20 Mm propagation distance. The model's validity will be largely determined through experience gained in its use.

Appendix D

Long-path/Short-path Effects Data Analysis

OVERVIEW

In this appendix fixed-site data are evaluated for evidence of long-path/short-path interference effects and are compared with the predictions derived in Appendix C. The primary evidence on fixed-site data for the existence of long-path signals within the short-path region, is a reversal from normal of the diurnal pattern of phase. For example, the phase changes as if transitioning from day to night propagation during a time interval when normally either no phase change or a night-to-day transition would occur. Also, the long-path signal can have a very different phase than the short-path signal. If it does, the emerging long-path can cause the received phase to change in an unpredictable manner. The observed phase change should not occur if only the short-path signal is received. A major complication, encountered here and in the South Pacific validation, is that the signals we attempt to analyze for long-path also undergo equatorial zone mode conversion when night is on the short-path. Sorting out the two effects is a major challenge that is not always feasible from the available data.

DATA INTERPRETATION

We evaluate those signals at locations where long-path may be detectable based upon the predictions of Appendix C. The following material describes the analysis conducted on fixed-site data to test for long-path effects:

NORWAY: No long-path interference is predicted in this validation region and none was detected.

LIBERIA: The maximum extent of the eastern long-path boundary was found in the South Pacific validation to extend far beyond the eastern edge of this validation region. An important prediction, not tested in the South Pacific validation, is the western extent of the long-path from the antipode. The lobe west of the antipode extends much farther than that predicted for any other station. The analysis results of the Liberia signals are as follows:

Hawaii: The Hawaii site is predicted to incur long-path when daylight is to the east of the antipode. The measured short-path daytime phase shows very marked deviations from the predicted daytime pattern at all frequencies. Long-path typically occurs at this site between 1100 and 2200 GMT. The measurements confirm the expected, since we have determined previously that long-path occurs far to the east of this site.

Brisbane: This is the closest fixed site on the west side of Liberia's antipode. The long-path lobe in this direction is predicted much shorter than to the east. The maximum ratio of night on the long-path to day on the short-path occurs around 01 July. Thus, if long-path signals reach Brisbane, the most favorable time to detect them is around July near 0600 GMT. In Figure D-1, we show Liberia phase data recorded at Brisbane from 25 to 31 July 1986 that evidences long-path effects. This data, which are representative for this season, show that long-path interference is quite variable from day to day. For most days, the long-path disturbance in minimal to moderate, similar to the bottom three groups of records. On some days, the evidence for long-path effects is quite strong, similar to that illustrated by the three top groups of records. On the record set starting 25 July, the long-path interference causes the 11.3 kHz phase to reverse its trend several hours before its normal maximum advance. The result is that this frequency incurs a full cycle offset during the 24 hour period. On the set beginning 26 July, both the 11.3 kHz and 13.6 kHz signals end with a cycle offset. Here the phase of these two signals first shows an added advance before reversing their direction. For the set starting 27 July, both the 10.2 and 13.6 kHz signals reverse direction of change over an hour early. While the record sets for the last three days show minimal long-path effects, the set marked 30 July evidences complex behavior. We find that cycle jumps occur about ten percent of the days during this season. This assessment covers the time interval when conditions are most favorable for the long-path to reach Brisbane.

At other seasons the long-path may not extend to Brisbane. In Figure D-2 we show data for the 03 to 09 March 1986 period. For this data set, we are not able to identify evidence of a long-path signal reaching Brisbane.

Darwin: We do not detect any evidence of long-path signal at this site.

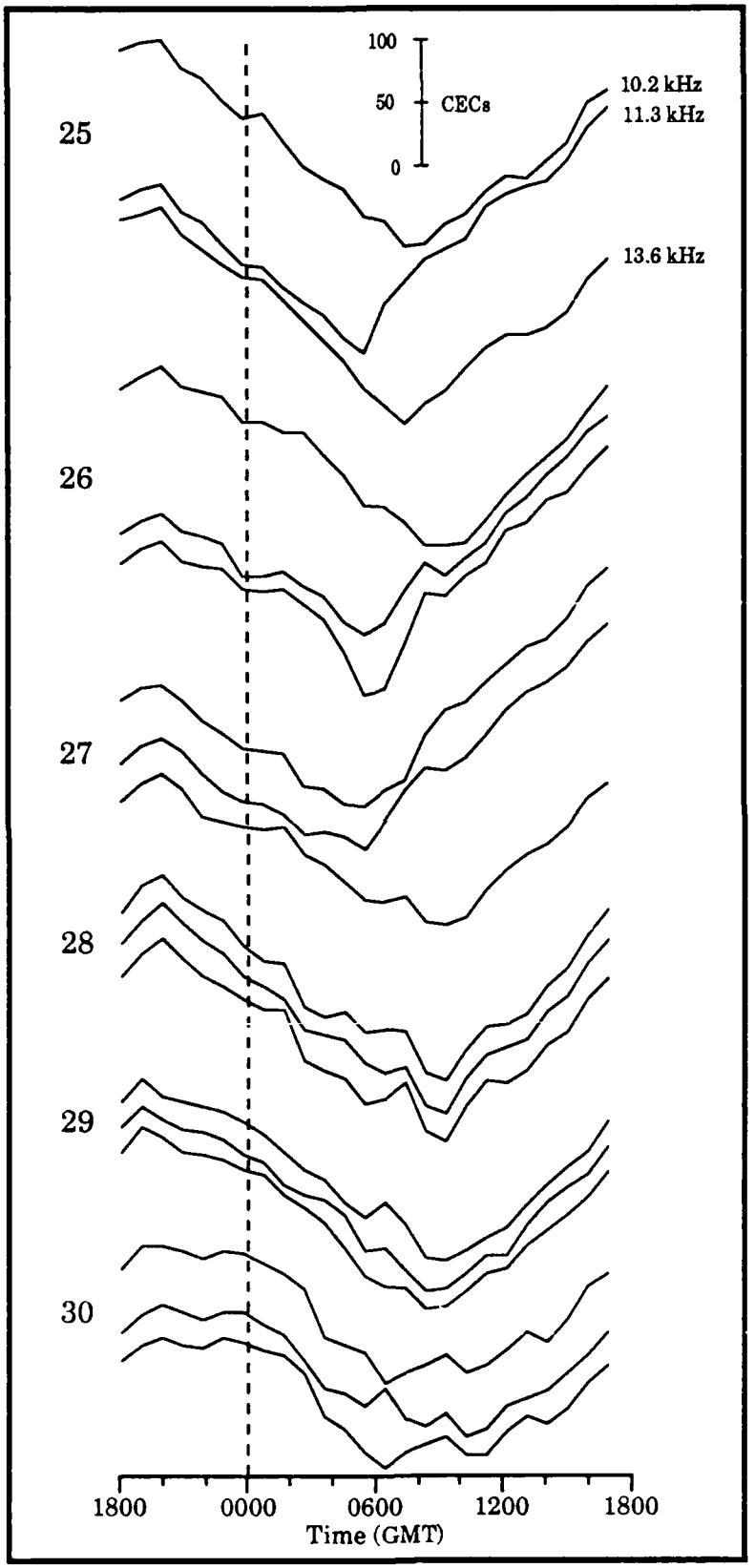

Figure D-1. Liberia Received Phase at Brisbane; 25-31 July 1986

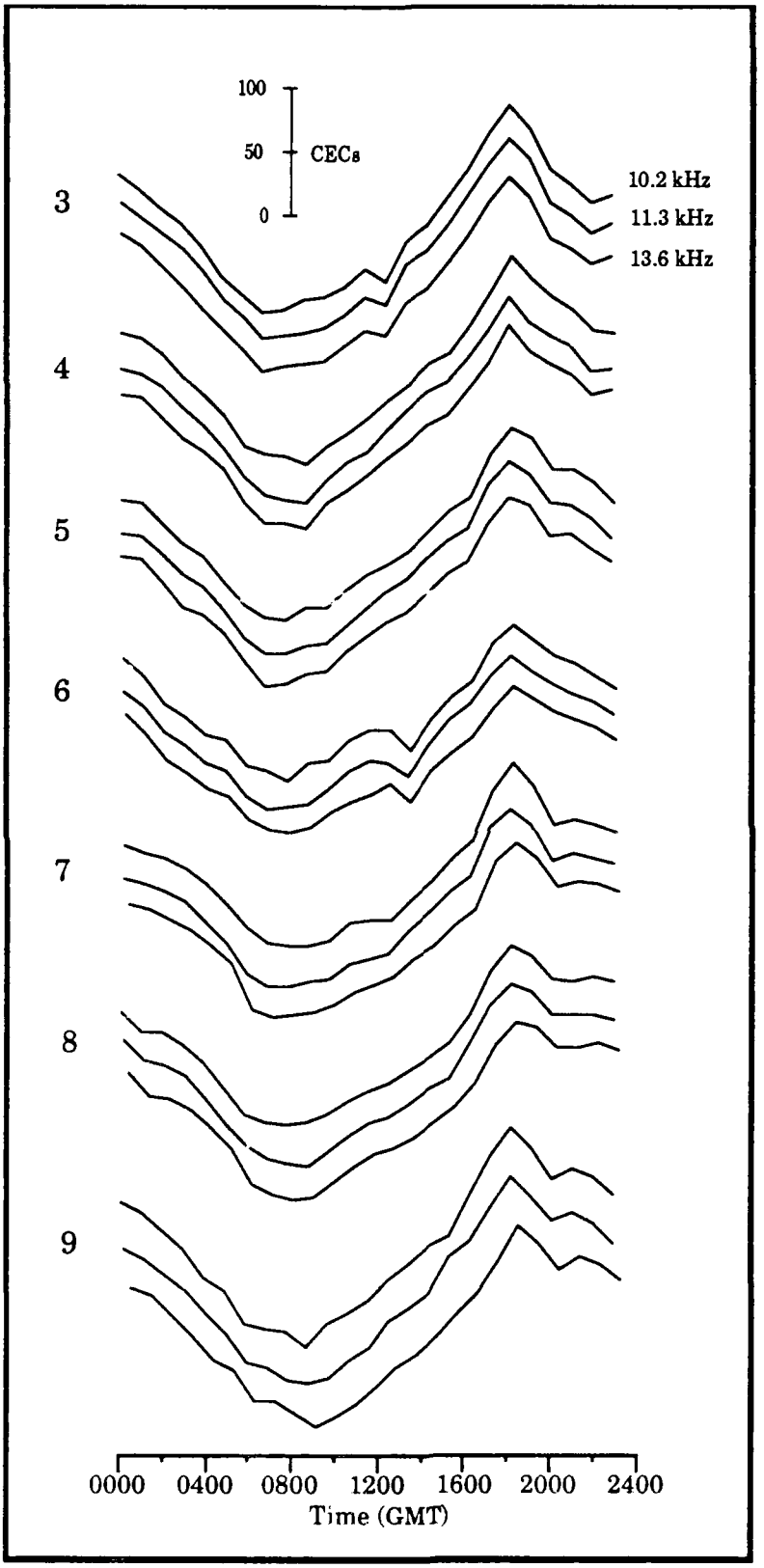

Figure D-2. Liberia Received Phase at Brisbane; 03-09 March 1986

Yap: The Liberia signals produce a very clean diurnal phase curve that closely track at all frequencies and at all times.

Liberia Discussion: We estimate that the westward maximum extent of long-path interference is shorter than our prediction. The boundary during at least June and July is a few hundred kilometers west of Brisbane. The boundary probably does not reach Darwin. From the onset times of long-path interference at Brisbane, we believe that the boundary occasionally could reach within 500 Km of Darwin. During the rest of the year this boundary is probably to the east of Brisbane. These data do not provide much support for adjusting the position and shape of the boundary. If data are available from any other sites in eastern Australia, a more detailed analysis should be conducted. We note that the long-path extension to the west, while less than we predicted, is greater than any other prediction we are aware of.

In the South Pacific validation we found that to the east, the long-path extends several megameters further than we estimated from the calculations. That finding, along with this finding, supports other observations that low latitude propagation to the west incurs more loss than presently predicted (LYNN 1983, Ref. 26). Thus, the ratios of signal levels shift boundaries eastward.

HAWAII: No evidence of long-path effects is expected or detected in the data.

NORTH DAKOTA: The long-path boundary at maximum eastward extent for North Dakota is predicted to penetrate into the the validation region almost to New Zealand. Sites where possible long-path might be detected are Brisbane, Cubi Point, Darwin and Singapore.

Brisbane: The optimum period for long-path extending to Brisbane is December and January. The data we have closest to this period are for March. The North Dakota signals at Brisbane are weak, and they contain multi-mode effects from propagation on the short-path through the equatorial zone. The poor signal quality masks any possible evidence of long-path effects.

Darwin: This channel was used for the calibration signals; thus no data are available.

North Dakota Discussion: We are unable to reliably assess the possible occurrence of long-path interference because of inadequate data.

LA REUNION: No evidence of long-path effects is expected or detected in the data.

ARGENTINA: The maximum penetration of the long-path boundary into the validation region is predicted to extend across south Australia, going just below Brisbane and exiting the western edge after passing near Samoa. The antipode lies about a megameter to the northwest of Japan. We examine data from sites in the order of increasing distance from the antipode.

Japan: The Argentina channel was used for the calibration signal, therefore no data was acquired.

Cubi: The Argentina channel was used for the calibration signal, therefore no data was acquired.

Yap: The Argentina channel was used for the calibration signal, therefore no data was acquired.

Hawaii: The data recorded at Hawaii are masked by short-path modal effects and by tracking loss on most days at the times of most interest. We could not determine if long-path interference extends to Hawaii.

Darwin: The maximum extent of the long-path signal will occur when the day/night terminator just reaches the short propagation path over Antarctica. The two most favorable date intervals are early March to late April and early August to mid October. The available data cover May and June of 1986, when the Antarctic portion of the propagation path was in darkness. We do not detect any long-path effects for this period.

Brisbane: If long-path signals reach Brisbane, the most favorable time to detect them is around July near 2130 GMT. In Figure D-3, we show Argentina phase data recorded at Brisbane from 05 to 09 July 1986 that evidence long-path effects. This data, which is representative for this season, show that the diurnal phase patterns of the 10.2 kHz and 11.3 kHz signals differ quite a bit from the pattern of the 13.6 kHz signal. We interpret the small day/night phase change of the two lowest frequencies to be

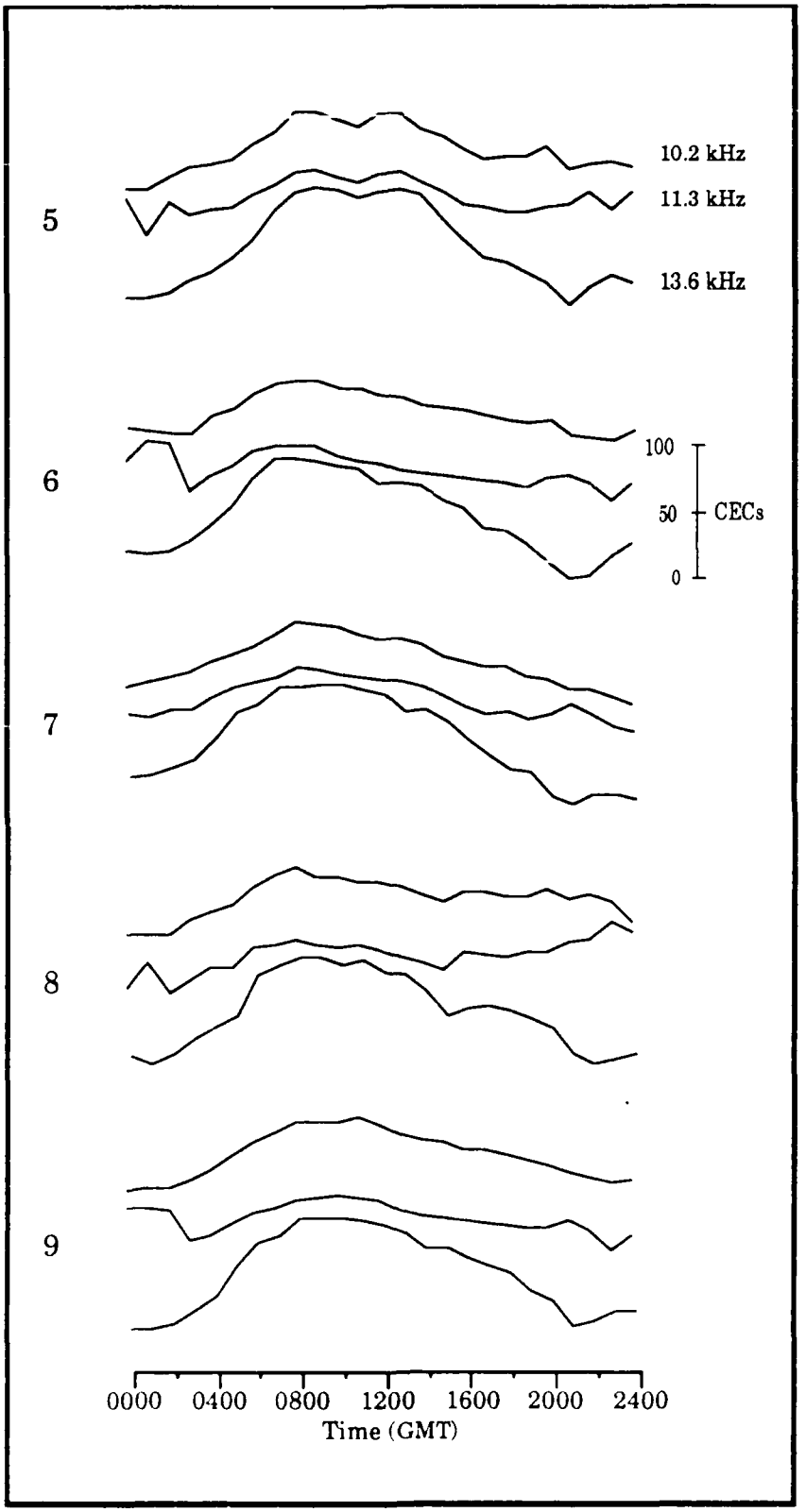

Figure D-3. Argentina Received Phase at Brisbane; 05-09 July 1986

caused by the presence of long-path signals. Data showing more typical diurnal phase patterns are shown in Figure D-4, for the period 06 to 12 August 1986. In this figure, the first five days show diurnal phase curves that we interpret to be almost free of long-path interference. Possibly the short all daylight periods, 1900 to 2300 GMT on 8 and 9 August, evidence some long-path presence. On 11 August, a phase cycle jump occurs at 11.3 kHz that spans the propagation path full daytime period. Following the middle of August very little evidence of modal effects are detected. Going back to 25 to 31 July, we show in Figure D-5 seven days of data with uncharacteristic phase behavior on all three frequencies. For all days in July 1986 the long-path disturbance is moderate to strong, similar to that shown in Figures D-3 and D-5. For June of 1986, we find no evidence of long-path effects. Data for 21 to 30 June, shown in Figure D-6, illustrate that the diurnal phase histories of all three frequencies closely follow each other and show a consistent pattern from day to day. This assessment covers the time interval when conditions are most favorable for the long-path to reach Brisbane. We find as with the Liberia signal that the maximum extent of long-path interference varies significantly with season.

AUSTRALIA: No evidence of long-path effects is expected or detected in the data.

JAPAN: No evidence of long-path effects is expected or detected in the data.

GENERAL DISCUSSION: Identifying long-path effects in the presence of other effects is very difficult using the monitoring site data. The prediction model seems reasonably consistent with observations of boundary transitions across sites. Some adjustments are definitely needed, these being the placement of the western boundary for Liberia to the west of Brisbane and the boundary for Argentina south of Brisbane. We show that the positions of these boundaries are dependent upon season.

Much more analysis than was possible is needed to produce a useful test of long-path effects. Useful products of this model presentation and the associated data analysis are (1) to place a time history on the movement of the boundary between the extreme locations, (2) to illustrate the complexity of the boundary curve that results from variations in propagation attenuation with azimuth, and (3) to show the large changes in rate of boundary movement as the terminator orientation changes with season.

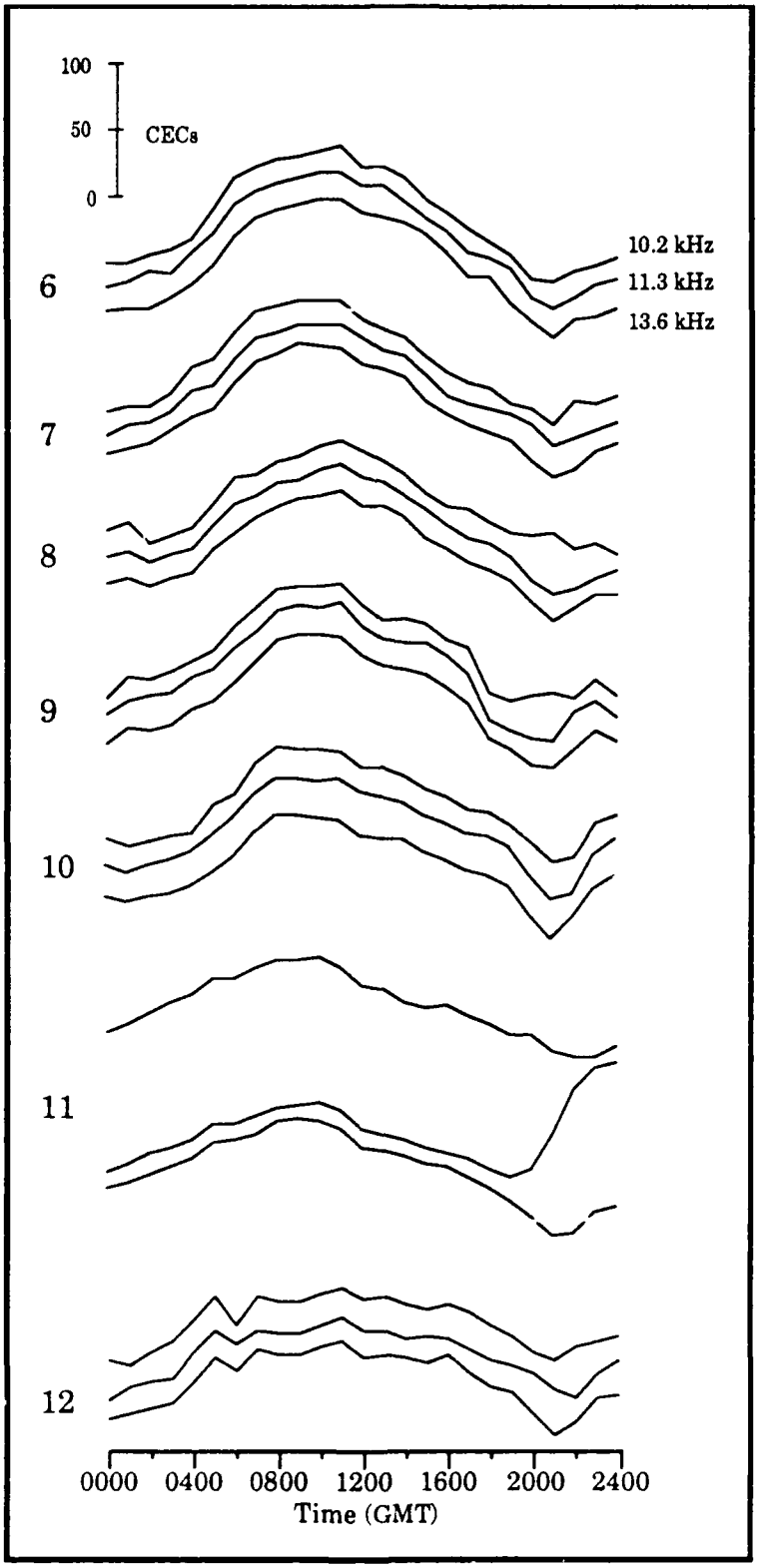

Figure D-4. Argentina Received Phase at Brisbane; 06-12 August 1986

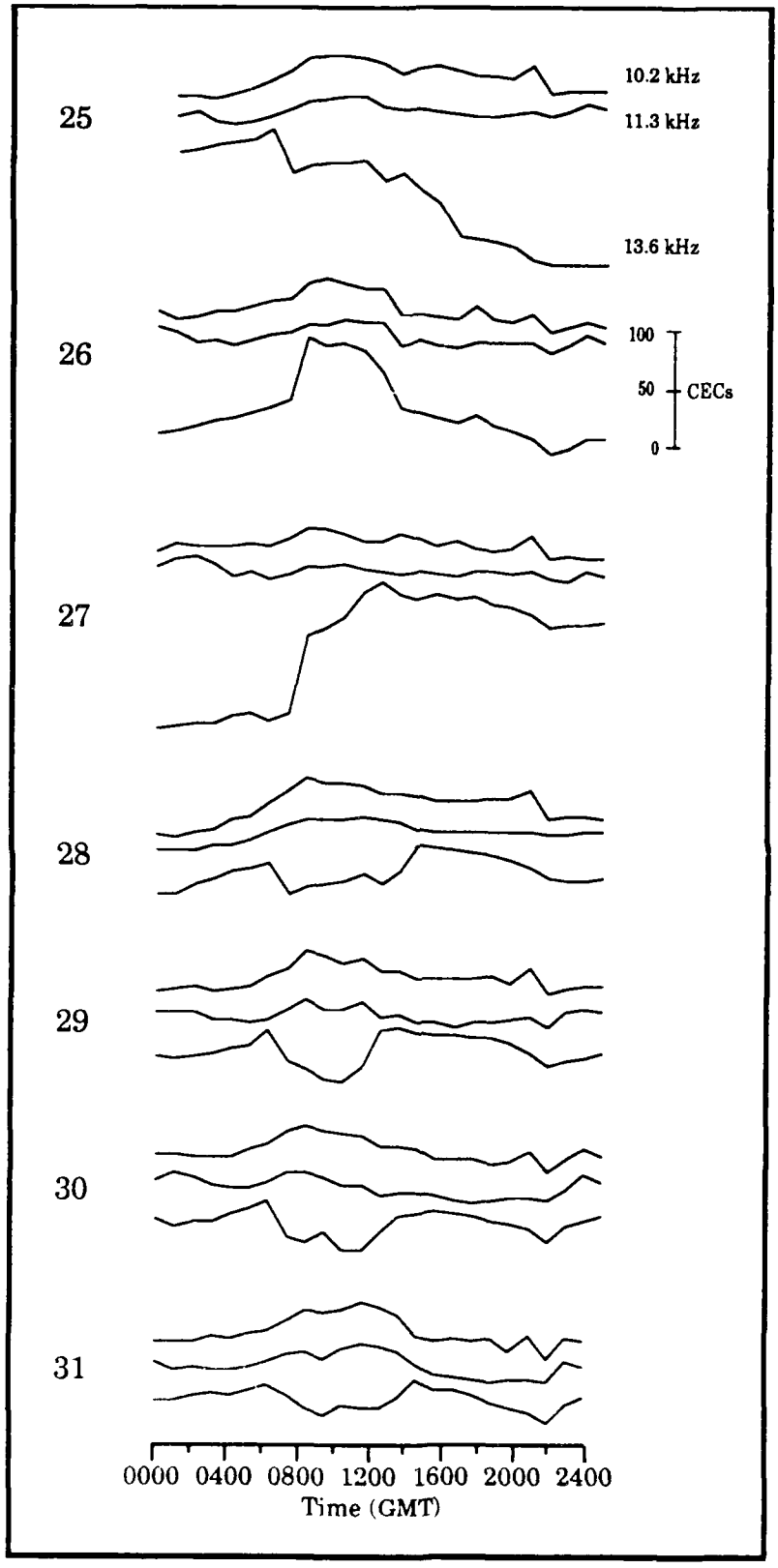

Figure D-5. Argentina Received Phase at Brisbane; 25-31 July 1986

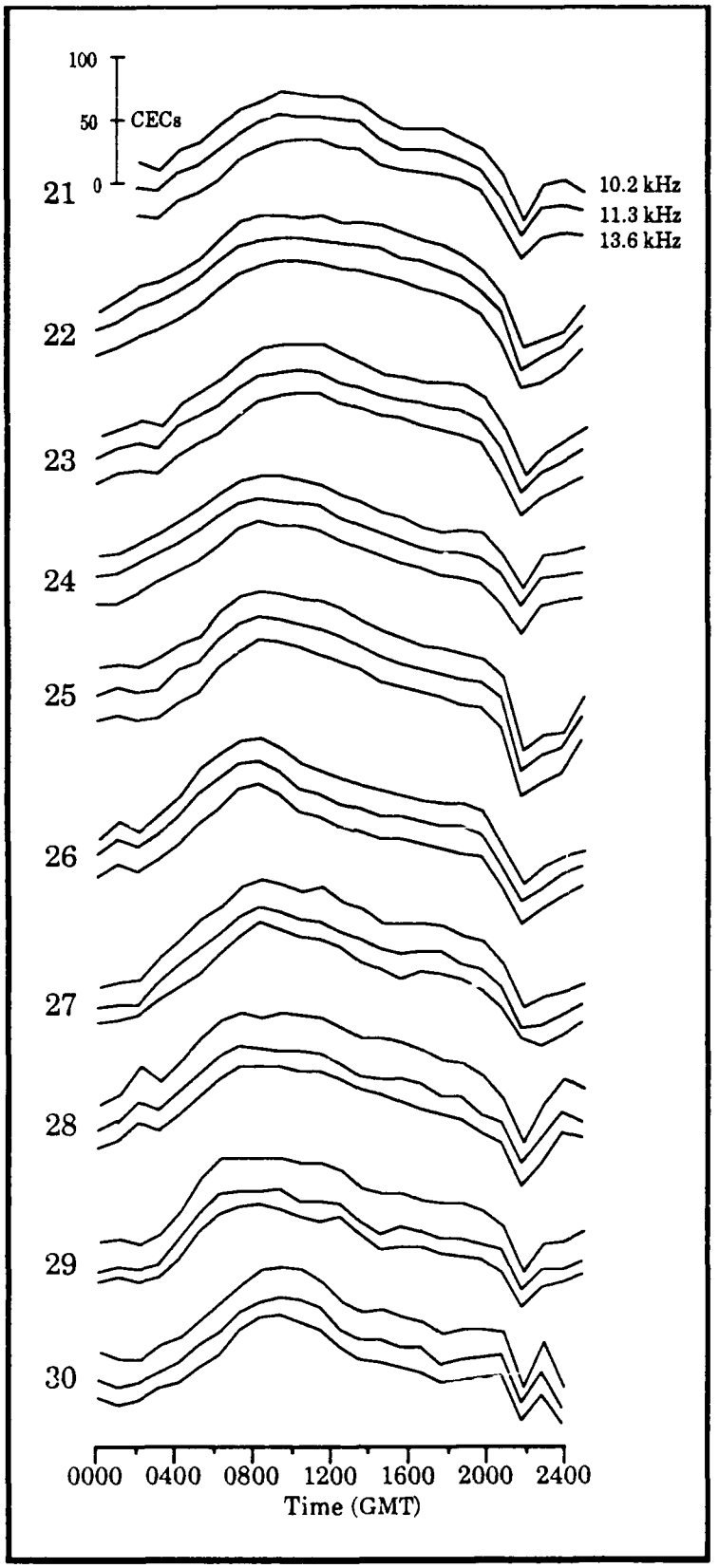

Figure D-6. Argentina Received Phase at Brisbane; 21-30 June 1986

THIS PAGE INTENTIONALLY LEFT BLANK

Appendix E

Navigation Fix Accuracy Assessment

OVERVIEW

This navigation fix accuracy assessment is presented in two parts:

- The first part describes comparisons made between Predicted Phase Difference (PPD) calculations and measured phase-difference at fixed sites. We use phase difference measurements to circumvent problems caused by unstable reference oscillators. Illustrations are given of representative observed conditions. The first part assumes the reader is familiar with phase-difference measurements and Propagation Phase Corrections (PPC).
- The second part extends the observations to the use of shipboard navigation data. The shipboard data are particularly valuable in confirming many of the observations of part one at additional locations. The analysis of shipboard data serve to illustrate that real-world navigation accuracy is consistent with that expected from fixed-site phase accuracy *determination.*

PART I: ACCURACY ASSESSMENT DESCRIPTION

The objective for this phase of the validation analysis is to check the basic ability to derive a position fix from provided predictions. Our perspective is that of the navigator who has to use the signals, associated correction aids, and auxiliary support, as they exist at the time of a fix. We concentrate on the information content in the measured phase of each signal available for navigation. The signal processing aspects of the navigation fix are more appropriately assessed on a laboratory bench. By concentrating on assessment of phase prediction, the complexity of interpretation is minimized and navigation model capabilities are more directly evident. In this analysis, we generally only check signals that do not have known self-interference problems during the time interval of assessment. To amplify, if our assessment is for daytime propagation and the night on a path is known to incur modal effects, the day signal is considered good for our assessment purpose.

Obtainable OMEGA navigation fix accuracy is dependent upon two components of received phase, the predictable and unpredictable. The predictable component

must be large enough to ensure the needed accuracy. By improving prediction methods, the predictable component is made a larger portion of the total signal. By comparing numerous measurements with predictions, some estimate can be derived of the relative magnitude of the predicted and unpredicted components.

Propagation prediction calculations are produced for semi-monthly intervals and include diurnal, seasonal, and long-term parameters. We choose this semi-monthly interval as the basic interval to check predictions. Several types of checks are described which include estimates for predicting phase at midpath noon, the day-to-night phase change, and the accuracy of predicting the phase change during sunrise and sunset transitions. Checks are also made on the variation about the predicted and observed medians.

The examples illustrating these types of checks are taken from sites having general good quality measurements. The data, presented in Tables E-1 through E-9, show the received phase for selected hours for each day of a semi-monthly interval. The hours selected were chosen to match conditions of propagation; i.e., day, night or day/night transition. Other values shown for each hour include: the median value for the semi-monthly interval, the range of phase values, the Predicted Phase Difference (PPD) and the Median plus PPD. Predicted phase difference is computed by subtracting the predicted phase of station two from station one. Our term predicted phase difference includes all of the parameters that must be included to compare predictions with measurements. Parameters included are: calculations of Predicted Propagation Corrections (PPCs) and adjustments for site location (centicycles from the PPC calculation). Data items considered of most interest in these tables are the range about each hourly median, the variation in the values of (M+PPD), and the comparison between M and PPD of the day-to-night phase change. (PPDs are constructed so they vary, from hour to hour, in the same direction as the PPCs).
The comparison between median phase and predicted phase cannot be absolute because the clock at each site has a small but unknown time drift. This drift is not important for LOP determination as the phase difference measurements remove the unknown time offset.

The significance of each data category selected for presentation can be illustrated by example. Referring to Tables E-1 through E-3 for signals reviewed at Japan, we have the benefit of checking data against the measurements of the

Day \ Time	0	100	500	800	1000	1200	1400	1700	2000
1	–11	6	42	41	31	7	–8	3	9
2	–13	0	31	44	30	–6	–23	–9	–22
3	–46	–23	24	21	22	–6	–25	–13	–29
4	–64	–13	27	–17	60	–47	10	–26	–33
5	–30	–12	23	21	18	–7	–33	–27	–31
6	–32	–21	19	21	11	–10	–37	–24	–45
7									
8			37	29	28	1	–19	–21	–41
9	–25	–7	25	34	21	–7	–21	–12	–41
10	–23	–26	24	34	13	–3	–25	–21	–36
11	–13	4	39	39	31	–4	–17	5	–28
12	–17	2	17						
13									
14			46	36	27	–10	–32	–24	–36
15	–11	6	29	30	23	0	–29	–20	–38
Entries	11	11	13	12	12	12	12	12	12
M	–23	–7	27	32	25	–6	–24	–21	–34
Range	53	32	29	61	49	54	47	32	54
PPD	19	33	40	38	33	11	–18	–17	–31
M+PPD	–4	26	–33	–30	–42	5	–42	–38	35

Table E-1. Japan Phase Difference A–E; 01-15 May 1986

Day \ Time	0	100	500	800	1000	1200	1400	1700	2000
1	–24	–33	–18	28	–8	37	–28	46	0
2	–28	–45	–14	39	7	60	- .	69	28
3	23	9	25	67	30	61	–1	56	24
4	–47	–36	2?	44	47	86	–5	76	18
5	4	–14	10	59	25	66	0	69	39
6	28	–3	11	72	43	68	16	84	57
7									
8			16	64	34	66	6	60	21
9	–12	–15	21	61	39	85	–10	50	12
10	–27	–36	–23	55	31	57	14	63	30
11	–18	–24	–3	60	34	61	–19	46	11
12	–27	–40	20						
13									
14			–6	47	25	50	–21	44	15
15	–16	–24	–7	47	26	21	–25	38	17
Entries	11	11	13	12	12	12	12	12	12
M	–18	–24	10	57	30	61	–8	58	20
Range	75	54	48	44	55	65	44	46	57
PPD	66	54	–18	–50	–74	–45	–34	34	11
M+PPD	48	30	–8	7	–44	16	–42	–8	31

Table E-2. Japan Phase Difference B–D; 01-15 May 1986

Day \ Time	0	100	500	800	1000	1200	1400	1700	2000
1	23	21	15	–55	–75	–53	–51	–51	35
2	19	19	17	–41	–55	–30	–12	–19	54
3	55	52	45	–17	–17	–17	–17	–30	45
4	98	30	56	–44	7	–10	–32	–17	49
5	53	48	40	-37	–2	–38	–26	–27	60
6	63	48	43	–19	–29	–14	5	–9	74
7									
8			45	–32	–34	–23	–9	–26	43
9	38	45	47	–41	–35	0	–19	–41	37
10	26	25	0	–46	–46	–27	4	–32	54
11	36	43	19	–39	–36	–16	–18	–37	35
12	22	23	44						
13									
14			26	–42	–47	–31	–34	–36	39
15	37	40	23	–36	–44	–58	–29	–43	43
Entries	11	11	13	12	12	12	12	12	12
M	37	40	40	–40	–35	25	–19	–31	44
Range	79	33	56	38	82	58	56	42	39
PPD	28	26	21	–53	–53	–34	–41	–51	34
M+PPD	–35	–34	–39	7	12	41	40	18	–22

Table E-3. Japan Phase Difference C–D; 01-15 May 1986

Japan transmitter. From Table E-1 for phase difference measurements of station pairs A–E, we note the following: (1) the range of measured phase difference values varies from a minimum of 29 to a maximum of 61 CECs, (2) the values of (M+PPD) range from –42 to +35 CECs, and (3) the median measured diurnal phase change (0800 minus 0000 GMT), is 55 CECs and the predicted is 19 CECs. These sets of values are typical of observations at this and the other sites. Some general comments for all three sites are as follows. The agreement between diurnal phase change, i.e. day-to-night, for various station pairs is generally good. We hesitate to place high value on comparisons of data because of the large variations involved and because we have not tracked the phase difference history between selected times. In the tables we selectively, but arbitrarily, add or subtract full cycles of phase in an attempt to produce what appears to be consistency in diurnal and daily trends. In our estimation, this process has not worked well and we feel a better process has to be devised.

Day \ Time	0	100	500	800	1000	1200	1400	1700	2000
1	–18	0	–34	27	16	18	32	49	16
2	–34	–12		–21	–28	66	11	46	0
3	–33	–7	–31	25	19	23	28	49	–24
4	–69	–7	17	25	15	54	9	50	–42
5	–6	12	–31	27	17	25	27	54	–45
6	–10	8	–33	24	16	23	32	50	–26
7	3	17	–31	30	21	28	21	2	–34
8									
9				33	21	17	16	43	–36
10	–14	2	–30	31	21	13	24	46	–45
11	–10	6	–24	29	19	23	28	46	–45
12	–16	–4	–30	28	23	26	33	47	–45
13	0	1	–40	28	19	25	32	56	–36
14	–7	7	–38	28	21	19	22	48	–30
15	–24	–1	–28	21	20	25	18	52	–29
Entries	12	13	13	14	14	14	14	14	14
M	–15	1	–31	28	19	25	27	49	–34
Range	72	29	57	57	51	53	24	54	61
PPD	61	62	21	10	4	–5	–8	30	–40
M+PPD	46	–37	–10	38	23	20	19	–21	–26

Table E-4. Cubi Phase Difference B–E; 01-15 January 1986

Day \ Time	0	100	500	800	1000	1200	1400	1700	2000
1	44	37	64	18	14	41	75	12	86
2	25	23	69	15	17	39	67	10	11
3	31	31	67	15	14	45	74	4	28
4	29	82	11	38	57	33	94	29	40
5	59	52	69	19	14	47	77	15	18
6	46	44	67	18	11	44	79	5	49
7	67	56	68	21	14	46	74	22	27
8									
9				23	19	42	72		23
10	50	39	68	19	11	39	80	7	17
11	48	38	73	17	15	42	71	12	25
12	46	33	68	18	17	45	79	17	20
13	0	41	60	18	18	11	80	12	21
14	61	47	60	20	16	11	78	12	20
15	43	39	70	6	13	39	71	17	42
Entries	12	13	13	14	14	14	14	14	14
M	46	39	68	18	14	41	76	12	24
Range	42	59	62	32	46	36	27	25	75
PPD	–6	–21	–80	7	–2	9	36	83	15
M+PPD	40	18	–12	25	12	50	12	–5	39

Table E-5. Cubi Phase Difference B–H; 01-15 January 1986

Day \ Time	0	100	500	800	1000	1200	1400	1700	2000
1	36		–40	32	31	63	–13	45	61
2	36	20	–42	42	42	57	–11	44	73
3	69	50	–36	47	31	50	–17	35	66
4	55	–10	–77	79	77	55	–54	36	58
5	56	25	–46	38	40	61	5	50	72
6	56	31	–55	42	39	61	–9	49	81
7	58	31	–47	37	40	57	–9		
8		20	–45	40	41	58	6	52	73
9	35	19	–42	36	40	58	–13	41	64
10	46	27	–41	38	43	61	–13	48	81
11	38	14	–44	34	43	58	–10	51	68
12	45	24	–45	34	41	65	–18	40	71
13	47	33	–41	35	44	63	–23	38	76
14	39	23	–43						
15			–38	33	45	56	–11	32	83
Entries	13	13	15	14	14	14	14	13	13
M	46	24	–43	38	41	58	–12	44	72
Range	34	60	41	47	46	15	60	20	25
PPD	–78	6	–54	–66	29	49	–22	26	68
M+PPD	–32	30	3	–28	–30	7	–34	–30	40

Table E-6. Yap Phase Difference B–H; 01-15 May 1986

Day \ Time	0	100	500	800	1000	1200	1400	1700	2000
1	30		–26	–42	52	–13	9	13	17
2	30	12	–31	–43	55	–4	25	26	25
3	29	16	–29	–45	50	–28	10	23	29
4	19	54	15	–6	93	–30	61	11	20
5	25	8	–31	–45	54	–7	15	7	23
6	24	8	–33	–42	52	–17	12	17	27
7	32	10	–31	–45	51	–21	3		
8		12	–31	–45	59	–16	–7	2	4
9	21	6	–30	–41	49	–34	–2	19	24
10	31	8	–31	–44	53	–16	9	17	17
11	22	5	–29	–40	48	–21	23	22	19
12	30	11	–30	–41	50	–15	18	17	24
13	30	8	–28	–42	52	–8	7	32	26
14	30	8	–33						
15			–29	–39	62	–6	6	8	8
Entries	13	13	15	14	14	14	14	13	13
M	30	8	–30	–42	52	–16	8	17	23
Range	13	49	48	39	45	30	68	30	25
PPD	4	90	69	46	–57	–26	2	9	12
M+PPD	34	–2	39	4	–5	–42	10	26	35

Table E-7. Yap Phase Difference E–G; 01-15 May 1986

Day \ Time	0	100	500	800	1000	1200	1400	1700	2000
1	0	–21	81	13	11	42	–4	6	–9
2	–14	18	98	20	13	42	–17	5	–7
3	–6	–8	25	46	0	–23	–6	5	14
4	38	28	24	7	14	4	6	0	4
5	–16	16	43	12	0	0	–4	5	–8
6	–10	–18	95	–2	0	–16	–25	–14	52
7	–19	–4	105	–11	34	14	–11	–33	–26
8	40	24	100	13	53	12	–13	–8	–3
9	45	10	94	18	19	38	–11	–30	–10
10	18	17	114	21	30	14	6	–9	6
11	–15	34	78	21	48	51	–17	–17	–8
12	22	32	91	13	–28	18	–24	–36	–10
13	13	–5	103	14	1	–35	–12	–3	–12
14	14	24	106	21	25	–24	14	–26	–5
15	40	39	77	17	–17	18	–33	–59	37
Entries	14	15	14	15	14	13	15	15	15
M	13	17	94	14	13	14	–11	–9	–7
Range	64	60	90	57	91	86	47	65	78
PPD	52	61	10	26	37	–60	–72	2	–15
M+PPD	–35	–22	–4	40	50	–46	17	–7	–22

Table E-8. Darwin Phase Difference A–B; 01-15 May 1986

Day \ Time	0	100	500	800	1000	1200	1400	1700	2000
1		16	–18	72	–33	4	41	35	33
2	34	17	–18	70	–34	23	36	34	38
3	29	16	–11	77		–6	30	33	34
4	31	31	–39	39	–11	49	–7	34	39
5	31	13	–13	79	–26		23	28	33
6	27	14	–33	54		–12	18	24	28
7	13	0	–33	50	–41	–12	14	27	18
8	17	1		53	–43	–11	19	19	12
9	1	–5	–33	51	–44	–7	18	27	31
10	17	0	–35	51	–41	–9	18	23	24
11	8	–3	–36	51	–43	–5	22	24	23
12	9	1	–36	52	–42	–7	15	22	3
13	13	–1	–35	52	–42	–4	18	26	20
14	11	–2	–37	50	–39	–11	15	24	21
15	10	–2	–35	51	–37	–7	19	25	18
Entries	14	15	14	15	13	14	15	15	15
M	15	1	–34	52	–41	–7	18	26	24
Range	33	36	28	40	33	61	48	16	36
PPD	–10	–25	–43	44	50	–24	0	5	6
M+PPD	5	–24	–77	96	9	–31	18	31	30

Table E-9. Darwin Phase Difference E–G; 01-15 May 1986

PART II: ANALYSIS OF SHIPBOARD LOP MEASUREMENTS

Shipboard recorded phase data are used to selectively validate navigation accuracy and to check findings from other analysis phases. In general we find that the shipboard data confirm that OMEGA position fixes, when compared to satellite fixes, produce position differences consistent with observed variations in signal propagation. Our checks of accuracy are primarily for median values of the LOP difference between the Omega and Satellite measured positions. Ideally, the medians are determined for periods of all-day or all-night propagation. Unfortunately our data samples mostly cover late daytime and sunset periods. Since much uncertainty is involved regarding propagation variability, the data were not as informative to us as were plots showing LOP errors in relation to the calculated PPDs. Thus, we choose to describe sample plots of data along with some interpretations.

We select four sample segments of the ship Tsushima's transits that illustrate typical trends; these are: (1) along the top leg of the eastern loop, (2) along the western leg of this same loop, (3) along the western side of the eastern loop from southeast of Japan to near Singapore, and (4) along the eastern side of the western loop, traversing northward just below the Philippines. The data are presented sequentially by measurement dates in Figures E-1 through E-4. Each figure used a consistent display format, as illustrated in Figure E-1. On the top two rows, we plot the predicted propagation phase correction at 10.2 kHz for each station of the selected station pair. The scale in centicycles has a tic mark for each 20 centicycles. The PPC curves are quite useful for showing predicted propagation conditions on each path. In this figure we note that the Norway signal begins transitioning from day to night at the start of each daily measurement sequence. (Note that the PPC curves are the inverse of diurnal phase curves.) The La Reunion signal completes transition to daytime, then about halfway through the measurement period, enters the sunset transition. The measurement period ends before the La Reunion signals reach full nighttime conditions. On lines 3 through 5, we show the measured phase difference corrected for diurnal and distance propagation parameters for each of three frequencies. Perfect correction would result in horizontal lines along the marked axis.

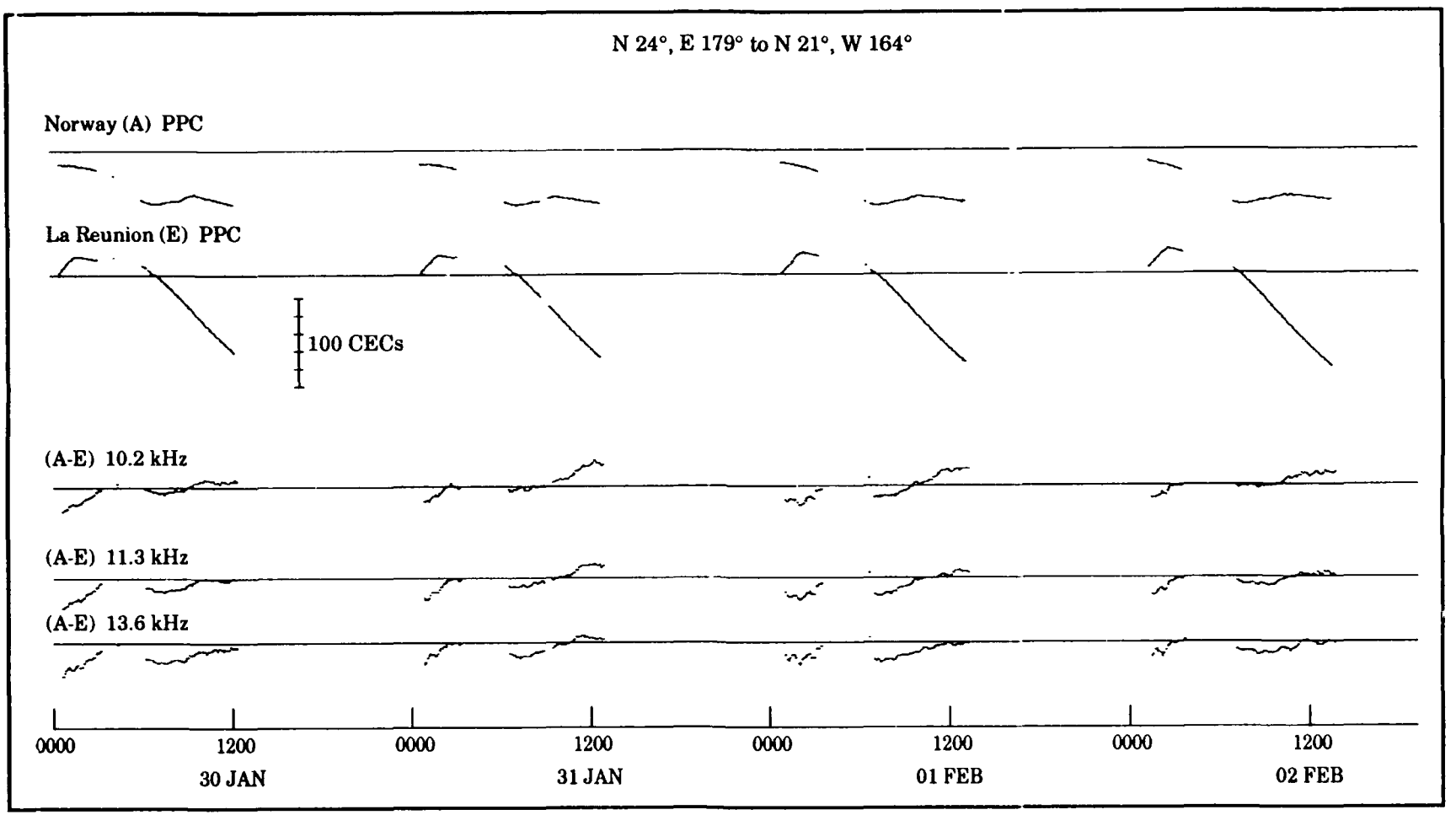

Figure E-1. Phase Difference Error Measured on TSUSHIMA, 30 January-03 February

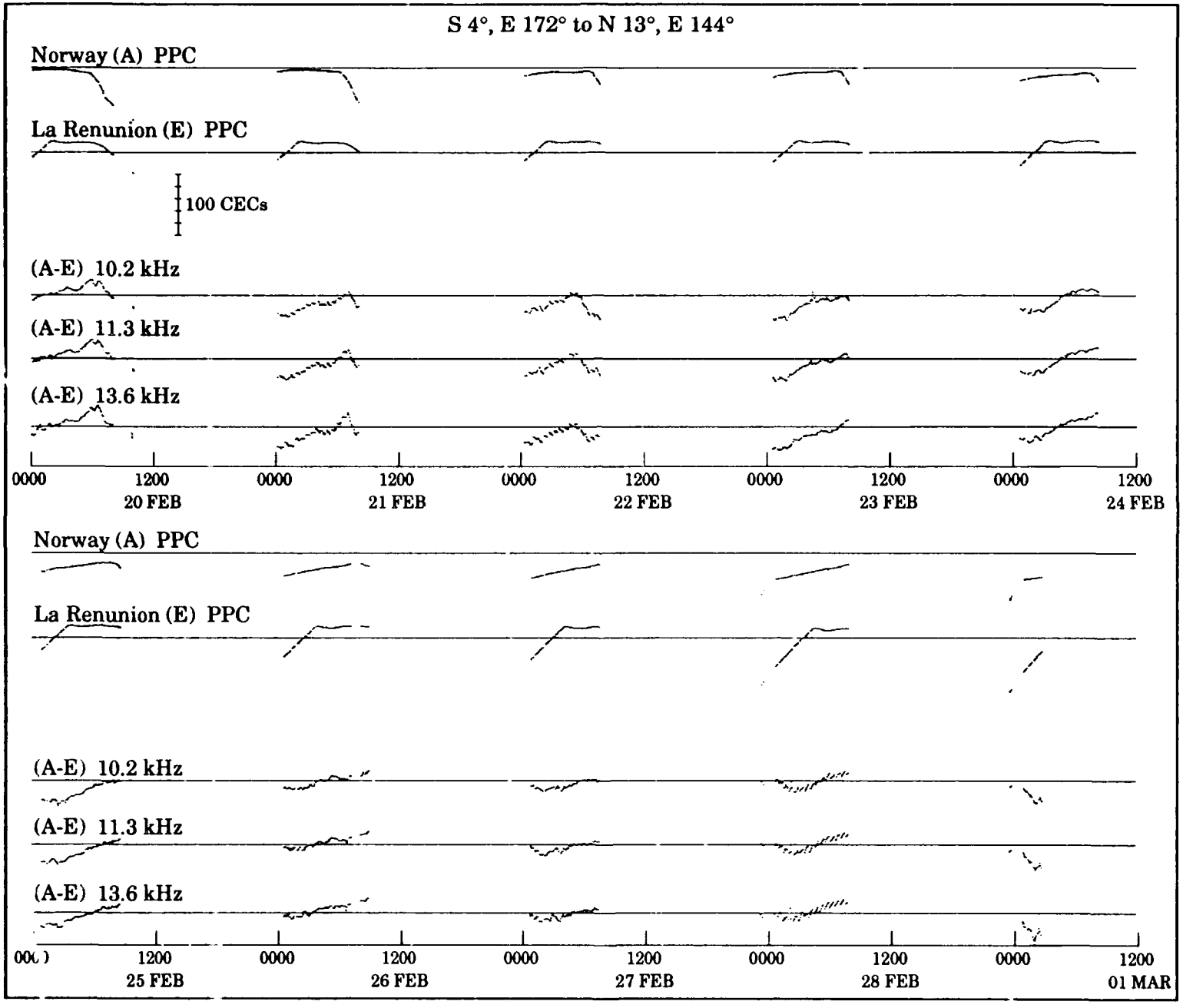

Figure E-2. Phase Difference Error Measured on TSUSHIMA, 20 February-01 March

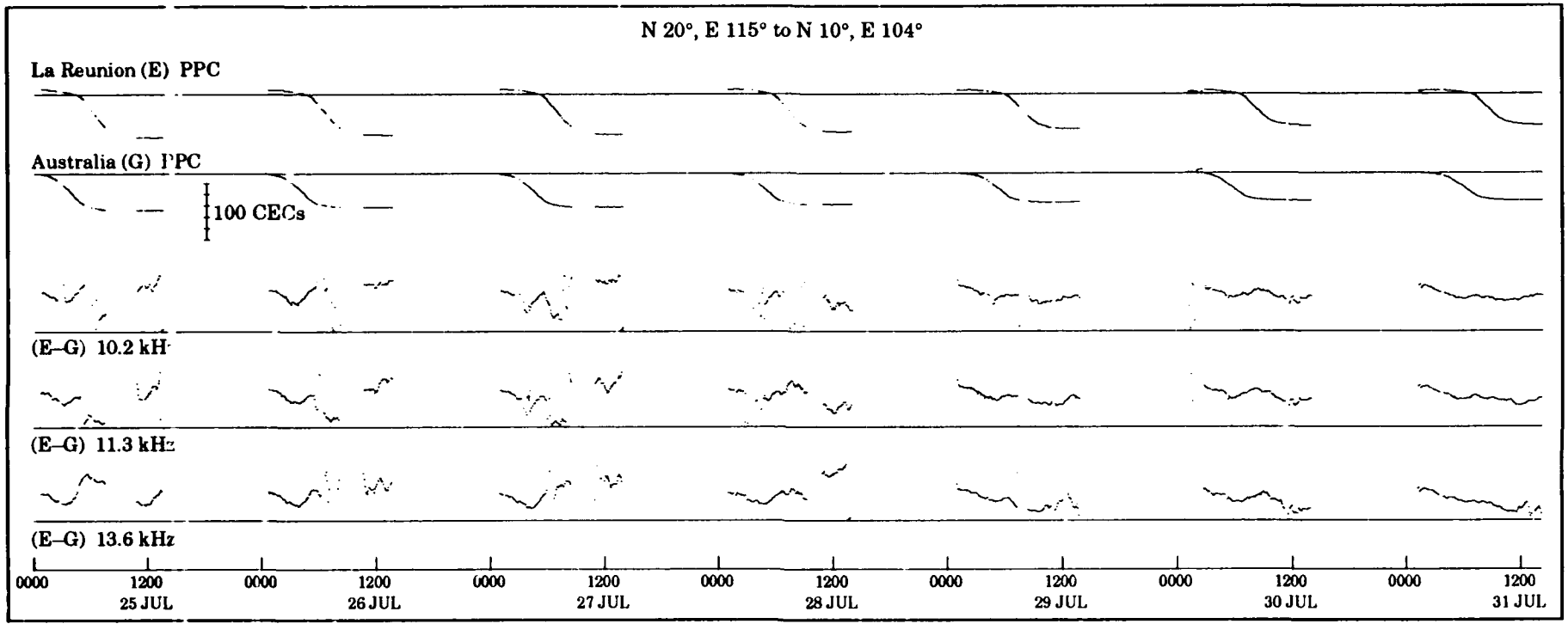

Figure E-3. Phase Difference Error Measured on TSUSHIMA, 25 July-01 August

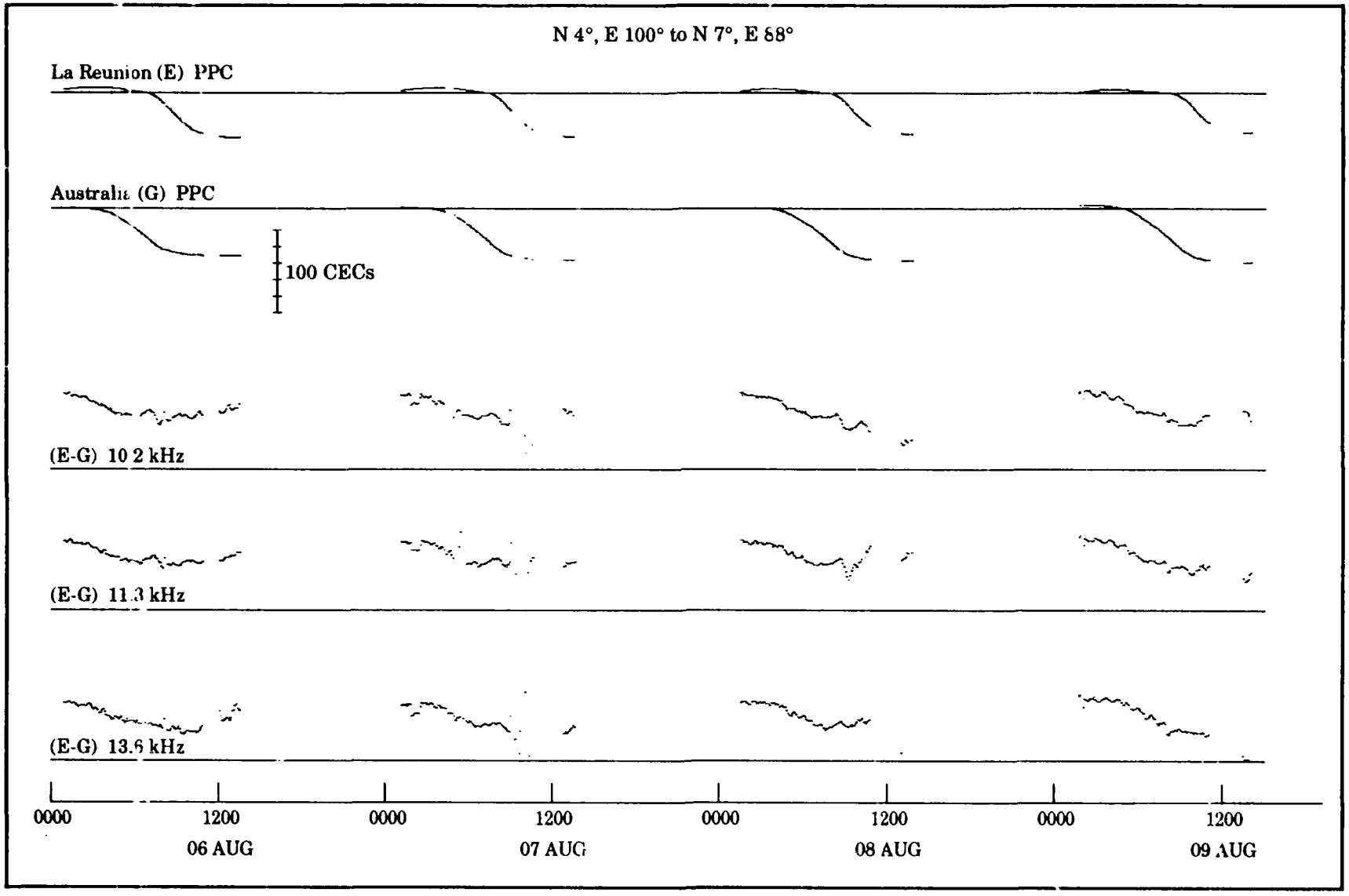

Figure E-4. Phase Difference Error Measured on TSUSHIMA, 06-10 August

Figure E-1 is chosen to show an example of typical low navigation error conditions. The phase difference errors are almost always within ±20 CECs. What is particularly interesting to us, is the repeatable pattern between frequencies and from day-to-day. Clearly, these trends are due to propagation.

In Figure E-2 we show the same station pair (Norway and La Reunion), for a later time sequence covering a ten-day interval. We note that the measurements cover slightly different diurnal segments. We note that the trends for each measurement interval are similar to those in Figure E-1. However, careful examination of the daily sequence reveals a cyclic pattern to the mean error for each period. This mean error is slightly positive on 20 February, drifts to a negative value by 22 February and then gradually drifts in a positive direction through 28 February. The cyclic drift accounts for most of the errors outside of ±20 CECs. We have no explanation for these observations.

The data of Figure E-3 are selected to show the consequences of disturbed propagation. This transit segment is to the southwest in a region that is generally within the equatorial conversion zone for the Australia signals. We note in the data for 25 July, that essentially as soon as the night transition for Australia is complete, the phase error patterns diverge for the three frequencies. The same situation occurs for the next three nights. By 29 July, the disturbance conditions are much reduced and on following nights, are negligible during the measurement period. We note that on these last three nights, a phase error bias is evident. This bias is frequency dependent, averaging almost 50 CECs for the 10.2 kHz signal. Again, this bias gradually changes over these three days.

The data of Figure E-4 are selected to show an example of navigation errors that are consistently large, yet the trends on all frequencies are similar. On 08 August, the biases on 10.2 kHz and 11.3 kHz exceed 60 CECs. Our total sample of data is too small to provide statistics. However, most of the errors observed are under or near ±20 CECs.

These data represent a cross section of the various characteristics evident in the shipboard data.

General Comments on Part II: We found the shipboard data a very useful addition to the validation database. The wealth of information contained in this database could easily warrant an independent analysis. We found the time plots particularly interesting because of the revealed patterns and trends. Because of uncertainties in determining true ship position, we are hesitant to draw conclusions from the measured median LOP errors. Nevertheless, it is evident that good quality navigation was taking place. We believe that some of the larger observed offsets are attributable to the PPC predictions. In particular, the very consistent trends on a daily basis and between frequencies suggest that the offsets are part of propagation prediction. We found that the day-to-night transition interval on most station pair combinations consistently had relatively large LOP errors. These errors generally are systematic, indicating that better predictions are feasible. Finally, we note that several of the nearest stations are modal at night and during transition. The station pairs without modal effects can incur transition intervals that occupy one-hundred percent of the time. This makes accurate prediction of transition intervals all the more important.

REFERENCES

1. Swanson, E.R., "OMEGA," Proceedings of the IEEE, Vol. 71, No. 10, Pages 1140–1155, October 1983.

2. Scull, D.C., "Omega Worldwide Calibration and Validation," Proc. of Conference on Navigation in Transportation, DOT-TSC-RSPA 78-22, September 1978.

3. Doubt, R.J., "OMEGA Navigation System Regional Validation Program," Navigation: Journal of The Institute of Navigation, Vol. 31, No. 3, pp 155–164, Fall 1984.

4. Karkalik, F.G., G.F. Sage and W.R. Vincent, "Western Pacific OMEGA Validation, Volume I, Technical Report," International OMEGA Navigation System, April 1978.

5. Karkalik, F.G., "OMEGA Validation Over the Western Pacific Area," Navigation: Journal of The Institute of Navigation, Vol. 25, No. 4, pp 395–404, Winter 1978-79.

6. Campbell, L.W., Dr. T.M. Servaes and E.R. Grassler, "North Atlantic OMEGA Navigation System Validation, Final Report," Analytical Systems Engineering Corp., 21 July 1980.

7. Campbell, L.W., "OMEGA Validation in the North Atlantic," Proc. 5th Annu. Meet. of the Int. Omega Assoc. (Aug 5–7, 1980). p 24.

8. Levine, P., Megatek Corporation, "North Pacific OMEGA Navigation System Validation: Draft Final Report," October 1980.

9. Levine, P. and R. Woods, "North Pacific OMEGA Navigation System Validation," Proc. 6th Annu. Meet. of the Int. Omega Assoc. (Aug 18–20, 1981). p 3.

10. Watt, T.M., G.J. Bailie and M. Sutphen, "South Atlantic OMEGA Validation," Vol. I: Summary, Analysis, Appendices A–E, Systems Control Technology, Inc., Palo Alto, CA, January 1983.

11. Watt, T., "Results of the South Atlantic OMEGA Validation," Proc. 8th Annu. Meet. of the Int. Omega Assoc. (July 18–22, 1983). p 17.

12. Kugel, C.P., "Indian Ocean OMEGA Signal Validation," Proc. 9th Annu. Meet. of the Int. Omega Assoc. (Aug 6–10, 1984). p 20.

13. Swanson, E.R., R.J. Doubt and C.P. Kugel, "Indian Ocean Validation," Proc. 10th Annu. Meet. of the Int. Omega Assoc. (July 22–26, 1985). pp 11-1 to 11-11.

14. Swanson, E.R. and C.P Kugel, "Indian Ocean Validation," Omega Navagation System Center Report, No. CG-ONSCEN-02-87, AD-A 194458, 1987.

15. Hildebrand, V.E., "South Pacific Omega Validation Analysis, Omega Navagation System Center Report, No. CG-ONSCEN-02-89, August 1989.

16. Ferguson, J.A., "A Report on the NELC Integrated Prediction Program (PREDPROG)," NELC TN 1630, 16 February 1970.

17. Bickel, J.E., J.A. Ferguson and G.V. Stanley, "Experimental Observation of Magnetic Field Effects at Night," Radio Science, Vol. 5, No. 1, p 19, 1970.

18. Pappert, R.A. and F.P. Snyder, "Some Results of a Mode Conversion Program for VLF," Radio Science, Vol. 7, No. 10, p 913, 1972.

19. Snyder, F.P., "Trans-Equatorial Propagation of Very Low Frequency Radio Waves," NOSC TD 431, 15 April 1981.

20. Gupta, R.R., B.E. Griffiths and P.M Creamer, "An Extended Omega Amplitude Prediction Model," The Analytical Sciences Corporation TR-1319-2, December 1979.

21. Gupta, R.R., S.F. Donnelly, P.B. Morris and R.L. Vence, Jr., "Omega System 10.2 kHz Signal Coverage Diagrams," Proc. 5th Annual Meeting of the Int. Omega Assoc. (Bergen Norway, Aug 5–7 1980(a)). pp 22-1 to 22-36.

22. Nalbandian, J.Y. and K.A. Tench, "OMEGA Access User's Guide," The Analytic Sciences Corporation, Reading, MA, May 1986.

23. Gupta, R.R., "Radial Profiles of 10.2 and 13.6 kHz Omega Signals," The Analytical Sciences Corporation EM-2687 (eight volumes), July 1988.

24. Zacharisen, D.H. and W.B. Jones, "World Maps of Atmospheric Radio Noise in Universal Time by Numerical Mapping," Institute for Telecommunication Sciences. OT/ITS Research Report 2, October 1970.

25. Gupta, R.R., S.F. Donnelly, P.M. Creamer and S. Sager, "Omega Signal Coverage Prediction Diagrams for 10.2 kHz," Volume I: Technical Approach and Volume II: Individual Station Diagrams. The Analytic Sciences Corporation, October 1980(b).

26. Lynn, K.J., "Transequatorial Omega/VLF Reception in Australia," Proc. Eighth Annual Meeting Intr. Omega Assoc., Lisbon, Portugal, 18–22 July 1983.